Identification of differentially expressed transcription factors and dissecting the role of DREAM complex associated components in cellular senescence

A thesis submitted in partial fulfilment of the requirements for the degree of Doctor of Philosophy from University College London

Ruchi Kumari

MRC Prion Unit at UCL

Institute of Prion Diseases

University College London

2018

This thesis is dedicated to loving memories of my Babaji, Shri Jai Narain Shastri and my dear friend Laura Jane Pulford!

Declaration

I, Ruchi Kumari, confirm that the work presented in this thesis is my own. Where information has been derived from other sources, I confirm that this has been indicated in the thesis.

Acknowledgements

Firstly, I would like to thank GOD who makes all things possible!

I am extremely thankful to my primary supervisor Prof. Parmjit Jat for giving me the golden opportunity to work in his lab, constant support, guidance throughout my PhD and always being willing to discuss. I am immensely thankful to you for being patient and helping me improve my writing style. My sincere thanks are due to all my teachers until now, without their guidance and unstinting support, I would not have been where I am!

I am indebted to Commonwealth Scholarship Commission for funding my PhD and giving me once in a lifetime opportunity and a wonderful experience to cherish that helped me grow immensely both professionally and personally. I thank Prof. John Collinge for allowing me work in his department.

I can never thank enough my inside out beautiful best friend Alexandra Philiastides for her constant support both in and out of the lab. Thank you for being a great pillar of support both professionally and personally. You are the reason why I survived this PhD! Thank you for going out of your way to help me! I am indebted to you and forever grateful to you! Thanks for putting up with me and helping me with figures for the thesis innumerable number of times and counting all my flasks. Thank you letting me use your laptop to write my thesis, when mine died midway while writing, it obviously would not have been possible without it! I can never express in words how eternally grateful I am to have met you through this PhD and share the journey of highs and lows together. I am equally thankful to Alex's family for loving me and supporting me like their own daughter. Special thanks to Alex's dad Dr. Antony Philiastides for all the discussions, words of motivation and good food we had together.

I must thank Dr. Jim DeCaprio for accidentally sending the LIN52-Ala form, because of which my first reconstitution experiment worked and helped the project take an interesting direction.

I must thank Richard Newton for his help with figures and scanning my mind-blowing number of flasks. Thanks to Matthew Ellis for his help with developing the computational method, Gary for help with sequencing and Dr. Holger Hummerich for the bioinformatic analysis. My gratitude is also extended to Marta for her help in the project and helping with my experiments after I developed the repetitive strain injury and for being such a lovely person. I thank Karthik for help with the figures. I thank everyone who has worked on this project before.

I want to express my gratitude to Nunu for training me. My warmest thanks to you for the continuous supply of delicious homemade food which made me feel closer to home, away from home! I also must thank Waitrose for their free coffee and Hare Krishna for free food.

This PhD journey has been very tough as I lost my loved and dear ones. My Babaji, thank you always believing in me and making me feel special and proud always. My dear friend Laura

Pulford who made me enjoy my time in London the most. I have the happiest, craziest and most beautiful memories with you in London. You are missed every single day my friend! My brave tuition friend Preeti Dahiya!

A very special thank you goes out to my best friend Shubhra Meena, you are one pure hearted person who has always stood by me no matter what! I am immensely thankful to all the current and past members of the student office. You have all helped make these past years a very enjoyable and memorable time. Special thanks to Mike farmer for all the Friday night fun nights! Special thanks to Xun Yu Choong for being extremely helpful and organizing all the plays, dimsums. My heartfelt thanks to my dear friend Justin Tosh and Lucy Sheytanova for being in this journey together always. I am very thankful to Justin for suggesting the idea of computational method to verify my results which improved my thesis a lot. I thank Iryna, Madeleine Reily, and Justin for statistics related help. I thank all my Commonwealth fellow Scholars family. Dr. Himadri Bhushan Das has been an unfailing source of encouragement, advice and reassurance. I owe a great deal to all my good friends I made along the way. Special thanks to my wonderful friend Danish Umer. I thank Himanshu Batra and Amit Krishna Dwivedi for being there specially towards the end of thesis writing.

Heartfelt thanks to Abhishek Mishra. I would like to thank Vibhav Mishra for all the great times and fun we had from July 2015 to September 2016 when lab work was overwhelming. After September 2016 I thank you making me realize my own potential to deal with hardships and continue to work despite that and be strong.

My acknowledgements would not be complete without thanking my beautiful parents for letting me pursue my dreams and always having my back. I feel very blessed and proud to have such amazing star parents like you. Thank you for constant love, chats, support, words of encouragement and your undying faith and belief in me. It kept me going! Special mention to my brother, my biggest strength, my star, my life, thank you for making me feel special and loved every single day and visiting me in London on Rakshabandhan, when I was missing you the most. Thank you for making me feel positive, believe in myself and have the motivation to move ahead when thesis writing felt impossible. Special heartfelt thanks to my Alipur family for their love and support throughout my PhD, every weekend! I am deeply grateful to my Badi Maa for the unconditional love and countless blessings and prayers!

I thank one and all who have helped me in some way or the other in coming this far!!

Abstract

Cellular senescence is a stable cell cycle arrest that normal cells undergo in response to a variety of intrinsic and extrinsic stimuli. Being implicated in ageing and age-related diseases including cancer it is of great importance to elucidate the signalling pathways involved in regulating the senescent state. The p53/p21^{WAF1} and p16^{INK4A}/pRB tumour suppressor pathways have clearly been implicated in senescence, but the critical downstream targets of these pathways are unclear. Transcription factors (TFs) regulate gene expression at different stages of embryonic development and are key to the establishment and maintenance of specific cell fates. My primary goal is to identify TFs that act downstream of these pathways.

To identify the TFs that act downstream of the p53/p21^{WAF1} and p16^{INK4A}/pRB pathways, the previously identified list of differentially expressed transcripts were overlaid with known sequence-specific DNA binding factors. The list was then refined by examining what happens to their expression, when senescence was bypassed and if the change in expression upon senescence is inversely correlated with expression in cancer.

This identified 10 upregulated and 74 downregulated TFs. Their ability to directly bypass senescence was examined in the conditionally immortalized fibroblasts by lentivirus mediated RNA silencing or ectopic expression. The MuvB complex (LIN9, LIN37, LIN52, LIN54 and RBBP4) associates with the RB-like proteins, DP1 and E2F4 to form a repressive complex, DREAM, that induces quiescence. When cells re-enter the cell cycle, MuvB dissociates from DREAM and sequentially recruits MYBL2 (B-MYB) and FOXM1 to promote cell cycle progression. Reconstitution of B-MYB-MuvB-FOXM1 i.e. MMB-FOXM1 complex demonstrated that it can bypass senescence under very stringent conditions and that LIN52, FOXM1 and B-MYB were the crucial components. Moreover, this required non-phosphorylated LIN52, suggesting a role for phosphorylated LIN52 and the DREAM complex in inducing senescence, which is not very widely studied.

Further reconstitution experiments using a cocktail of TFs targeting the up- and down-regulated factors has revealed the presence of synergy indicating that there are other key TFs which remain to be identified. This study has enabled us to identify TFs that play a causal role in senescence. This opens the door to identifying their downstream targets and lays the foundation for a better understanding of the pathways underlying cellular senescence and its therapeutic intervention in cancer and age-related diseases.

Impact Statement

Normal somatic cells divide a fixed number of times before they stop dividing and enter a state known as cellular senescence. Senescent cells are not dead; they are metabolically active, remain viable, have a characteristic distinct appearance, but cannot divide. Cellular senescence can compromise repair of damaged tissues, wound healing and contribute towards ageing, as these processes require cells to divide. Removal of senescent cells can attenuate age-related tissue dysfunction and therefore extend healthspan. Senescence can also act as a potent anti-cancer mechanism, by preventing proliferation of potentially cancerous cells. Bypass of cellular senescence which leads to a limitless replicative potential, is a key hallmark of cancer cells.

The mechanisms underlying cellular senescence are not completely understood, such as, why cells stop dividing; how do they stop; how do they know when to stop; what the critical players are; the pathways involved in making them stop dividing; and how they are all integrated. Transcription factors (TFs) are proteins that can simultaneously control the expression of many other proteins and thus play a central role in regulating biological processes. The aim of my thesis was to systematically study transcription factors whose expression is altered during senescence to determine if they have a causal role in making normal cells stop dividing.

This thesis presents the identification of 10 TFs which are up-regulated and 74 TFs that are down-regulated in senescence. This differential regulation is opposite to that in cancer, as cancer is the flip side of senescence. Some of the identified factors are components of a complex called DREAM and its associated components i.e. MMB-FOXM1 which are formed after disassembly of DREAM complex. The DREAM complex has previously been shown to play a role in regulating quiescence, another form of cell cycle arrest which is reversible in contrast to senescence which is essentially irreversible. The role of DREAM complex in senescence is not widely studied. Results presented within this thesis highlight an important role for DREAM and the associated MMB-FOXM1 complex in regulating entry into senescence and how it may be bypassed in cancer. Pooling of multiple different TFs has further shown that there may be other additional components that remain to be identified and studied further.

Together this study has contributed in understanding the role of DREAM complex and associated components in regulating senescence and has laid the foundation for identification of their downstream targets, particularly those targets that may be involved in the stability of the senescence as it is a stable growth arrest. Eventually it is hoped

that these targets will represent novel, important and direct targets for developing new therapies that promote healthier ageing and increase vitality of the older population through stimulating regeneration, repair and wound healing, while retaining the tumour suppressor properties of senescence, if possible. These key components also have the potential to be new therapeutic cancer targets, for developing small molecule inhibitors and activators aimed at inducing senescence in tumours.

Table of Contents

List of Figures

List of Tables

List of Abbreviations

AKT	Protein Kinase B
AMP	Adenosine monophosphate
AMPK	5’ adenosine monophosphate activated protein kinase
ARID2	AT-rich Interaction domain 2
ATF6-α	Activating transcription factor 6 alpha
ATM	Ataxia telangiectasia mutated
ATR	Ataxia telangiectasia and RAD3-related (ATR)
B2MG	Beta 2 microglobulin
bHLH	Basic helix loop helix
BiP	Binding immunoglobulin protein
bp	Base pair
CCF	Cytoplasmic chromatin fragments
CDE	Cell-cycle dependent element
CDK	Cyclin dependent kinase
CDKI	Cyclin dependent kinase inhibitor
cGAMP	2’3’ cyclic GMP-AMP
cGAS	Cyclic GMP–AMP synthase
ChIP	Chromatin immunoprecipitation
CHR	Cell cycle genes homology regions
$CL3^{EcoR}$	Clone 3 of Human Mammary Fibroblasts used in this study
CLE	CHR-like element
DDR	DNA damage response
DEP-1	Density-enhanced phosphatase-1
DNA-SCARS	DNA segments with chromatin alterations reinforcing senescence
DP	Dimerization partner
DPP4	Dipeptidyl peptidase 4
DREAM	Dimerization partner (DP), retinoblastoma (RB)-like, E2F and MuvB complex
ds	Double stranded
DSB	Double Stranded break
DYRK1A	Dual-specific tyrosine-(Y)-phosphorylation regulated kinase 1A

E2A	2A peptides derived from equine rhinitis virus
E2F	E2 factor family
EB	Elution buffer
EBLN1	Endogenous bornavirus-like nucleoprotein 1
EcoR	Murine ecotropic receptor
EPAS1	Endothelial PAS Domain Protein1
ER	Endoplasmic reticulum
F2A	2A peptides derived from foot-and-mouth disease virus
FCS	Foetal Calf Serum
FM	Multicistronic construct containing FOXM1ΔNΔKEN and B-MYB
GA	Growth arrest
GIST	Gastrointestinal stromal tumours
GMP	Guanosine monophosphate
HCV	Hepatitis C virus
HGPS	Hutchinson-Gilford Progeria Syndrome
HMF	Human mammary fibroblasts
HRP	Horse radish peroxidase
hTERT	Catalytic component of human telomerase
IL	Inter leukin
KLF	Krüppel-like factor
LB	Luria Base
LF	Multicistronic construct containing LIN52 and FOXM1ΔNΔKEN
LFM	Multicistronic construct containing LIN52, FOXM1ΔNΔKEN and B-MYB
LM	Multicistronic construct containing LIN52 and B-MYB
MiDAS	Mitochondrial dysfunction associated senescence
miRNA	Micro RNA
MMB-FOXM1	Reconstituted whole complex containing B-MYB, MuvB and FOXM1 complex
MMP	Matrix metallo proteinases
mTOR	Mechanistic target of Rapamycin

MuvB	Multivulval class B
NHDF	Normal human dermal fibroblasts
NR1H4	Nuclear receptor sub family 1
OIS	Oncogene induced senescence
ORF	Open Reading Frame
P2A	2A peptides derived from porcine teschovirus-1
PATZ1	POZ/BTB and AT-hook-containing zinc finger protein 1
PBS	Phosphate buffered saline
PDS5B	PDS5 Cohesin Associated Factor B
PLXNA3	Plexin A3
POK	POZ/BTB and Kruppel TF family
RGS7	Regulator of G-protein Signalling 7
ROS	Reactive oxygen species
RPA	Replication protein A
SA	Senescence associated
SAHF	Senescence-associated heterochromatin foci
SASP	Senescence associated secretory protein
SBB	Sudan Black B
SD	Standard deviation
shRNA	Short hairpin ribonucleic acid
SIPS	Stress induced premature senescence
SIRT1	Sirtuin1
STING	Stimulator of interferon genes
SV40-LT	Simian Virus 40 large T antigen
T2A	2A peptides derived Thosea asigna virus
TERC	Catalytic ribonucleic component of human telomerase
TF	Transcription Factor
TGF-β	Transforming growth factor beta
TIF	Telomere-dysfunction induced foci
TNF-α	Tumour necrosis factor alpha
ts	Temperature sensitive
UPR	Unfolded protein response
VEGF	Vascular endothelial growth factor

WC	Reconstituted Whole Complex containing B-MYB, MuvB and FOXM1 i.e. MMB-FOXM1
WT	Wild type
ZBTB7A	Zinc Finger and BTB Domain containing 7A
ZC3H4	Zinc Finger CCCH-Type Containing 4

Chapter 1 Introduction

An early study published in 1921 by French Nobel laureate, Alexis Carrel claimed to have successfully cultured population of cells derived from embryonic chick heart tissue in vitro for 34 years (Carrel and Ebeling 1921). This set the prevailing belief in the early twentieth century, that all vertebrate cells inherently capable of dividing can grow indefinitely when cultured in vitro in the right milieu suggesting them to be immortal. This was contradicted in 1961 by the pioneering study consisting of a series of experiments conducted by Leonard Hayflick and Paul Moorhead. In this study, for the first time they observed that normal diploid human cells when cultured in vitro had a limited proliferative potential. After a fixed number of divisions, the cells stop dividing which is defined as the 'Hayflick limit' (Hayflick and Moorhead 1961). This stage in which the cells stop dividing is now widely known as the biological phenomenon, cellular senescence.

Hayflick demonstrated that human diploid cell strains stop dividing in vitro after a fixed number (40-60) of population doublings. Furthermore, he suggested the presence of memory within cultured normal human cells as he observed that both human diploid adult and foetal strains which had been cryopreserved, remember the population doubling level at which they were frozen and upon revival would undergo further population doublings only up to the fixed maximum pre-determined population doubling. This led to the conclusion that onset of cellular senescence is not related to the absolute calendar time but rather depends on the time during which the culture is actively proliferating. Another key finding was that the passage potential for adult lung strains was found to be significantly lower than the passage potential of foetal lung strains. This for the first time suggested the idea of cellular ageing as invitro culture mimics cellular ageing (Hayflick 1965). Since this crucial discovery of cellular senescence in 1961, apart from notable exceptions of most cell lines and embryonic stem cells, senescence has been demonstrated in many different cell types of different species including stem cells (Hayflick 1974).

Senescence can potentially compromise tissue repair and regeneration and contribute to tissue and organismal ageing due to the accumulation of senescent cells and depletion of stem/progenitor cell compartments and secretion of an

array of inflammatory cytokines, chemokines and matrix metalloproteinases described as Senescence Associated Secretory Phenotype proteins (SASP) (Campisi et al. 2011; Coppé et al. 2010a). Senescence can also lead to the removal of defective and potentially cancerous cells from the proliferative pool, thereby limiting tumour development and act as a potent tumour suppressor mechanism (Campisi 2005). Removal of senescent cells can prevent or delay age-related tissue dysfunction and extend healthspan (Baker et al. 2011, 2016). Even though the acquisition of limitless replicative potential has been proposed to be one of the key events required for malignant transformation, underlying signalling pathways and regulating mechanisms controlling senescence are poorly understood (Hanahan and Weinberg 2011). A greater understanding of the molecular events that lead to cellular senescence is therefore essential if we are to prevent tissue dysfunction without increasing the risk of cancer.

From recent developments in the senescence field, it is now clear that senescence entails much more than just growth arrest. Hence, in this chapter, I will discuss cellular senescence as a biological phenomenon, its causes, characteristic hallmarks and the pathways involved in manifesting cellular senescence. Cell cycle and its key regulators will also be discussed. The significance of this biological phenomenon in different contexts such as its role in vivo, in cancer and ageing will be discussed. Furthermore, this thesis focusses on studying the role of the DREAM complex and associated components in senescence, the DREAM complex is also discussed. Finally, the model of study used in this thesis ($CL3^{EcoR}$) is explained.

1.1 Causes of Cellular Senescence

Since its discovery, several studies have revealed that cellular senescence can be caused by a variety of intrinsic and extrinsic stimuli. This led to the identification of different types of senescence. Replicative senescence is the term coined for the cellular senescence arising due to the limited proliferative potential of cells in culture as observed by Hayflick upon serial cultivation (Hayflick and Moorhead 1961). However, it is now known that apart from replicative senescence, premature senescence can be induced by a variety of intrinsic and extrinsic stimuli commonly referred to as Stress-Induced Premature

Senescence (SIPS). Morphological and biochemical changes that occur upon SIPS is quite similar to replicative senescence. Not much can be said about whether all types of senescence induced in vitro in different cell model systems, actually occur in vivo within an organism.

1.1.1 Telomere-dependent Replicative Senescence

Several studies after Hayflick's key finding focussed on examining the reason behind the finite proliferative potential. One of the well understood intrinsic stimuli responsible for this form of growth arrest arising due to proliferative exhaustion is shortening of telomeres (Harley et al. 1990; Sedivy and van Deursen 2013). Telomeres are the ends of chromosomes which are normally protected by a complex of six telomere-specific proteins called the shelterin complex (de Lange, 2010). Due to the 'end replication problem' faced by linear chromosomes, the telomeres shorten with each cell division. This arises due to the restricted 5'- to 3'- unidirectional nature of DNA replication along with the requirement of a primer for initiation of DNA synthesis which leads to continuous DNA replication on the leading strand as opposed to the discontinuous process on the lagging strand, producing short DNA fragments known as Okazaki fragments. These fragments are covalently joined by DNA ligase activity later to complete the DNA synthesis on the lagging strand. At the 5'- end of the lagging strand, the last primer which was added to form the last Okazaki fragment cannot be replaced by DNA, giving rise to the end replication problem and hence the loss of 50-200 base pairs of telomeric DNA from the end of a chromosome during each S-phase replication (Harley et al. 1990; Olovnikov 1973). Hence, continuous cell divisions lead to the removal of protective shelterin complex resulting in progressively short and dysfunctional telomeres (Martens et al. 2000).

As telomere shortening induces senescence growth arrest, cancer cells must, therefore, overcome this in order to grow indefinitely. This is done by the presence of a ribonucleoprotein enzyme called Telomerase which comprises the catalytic subunit, telomeric reverse transcriptase (hTERT) and the catalytic RNA component (TERC) which acts as a template for hTERT for adding hexanucleotide repeats. Telomerase can restore the repetitive telomere DNA de novo and prevent telomere shortening (McEachern et al. 2000). In humans,

telomerase is found only in a few cells like cancer cells, germ cells and some stem cells whereas in mice the number of telomerase expressing cells is greater (Campisi 2013). The catalytic RNA is ubiquitous. Human somatic cells lack the catalytic subunit of telomerase at a level sufficient to constantly maintain telomeres. Therefore, in somatic cells, repeated cell division without telomerase leads to critically short and dysfunctional telomeres which elicit a DNA damage response (DDR) via the tumour suppressor protein p53. Prolonged DDR signalling and p53 activation enforce senescence growth arrest (Fumagalli et al. 2012).

1.1.2 Stress-Induced Premature Senescence (SIPS)

Premature senescence can be induced by other forms of genotoxic stress apart from telomere shortening. Genotoxic stress can be caused by endogenous factors, for example, progressive telomere shortening due to other factors apart from normal cell division like changes in telomeric structure. Exogenous factors such as oncogene activation, oxidative stress, DNA damage caused by radiation and other small molecules can also lead to genotoxic stress. To combat these stresses, premature cellular senescence is induced in cells before achieving the maximum fixed doubling potential. Most of the genotoxic stress results in a DDR, and growth arrest via activation of p53. Other forms of stress lead to senescence via activation of the pRB pathway (Campisi and D'Adda Di Fagagna 2007). A recent extensive study conducted by Petrova and colleagues in 2016 analysed more than 50 small molecule chemical compounds that can induce premature cellular senescence and senescence-like states (Petrova et al. 2016). Their study described in detail the basic mechanism of action of different small molecule compounds studied, the treatment used, documenting the biological senescence markers studied and the signalling pathways involved in manifesting senescence (Petrova et al. 2016). It is not very clear whether all these different forms of stresses manifest senescence via distinct pathways or a common biochemical pathway.

1.1.2.1 Oncogene-Induced Senescence (OIS)

OIS was discovered by Serrano and colleagues in 1997 when they demonstrated premature permanent senescence growth arrest occurring in G1 phase of the

cell cycle due to oncogenic Ras overexpression after a brief period of hyperproliferation in the presence of p53 or $p16^{INK4A}$ in vitro (Serrano et al. 1997). OIS observed in this study was phenotypically indistinguishable from replicative senescence. This study suggested that in addition to replicative senescence which occurs due to the cell division counting mechanism, premature senescence can occur as a dynamic response to an aggressive mitogenic stimulus suggesting a role of OIS as a tumour suppressor mechanism (Serrano et al. 1997).

After this key discovery of OIS, this area was widely researched, which led to the identification of several other oncogenes capable of inducing senescence. Not only, the expression of an oncogene can lead to OIS but also the loss of tumour suppressor is capable of inducing senescence (Gorgoulis and Halazonetis 2010). Multiple studies after its discovery in vitro, have subsequently shown the presence of OIS in vivo as a potent anti-tumour barrier (Chen et al. 2005; Sharpless and Sherr 2015).

Extensive research has shown that OIS can be manifested by different overlapping pathways (Gorgoulis and Halazonetis 2010). One of the key pathways of OIS manifestation involves DDR arising due to aberrant DNA hyper-replication (Di Micco et al. 2006), increased levels of reactive oxygen species (ROS) (Lee et al. 1999), replication fork reversal (Neelsen et al. 2013) and depletion of nucleotide pools (Mannava et al. 2013). Derepression of the CDKN2A locus is also a general feature associated with OIS (Kim and Sharpless 2006; Gil and Peters 2006). The relative importance of one mechanism over the other depends on the cell type and varies across species.

Other strong, persistent or deranged mitogenic signals can also induce cellular senescence to suppress tumour formation (Blagosklonny 2003). Cells can undergo senescence in response to other forms of proliferative mitogenic signals in addition to the aberrant expression of oncogenes; for example, persistent stimulation by cytokines like interferon-β triggers senescence mediated by p53 activation and DDR arising due to the accumulation of ROS (Moiseeva 2006).

1.1.2.2 Unresolved DNA Damage Induced Senescence

Apart from telomere shortening, many cells undergo cellular senescence in response to other forms of DNA damage (Nakamura et al. 2008). Directly or indirectly generated DNA DSBs (Double-stranded breaks) are potent inducers of cellular senescence mostly regulated via the p53-$p21^{WAF1}$ pathway. DNA DSBs can be caused by ionizing radiation, topoisomerase inhibitors, cytotoxic chemotherapies and also oxidative stress (Robles and Adami 1998; Chang et al. 2002; Barascu et al. 2012). It has been observed that a single unresolved DNA DSB can induce senescence (Di Leonardo et al. 1994).

Many anticancer drugs, for example, bleomycin and doxorubicin are capable of inducing senescence by causing DNA damage whereas others such as palbociclib induce senescence through a different mechanism by inhibiting cyclin dependent kinase (CDK) (Petrova et al. 2016). Additionally, oxidizing agents (e.g. H_2O_2) which lead to the formation of ROS can also cause senescence. ROS is also generated by mitochondria via TCA cycle. The DDR is one of the overlapping pathways used by oxidizing agents to manifest senescence (Correia-Melo et al. 2016). ROS are one of the different stimuli commonly used to induce premature senescence in in vitro studies.

1.1.2.3 Epigenetically Induced Senescence

As mentioned later in the senescence markers section, cellular senescence entails changes in chromatin organization which include the formation of repressive heterochromatin, known as Senescence-associated heterochromatin foci (SAHFs) at many loci which mainly encode pro-proliferative genes (Narita et al. 2003). Disruption in the epigenome can also induce cellular senescence. For example, histone deacetylase inhibitors (Munro et al. 2004), suboptimal c-Myc (Guney et al. 2006) or downregulation of p300 histone acetyltransferase (Bandyopadhyay et al. 2002) are considered to act by perturbing chromatin organization.

Epigenetically induced senescence mostly acts by inducing $p16^{INK4A}$ expression as opposed to DNA damage-induced senescence which relies mainly on the cyclin dependent kinase inhibitor (CDKI), $p21^{WAF1}$ (Petrova et al. 2016).

Therefore, as epigenetic modifiers are capable of maintaining the senescent state without inducing any cell stress, epigenetically induced senescence has been characterized as ‘causeless’ which makes it similar to the senescence observed during developmental stages or during ageing as opposed to DNA damage-induced senescence which occurs prematurely due to induction of different forms of stress (Petrova et al. 2016).

1.1.2.4 Mitochondrial Dysfunction Associated Senescence (MiDAS)

A recent study by Wiley et al., 2016, has set out to show another cause of senescence growth arrest, which occurs due to mitochondrial dysfunction and which is different from the senescence due to genotoxic stress (Wiley et al. 2016). Mitochondria normally oxidize NADH to NAD^+. Hence, mitochondrial dysfunction decreases the NAD^+/NADH ratio mostly in the cytosol, leading to activation of 5’ adenosine monophosphate activated protein kinase (AMPK), followed by subsequent activation of p53 and manifestation of miDAS (Wiley et al. 2016).

The key feature of miDAS is the distinct secretory phenotype which is different from SASP caused by genotoxic stress. The SASP caused by miDAS includes interleukin (IL)-10, tumour necrosis factor alpha (TNF-α) and chemokine (C-C motif) ligand 27 (CCL27) but lacks the normal IL-1 mediated signalling arm. This distinct SASP has the potential to alter the differentiation of certain cell types like preadipocytes and keratinocytes. Interestingly, miDAS has also been shown to occur in vivo in a progeroid mouse which accumulates dysfunctional mitochondria suggesting the involvement of dysfunctional mitochondria in driving ageing phenotypes (Wiley et al. 2016).

1.1.2.5 Paracrine Senescence

It has been recently discovered that senescence can be induced in neighbouring healthy, proliferation competent cells by a primary senescent cell (Nelson et al. 2012; Acosta et al. 2013). This type of non-cell autonomous stable growth arrest is called paracrine senescence. The manifestation of non-cell autonomous senescence occurs mainly because of the SASP produced by a primary senescent cell. A study by Acosta et al., 2013, has demonstrated beautifully the

non-cell autonomous paracrine transmission of senescence by cells undergoing OIS in vivo in both mouse and human models of OIS and also provides insights into pathways regulating paracrine senescence (Acosta et al. 2013). Their study has identified multiple different SASP components namely, vascular endothelial growth factor (VEGF), transforming growth factor (TGF)-family members and the chemokines CCL2 and CCL20 mediating paracrine senescence. The TGF pathway identified in their study suggests $p15^{INK4B}$ and $p21^{WAF1}$ involvement (Acosta et al. 2013).

Another study by Nelson et al., 2012, has shown a similar senescence bystander effect (Nelson et al. 2012). This study set out to show that senescent cells induce a DDR, a characteristic feature of senescence, in neighbouring cells. They found that senescence occurs via gap junction-mediated cell to cell contact which leads to transfer of ROS, thereby suggesting the involvement of ROS in paracrine senescence (Nelson et al. 2012, 2018).

1.2 The Cell Cycle

The cell cycle is a sequence of coordinated phases which leads to cell division, critical for both development and viability of multicellular organisms. Completion of the cell cycle leads to production of two daughter cells upon mitosis. To maintain the integrity of the genetic material of the daughter cells, accurate replication of DNA must be ensured.

The cell cycle can be divided into two main phases i.e. Interphase where a cell prepares to divide, and the Mitotic phase, where the actual cell division occurs. Interphase can be further divided into G1, S and G2 phases (Figure 1.1). Mitosis consists of prophase, metaphase, anaphase and telophase (Vermeulen et al. 2003; Norbury and Nurse 1992).

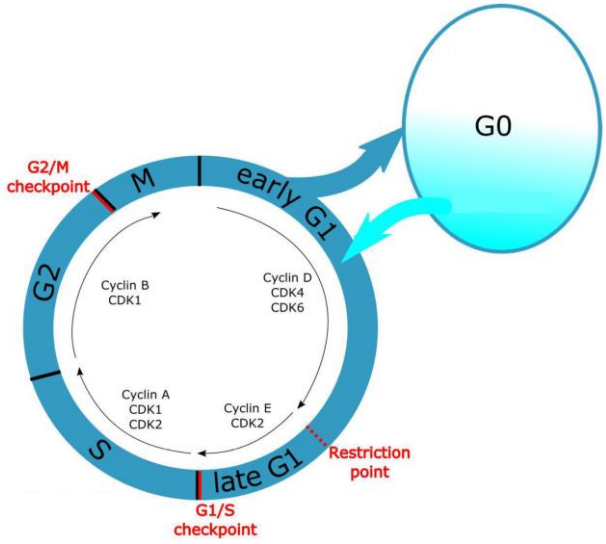

Figure 1.1 Schematic representation of the mammalian cell cycle
The cell cycle is divided into four phases, G1, S, G2 and M. Different cyclin/CDK complexes that are active during specific phase of the cell cycle are indicated. For accurate and efficient functioning of the cell cycle, different checkpoints marked in red exist. Cells which are not preparing to divide enter the resting G0 phase, such as quiescent cells, senescent cells or terminally differentiated cells.

For accurate progression of the cell cycle, it is regulated at various points called cell cycle checkpoints. Two-thirds into the G1 phase, there occurs a point called the Restriction point (R point) after which the cell commits to enter into mitosis (Pardee 1974). Mitogenic signals like growth factors affect cells in G0 and G1 phase. Before the restriction point, growth factors allow cells to proceed to G1 phase from G0 and cells are capable of reverting back to G0 phase upon removal of growth factors. In contrast, after the restriction point, cells no longer respond to the growth factors/mitogenic signals and can progress to S phase even after removal of growth factors. Additionally, other checkpoints exist to ensure correct cell cycle at different stages such as, the DNA damage checkpoint and the spindle checkpoint (Hartwell and Weinert 1989; Paulavich and Hartwell 1995).

1.2.1 Cell cycle regulation by cyclins, CDKs and CDK inhibitors

The tight regulation of the cell cycle is achieved by the action of a group of proteins called cyclins and cyclin dependent kinases (CDKs). CDKs are a family of heterodimeric serine-threonine protein kinases (Malumbres 2014; Malumbres and Barbacid 2005). CDKs were the first regulators of the cell cycle to be discovered. The original member now known as CDK1 was first identified in

genetic screens as CDC28 (Hartwell et al. 1970) in the budding yeast *Saccharomyces cerevisiae*, and as Cdc2 (Nurse 1975) in the fission yeast *Schizosaccharomyces pombe*, and were demonstrated to be critical for cell cycle progression (Russell and Nurse, 1986; Morgan, 1997). Later, using complementation approach, homologues in humans were identified (Draetta et al. 1987; Lee and Nurse 1987; Hanks 1987).

In independent experiments in sea urchin eggs, cyclins were discovered after observing that they were degraded periodically at each cell division (Evans et al. 1983). Since their discovery several different cyclins have been identified that associate with specific CDKs during a specific phase of the cell cycle (Pines 1991). Multiple different CDKs have been identified, which include CDK2, CDK4 and CDK6 active during G1 phase, CDK2 during S phase and CDK1 during G2 and M phases (Vermeulen et al. 2003). The levels of CDKs remain relatively constant during the cell cycle but their activation at specific stages of the cell cycle is achieved by association with cyclins. As is obvious by the name, the levels of cyclins oscillate during the cell cycle, which eventually leads to periodic activation of CDKs. To control the activity of their target proteins CDKs phosphorylate their target proteins during the cell cycle. These proteins work together to ensure the co-ordinated and timely regulation of specific transcription factors which are required to be active during a particular stage in cell cycle to guide cells through cell cycle in orderly fashion (Malumbres 2014).

In addition to cyclins, the activity of CDKs is also regulated by CDK-Inhibitors (CDKI) which act by phosphorylating specific serine, threonine or tyrosine residue, in the cyclin-CDK complex. There are two different sub-groups of CDKIs which are known as the Cip/Kip family and the INK4A family. The Cip/Kip family is made up of three members i.e. CDKN1A ($p21^{WAF1}$), CDKN1B ($p27^{KIP1}$) and CDKN1C ($p57^{KIP2}$) and the INK4A family consists of CDKN2A ($p16^{INK4A}$), CDKN2B ($p15^{INK4B}$), CDKN2C ($p18^{INK4C}$) and CDKN2D ($p19^{INK4D}$) (Sherr and Roberts 1999).

1.2.2 The RB family of proteins

The RB family of pocket proteins is one of the main targets of cyclin-CDK complexes and their best-known function is binding to and inactivating E2F

leading to repression of transcription of E2F target genes. The three members of the pocket protein family are: RB1 (pRB), RBL1 (p107) and RBL2 (p130). These proteins share a common bipartite pocket region comprising a LXCXE motif, which allows them to interact directly with other proteins (Dyson 1998).

RB1 (pRB) is the product of retinoblastoma gene *RB1* which was initially identified as a gene responsible for causing a childhood cancer in the eyes, retinoblastoma (Knudson 1971). The wild type *RB1* gene is amongst the most extensively studied tumour suppressor genes and the product RB1 is known to be deregulated or absent in about 90% of cancers (Hanahan and Weinberg 2011).

The tumour suppressive action of RB1 can be disrupted by different mechanisms such as, dysregulated phosphorylation by cyclinD/CDK4,6 and cyclinE/CDK2 complexes or mutations in the *RB1* gene, most of which occur in the pocket domain of RB1 (Huang et al. 1990; Hu et al. 1990). Additionally, viral proteins such as SV40LT (Ludlow et al. 1989), HPV Type 16 E7 (Dyson et al. 1989) and Adenovirus type 5 E1A (Whyte et al. 1988) act as viral oncoproteins which are capable of binding and sequestering RB via the LXCXE motif and thereby inhibiting its tumour suppressor activity. It has been demonstrated that distinct patterns of phosphorylation of different sub-populations of RB by cyclin dependent kinases have the ability to alter the growth controlling functions of RB (Mittnacht et al. 1994).

The RB family of proteins act as ‘gatekeepers’ thereby controlling the cell cycle progression from G1 to S phase by interacting with specific TFs and promoter regions. pRB is a substrate of CDK which remains bound to the E2F TF thereby preventing the activation of the E2F target genes required for S phase entry. pRB when dephosphorylated remains bound to E2Fs thereby forming the RB-E2F repressive complex. These repressive complexes bind to the promoter regions of E2F target genes and inhibit the transcription of genes required for cell cycle progression (Fischer and Müller 2017). Additionally, to enhance the transcription repression they also recruit factors such as histone deacetylase enzymes (HDACs) and the histone methyltransferase SUV39H1. At the G1/S checkpoint this inhibition is removed by the phosphorylation of RB by cyclinE-CDK2 which

leads to release of E2Fs from RB, thereby promoting the transcription of S phase genes and hence the progression of cell cycle (Zhang et al. 2000). The gene expression during late S phase is controlled by association of MuvB (Multi vulva class B) with MYBL2 (B-MYB) whereas, during late G2 and M phase the gene expression is controlled by binding of MuvB with B-MYB and FOXM1. During G0 all cell cycle dependent gene expression is repressed by binding of MuvB to p130-E2F dimerization partner (DP) forming the repressive DREAM complex. This is discussed in detail in section 1.2.4.

RB plays a key role in skeletal muscle differentiation by associating with myoD, a basic helix-loop-helix (bHLH) protein (Magenta et al. 2003; Thorburn et al. 1993). In addition to the critical functions performed by the RB family of proteins in cell cycle regulation, recently a direct functional involvement of the RB family of proteins has been reported in DNA repair by non-homologous end-joining (Huang et al. 2016; Cook et al. 2015).

1.2.3 E2Fs

The E2 factor family (E2F) is a family of TFs which act downstream of the pRB family of pocket proteins, therefore play a crucial part in cell cycle regulation. E2Fs interact with the members of the pRB family of pocket proteins as well as with DP1, DP2 and DP3 as heterodimers (Dyson 1998). RB can interact with E2Fs to inhibit their function. The ability of E2Fs to bind to and activate E2 adenoviral gene promoter led to their discovery (Kovesdi et al. 1986). Eight E2F members (E2F1-E2F8) are known in mammals, which play different roles during cell cycle regulation by interacting with the target nucleotide sequences present in the promoter region of other genes which are essential for transit through the cell cycle (Dyson 1998; Helin 1998; Trimarchi and Lees 2002).

E2Fs perform varied functions and depending on that they can be divided into main functional groups: activating (E2F1, 2 and 3) and repressing E2Fs (E2F4 and E2F5) (Trimarchi and Lees 2002). Activating E2Fs (E2F1-3) are positive regulators of transcription which are required for cell cycle progression and mainly associate with pRB (Leone et al. 1998, 2000). The importance of activating E2Fs is obvious from a study which demonstrated that mutating all three activating E2F1-3, leads to complete blocking of proliferation (Wu et al.

2001). In contrast, E2F4 and 5 mainly act as negative regulators of the E2F regulated promoters and therefore are known to play an important role in cell cycle exit and differentiation (Sardet et al. 1995). They are known to interact with other members of the RB family. E2F4 can form complexes with all the members of family i.e. p130, p107 and RB in some cell types. On the other hand, E2F5 only forms complexes with p130 (Dyson 1998). It has been shown that in response to some cell cycle arrest signals, cells which do not have repressive E2Fs are unable to undergo G1 arrest (Gaubatz et al. 2000). E2F7 and 8 act as repressive E2Fs. They replace the activating E2F1-3 in late S phase after DNA synthesis is completed to reduce the G1/S gene expression in G2/M stage (Westendorp et al. 2012; Di Stefano et al. 2003; Christensen et al. 2005).

1.2.4 The DREAM complex

Sadasivam and DeCaprio have described the DREAM complex as the master coordinator of cell cycle-dependent gene expression (Sadasivam and DeCaprio 2013). DREAM is a multi-subunit complex formed by the assembly of p130 and p107 (RB family of pocket proteins) with Dimerization partner (DP), E2F4-5 and a Multivulval class B (MuvB) core complex which represses most if not all gene expression in quiescence (Litovchick et al. 2007). The MuvB core complex comprises LIN9, LIN37, LIN52, LIN54 and RBBP4 (Sadasivam et al. 2012). MuvB complexes, which share an evolutionarily conserved protein core (Sadasivam and DeCaprio 2013), were first identified in *Caenorhabditis elegans* where they controlled vulva development (Harrison et al. 2007, 2006; Ferguson et al. 1987), *Drosophila melanogaster* (Lewis et al. 2004), and later in mammalian cells (Litovchick et al. 2007; Schmit et al. 2007; Pilkinton et al. 2007) and plants (Kobayashi et al. 2015).

Recent work on studying the DREAM complex in depth has helped to uncover and provide a better understanding of the molecular mechanisms controlling the precisely timed expression of specific cell cycle-related genes at a specific stage. The DREAM complex displays two notable characteristic features. First, the DREAM complex can switch functions and exerting opposite effects by associating with different components. Second, it consists of different subunits

that are capable of binding to distinct promoter DNA elements to regulate gene expression.

1.2.4.1 Co-ordinated Cell cycle gene regulation via DREAM complex and associated components

Discovery of DREAM has offered a more detailed understanding of cell-cycle-dependent gene regulation by a coordinated and precisely timed expression of specific G1/S and G2/M cell cycle genes. The MuvB core complex does not change in its composition but it regulates the cell cycle by associating with different protein components at different stages during cell cycle progression. This allows it to switch its function from a transcription repressor in G0 and G1 to an activator in S, G2 and M phases of the cell cycle (Sadasivam et al. 2012).

E2F4,5 and pocket proteins p130/p107 were long known for their role in transcriptional repression via E2F sites (Van Den Heuvel and Dyson 2008). Therefore, DREAM was initially identified as a complex which binds promoters through E2F sites (Litovchick et al. 2007; Schmit et al. 2007; Sadasivam and DeCaprio 2013). The mechanistic characteristic of gene regulation by DREAM is shared with the RB tumour suppressor which also acts through E2F elements by forming similar RB/E2F transcriptional repressor complexes (Fischer and Müller 2017).

DeCaprio and colleagues have shown that in mammalian cells, the MuvB core complex dissociates from p130 and sequentially recruits B-MYB, during S phase to activate late S-phase genes, and FOXM1, in G2 phase, to activate mitotic gene expression (Schmit et al. 2007; Sadasivam et al. 2012; Litovchick et al. 2007). The DREAM complex in addition to the E2F sites is capable of binding to DNA with cell cycle genes homology regions (CHRs) like all other MuvB derived complexes (Figure 1.2) (Schmit et al. 2009; Müller and Engeland 2010; Müller et al. 2012). As the MMB complex does not contain any E2F which would allow its binding to the E2F site, therefore, MMB complex exclusively binds to the CHR promoter element via the LIN54 component of the MMB complex (Müller et al. 2012, 2014; Marceau et al. 2016). Interestingly, the CHR promoter element has emerged as a key site that plays a central role in cancer signalling pathways (Paci et al. 2017). As it is now known that the DREAM complex binds to CHR in

addition to E2F, DREAM therefore, has the potential to regulate a larger set of genes than RB and perform distinct regulatory functions apart from RB/E2F complexes (Müller et al. 2012; Fischer and Müller 2017; Guiley et al. 2015).

It is still not clear if additional direct binding to DNA occurs via B-MYB and FOXM1 when they are present as part of the MMB-FOXM1 complex associated with MuvB. The evolutionarily conserved Myb sites for B-MYB binding and Forkhead binding motifs for FOXM1 binding are not enriched in the proximity of G2/M promoters as opposed to the enriched CHR sites (Müller et al. 2012, 2014). This suggests the absence of any sequence-specific binding of B-MYB and FOXM1 to G2/M gene promoters and hence their inability in activating the genes required for cell cycle progression on their own, without association with MuvB complex. However, it has been demonstrated that FOXM1 is also capable of binding to non-forkhead binding sites in the genome in addition to binding via canonical RYAAAYA forkhead binding motifs (Chen et al. 2013; Sanders et al. 2015). This atypical and nonspecific binding of FOXM1 might help in enhancing the binding of MuvB to the DNA, maybe in a non-canonical way.

Therefore, the repressive DREAM complex which contains both E2F and MuvB can bind to both E2F and CHR elements and repress both G1/S and G2/M genes whereas the activator MMB-FOXM1 complex which only has MuvB and lacks E2F is capable of only binding to CHR sites and hence is only capable of activating G2/M genes. The DREAM complex ensures coordinated and timely downregulation of cell cycle genes during cell cycle exit and growth arrest. MuvB based complexes can switch by associating with different components which turn the MuvB core from a repressor to activator, thereby explaining how MuvB binding to the same DNA elements can switch/alter functions from repression to activation (Engeland 2017; Fischer and Müller 2017).

In addition to binding via single E2F or CHR sites, two other DNA elements i.e. CDE (cell-cycle dependent element) and CLE (CHR-like element) sites are also present to further support the binding of the DREAM complex. CDE and CLE augment the binding of the DREAM complex to DNA. CDE augments the binding of DREAM complex to the CHR sites located within promoters. Similarly, CLE enhances the binding of the DREAM complex to E2F sites. CDE and CLE are

weak binding sites and are not enough for the DREAM complex to bind to these sites alone. Hence, they act in tandem with the main binding sites i.e. CHR and E2F respectively. Also, a spacer of four nucleotide bases is required between E2F and CLE and between CHR and CDE sites (Müller et al. 2016). Binding of DREAM complex to CHR and CLE sites is through LIN54 as LIN54 is the only component of the MuvB complex which can interact with DNA in a sequence-specific manner to regulate G2/M gene expression. Hence, the DREAM complex can bind to promoter DNA by four different modes as shown in Figure 1.2 (Müller et al. 2016).

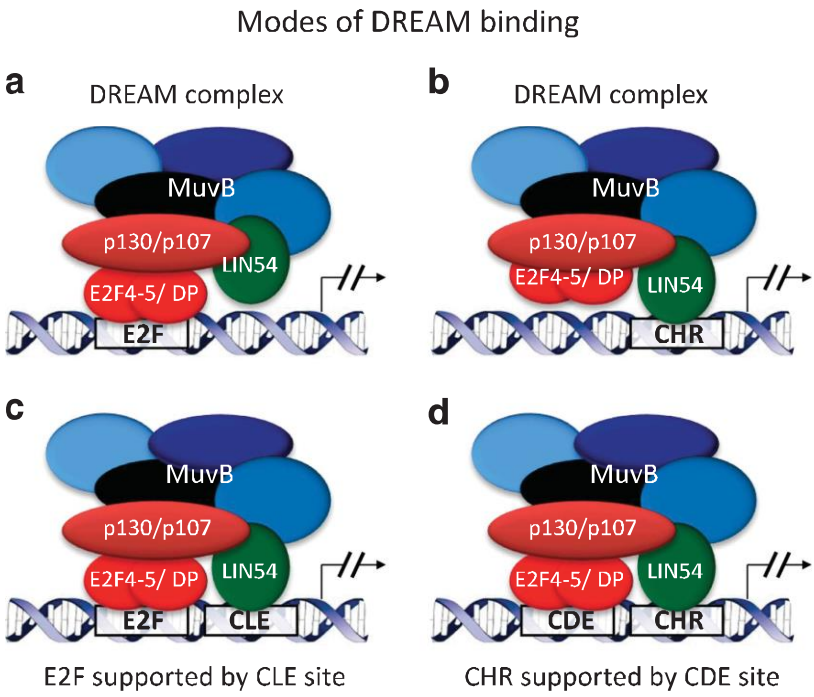

Figure 1.2 Different modes of the DREAM complex binding
The DREAM complex can form two distinct contacts with DNA, namely binding to main elements (a) E2F or (b) CHR by E2F4-5 heterodimers and the LIN54 component of MuvB respectively. The binding to main promoter elements E2F and CHR can be supported by the (c) CLE and (d) CDE sites respectively. CLE and CDE sites are different from E2F and CHR elements and are unable to bind to DREAM on their own. As the MuvB complex binds to DNA via the LIN54 component, therefore, only LIN54 component of MuvB complex is labelled in the diagram. Figure from (Engeland 2017).

One-way progression through the cell cycle is ensured by the timely degradation of specific proteins via ubiquitin-mediated proteasomal degradation (Teixeira and Reed 2013). For example, SCF and APC/C^{Cdh1} have been reported to ubiquitinate B-MYB and FOXM1 respectively to cause their ubiquitin-mediated proteolysis (Charrasse et al. 2000; Laoukili et al. 2008).

After the completion of the cell cycle, the repressive DREAM complex is reformed to promote cell cycle exit or to prevent the entry into the next G1 phase (Figure 1.3). To reform the DREAM complex after completion of the cell cycle it is important to dephosphorylate the pocket proteins phosphorylated by cyclin/CDK complexes. Two enzymes which have been implicated in regulating this dephosphorylation of pocket proteins are PP1 and PP2A (Kolupaeva and Janssens 2013). Interestingly, in a cell, PP1 and PP2A are the most abundant family of serine-threonine phosphatases (Virshup and Shenolikar 2009). Dephosphorylation of pocket proteins p107 and p130 is conducted by PP2A. On the other hand, PP1 is the major phosphatase for dephosphorylating and activating RB (Kolupaeva and Janssens 2013; Kurimchak and Grana 2015). This dephosphorylation promotes the formation of transcriptionally repressive complexes i.e. DREAM and RB-E2F complexes.

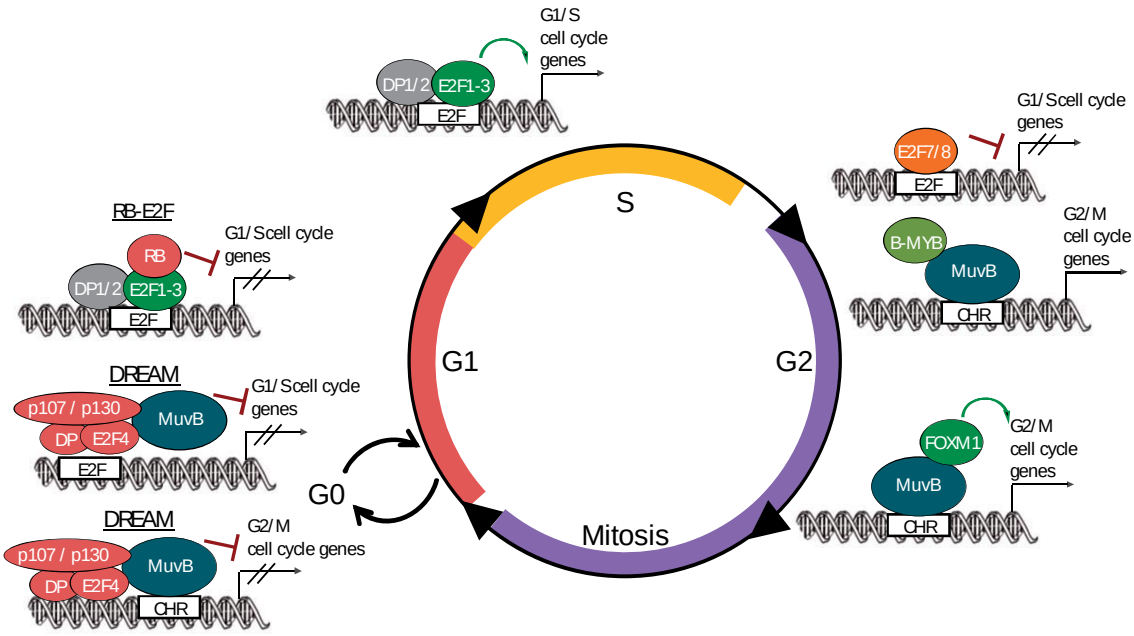

Figure 1.3 Role of the DREAM complex in cell cycle regulation.
Association of MuvB complex (LIN9, LIN37, LIN52, LIN54, and RBBP4) with different factors at different phases in cell cycle regulates gene expression during different stages of cell cycle. In early phases of cell cycle G0/G1 stage, when cells are arrested, MuvB binds to p130/p107, E2F4/DP to form the repressive DREAM complex, which inhibits all cell cycle-dependent gene expression and hence arrests cell growth. When cells exit the G0/G1 stage, transcriptional repression is released as p130 dissociates from MuvB and E2F allowing activator E2Fs (E2F1-3) to activate genes required for progression into S phase. MuvB binds to B-MYB in S phase to regulate late S phase genes. In G2 phase, MuvB-B-MYB complex recruits FOXM1 followed by proteasomal degradation of B-MYB. Active FOXM1 remains bound to MuvB and regulates the expression of genes required in the G2-M transition. Figure from (Fischer and Müller 2017).

Assembly of the DREAM complex also requires phosphorylation of the LIN52 component of MuvB core complex at Serine-28. This phosphorylation is achieved by DYRK1A kinase, an enzyme identified by Litovchick and colleagues (Litovchick et al. 2011). It has been shown by structural analysis that this phosphorylation supports the binding of pocket proteins to LIN52 and the MuvB core complex (Guiley et al. 2015). The kinase LATS2 is known to phosphorylate and activate DYRK1A, eventually leading to gene downregulation and cell cycle arrest mediated by the DREAM complex (Tschöp et al. 2011). Active DYRK1 phosphorylates LIN52-S28 enabling the formation of the DREAM complex and thereby shifting the balance from activating MMB-FOXM1 complex to repressive DREAM complex. Even though the role of the DREAM complex in cellular senescence is not fully understood, Litovchik et al., 2011, have shown that disorganization of DREAM complex leads to suppression of Ras-induced senescence (Litovchick et al. 2011).

1.2.4.2 Cell stress and p53 mediated downregulation of cell cycle-related genes

Initially, the detailed mechanism by which p53 mediates transcriptional repression of a plethora of genes was not evident, however this changed after the availability of genome-wide ChIP data on binding of p53 and the discovery of the mammalian DREAM complex along with its target genes (Litovchick et al. 2007; Schmit et al. 2007). This led to the observation that p53 induction led to the formation of a repressive DREAM complex and therefore the identification of the p53-DREAM pathway (Quaas et al. 2012).

Recently it has been shown that p53 dependent repression is mediated via the p53-p21^{WAF1}-DREAM-E2F/CHR pathway (Figure 1.4). Discovery of this pathway has also led to the identification of a clearer mechanism explaining how p53 downregulates a plethora of genes with p21^{WAF1} being the key mediator. Also, it demonstrates the role played by the p53-DREAM pathway in halting cell cycle progression in response to a number of stress signals including DNA damage as it leads to activation and stabilization of p53 (Horn and Vousden 2007).

The key step in the p53-DREAM pathway is the upregulation of a CDKI i.e. p21^{WAF1}. p21^{WAF1} was the first identified transcriptional target for p53 (El-Deiry et al. 1993). The transcriptional upregulation of p21^{WAF1} following p53 activation

occurs via direct binding of p53 to sites present in the $p21^{WAF1}$ promoter (Quaas et al. 2012). As $p21^{WAF1}$ is a CDKI it blocks phosphorylation of the pRB related pocket proteins, p107 and p130 as well as RB. As described above in the unphosphorylated state p107 and p130 proteins bind to the MuvB core complex promoting the assembly of repressive DREAM complex. Therefore, activation of p53 can shift the equilibrium from the activating MMB-FOXM1 complex to the repressive DREAM complex in a $p21^{WAF1}$ dependent manner (Quaas et al. 2012). During this stage, the DREAM complex shows parallel regulation along with pRB mediated regulation because lack of phosphorylation of pRB leads to the formation of repressive RB/E2F complexes (Dyson 2016).

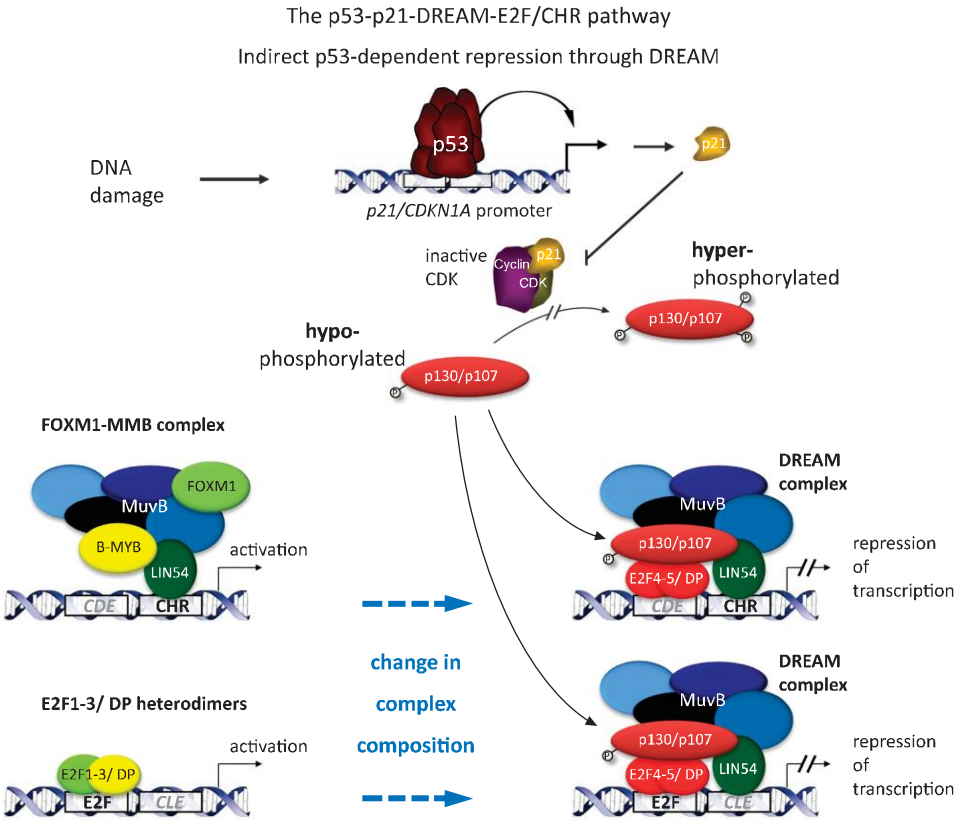

Figure 1.4 Indirect p53-dependent repression via DREAM (p53-DREAM pathway)
Activation of p53 leads to downregulation of a plethora of genes. This regulation mediated by p53 is mostly indirect as p53 does not bind directly to the genes. Instead, p53 directly binds and activates CDKI $p21^{WAF1}$ which leads to hypophosphorylation of p107/p130. Hypophosphorylated p107/p130 promote assembly of repressive DREAM complex. DREAM complex then displaces the activating MMB-FOXM1 and E2F1-3/DP complex from their target promoters. This switch mediated by p53 leads to the indirect downregulation of previously activated genes and hence shifts the equilibrium from activating complexes to the repressive complexes. Only LIN54 component of MuvB is labelled. Figure from (Engeland 2017).

Before p53 dependent downregulation, target genes are activated by two different mechanisms involving both groups of promoter elements. Activator E2F1-3 proteins bind to E2F elements for maximum expression of the genes involved in S phase whereas MMB-FOXM1 complex binds to CHR promoter elements to upregulate the genes expressed in late G2 and M phase of cell cycle. Following activation, E2F or E2F/CLE and CHR or CDE/CHR promoter elements bind to DREAM complex to allow downregulation of the upregulated early and late cell cycle regulating genes respectively (Müller et al. 2016).

A recent study by Kurt Engeland using meta-analyses of genome-wide studies has identified a catalogue of more than 250 high confidence target genes for the p53-DREAM pathway (Engeland 2017). The three pivotal criteria used in the identification of these targets were: downregulated mRNA expression of the target gene following p53 activation, binding of DREAM component to the target gene by ChIP and the presence of E2F or CHR elements in the proximal promoter of the target gene (Engeland 2017).

The data obtained showed that the p53-DREAM pathway regulates a plethora of genes grouped into functional groups. These functional groups control different cellular functions such as DNA repair, telomere maintenance, cell cycle checkpoint control and various other functions. The p53-DREAM pathway controls an entire set of genes important for complete cell functions spanning from start (G1 phase) to the end of the cell cycle (M phase). This implies that p53 controls not just partial but entire function of a cell, employing its master coordinator functions via DREAM complex mediated mainly by $p21^{WAF1}$. Hence, defects in the p53-pathway contribute to loss of checkpoint control not only at the G1/S transition but to all checkpoints up to completion of the cell cycle.

p53 is known to indirectly downregulate expression of many cell cycle associated genes which are required for cell cycle progression. Essentially all the genes are downregulated indirectly by p53 as a study has shown that a very small percentage of genes about 3% that are downregulated by p53 are also bound by p53 (Fischer et al. 2014) Indirect transcriptional repression by p53 via $p21^{WAF1}$ is shown in Figure 1.4. Repression by p53 is largely indirect which involves direct

activation of p21^{WAF1} by p53, followed by formation of different repressive complexes such as RB/E2F and DREAM (Fischer et al. 2014).

Taken together, identification and detailed understanding of the DREAM complex has provided the explanation for the precisely timed regulation of the G2/M cell cycle genes in addition to the well-established regulation of G1/S cell cycle genes by RB mediated repression of E2F TFs. The detailed mechanism of regulation of different TFs involved in the cell cycle is presented below in Figure 1.5.

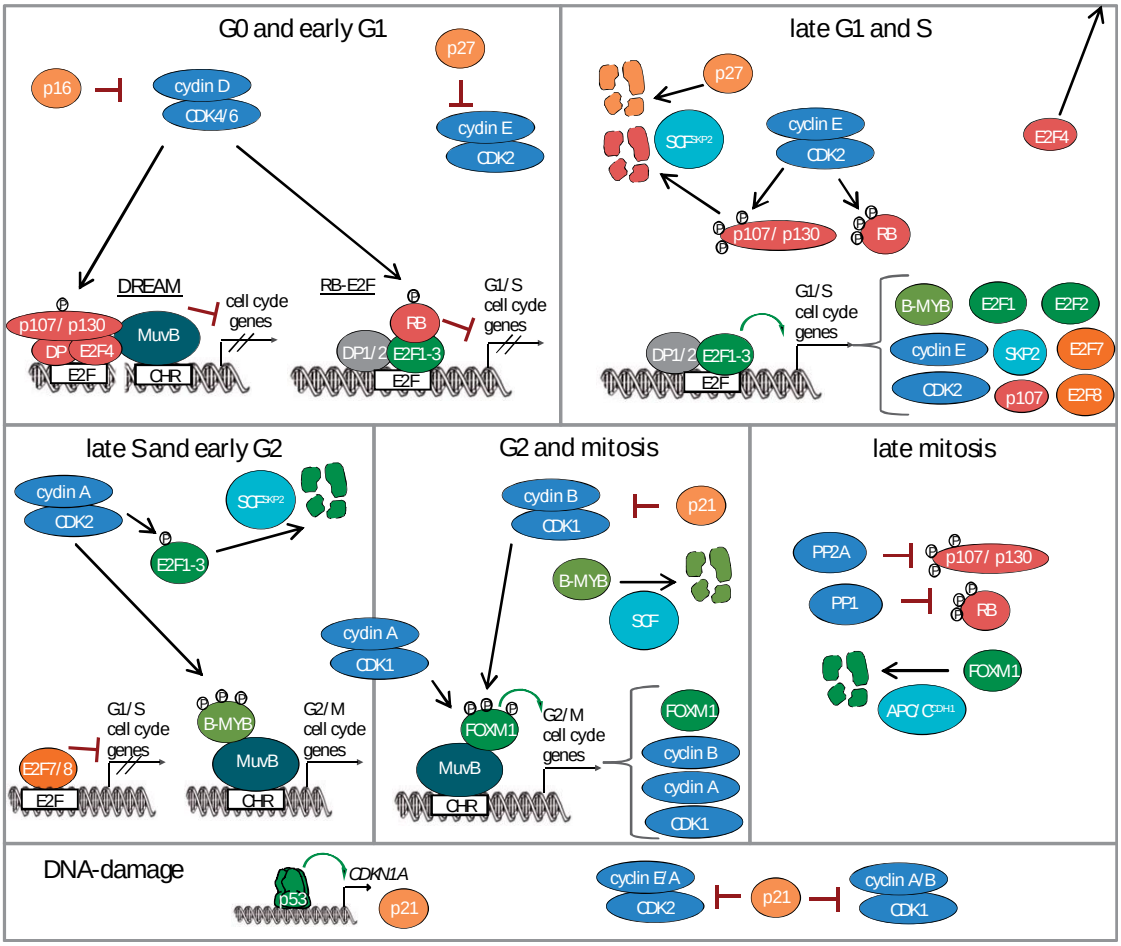

Figure 1.5 Regulation of different Transcription Factors involved in the cell cycle
Diagrammatic representation showing the detailed regulatory mechanisms of different TFs which regulate gene expression of specific genes required during different stages of cell cycle. Figure from (Fischer and Müller 2017).

1.3 Hallmarks of cellular senescence

Mammals contain both mitotic and post-mitotic cells. Only the cells which can divide have the potential to initiate cancer and undergo senescence. Apart from growth arrest, a number of characteristics and molecular markers are used to identify senescent cells. Till date there is no single characteristic marker which is exclusive to senescent cells, nor do all senescent cells display every known senescence marker (Campisi 2013).

1.3.1 Signalling pathways as Hallmarks of senescence

Cellular senescence growth arrest is largely established and maintained by engaging either one or both p53/$p21^{WAF1}$ and $p16^{INK4A}$/pRB tumour suppressor pathways. Both these pathways are complex as they involve many upstream regulators and downstream effectors along with varying side branches (Levine and Oren 2009; Chau and Wang 2003). Both pathways are also interlinked and crosstalk and regulate each other (Yamakoshi et al. 2009; Zhang et al. 2006; Martín-Caballero et al. 2001). These pathways maintain the senescence state mainly by inducing widespread changes in gene expression. p53 and pRB are the key transcriptional regulators. $p21^{WAF1}$ acts downstream of p53 and $p16^{INK4A}$ acts upstream of pRB. They are crucial components of each pathway as they are CDKIs (cyclin-dependent kinase inhibitors) and act as negative regulators of cell cycle progression. Hence, prolonged overexpression of any of the above mentioned four critical components (p53, pRB, $p16^{INK4A}$, $p21^{WAF1}$) is sufficient to induce senescence (McConnell et al. 1998).

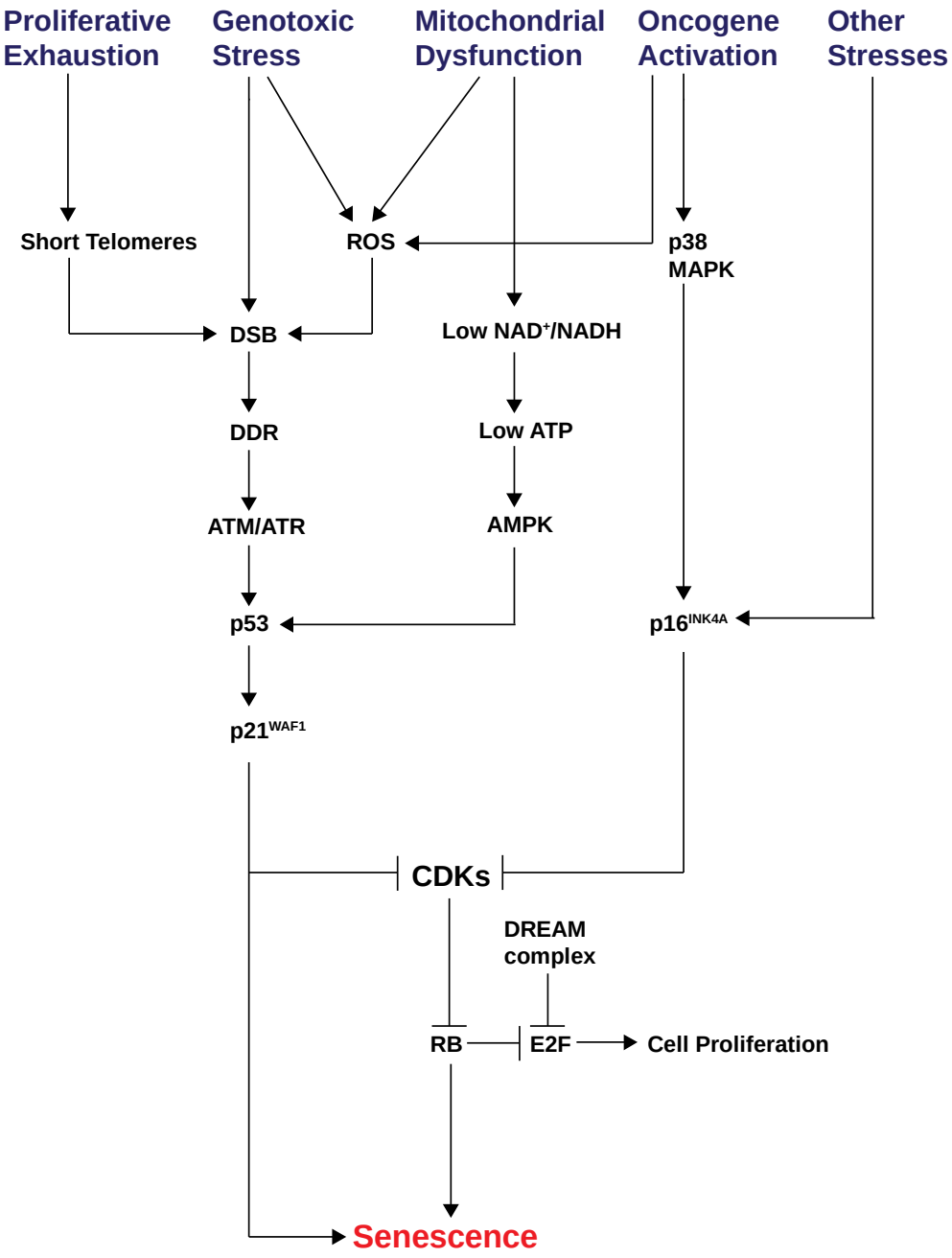

Figure 1.6 Signals and pathways involved in regulating cellular senescence
The figure depicts various intrinsic and extrinsic stimuli that induce senescence. Major pathways involved in manifesting senescence are indicated. It also shows how the two key tumour suppressor pathways are interlinked as well.

1.3.1.1 Cell Cycle Arrest and key effector proteins

Growth arrest which marks the inability of the cell to continue in the cell cycle is obviously a key hallmark of a senescent cell. It is different from another form of growth arrest known as quiescence, in that senescence occurs in G1 and possibly G2 phase of cell cycle (Di Leonardo et al. 1994) as opposed to

quiescence which happens in G0 phase. Also, another crucial difference is that quiescent cells can resume proliferation in response to appropriate signals whereas senescent cells cannot (Campisi and D'Adda Di Fagagna 2007). This is beautifully explained by Blagosklonny's theory of 'hyperfunction' which states that ageing is a quasi-programme, which occurs as a consequence of the continuance of the processes occurring during development and growth in early life (Blagosklonny 2013). For example, during growth arrest, the nutrient sensing pathways like mTOR (mechanistic target of Rapamycin) remains active but now as opposed to cell proliferation and growth, it initiates cellular senescence. Therefore, the choice between senescence and quiescence is governed by the mTOR pathway. Cells with persistent activation of mTOR undergo a stable senescent growth arrest, whereas cells in which mTOR is inhibited, undergo a reversible quiescence growth arrest (Blagosklonny 2012; Korotchkina et al. 2010). Apoptosis is defined as a phenomenon of programmed cell death in which the remains of a dead apoptotic cell are removed by engulfment by another cell, whereas in senescence, the senescent cell is not immediately eliminated and remains metabolically active.

Senescent cells show significant changes in gene expression. These changes in gene expression include changes in the expression of genes like cell cycle inhibitors (CDKI) (Shelton et al. 1999). CDKs regulate cell cycle progression by phosphorylating different proteins. Two key cell cycle inhibitors that are expressed by senescent cells are the cyclin-dependent kinase inhibitors $p21^{WAF1}$ and $p16^{INK4A}$. Both of these CDKI are key components of the two major tumour suppressor pathways in mammalian cells: which are p53 and pRB pathways respectively (Campisi 2001).

As mentioned before the general block of proliferation is a key feature of a senescent cell. Exit from cell cycle can be demonstrated using colony-formation assays which gives a direct measure of the proliferation potential of the cells or by BrdU/EdU-incorporation assays that measures the DNA synthesis rate. Although, this is not very accurate as there could be DNA repair mediated synthesis still occurring. Measuring the expression levels of CDKIs $p16^{INK4A}$ and $p21^{WAF1}$ are also key in detecting cell cycle arrest. Despite this, growth-arrest is

not a specific unique marker for senescent cells especially because of the inability and impracticality to measure it in vivo and in post-mitotic cells.

Senescent cells in order to maintain their growth arrested state are known to repress the expression of genes required for cell cycle progression (Pang and Chen 1994). Repression of some of these genes is due to the inactivation of transcription factor E2F by pRB by forming the transcriptionally repressive RB-E2F complex. In some senescent cells, senescence associated heterochromatin foci formation by pRB dependent reorganization of chromatin leads to silencing of the E2F target genes (Narita et al. 2003).

1.3.1.1.1 p53

Nuclear phosphoprotein p53 was identified as a protein that formed an oligomeric complex with T antigen of simian virus 40 (SV40) and ironically was initially thought to be an oncoprotein (Lane and Crawford 1979; Linzer and Levine 1979).

p53 is a member of a unique protein family which includes proteins p63 and p73.The members of this family are structurally related to each other and they can homo-oligomerize and bind to DNA. Although structurally related the members of the family perform different functions; p53 acts as a key tumour suppressor protein whereas p63 and p73 are mainly involved in organismal development (Irwin and Kaelin 2001a, 2001b). p53 is one of the most studied proteins. This is not surprising because of the multitude of cellular functions it performs such as a key tumour suppressor protein, maintains genome integrity, plays role in apoptosis, metabolic regulation, development and DNA repair to name a few. Hence, p53 is famously known as a ‘guardian of the genome’ (Lane 1992; Kastenhuber and Lowe 2017).

In line with the key role of p53 in tumour suppression as well as in maintaining genome integrity, p53 is known to act as a key regulator in cellular senescence, via several different mechanisms. Activation of p53 is dependent on various post translational modifications such as phosphorylation, methylation, acetylation, sumoylation, ubiquitination and neddylation (Kruse and Gu 2009). Interestingly, a study by Katherine Webley and colleagues studied different phosphorylated states of p53 by using antibodies with phosphorylation sensitive epitopes in

senescent fibroblasts (Webley et al. 2000). Distinct post translational modifications were demonstrated upon comparing phosphorylation of amino acid residues present in both amino and carboxy terminals of p53 during replicative senescence and DNA damage induced senescence. Increased Ser-15 phosphorylation resulting in p53 stabilization was found to be the only common change in both types of senescence studied in this study (Webley et al. 2000).

1.3.1.1.2 $p21^{WAF1}$

$p21^{WAF1}$ is a 21 kDa CDKI protein which is one of the members of the Cip/Kip family of CDKI in addition to p27 and p57. It is encoded by the CDKN1A gene. $p21^{WAF1}$ is capable of inactivating all different CDKs, thereby inhibiting cell cycle progression. This role was discovered when Harper and colleagues noticed a 21kDa protein interacting with and inhibiting different cyclin dependent kinase proteins in their immunoprecipitation experiments (Wade Harper et al. 1993). $p21^{WAF1}$ inhibits the kinase activity of cyclin-CDK complexes by interacting with cyclins through two copies of cyclin binding motifs present in p21 (Cy1 and Cy2). This inhibits binding of cyclin/CDK complexes to the RB family of proteins which eventually inhibits their phosphorylation and subsequent release of E2Fs and hence induces $p21^{WAF1}$ mediated cell cycle arrest (Chen et al. 1996). As $p21^{WAF1}$ is known to interact with and inactivate various cyclin/CDK complexes, it is capable of inducing cell cycle arrest at any stage of cell cycle as opposed to INK4A family of CDKI which specifically bind and inactivate CDK4 and CDK6, hence can induce cell cycle arrest only during G0/G1 phase (Wade Harper et al. 1993; Pavletich 1999; Sherr 2000).

$p21^{WAF1}$ has been shown to be consistently upregulated during senescence response induced by different stimuli (Noda et al. 1994; Hernandez-Segura et al. 2017). During DNA damage $p21^{WAF1}$ expression is mainly upregulated by direct transactivation by p53; additionally, p53 can also activate $p21^{WAF1}$ in response to Ras activation (Macleod et al. 1995). Furthermore, $p21^{WAF1}$ can be upregulated independently of p53 by various other stimulators such as by different nuclear receptors including androgen receptors, vitamin D receptors and retinoid receptors. Also members of the Krüppel-like factor (KLF) TF family can cause

activation of *CDKN1A* gene by cooperating with p300-CREBBP (Abbas and Dutta 2009).

In addition to the transcriptional control of $p21^{WAF1}$ by p53 dependent and independent mechanisms, $p21^{WAF1}$ is also controlled at the post translational level. As $p21^{WAF1}$ is an unstable protein, newly synthesized $p21^{WAF1}$ is stabilized by WISp39, a Hsp90 binding tetratricopeptide repeat, which stabilises $p21^{WAF1}$ by preventing its proteasomal mediated degradation (Jascur et al. 2005). Also, additional post-translational modification such as phosphorylation of $p21^{WAF1}$ can modulate the binding partners of $p21^{WAF1}$ or change the subcellular location of $p21^{WAF1}$, which ultimately has the potential to alter $p21^{WAF1}$ function blocking its ability to act as a CDKI (Child and Mann 2006). For example, $p21^{WAF1}$, when present inside the nucleus, inhibits cell cycle progression, whereas after phosphorylation it gets transported to the cytoplasm where it functions as anti-apoptotic (Ping et al. 2006). Therefore, $p21^{WAF1}$ plays multiple different functional roles within the cell by regulating different processes (Georgakilas et al. 2017; Karimian et al. 2016).

1.3.1.1.3 $p16^{INK4A}$

Replicative senescence is also linked to the derepression of the CDKN2A locus which encodes two key tumour suppressor proteins namely $p16^{INK4A}$ and $p14^{ARF}$. $p14^{ARF}$ regulates the stability of p53 by binding and inhibiting MDM2 activity which is responsible for proteasomal-mediated degradation of p53 (Kim and Sharpless 2006; Gil and Peters 2006). In young tissues, the CDKN2A locus is normally expressed at a very low undetectable level whereas it becomes derepressed leading to its high-level expression during ageing (Krishnamurthy et al. 2004). The molecular mechanisms underlying this derepression are not completely understood but to a large extent the derepression has been associated with loss of polycomb group of proteins and is independent of p53 (Jacobs et al. 1999; Bracken et al. 2007).

$p16^{INK4A}$ is a 16 kDa protein that directly binds to CDK4/6 and blocks the formation of cyclinD-CDK4/6 complex, thereby preventing phosphorylation of RB and promoting repression of E2F target genes (Serrano et al. 1993). $p16^{INK4A}$ is frequently used as a specific and unique marker for senescence as its expression

in most normal, untransformed cells and tissues is low or undetectable as opposed to accumulated high levels of $p16^{INK4A}$ after senescence induction by various stimuli (Hara et al. 1996; Wiley et al. 2017).

Transcriptional activation of $p16^{INK4A}$ has also been extensively used to report senescence in vivo (Demaria et al. 2014; Burd et al. 2013). The expression of $p16^{INK4A}$ is also a functional marker of ageing as it has been reported to increase in several vertebrate tissues with age (Baker et al. 2016; Waaijer et al. 2012; Krishnamurthy et al. 2004; Liu et al. 2009). Loss of the $p16^{INK4A}$ gene or inherited mutations in the $p16^{INK4A}$ gene have been related to several cancers particularly melanoma (Li et al. 2011a). The inducers of $p16^{INK4A}$ are mostly related to the epigenetic changes.

1.3.1.2 The DNA Damage Response (DDR)

The DDR is a classical, evolutionarily conserved, robust response that is activated in cells with DNA damage such as single-stranded and double-stranded breaks. Cells are able to deal with DNA damage, but if the damage is irreparable, in order to prevent the duplication and passing of damaged DNA to the daughter cells, cells must undergo either apoptosis or senescence. Initially, it was not clear how a cell decides to choose between apoptosis and senescence but now it has been suggested that prominent short-term DNA damage activates apoptosis whereas prolonged mild DNA damage induces cellular senescence (Petrova et al. 2016). Therefore, it is suggested that persistent DDR signalling leads to cellular senescence.

Classical DDR mainly involves the $p53/p21^{WAF1}$ tumour suppressor pathway. Multiple different DNA damage sensors such as replication protein A (RPA) (Zou and Elledge 2003) and the RAD9-RAD1-HUS1 (9-1-1) (Weiss et al. 2002) complex detect exposed single-stranded breaks and MRE11-RAD50-NBS1 (MRN) (Stracker et al. 2004; Moreno-Herrero et al. 2005) complex detect DNA double-stranded breaks and recruit the upstream protein kinases ataxia telangiectasia mutated (ATM) and ataxia telangiectasia and RAD3-related (ATR) to the site of damage (D'Adda Di Fagagna 2008). Although both ATM and ATR are activated upon DNA damage, they are known to have distinct DNA specificities such as: ATM gets activated predominantly by DSBs whereas ATR

in addition to double strand breaks responds to a broad spectrum of DNA damage such as genotoxic stress caused by DNA replication stress initiated by oncogenes (Maréchal and Zou 2013). Once at the site of damage ATM and ATR further phosphorylate and amplify the DDR signal by phosphorylating other DNA damage mediator proteins, such as phosphorylation of histone H2AX to form γ-H2AX which aids in the assembly of other specific DNA repair complexes, forming nuclear foci that are stable sites of dynamic accumulation of different DDR proteins (Lukas et al. 2003). Dynamic changes in histone modification such as histone methylation are also critical for regulating DNA double-strand break (DSB) repair by activating ATM kinase (Ayrapetov et al. 2014). This process of activation of ATM kinase also contributes to the formation of transient repressive chromatin structures which serve to stabilize the damaged chromatin and promote assembly of DSB-signalling proteins (Ayrapetov et al. 2014).

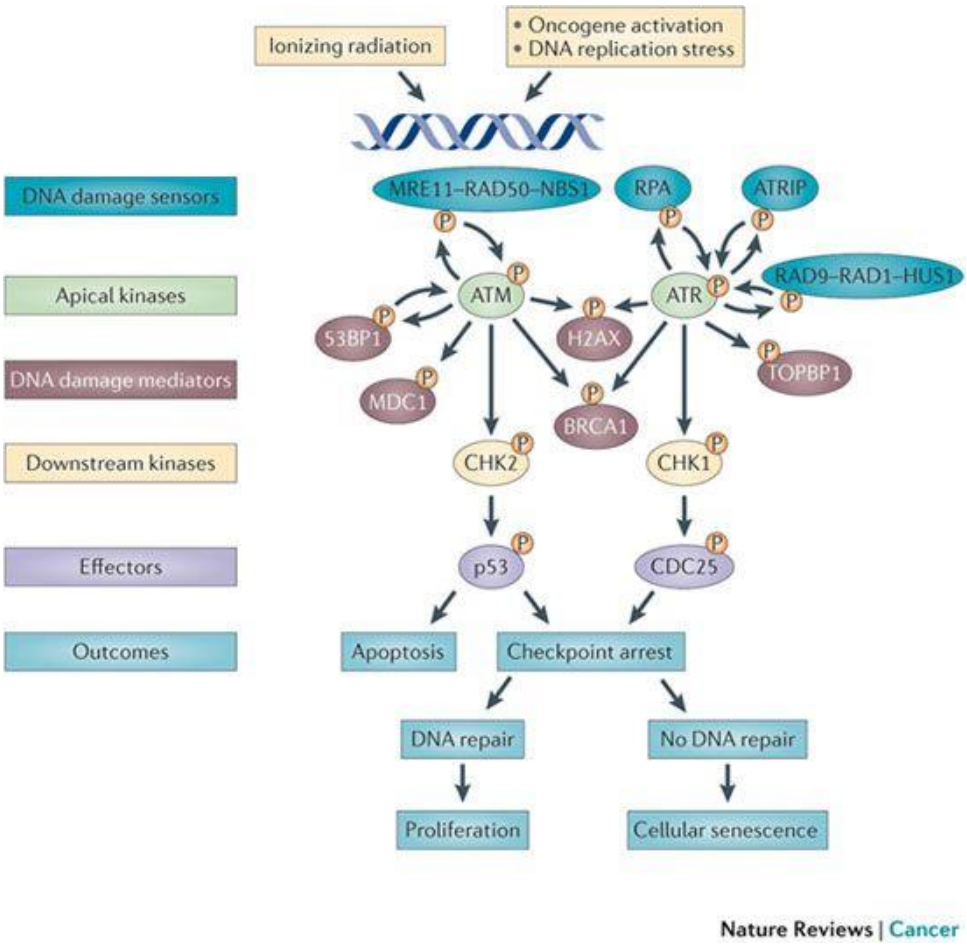

Figure 1.7 The DNA Damage Response (DDR) Signalling Pathway
Diagrammatic representation of the DDR signalling pathway showing the key DNA damage sensors, different kinases involved and the effector molecules. Figure from (Sulli et al. 2012).

Other downstream diffusible kinases which act far from the site of DNA damage such as CHK1 and CHK2 propagate the damage signal by further phosphorylating the final effector substrates like p53. Phosphorylation of p53 on Serine-20 by CHK2 leads to a reduction in binding affinity of E3 ubiquitin-protein ligase MDM2 to p53, leading to an increase in p53 level. p53 is also phosphorylated at Serine-15 directly by ATM (Chehab et al. 1999). CHK1 negatively regulates CDC25, a dual-specificity protein phosphatase which usually promotes G2 to M transition, by phosphorylating Serine-216 leading to G2 growth arrest (Peng 1997) Figure 1.7. Eventually, the phosphorylated p53 activates and upregulates the expression of its transcription target $p21^{WAF1}$ which is a potent universal CDKI and therefore an inhibitor of cell cycle resulting in cell cycle arrest (Sulli et al. 2012).

As most of the senescence-inducing signals eventually impinge on DNA directly or indirectly, persistent DDR signalling is a characteristic feature of many senescent cells. The DDR signalling pathway has associated features like DNA damage foci which can be detected by immunostaining of γ-H2AX; telomere-dysfunction induced foci (TIF) (Herbig et al. 2006) and DNA segments with chromatin alterations reinforcing senescence (DNA-SCARS) (Rodier et al. 2011). These, or phosphorylated p53, can be used as markers for cellular senescence. The challenge relies on the fact that DDR can also be activated by other DNA-damaging stimuli which do not lead to the senescent state. Furthermore, not all forms of senescence are manifested via DDR (Salama et al. 2014).

1.3.1.3 The Senescence-Associated Secretory Phenotype (SASP)

It has been known for a while that senescent cells affect their microenvironment by secreting a number of factors into the vicinity, which affect the behaviour of nearby non-senescent cells (Aravinthan 2015). The SASP, therefore, is considered as a crucial feature of many senescent cells. It is hypothesized that DNA damage is an essential driver of the SASP. The SASP is expressed by cells in which senescence was caused by genomic damage or epigenomic perturbation leading to prolonged DDR (Campisi 2013). Normal cells in which senescence is induced by ectopically expressing $p21^{WAF1}$ or $p16^{INK4A}$, do not

express SASP despite displaying other characteristic senescence markers (Coppé et al. 2011). On the other hand, cells that undergo senescence because of DNA damage, dysfunctional telomeres, epigenomic perturbation, mitogenic proliferative signals, oxidative stress or other senescence-inducing stimuli are known to develop SASP to different extents (Rodier et al. 2009; Pazolli et al. 2012; Coppé et al. 2010b; Acosta et al. 2008; Kuilman et al. 2008). Similarly, induction of senescence by mitochondrial dysfunction presents a distinct secretory phenotype (Wiley et al. 2016).

The main components of SASP include a plethora of soluble signalling factors, for example, inflammatory cytokines, chemokines, growth factors and matrix metalloproteinases (MMPs) (Coppé et al. 2010a). IL-6 and IL-8 are two main SASP components. These factors have been shown to play both positive and negative roles in various biological processes such as tissue repair, wound healing and tumour progression (Demaria et al. 2014; Coppé et al. 2010a). The SASP plays a key role in mediating the pathophysiological activity of senescent cells. Hence, SASP factors have been suggested to have deleterious as well as beneficial effects (Rodier and Campisi 2011).

SASP factors control a multitude of functions by playing a role in enhancing immune surveillance, tissue repair and remodelling and have also been shown to promote reorganization of embryonic structures during developmental stages (Demaria et al. 2014; Adams 2009). On the contrary, chronic presence of some of the tissue remodelling and pro-inflammatory SASP factors like interleukins and MMPs have been shown to play a role in ageing phenotypes and disease states (Coppé et al. 2010a). The beneficial or deleterious effect of the SASP depends on the physiological context.

SASP factors can exert their effects in both autocrine and paracrine fashion. Factors like IL-1α and IL-6 act in a cell-autonomous manner to reinforce the senescent state whereas many other SASP factors act by exerting non-cell-autonomous function, enabling alteration in the behaviour of neighbouring cells (Acosta et al. 2008, 2013). SASP members can be secreted into the extracellular environment by different methods. Many members are produced as soluble proteins which can be directly secreted, whereas some are initially expressed as

transmembrane proteins that require ectodomain shedding for secretion (Stow and Murray 2013). Sheddase enzymes like ADAM17 have been reported to be upregulated in OIS and cancer and are responsible for regulating the ectodomain shedding of many cell membrane-bound SASP factors (Morancho et al. 2015; Effenberger et al. 2014). Additionally, to enable more distal functions, such as enhancing cancer cell proliferation, some SASP members are secreted in small exosome-like extracellular vesicles (Takasugi et al. 2017).

Triggers activating the SASP are not completely understood but to a large extent have been shown to be related to DDR initiated NF-κB activation that mainly induces expression of inflammatory cytokines (Ohanna et al. 2011). Studies have also demonstrated the involvement of the mTOR pathway in regulating the SASP at the post-transcriptional level (Laberge et al. 2015; Herranz et al. 2015; Bent et al. 2016). Recent findings have indicated dynamic signalling by NOTCH1, a cell surface receptor, as a crucial regulator of SASP composition (Hoare et al. 2016; Ito et al. 2017).

Interestingly last year three different studies collectively implicated the essential role of yet another pathway, called cyclic GMP–AMP synthase linked to stimulator of interferon genes (cGAS-STING) in mediating SASP and thereby regulating cellular senescence (Dou et al. 2017; Yang et al. 2017; Glück et al. 2017). As described later in section 1.3.2.3, nuclear integrity is compromised during senescence due to loss of the nuclear lamina protein, LaminB1, which leads to the unusual presence of cytoplasmic chromatin fragments (CCFs) in the cytoplasm. The functional relevance of CCFs in the cytoplasm is not clear, but the discovery of the cGAS-STING pathway has shown that it promotes SASP in primary human cells and in mice and has been shown to play a role in tumour suppression due to immune-mediated clearance of premalignant cells (Dou et al. 2017; Umbreit and Pellman 2017).

cGAS is a 522 amino acid protein which is a cytosolic DNA sensor that activates innate immunity on sensing aberrant double stranded (ds) DNA molecules and responds equally to microbial as well as endogenous ligands. After activation by binding to CCFs present in cytoplasm, cGAS in the presence of ATP and GTP catalyses production of the second messenger molecule 2’3’ cyclic GMP-AMP

(cGAMP), which recruits STING thereby activating NF-κB which will lead to production of pro-inflammatory molecules (Diner et al. 2013; Ablasser et al. 2013; Zhang et al. 2013; Gao et al. 2013; Ablasser and Gulen 2016; Chen et al. 2016). Hence, the two key downstream pathways which function after activation of cGAS-STING involve activation of interferon and NF-κB (Barber 2015; Glück et al. 2017).

Results obtained from the study by Yang et al., 2017, have demonstrated that cGAS is localised in the cytoplasm of non-proliferating cells whereas it enters the nucleus and accumulates on chromatin DNA during mitosis in proliferating cells (Yang et al. 2017). This explains the diffuse pattern obtained for cGAS in proliferating cells as opposed to the consolidated sharp, bright puncta which colocalized with CCFs in senescent cells in the study conducted by Dou and colleagues (Dou et al. 2017). Further studies have reported the engagement of the cGAS-STING pathway both in vitro and in vivo where cellular senescence was induced by different stimuli (Glück et al. 2017; Yang et al. 2017). Loss of cGAS compromised senescence in different in vivo models and also accelerated the spontaneous immortalisation of mouse embryonic fibroblasts thereby highlighting the importance of cGAS in regulating SASP and senescence (Glück et al. 2017; Yang et al. 2017). Identification of the cGAS-STING pathway provides new insights that nuclear genomic DNA not only acts as a stable nuclear entity that encodes genetic information but also serves to act as a 'danger-signal' to alarm the immune system by inducing the proinflammatory SASP pathway and the interferon response. This suggests that this pathway might have evolved for fighting infectious DNA in the cytoplasm. Findings till now suggest that the function of the SASP might be to help the damaged senescent cell communicate with neighbouring cells about their compromised state and initiate tissue repair, if feasible, or to stimulate their immune clearance by the immune system (Campisi 2013; Iannello et al. 2013).

The nature of the SASP is nonspecific and immensely heterogeneous which can be regulated at multiple different levels. Difficulty in the identification of a general regulatory mechanism restricts the use of SASP as an unequivocal marker for senescence (Hernandez-Segura et al. 2017; Coppé et al. 2010a). However, the

advantage in studying the composition of SASP is that it can be helpful in defining different senescence programs and its context (Lecot et al. 2016). For example, the presence of growth factors like VEGF and PDGF-A and different MMPs indicate the involvement of senescent cells in wound healing and tissue repair (Demaria et al. 2014; Jun and Lau 2011) whereas, therapy-induced or age-related senescent cells are mainly associated with secretion of inflammatory factors (Demaria et al. 2017; Baker et al. 2016).

1.3.1.4 Resistance to Apoptosis

It is seen that many cells that undergo senescence acquire resistance to apoptotic signals (Ryu et al. 2007; Marcotte et al. 2004; Sanders et al. 2013; Hampel et al. 2004). Since senescent cells are resistant to apoptosis, it may explain why senescent cells keep on accumulating with age. It is still not completely clear as to what decides whether a cell will undergo apoptosis or senescence. Cell type, nature and intensity of the stress and damage are expected to play a role in this decision. Most cells can undergo both senescence and apoptosis and both of these pathways communicate with each other and can be regulated by p53 (Seluanov et al. 2001). The mechanisms by which senescent cells resist apoptosis are not very well understood. For some cells this might be due to changes in proteins governing apoptosis (Marcotte et al. 2004; Murata et al. 2006) whereas for others, it might be due to preferential activation of genes related to senescence growth arrest and by suppression of genes which activate apoptosis by p53 (Jackson and Pereira-Smith 2006).

It has been reported by various studies that senescent cells are resistant to apoptosis and anti-apoptotic BCL2 has been shown to play a crucial role in this observed resistance to apoptosis. Findings from the study by Ryu et al., 2007, confirm that failure to downregulate BCL2 in senescent HDFs is responsible for resistance to apoptosis (Ryu et al. 2007). Sanders et al., 2013, explored the epigenetic mechanisms involved in conferring resistance to apoptosis in senescent HDFs. ChIP experiments demonstrated significant enhancement of antiapoptotic BCL2 gene, upon H4K16 acetylation and depletion of H4K20 methylation. Active transcription of BCL2 in senescent HDFs contribute to apoptosis resistance (Sanders et al. 2013). Antiapoptotic members of the BCL2

family such as BCL-XL and BCL-W are upregulated through a combination of increased transcription and cap-independent translation in senescent cells, allowing them to survive by resisting apoptosis. This study clearly showed specific induction of apoptosis in senescent cells after inhibition of BCL-W and BCL-XL by siRNA or small molecule inhibitor ABT737 (Yosef et al. 2016).

The CDKI $p21^{WAF1}$ maintains the viability of senescent cells under persistent DNA damage by protecting them from cell death by restraining caspase and JNK signalling pathways (Yosef et al. 2017). HSP90 aids in the survival of senescent cells by stabilization of factors such as Protein Kinase B (AKT) (Fuhrmann-Stroissnigg et al. 2017). Consistent with established resistance to apoptosis of senescent cells, transcript analysis showed increased expression of multiple different pro-survival factors in senescent cells making them resistant to apoptosis (Zhu et al. 2015; Childs et al. 2014). Hence the resistance to apoptosis can be the cause of accumulation of senescent cells and their retention in tissues with ageing.

1.3.1.5 Metabolism

A number of studies have reported notable changes in cell metabolism in OIS which includes changes in glucose, lipid, nucleotide and mitochondrial metabolism (Aird and Zhang 2014). As the changes observed in cell metabolism during OIS are mostly opposite to the changes observed in tumorigenesis, this indicates the involvement of these pathways in the tumour suppressive role of OIS (Aird and Zhang 2014). Additionally, to identify novel non-invasive biomarkers, a study by James et al., 2015, has analysed the extracellular senescence metabolomes generated from fibroblasts rendered senescent by proliferative exhaustion and irradiation induced DNA double-strand breaks. Interestingly the ECM found in these senescent cells was also found to be accumulated in a variety of pathological states such as ageing, inflammation, neoplasia and fibrosis (James et al. 2015). Furthermore, a recent study by Wu et al., 2017, used a combination of metabolomics and proteomics to show distinct metabolic profiles for chemotherapy-induced senescent cells and apoptotic cells (Wu et al. 2017).

The observed metabolic changes are regulated by p53 and pRB (Wiley et al. 2016; Takebayashi et al. 2015; Nicolay and Dyson 2013). mTOR activation and mitochondrial dysfunction are also capable of inducing metabolic changes (Correia-Melo et al. 2016). As described previously in 1.1.2.4, mitochondrial dysfunction can manifest senescence by activating AMPK which leads to an increase in NAD+, therefore contributing to metabolic changes observed in senescence (Wiley et al. 2016).

Even though changes in metabolism have the potential to be exploited as a marker for senescence, challenges which exist are first, alterations in metabolism can occur as a consequence or cause of other hallmarks of senescence (Wiley and Campisi 2016). Secondly, only a few studies have considered the whole metabolome of senescent cells, which is very important (Kim et al. 2011b; Wu et al. 2017). Furthermore, in depth characterization may help to identify specific metabolites as markers for cellular senescence.

1.3.1.6 Endoplasmic Reticulum (ER) Stress

ER stress caused by different stimuli such as mutations, oxidative stress, lack of chaperones and infections can lead to perturbations in the critical functions of ER such as regulating protein synthesis, assembly, folding and transport, leading to accumulation of misfolded proteins and proteotoxicity. The unfolded protein response (UPR) is a coordinated system of transcriptional and translational control that is activated by ER to deal with ER stress. UPR is associated with enlargement of ER, reduced protein synthesis and secretion of misfolded proteins (Pluquet et al. 2015).

The UPR involves at least three ER membrane resident proteins, namely: pancreatic ER kinase-like ER kinase (PERK), inositol-requiring enzyme 1 alpha (IRE1α) and activating transcription factor 6 alpha (ATF6α) (Pluquet et al. 2015). Binding immunoglobulin protein (BiP) is known to bind to PERK, IRE1α and ATF6α of UPR and inhibit their function. Upon ER stress, as a consequence of UPR, BiP binds to the misfolded and unfolded proteins releasing its binding with PERK, IRE1α and ATF6α (Wang and Kaufman 2014). As BiP plays a key role in the UPR upon ER stress, this suggests a possible role of BiP in

senescence. It was shown by Gulow et al., 2002, that the translational efficiency of BiP is markedly increased upon UPR activation (Gülow et al. 2002).

Data from a study conducted by Druelle et al., 2016, provided the first evidence of the involvement of the ATF6α arm of UPR in response to ER stress in the induction of senescence in normal human dermal fibroblasts (NHDF) (Druelle et al. 2016). By genetically inactivating the three UPR sensors in NHDF, it was demonstrated that the ATF6α arm plays a crucial role in regulating the common morphological changes related to the senescent phenotype such as cell enlargement, cell shape, increase in SA-β gal activity and ER expansion (Druelle et al. 2016). Hence, it can be stated that UPR may control the establishment of some of the senescence markers. A recent study regarding the ATF6α arm of UPR was shown to mediate replicative senescence in normal human dermal fibroblasts via upregulation of the COX2/Prostaglandin E2 intracrine pathway (Cormenier et al. 2018). ER stress-related senescence has also recently been shown to play a role in the pathology of Osteoarthritis chondrocytes (Liu et al. 2017).

Expansion of ER during cellular senescence could also be a consequence of the increased demand for protein synthesis, maturation and secretion for production of SASP. Hence, increased protein secretory activity caused by activation of the SASP leads to pressure on the ER-resident protein folding system, resulting in increased amounts of unfolded protein species, which as a consequence activate the UPR.

To better characterize the molecular and functional connections between UPR and senescence and to identify universal markers, further research is required into monitoring ER stress in senescence as it is not a common practice in the senescence field. Only a few studies have monitored the role of ER stress in senescence, by using RT-qPCR of different downstream genes (Chen et al. 2015).

1.3.2 Morphological alterations as Hallmarks of senescence

1.3.2.1 Cell Size and Shape

One of the most characteristic features of senescent cells in vitro is the enlarged and irregular cell shape. Results obtained from a recent study by Bent et al., 2016, have implicated the activation of PI3K /AKT/mTOR signalling in enlarged endothelial senescent cells (Bent et al. 2016). mTORC1 is a key mediator of the PI3K /AKT/mTOR, which is known to integrate different stress stimuli and modulate cell growth (Lloyd 2013). mTORC1 activation occurs upon senescence induction by a variety of stimuli (Blagosklonny 2012).

One of the contributors to the senescence-associated changes in cell shape is the overproduction of vimentin, an intermediate filament protein (Nishio et al. 2001). Quantitative and structural changes in vimentin are particularly found in different types of senescent cells and aged tissues (Hwang et al. 2009). The ATF6α arm of UPR described above also controls the changes in cell shape upon senescence in addition to enlargement of ER. These changes in cell shape are linked to remodelling of the intermediate filament protein vimentin, thereby showing that the observed changes related to increased vimentin expression are partly under the control of ATF6α arm of UPR (Druelle et al. 2016).

Even though it is easy to detect a change in cell size and shape by regular bright-field microscopy, additionally, targeting cytoplasmic proteins such as vimentin or actin using immunofluorescence can also be used to assess changes in cell shape. The challenge here lies in detection and quantification of change in cell size and shape in vivo within an organism.

1.3.2.2 Increased Lysosomal Content

Increased lysosomal content and upregulation of many lysosomal proteins is a key feature of the senescent state. Enhanced lysosome biogenesis or accumulation of old lysosomes could be the reason behind increased lysosomal content observed during senescence. The lack of lysosomal removal leading to accumulation of lysosomes and hence the enhanced lysosomal content is supported by the presence of residual bodies called lipofuscins which consist of lipid-containing residues from lysosomal digestion (Georgakopoulou et al. 2013).

To detect the enhanced lysosomal content, the most commonly and widely used senescent cell marker is measuring the activity of lysosomal enzyme β galactosidase at a suboptimal pH of 6.0, designated as senescence-associated (SA)-β galactosidase (Kurz et al. 2000; Dimri et al. 1995). Surprisingly, the mechanism behind the overexpression of SA-βgal in the senescent state remains to be fully explored. Only recently, a study by Hoare et al., 2016 has shown that the NOTCH1 pathway negatively regulates GLB1, the gene encoding SA-βgalactosidase enzyme at the transcriptional level (Hoare et al. 2016). Even though SA-β gal staining is arguably the most common marker used for senescence, the challenge relies in its use in live cells and paraffin-embedded tissue, limiting its application only to fresh samples.

Sudan Black B (SBB) can be used as an alternative marker to detect accumulation of lysosomes as it selectively binds to lipofuscins. SBB has the added advantage that it can be used for paraffin embedded tissue sections unlike SA-β gal (Georgakopoulou et al. 2013). Very recently a lipophilic biotin-linked SBB-inspired analogue GL13 was designed and synthesized that allowed sensitive and specific, antibody enhanced detection of senescent cells containing lipofuscin in a wide variety of biological specimens (Evangelou et al. 2017).

However, increased lysosomal activity is not a very specific senescence marker; the constitutive expression of SA-β gal activity has been observed in non-senescent cells suggesting that it is not a marker exclusive to the senescent state, nonetheless the most commonly used (Kopp et al. 2007). Even more importantly it suggested that senescence was not only an artefact of in vitro culture but also occurred in the organism. As it also increases with age, so acts as an ageing marker.

1.3.2.3 Nuclear Changes

Senescent cells, along with morphological changes in cell size and shape, also present characteristic changes in their nucleus such as an enlarged nucleus, mostly irregular shaped nuclei and chromatin reorganization. Loss of a structural protein of the nuclear lamina, LaminB1, is a widespread marker used for detection of different types of senescence (Hernandez-Segura et al. 2017;

Sadaie et al. 2013). This decline in LaminB1 leads to other nuclear changes such as extrusion of fragments of chromatin from the nucleus to cytoplasm called CCFs, arising due to the unselective permeability of nuclear envelope (Adams et al. 2013).

The decline in LaminB1 is regulated at the mRNA level due to the reduced LaminB1 mRNA stability rather than caspase-mediated degradation observed in apoptosis (Freund et al. 2012). Furthermore, a study by Dreesen et al., 2013, has reported the involvement of miR-23a, which is upregulated in senescence. This targets LaminB1 and reduces its expression (Dreesen et al. 2013). Expression of LaminB1 is downregulated by the p53 and pRB pathways and does not depend on other senescence associated pathways such as p38 MAPK, DDR, ROS and NF-κB (Freund et al. 2012).

Chromatin reorganization because of senescence induction can also lead to the formation of SAHFs, which are heterochromatin domains densely stained by DAPI and rich in HP1γ and H3K9me3 of DNA. These appear possibly to silence pro-proliferative genes like E2Fs (Narita et al. 2003). However, SAHFs cannot be used as a universal marker for senescence as they can be detected only in vitro and are mainly observed during OIS.

1.3.2.4 The composition of the Plasma Membrane

The plasma membrane of eukaryotic cells allows cells to communicate with the extracellular space via regulation of signal transduction pathways and with neighbouring cells. A number of studies have reported one consistent change in the plasma membrane composition of senescent cells i.e. upregulated expression of caveolin-1, an integral structural plasma membrane protein that binds tightly to cholesterol (Park et al. 2000; Volonte et al. 2002; Cho et al. 2003, 2004). Caveolin-1 has been shown to be responsible for altering the morphology and adherent properties of senescent cells (Cho et al. 2004; Inomata et al. 2006).

Direct interaction of caveolin-1 with signalling molecules in the MAPK pathway possibly explains the role of caveolin-1 in promoting cellular senescence (Ohno-Iwashita et al. 2010). Additionally, findings from the study by Volonte et al., 2015, indicate that the main mechanism through which overexpression of caveolin-1

promotes stress-induced premature senescence is via increased p53 activity (Volonte et al. 2015). This increased p53 activity is achieved by downregulating silent information regulator 2 homologue 1 (SIRT1), activating ATM and inhibiting MDM2 (Volonte et al. 2015).

Apart from caveolin-1, other plasma membrane proteins have also been reported to show altered expression during senescence. Althubiti et al., 2014, identified 107 plasma membrane-associated proteins by a proteomics screen, that were preferentially expressed in senescent cells (Althubiti et al. 2014). The authors also developed a simple and specific flow cytometry-based staining protocol for two of them, namely density-enhanced phosphatase-1 (DEP-1) and Beta-2 Microglobulin (B2MG), for rapid detection of senescent cells in culture (Althubiti et al. 2014).

Another very recent study observed the specific expression of an oxidized form of vimentin in the plasma membrane of senescent primary human fibroblasts. As oxidized vimentin is secreted, it has the potential to be used as a vital and non-invasive biomarker for studying senescence (Frescas et al. 2017). Remarkably, mass spectrometric analysis conducted by Kim et al., 2017, revealed yet another cell membrane-associated protein i.e. dipeptidyl peptidase 4 (DPP4) selectively expressed on senescent cells and not on proliferative human diploid fibroblasts (Kim et al. 2017). Differential expression of DPP4 allows FACS mediated sorting of senescent cells using anti-DPP4 antibody. Furthermore, antibody-dependent cell-mediated cytotoxicity (ADCC) assays can also be used for therapeutic intervention in conditions where it is desirable to eliminate senescent cells, making it a promising target (Kim et al. 2017).

Multiple different studies have indicated the immense potential for development of a plasma membrane based novel marker that will allow specific identification of senescent cells. Use of this strategy, provides the added advantage of allowing the sorting of senescent cells by targeting specific cell membrane-associated proteins.

1.3.2.5 Accumulation of Dysfunctional Mitochondria

Many studies have shown close links between mitochondrial dysfunction and its role in driving and maintaining senescence (Passos et al. 2007; Correia-Melo et al. 2016; Wiley et al. 2016). Senescent cells have an increased mitochondrial mass in replicative as well as oncogene-induced senescence and other stress-induced senescence (Passos et al. 2007; Moiseeva et al. 2009; Passos et al. 2010; Tai et al. 2017). The membrane potential of these accumulated mitochondria is reduced which leads to release of mitochondrial enzymes such as endonuclease G, and enhanced ROS production, showing that the mitochondria that accumulate during senescence are dysfunctional (Studencka and Schaber 2017; Passos et al. 2007).

Mitophagy is a selective process which predominantly maintains mitochondrial turnover by specifically targeting dysfunctional mitochondria to lysosomes for hydrolytic degradation by autophagic sequestration (Kim et al. 2007). The accumulation of old and dysfunctional mitochondria mainly occurs due to reduced mitophagy in senescent cells which is observed both in vitro and in vivo (Dalle Pezze et al. 2014; García-Prat et al. 2016). As mitophagy is a selective autophagy for mitochondria, the specificity is achieved by dedicated proteins such as Parkin and PINK1 which target mitochondria with reduced membrane potential for degradation by tagging them with polyubiquitin chains (Deas et al. 2011). Increased cytoplasmic p53 during cellular senescence has been reported to bind to Parkin and inhibit its translocation to dysfunctional mitochondria (Hoshino et al. 2013; Ahmad et al. 2015). This provides an explanation for the decline in mitophagy and therefore, accumulation of dysfunctional mitochondria in senescence.

Further research by Dalle Pezze et al., 2014, suggested increased mTOR-dependent mitochondrial biogenesis and decreased mitochondrial fission during reduced mitophagy to be the potential driving force behind the accumulation of mitochondria during senescence (Dalle Pezze et al. 2014). This study showed that mitophagy only affected new mitochondria but not old ones thereby providing an explanation for the accumulation of dysfunctional mitochondria possibly due

to the impairment in mitochondrial turnover together with increased mitochondrial biogenesis (Dalle Pezze et al. 2014).

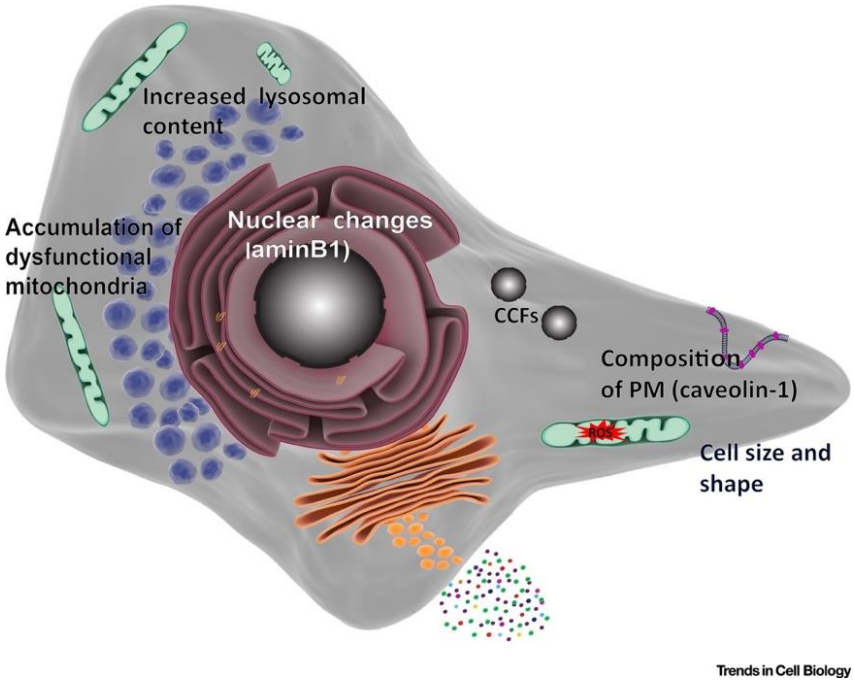

Figure 1.8 Morphological alterations as Hallmarks of senescence
This figure depicts the morphological changes that occur during cellular senescence arising as a consequence of different molecular pathways involved in senescence. Figure from (Hernandez-Segura et al. 2018).

1.4 Significance of senescence

Why did senescence originate in the first place?

Recently it has been shown that senescence can be a normal programmed event which occurs during mouse development. Storer et al., 2013, found that senescence-associated β-galactosidase positive cells were present at two signalling centres in embryonic patterning, namely, the apical ectodermal ridge and the neural roof plate (Storer et al. 2013). These senescent cells displayed features similar to oncogene-induced senescence. Munoz-Espin et al., 2013, discovered that senescence occurs at multiple locations including the mesonephros and the endolymphatic sac of the inner ear during mammalian embryonic development (Muñoz-Espín et al. 2013). It was also shown that senescence was strictly dependent only on $p21^{WAF1}$ and independent of DNA damage as cells were found to be negative for the DDR protein γH2AX, p53 or other cell cycle inhibitors. Another very recent study by Davaapil et al., 2017, has demonstrated cellular senescence to play an intrinsic part in amphibian development, uncovering conserved and new roles of senescence in vertebrate organogenesis (Davaapil et al. 2017). Overall, these studies suggested that senescence is a programmed mechanism during embryonic development and might also be the evolutionary origin of damage-induced senescence (Davaapil et al. 2017; Storer et al. 2013; Muñoz-Espín et al. 2013).

It can be hypothesized that senescence was later co-opted during the reproductive age as it provides the beneficial effect of tumour suppression. As senescence is a form of growth arrest, this inhibition of cellular proliferation can then be beneficial as it prevents tumour formation in early life. Cellular senescence-related phenotypes can be both beneficial and deleterious, depending on the age of the organism (Campisi 2003). Senescence can be deleterious in the later part of life as it blocks tissue repair and renewal, promoting age-related phenotypes including tumorigenesis (Campisi 2005). This paradox of contrasting roles of senescence is a very good example of an important evolutionary theory of ageing called ‘Antagonistic Pleiotropy’ which states that pleiotropic traits with beneficial early effects would be favoured by natural

selection even if these genes had deleterious at later age (Kirkwood and Austad 2000; Williams 1957).

1.4.1 Senescence in vivo

Since Hayflick's discovery about senescence using cultured cells, most of what has been known about senescence has largely come from cell culture studies. There is now enough evidence to show that senescence is important and occurs in vivo (Jeyapalan et al. 2007). With the help of a number of recently discovered senescence markers described above, it has been possible to identify senescent cells in vivo.

In addition to the senescent cells detected during development stages, senescent cells have also been found in vivo in many renewable tissues like epithelia, stroma, haematopoietic system and vasculature of humans, primates and rodents (Dimri et al. 1995; Krishnamurthy et al. 2004). Additionally, a study by Demaria et al., 2014, has provided another example of the functional relevance of senescent cells in vivo (Demaria et al. 2014). This study demonstrated the role of senescent endothelial and fibroblast cells in accelerating the closure of cutaneous wound by secreting PDGF-AA at the wound site, and inducing differentiation of myofibroblasts (Demaria et al. 2014).

An increase in the frequency of senescent cells is also observed in normal and premature ageing skin of primates (Herbig et al. 2006). It has been found that cells which express multiple senescence markers accumulate with age (Campisi and D'Adda Di Fagagna 2007). Importantly, senescence has now also been reported to play a role in regeneration in salamanders (Yun 2015; Yun et al. 2015). This has provided new insights as it demonstrates that unlike mammals where the regenerative capacity deteriorates with age, in species such as salamander it remains intact which allows them to undergo multiple rounds of regeneration during their lifespan. Surprisingly, during salamander limb regeneration, the unexpected presence of a large number of senescent cells is observed. Although, by the time the limb had regrown, these senescent cells had disappeared by effective and rapid senescent cell clearance which was found to be mainly mediated by macrophages. Due to this effective and rapid clearance of senescent cells, the number of senescent cells does not increase upon ageing

in salamander as opposed to the observed increase of senescent cells in mammals (Yun et al. 2015). This suggests the potential use of effective surveillance of senescent cells in boosting the ability to recover from injuries as well as in anti-ageing therapies.

1.4.2 Senescence and Cancer

The Bright Side: The novel and crucial role of senescence growth arrest which has been established until now is that senescence plays a significant role in tumour suppression, preventing the organism from developing cancer (Prieur and Peeper 2008; Collado and Serrano 2010). There are many examples of studies which have demonstrated the role played by senescence in tumour suppression in the presence of an oncogene or during the loss of a tumour suppressor protein to prevent uncontrolled neoplastic growth (Salama et al. 2014; Muñoz-Espín and Serrano 2014).

One such key example is presence of multiple links between genetics of melanoma and cellular senescence such as the CDKN2A gene, the commonest known high penetrance melanoma susceptibility gene which as described previously encodes two key effectors of senescence i.e. $p16^{INK4A}$ and $p14^{ARF}$. The presence of large number of senescent melanocytes that express multiple different senescence markers in cutaneous benign nevi also shows the role played by senescent cells in tumours. Therefore, evasion of cellular senescence is crucial to generation of metastatic cutaneous melanoma (Bennett 2016).

It is also known that some of the SASP components under certain circumstances help in establishing the tumour suppressive growth arrest of senescent cells. For example, IL-6, IL-8, IGFBP7 and GROα help establish oncogene-induced senescence caused by oncogenes like RAS and BRAF (Kuilman et al. 2008; Wajapeyee et al. 2008; Yang et al. 2006; Campisi 2013). If senescence is bypassed by disruption of tumour suppressor pathways, cells undergo crisis, which occurs when cells continue to divide with short telomeres. During crisis, the fusion of chromosomes stimulates mitotic arrest leading to mitotic telomere de-protection and cell death which eventually eliminates precancerous cells from the population (Hayashi et al. 2015). Hence, two barriers namely replicative senescence and crisis block tumour formation.

The Dark Side: There is increasing evidence that senescent cells can drive hyperplastic pathology and therefore can stimulate cancer progression. Several components of SASP are incriminated in tumour progression, like VEGF, which promotes tumour cell driven angiogenesis, and MMP3 which enhances tumour cell invasion and metastases by degradation of the extracellular matrix, thereby, the basement membrane (Coppé et al. 2006; Liu and Hornsby 2007). Furthermore, SASP constituents can also induce the malignant phenotype in cell culture studies, the key phenotype being epithelial to mesenchymal transition (Laberge et al. 2012). This morphological transition allows transformed epithelial cells to intrude and migrate via tissues and promote metastasis by secretion of SASP components like IL-6 and IL-8 (Coppé et al. 2008; Parrinello 2005). SASP is also capable of causing inflammation by releasing inflammatory cytokines that induce infiltration of leucocytes, thereby generating reactive toxic species which have the potential to cause DNA damage and hence initiate cancer (Freund et al. 2010).

1.4.3 Senescence and Ageing

Hayflick for the first time interpreted senescence to be related to ageing at the cellular level and possibly at the organismal level in humans, after noticing the presence of an inverse correlation between the proliferative potential of isolated cells and the age of the donor (Hayflick 1965; Hayflick and Moorhead 1961). It is now well established that senescent cells promote organismal ageing. As described above, senescent cells are resistant to apoptosis, which leads to accumulation of senescent cells with age (Marcotte et al. 2004; Hampel et al. 2005; Wang et al. 2009a). It is also seen that cells expressing more than one senescence markers are comparatively rare in young organisms and their number keeps on increasing with age (Campisi and D'Adda Di Fagagna 2007).

This accumulation of senescent cells can promote age-related pathologies by three possible ways. First, senescent growth arrest can attenuate stem/progenitor cell reserves which can cause functional decline as a result of reduced tissue repair, regeneration and normal replenishment of cells (Drummond-Barbosa 2008; Aravinthan 2015). Second, factors secreted by senescent cells into their microenvironment affect crucial processes like

angiogenesis, differentiation, migration, tissue architecture and cell growth. This inappropriate presence can lead to disruption of tissue structure and function (Rodier and Campisi 2011). Third, SASP comprises several potent inflammatory cytokines (Freund et al. 2010). If not all, most of the age-related pathologies stem from low-level, chronic inflammation, a theory described as 'inflammaging' (Franceschi and Campisi 2014; Franceschi et al. 2007; Chung et al. 2009). The inflammatory oxidative damage caused by SASP components creates an inflammatory microenvironment which stimulates onset and progression of different age-related disorders including cancer (Lecot et al. 2016; Allavena et al. 2008; Grivennikov et al. 2010).

Furthermore, different epigenomic changes associated with senescence, such as changes in the chromatin state and transcriptional networks, can lead to altered gene expression with age and contribute to the age-associated decline (Booth and Brunet 2016). The number of studies reporting the involvement of senescence in multiple different age-related disorders such as osteoarthritis, atherosclerosis, obesity, hair-greying, macular degeneration and sarcopenia is constantly increasing (He and Sharpless 2017; Campisi 2013; De Keizer 2017).

One of the most fundamental questions about the role of senescence in ageing is that of whether the removal of senescent cells has the potential to increase the lifespan? This is demonstrated very well by experiments conducted by Baker and colleagues (Baker et al. 2011). A transgenic progeroid BUBR1-mouse model was used in these experiments in which senescent cells, mainly $p16^{INK4A}$ positive cells, could be eliminated by administration of a drug (AP20187). This was based on a transgenic strategy wherein a novel transgene INK-ATTAC was designed for inducible elimination of $p16^{INK4A}$ positive cells. The removal of $p16^{INK4A}$ senescent cells in the premature ageing mouse model protected them from several age-related pathologies consisting of cataracts in the eye, sarcopenia in skeletal muscle and loss of subcutaneous fat from adipose tissue, thereby extending the healthspan (Baker et al. 2011). In a more recent study using the same transgene experiments performed in a wild-type non-progeroid mice, Baker et al., 2016, demonstrated that naturally occurring $p16^{INK4A}$ cells are also involved in the age-related deterioration of multiple organs including eye, kidney,

heart and progression of neoplasia (Baker et al. 2016). These experiments suggest the possibility of therapeutic removal of senescent cells in preventing or delaying dysfunction and extending healthy lifespan.

As described above in section 1.3.2.3, senescent cells present characteristic nuclear changes with compromised nuclear lamina integrity. Recently, a premature ageing disease called Hutchinson-Gilford Progeria Syndrome (HGPS) has been found to be caused by mutations in the LMNA gene. In HGPS, aberrant splicing of the LMNA gene leads to accumulation of a mutant Lamin A protein called progerin which interestingly is also produced in senescent cells, suggesting the accumulation of progerin to be a factor in physiological ageing (Gonzalo et al. 2017).

1.5 Model of Study

Cellular senescence is mainly studied by the serial cultivation of primary cells. One of the key stumbling blocks in studying senescence in vitro is the heterogeneous nature of cells growing in a culture. This heterogeneous behaviour occurs because, in a culture, cells tend to senesce asynchronously because of the genetic, epigenetic and phenotypic variations between cells. In such heterogeneous cultures, there can be senescent cells in early passages and proliferating cells towards later passages. Such a state can mask small changes in gene expression when comparing actively proliferating cells against senescent cells. Study with human cells is further complicated by genetic, epigenetic and proliferative variation between different donors as well as phenotypic differences between cells within cultures. To simplify this process many investigators study stress or irradiation or oncogene-induced senescence due to the expression of activated oncogenes such as K-RasV12, Raf or BRAFV600E, where it occurs prematurely and can be induced acutely in a variety of cell types (Collado et al. 2007).

To overcome the above-mentioned barriers, a unique conditionally immortalised Human Mammary Fibroblasts (HMF) cell model has been used in this study in which the cells in a culture can all be made to senesce synchronously. This cell line was immortalised by retrovirally introducing hTERT, the catalytic subunit of

telomerase (Vaziri and Benchimol 1998; Bodnar et al. 1998) and a temperature sensitive (ts) non-DNA binding mutant of SV40 LT antigen (U19tsA58) into early passage primary adult interlobular mammary fibroblasts, as either hTERT or SV40 LT antigen alone were not sufficient to immortalise these cells (Counter et al. 1998; Kiyono et al. 1998). Following this, four different cell lines were created (HMF 3A, B, C, D) depending on the discrete order and timing of transduction of the two components. It was found that the order and timing of introduction of tsLT antigen and hTERT subunit did not affect the generation of immortalised cell line, but it affected the genomic stability. Out of the four, HMF3A, was selected, where both genes were introduced at early passage with transduction of tsLT antigen first followed by hTERT subunit. HMF3A was identified to be the most like 'normal' cells in terms of phenotypic stability, temperature sensitivity and showed no transformation for more than 300 population doublings post-explantation (O'Hare et al. 2001; Hardy et al. 2005).

The beauty of the model arises from the use of a temperature-sensitive variant of the SV40LT antigen. The SV40LT antigen is known to bind and inactivate the activity of several proteins including p53 and RB that are known to be important in establishing and maintaining the senescent state (Ali and DeCaprio 2001). The reason why p53 is activated upon T antigen inactivation in CL3 cells is because T antigen is no longer active and thus it is not there to inactivate p53. This remarkable conditionally immortalised HMF3A cell line is stringently temperature sensitive. They are immortal when grown at a permissive temperature of 33°C - 34°C, as tsSV40LT antigen is active leading to inactivation of p53 and RB and hence senescence cannot occur. On the other hand, when cells are shifted to a higher non-permissive temperature of 38°C - 39.5°C, the tsSV40LT thermolabile antigen is inactivated, allowing the p53/$p21^{WAF1}$ and $p16^{INK4A}$/pRB pathways to act and hence stable cellular senescence occurs synchronously within seven days (Rovillain et al. 2011). The growth of these cells is entirely dependent on the tsLT antigen's activity to bind and inhibit p53 and pRB activity as telomerase remains constitutively active both at the permissive and non-permissive temperatures.

As these cells are now capable of inducing senescence synchronously in culture, making conditionally immortalised HMF3A an appropriate model for dissecting the pathways underlying cellular senescence, by investigating the ability of target genes to complement the growth of these cells under non-permissive conditions. Another reason why this conditionally immortalised HMF3A system represents a potential system for addressing the aims of this thesis, is due to the fact that the transcriptional changes that occur upon the conditional HMF3A growth arrest directly correlate with the transcriptional changes that occurred upon replicative senescence in normal human mammary fibroblasts (Hardy et al. 2005).

This HMF3A model was further refined by Drs Louise Mansfield and Emily Rovillain by engineering the HMF3A cells to express a full length murine ecotropic retroviral receptor to facilitate efficient retroviral infection. Introduction of the murine ecotropic receptor provided the advantage of increased transduction efficiency along with increased safety as ecotropic viruses unlike amphotropic viruses are incapable of infecting human cells. After the introduction of the murine ecotropic receptor, 24 single cell clones were selected to create a refined clonal model to produce a consistent and homogeneous population as opposed to studying senescence bypass in the mixed population of HMF3A^{EcoR} cells. After growing the 24 clones, 6 fast growing clones were selected for further analysis and compared to the mixed cell population of parental HMF3A^{EcoR} in terms of growth rates, irreversibility, infectibility with retroviruses and temperature dependent growth. Even though all 6 clones exhibited temperature-dependent growth, Clone 3 (CL3^{EcoR}) cells most closely mirrored the parental cells in their temperature dependent growth characteristics. They undergo stable growth arrest within seven days at the high non-permissive temperature of 38°C which is essentially irreversible, express SA-β- galactosidase, the most common and widely used marker for senescence and exhibit the same changes in morphology as mixed population of parental cell line HMF3A^{EcoR} (Rovillain et al. 2011). Hence, CL3^{EcoR} cells were validated to be a representative of the mixed population of parental HMF3A^{EcoR} cells.

Furthermore, CL3^{EcoR} cells demonstrated similar results like HMF3A^{EcoR} wherein the growth arrest was predominantly dependent upon p53/p21^{WAF1} pathway

since it is most efficiently abrogated when it is inactivated. While inactivation of the $p16^{INK4A}$/pRB pathway also prevented growth arrest, it was much less efficient and occur in a much smaller number of cells compared to when p53-$p21^{WAF1}$ was inactivated. This support the possibility of both pathways acting in parallel and pRB does not necessarily always act downstream of p53 to induce senescence. Microarray expression profiling studies were conducted on these $CL3^{EcoR}$ cells (Rovillain et al. 2011).

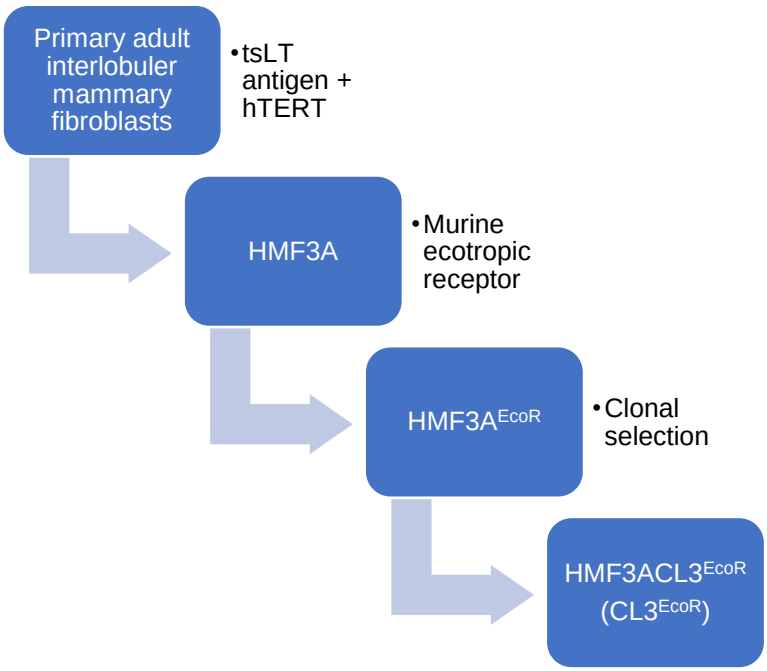

Figure 1.9 Generation of the $CL3^{EcoR}$ cells.
This figure describes the stepwise engineering of the conditionally immortalised human mammary fibroblasts $CL3^{EcoR}$ cells used in this thesis, from the human breast primary fibroblasts. The clonal selection was conducted to produce a homogeneous cell population.

1.6 Project aims

The aim of this project was to prioritize and identify TFs from the previously identified differentially expressed genes when $CL3^{EcoR}$ cells undergo senescence and investigate their functional role in cellular senescence of $CL3^{EcoR}$ cells. It is known that mechanisms underlying senescence growth arrest primarily involve $p53/p21^{WAF1}$ and $p16^{INK4A}$/pRB tumour suppressor pathways (Adams 2009), but it is not known what makes the growth arrest stable; what the critical targets are; and what downstream transcription factors are involved, as they are likely to be the key for the establishment and maintenance of the senescent state. Hence, the main aim of this thesis was to identify transcription factors that act downstream of the $p53/p21^{WAF1}$ and $p16^{INK4A}$/pRB pathways to regulate senescence growth arrest. To achieve this goal, I will:

- Prioritize and shortlist the differential TFs from the previous microarray study conducted in the lab in $CL3^{EcoR}$ cells.
- Prepare expression constructs for the prioritized TFs.
- Determine if silencing the expression of up-regulated TFs individually bypasses senescence.
- Determine if ectopic expression of down-regulated TFs individually bypasses senescence.
- Determine if reconstituting the active DREAM associated complex i.e. (MMB-FOXM1) bypasses senescence.
- Identify the critical components of the MMB-FOXM1 complex that play a crucial role in bypassing cellular senescence.
- Identify if there is a cocktail of TFs that when used in conjunction will synergize to bypass senescence efficiently.

Chapter 2 Materials and Methods

2.1 Mammalian cell culture

All the cell culture experiments were performed in a designated Class II biosafety cabinet within a containment level II laboratory following aseptic techniques to ensure sterility.

Cell lines used for the study:

- HMF3ACL3^{EcoR} (CL3^{EcoR}) cells were used to study bypass of senescence.
- HEK 293T cells were used to prepare lentiviruses for transducing CL3^{EcoR} cells.

Culture medium used: High glucose, pyruvate Dulbecco's Modified Eagle Medium from Life Technologies, Gibco® supplemented with 10% volume per volume (v/v) heat-inactivated Foetal Calf Serum (FCS), 100 units/ml Penicillin, 100 µg/ml Streptomycin and 2 millimolar L-Glutamine.

2.2 Maintaining the Cell Lines

CL3^{EcoR}: Cells were passaged at a stage when they were close to confluency, using 1 ml 1X Trypsin-EDTA solution (0.05%) per flask to detach adherent cells. Medium was removed, and the cells were washed with sterile phosphate buffered saline (PBS) without calcium and magnesium. This was done to remove traces of culture medium as it contains FCS which is known to inhibit trypsin activity. Trypsin was left on cells for one minute at 33°C, following which the cells were tapped to detach them from the flask. The flasks were then checked for complete detachment of cells under a microscope. The cells were resuspended in complete DMEM and centrifuged at 1000 rpm for three minutes. The cell pellet was then re-suspended in fresh medium.

If a specific number of cells were to be seeded, 13 µl sample of the suspension was added on to C-chip disposable haemocytometer from NanoEntek for counting. The appropriate volume of cell suspension (according to split ratio or cell number) was transferred to the required number of flasks and culture medium was added to make up the volume to 15 ml for T-75 and 7 ml for T-25.

$CL3^{EcoR}$ cells were maintained in T-75 flasks at 33°C at 5% CO_2, with 1:5 passaging twice a week (normally Monday and Thursday).

HEK293T: HEK293T cells were obtained from ATCC and grown in 10 cm culture dishes at 37°C at 5% CO_2. They were passaged at 1:5 on Mondays and Wednesday and at 1:6 on Fridays after checking for confluency. When re-suspending HEK293T, cells had to be vigorously pipetted to break up cell clumps to ensure that cells grew as a monolayer.

The experiments were all done at almost the same passage level, by repeatedly going back to frozen stocks.

2.3 Freezing cells

To keep stocks of the cell lines to be used for experiments, they were stored in liquid nitrogen. Cells when close to confluence were trypsinized, resuspended in medium and centrifuged at 1000 rpm for three minutes to remove trypsin. The cell pellet was then resuspended in Freezing Medium which comprised FCS supplemented culture medium with 10% DMSO (dimethyl sulfoxide). 1 ml aliquots of cells in freezing medium were then transferred to labelled cryovials. Cryovials were stored overnight at -80°C in several layers of tissue or in a freezing container to gradually decrease the temperature and prevent cells from the sudden shock of a very low temperature. Cryovials were then transferred to liquid nitrogen the next day.

2.4 Reviving cells from Liquid Nitrogen

Cells were thawed rapidly at 37°C in a water bath and added to 9 ml of complete medium and centrifuged at 1000 rpm for three minutes. The medium was aspirated quickly to remove DMSO which is toxic to cells at warm temperatures. The cell pellet was then gently resuspended in a required volume of fresh medium and plated in T25 flasks/10 cm dishes and incubated at the appropriate temperature and 5% CO_2. When the cells reached sub-confluence, they were then passaged as described above.

2.5 Packaging of Lentiviral Constructs

Lentiviruses were used to stably transduce $CL3^{EcoR}$ cells. The ORF's (Open Reading Frame) for each gene of interest was inserted into either pLX301 or pLEX-MCS lentiviral vectors by recombinational cloning or by DNA manipulation. shRNAmiRs for upregulated TFs were inserted into the pGIPZ lentiviral vector Figure 2.1. Lentiviral stocks were prepared in HEK293T cells using the following protocol:

Day 1: HEK293T cells were seeded by splitting a nearly confluent plate at a ratio of 1:5 and incubating the cells in complete DMEM overnight at 37°C.

Day 2: Transfection was carried out by preparing a mix consisting of 1.5 µg of lentiviral vector DNA, 1 µg of lentiviral Gag/Pol expression vector and 1 µg of VSV-G viral envelope expression vector pMDG.2 (UCL RNAi silencing consortium) in a total volume of 15 µl (made up with Tris: EDTA buffer, TE at pH 8.0). In a separate microcentrifuge tube, 200 µl of reduced serum Opti-MEM (Life Technologies, Gibco®) medium was added. To this tube 10 µl of FuGENE 6-Transfection Reagent (Promega) was added to the centre of the tube and mixed by flicking. 15 µl of prepared transfection mix was added to the Opti-MEM/FuGENE mix. This final mix was flicked to mix all the contents and allowed to stand for 15 minutes at room temperature. Meanwhile, the medium on the HEK293T cells was replenished with fresh medium very gently along the sides of the dish to prevent detachment as HEK293T cells detach rapidly. After 15 minutes the Opti-MEM/DNA/FuGENE mix was added dropwise to HEK293T cells and swirled gently and incubated overnight at 37°C and 5% CO_2 / 20% O_2.

Day 3: The medium was changed to high serum medium i.e. DMEM containing 15% FCS in the morning.

Day 4: To harvest Round 1 lentivirus, the supernatant was collected in a 10 ml syringe and filtered through a 0.45-micron filter into a fresh tube and frozen immediately at -80°C, if the infections were not done with the fresh lentivirus the same day. 10 ml high serum medium was again added gently to the cells and incubated at 37°C overnight.

Day 5: Round 2 viruses were collected the same way as described above and aliquots stored immediately at -80°C until required.

A.

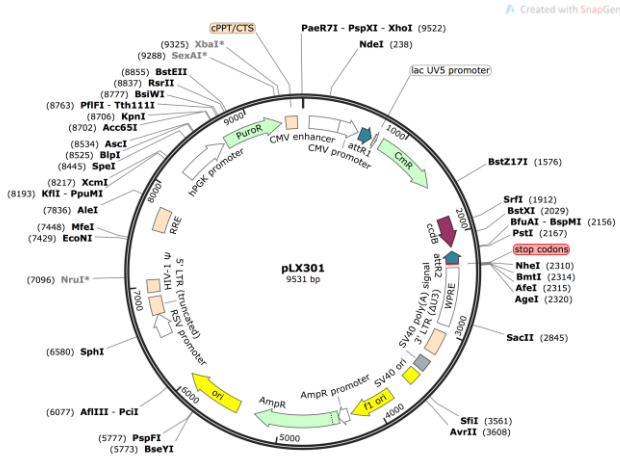

B.

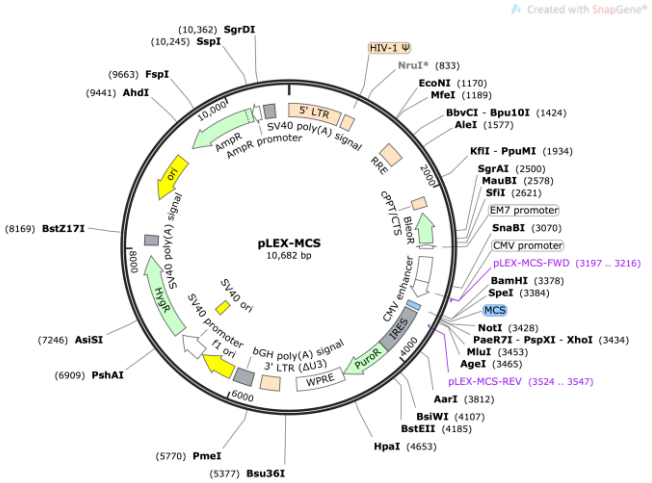

C.

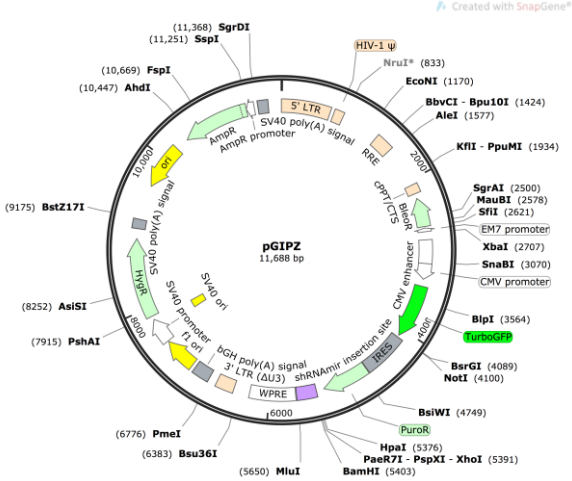

Figure 2.1 Maps of lentiviral vectors used.
A. pLX301 B. pLEX-MCS and C. pGIPZ

2.6 Lentiviral Infection

Lentiviral infections were carried out as follows:

Day 1: $CL3^{EcoR}$ cells were counted using a C-chip haemocytometer and seeded at a density of 100,000 cells per T-25 flask.

Day 2: Appropriate lentiviruses produced by above-described protocol were thawed, if the freshly harvested virus was not used. A 5 ml (for down-regulated TFs) or 2 ml (for up-regulated TFs) aliquot of lentivirus was added to each flask of $CL3^{EcoR}$ cells. To increase the efficiency of transduction, double infections were conducted where lentivirus was added twice within a span of 10 to 12 hours approximately. To facilitate infection Polybrene (hexadimethrine bromide, Millipore) was added at a working concentration of 8 µg/ml from the stock of 10 mg/ml. The volume of medium in the flask was made up to 7 ml by adding complete DMEM.

Day 3 and 4: Fresh medium was added, and flasks were incubated at 33°C for two days.

Day 5: To select for successfully and stably transduced cells, the medium was changed to selection medium which contained puromycin (2 µg/ml or 6 µg/ml) as puromycin is the mammalian selection marker for the lentiviral vectors used i.e. pLX301, pLEX-MCS and pGIPZ.

Day 6 and 7: Flasks containing the selection medium were incubated at 33°C for at least two days.

Day 8: Flasks were examined under a phase contrast tissue culture microscope to see if there were enough numbers of survivors to reseed 35,000 or 50,000 cells in triplicate. If yes, then cells were trypsinized and reseeded at the appropriate number in triplicate in T-75 flasks and incubated overnight at 33°C to adhere and stabilize. If not, the survivors were allowed to grow at 33°C until enough cells were present with a medium change. A control flask was always plated along with the experiment, in which non-infected $CL3^{EcoR}$ cells were maintained simultaneously. After adding selection medium by Day 8 normally

90% of the cells are dead in the control flask. This is done to confirm that selection had worked successfully, also confirmed successful transfection.

Day 9: The following day the cells were shifted to the non-permissive temperature: 37.8°C-38.9°C. Cells were then maintained at the non-permissive temperature for three weeks with weekly medium change with 15 ml of complete DMEM.

To determine the extent of senescence bypass, flasks were stained after three weeks with 2% Methylene blue stain in 50% ethanol and 50% distilled water. After removing the medium from the flasks, the stain was added and incubated for at least 30 minutes and then washed under running tap water. After air drying, the flasks were photographed, and the number of densely growing colonies visible as blue foci were quantified.

A combination of qualitative and quantitative approaches was used to determine the extent of senescence bypass. For quantitative analysis, two different approaches were taken. First, the growing dense blue colonies were independently counted twice manually on a lightbox, using a non-biased approach by randomly selecting the flask to be counted. The second approach used the Definiens Developer XD software wherein, an algorithm was developed by Dr Matthew Ellis (Image analyst, Division of Neuropathology, UCL) to calculate the area of the flask stained blue. This enabled determination of the extent of senescence bypass, as the higher the area covered in blue, the stronger is the bypass potential. To see if both the methods used generated similar results, the data for every experiment was plotted as ‘Number of growing colonies' when counted manually as well as ‘Percentage area stained' when calculated by the software.

2.7 Mycoplasma Testing

To maintain clean contamination free cell lines LookOut® Mycoplasma PCR detection kit (Sigma-Aldrich) was used. It is a highly sensitive method to detect Mycoplasma and Acholeplasma contamination in cell cultures. The whole procedure was done in four steps which are as follows:

Preparation of Sample: Samples to check for Mycoplasma were derived from the medium supernatant of cultures of cell lines i.e. CL3^{EcoR} and HEK293T after they had reached 90-100% confluence. DNA was extracted using GenElute^{TM} Blood genomic DNA Kit from Sigma Aldrich after boiling 500 µl of the supernatant collected at 95°C for five minutes.

PCR Set up: The DNA isolated after the extraction procedure was used to set up the PCR reaction as follows. The total volume for each PCR reaction was 25 µl.

Table 2.1 Constituents of PCR reaction for mycoplasma test

	Sample	**Positive Control**	**Negative Control**
DNA Polymerase/Rehydration Buffer	23 µl	25 µl	23 µl
Sample Volume	2 µl	-	-
DNA free water	-	-	2 µl

DNA Polymerase/Rehydration Buffer Preparation: The required volume of the Rehydration Buffer was pipetted into a clean amplification tube and the required volume of DNA polymerase was added. For JumpStart Taq Polymerase with 2.5 units/µl, a volume of 0.5 µl is required per reaction. The DNA Polymerase/Rehydration Buffer was carefully mixed by flicking the tube.

Tube preparation: Appropriate number of tubes for the negative control and samples were removed from the bag. Protective films from the tubes were peeled off and 23 µl of the prepared DNA polymerase/Rehydration Buffer was added to each reaction tube. 2 µl of DNA free water was added to the negative control and 2 µl of the sample was added to each sample reaction tube. The appropriate number of positive control reaction tubes were removed from the bag and labelled. 25 µl of the prepared DNA polymerase/Rehydration Buffer was added to each tube.

Incubation: The contents of each tube were mixed thoroughly by flicking the tubes. The liquid in the tube was collected at the bottom of the PCR tube and incubated at room temperature for five minutes, followed by thermal cycling.

Thermal Cycler Program: The following thermal cycler program was used for the PCR reaction on a MJ Research PTC-200 Thermal cycler:

40 cycles 94°C for 30 seconds

55°C for 30 seconds

72°C for 40 seconds

Cool down to 4-8°C.

Agarose Gel and Evaluation: 1.2% standard agarose gel was used with a 5 mm comb. 8 µl of each PCR reaction was directly loaded. The loading buffer was pre-included in the PCR mixture. Electrophoresis was stopped after the dye had migrated approximately 2.5 cm.

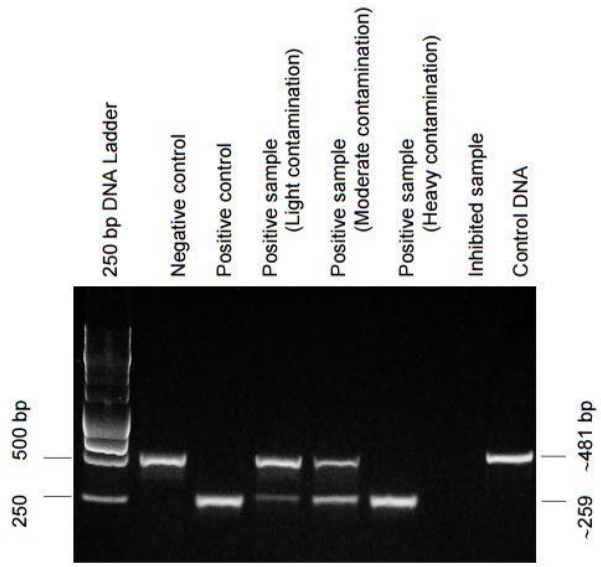

Figure 2.2 Relevant amplicon bands for Mycoplasma testing.
The negative control samples show a distinct 481 bp band. Internal controls appear in every lane indicating a successful PCR. The positive control shows a band at 259 bp along with the internal control 481 bp band. Mycoplasma positive samples, if any should show bands in the range of 260±8 bp. The intensity and thickness of the band (260±8 bp) is an indication of the extent of mycoplasma contamination.

2.8 Bacterial Manipulations

2.8.1 Bacterial strains

For most of the transformations, plasmid manipulation and preparations conducted in this study, competent cells made from the JS4 Escherichia coli strain, which is a recA derivative of MC1061 (a kind gift from J. Sedivy, Brown University) were used (Sedivy et al. 1987). DH5-α super-competent cells from ThermoScientific were also used. One Shot™ ccdB Survival™ 2 T1R Competent Cells (ThermoScientific) were used for propagation of plasmids containing the ccdB gene. In this thesis, they were used for propagating the Gateway destination entry vector pLX301.

2.8.2 Medium and Bacterial growth

E. coli were grown in Luria Base (LB) Broth (25 g/l Luria Broth Base; Invitrogen) or Super broth [(10 g MOPS (4- Morpholinepropanesulphonic acid) sodium salt (Sigma), 20 g yeast extract (Oxoid), and 32 g tryptone (Oxoid) per litre]. 15 g/l of agar (Oxoid) was added when LB agar was prepared. To make up the medium, all the components were dissolved in distilled water and autoclaved for 20 minutes at 121°C under high pressure. Desired antibiotics were added as appropriate: kanamycin (Sigma) was added at a final concentration of 50 µg/ml, ampicillin (Sigma), spectinomycin (Sigma) and carbenicillin (Sigma) was added at a final concentration of 100 µg/ml, and chloramphenicol was added to a final concentration of 30 µg/ml.

2.8.3 Bacterial Transformation

For bacterial transformations, competent JS4 cells were used. Each 50 µl aliquot of JS4 competent cells was thawed on ice. The JS4 strain can be made up to a maximum volume of 1 ml using cold sterile 0.1 M $CaCl_2$. The required number of sterile Eppendorf tubes were pre-chilled on ice. 100 µl of the JS4 cells were aliquoted into each pre-chilled tube. DNA was added to the bacteria and the reactions swirled gently and incubated on ice for 30 minutes. After 30 minutes, JS4 cells were given a heat shock for 90 seconds at 42°C. After the heat shock, tubes were incubated on ice for 2 minutes. 500 µl of LB broth was added to each tube and incubated at 37°C without shaking for an hour. After one-hour cells

were spun on a desktop centrifuge at 13000 rpm for one minute to pellet the bacteria. The pellet was re-suspended in a small volume and plated on a LB agar plate containing the appropriate antibiotic. Plates were then incubated at 37°C for >16hours.

For DH5-α super-competent cells and One Shot™ ccdB Survival™ 2 T1R Competent Cells the same transformation protocol described above was used with heat shock given for only 30 seconds and 250 µl of the S.O.C. medium provided with the kit was used.

2.9 DNA Manipulations

2.9.1 Genomic DNA isolation

From cell culture supernatant:

To extract DNA from the supernatant of cell cultures to check for Mycoplasma, GenElute™ Blood genomic DNA Kit Protocol from Sigma Aldrich was used.

To 200 µl of the supernatant boiled at 95°C for 5 minutes, 20 µl of Proteinase K solution was added in a 1.5 ml microcentrifuge tube and vortexed. 200 µl of Lysis Solution was added to the sample and vortexed thoroughly for 15 seconds as a homogeneous mixture is essential for efficient lysis. The tube was then incubated at 55°C for 10 minutes. 500 µl of the Column Preparation Solution was added to each pre-assembled GenElute Miniprep Binding Column and centrifuged at 12,000xg for one minute. Flow through liquid was discarded. This step maximises binding of DNA to the membrane resulting in more consistent yields. 200 µl of absolute ethanol (95-100%) was added to the lysate and mixed thoroughly by vortexing for 5 to 10 seconds to produce a homogenous solution. The entire contents of the tube were transferred to the treated column and centrifuged at ≥ 6500xg for 1 minute. The collection tube containing the flow through liquid was discarded and a new 2 ml collection tube was placed on to the column. 500 µl of Wash Solution diluted with ethanol was added to the column and centrifuged for 3 minutes at maximum speed. The collection tube containing the flow through liquid was discarded and a new 2 ml collection tube was placed on to the column. The column must be free of ethanol before eluting

the DNA. The column was centrifuged for an additional one minute at maximum speed to get rid of any residual ethanol. The collection tube containing the flow through was discarded and a new 2 ml collection tube was placed on to the column. To elute the DNA, 200 µl of the Elution Solution was directly pipetted into the centre of the column and incubated for five minutes at room temperature to increase the elution efficiency. After five minutes the tube was centrifuged at ≥6500g for one minute to elute the DNA.

From growing cells:

To extract genomic DNA from cells that were stably transduced with the mixture of 73 TFs (Pool 73) and had bypassed senescence at the non-permissive temperature, Illustra Nucleon Genomic DNA Extraction Kit from GE healthcare was used. The Illustra Nucleon blood and cell culture 1 (BACC1) protocol was used as it was designed for genomic DNA isolation from 1 to 3 x 10^6 cultured cells.

Cell Preparation: Stably transduced $CL3^{EcoR}$ cells growing at 38.9°C for three weeks were trypsinized and collected by centrifugation at 600xg for 5 minutes at 4°C. The supernatant was discarded very gently without disturbing the pellet.

Cell Lysis: The cell pellet was resuspended in 1.0 ml Reagent A provided in the kit and left on ice for 5 minutes. After five minutes, tube was centrifuged at 1300xg for 5 minutes and the supernatant was discarded. To the pellet, 350 µl of Reagent B was added. The tube was vortexed briefly to resuspend the pellet. The suspension was transferred to 1.5 ml microcentrifuge tube.

Deproteinization: 100 µl of sodium perchlorate solution was added. The tubes were mixed by hand, by inverting the capped tube at least 7 times.

DNA Extraction: 600 µl of chloroform was added and mixed by hand, by inverting the capped tube at least 7 times.150 µl of Nucleon resin was added without remixing the phases. The tube was then centrifuged at 350xg for 1 minute.

DNA precipitation: Without disturbing the Nucleon resin layer which is brown in colour, the upper phase (approximately 450 µl) was transferred to another clean

1.5 ml microcentrifuge tube. To precipitate the DNA, 2 volumes, i.e. 900 µl, of cold absolute ethanol was added. The preparation was then mixed by inversion until the precipitate appeared.

DNA Washing: To pellet the DNA the microcentrifuge tube was centrifuged at top speed for five minutes. The supernatant was discarded. The same step was repeated after addition of 1 ml of cold 70% (v/v) ethanol and mixing several times. The pellet was left for airdrying for at least 20 minutes to ensure that all the ethanol had evaporated. The DNA was then dissolved in an appropriate volume of TE buffer.

2.9.2 Small scale plasmid preparation

QIAprep Spin Miniprep Kit from Qiagen was used.15 ml of bacterial culture grown overnight from a single colony or glycerol stock was pelleted by centrifugation at 4000 rpm for 10 minutes at room temperature. The pelleted bacterial cells were resuspended in 250 µl of buffer P1 and the contents transferred to a microcentrifuge tube. 350 µl of buffer P2 was added and mixed thoroughly by inverting the tubes 4 to 6 times until the solution becomes clear. 490 µl of buffer N3 was added and mixed immediately and thoroughly by inverting the tube 4 to 6 times. The tubes were then centrifuged at 13,000 rpm in a bench top micro-centrifuge for 10 minutes. Supernatant from the tube was carefully pipetted on to a QIA prep spin column and centrifuged for one minute at 13,000 rpm. Flow through was discarded. The QIA prep spin column was washed by adding 500 µl buffer PB, centrifuged for a minute at 13,000 rpm and the flow through was discarded. QIA prep spin column was washed again by adding 750 µl of buffer PE, centrifugation for one minute at 13000 rpm and discarding the flow through. To remove any residual wash buffer, the column was centrifuged again for one min at 13,000 rpm. QIA prep column was placed in a clean 1.5 ml microcentrifuge tube. To elute DNA, 50 µl buffer EB (10 mM Tris.Cl, pH 8.5) was added to the centre of the QIA prep spin column and allowed to stand for three minutes. After the incubation, the tube was centrifuged at 13,000 rpm for two minutes to elute the DNA. The microcentrifuge tube was labelled and stored at -20°C.

2.9.3 Large scale plasmid preparation

Large-scale plasmid preparation was done for pMDG.2 and p8.91 plasmids used for lentivirus production by QIA filter plasmid Maxi Kit from Qiagen. 1 µl of each of these plasmids were transformed into JS4 cells when the quantity of DNA was running low. A single colony was picked and used to inoculate 10 ml of LB super broth with antibiotic overnight at 37°C with shaking at 220 rpm. Next day this culture was used to inoculate 250 ml of super broth plus antibiotic in a sterile conical flask. Cultures were grown at 37°C shaker incubator at 220 rpm for 48 hours. After 48 hours the bacterial culture was harvested by centrifugation at 8000 rpm for 15 minutes at 4°C. The pellet obtained was completely resuspended in 10 ml of buffer P1 by vigorous vortexing. 10 ml of buffer P2 was added and mixed by inverting the sealed tube 4 to 6 times. The tube was then incubated at room temperature for 5 minutes. During this incubation, the cap was screwed on to the outlet nozzle of the QIA filter Cartridge and placed in a QIA rack. After five minutes, 10 ml pre-chilled buffer P3 was added to the lysate and mixed immediately and thoroughly by inverting the tube 4 to 6 times. The lysate was then poured into the barrel of the QIA filer Cartridge and incubated at room temperature for ten minutes. Meanwhile, the QIAGEN-tip was equilibrated by applying 10 ml buffer QBT and allowing the column to empty by gravity flow. After ten minutes the cap from the QIA filter cartridge was removed from the outlet nozzle. The Plunger was gently inserted into the QIA filter Cartridge and the cell lysate was filtered into the equilibrated QIAGEN-tip. The lysate was allowed to enter the resin under gravity. The QIAGEN-tip was washed with 2 x 30 ml Buffer QC. The DNA was eluted into a clean 50 ml tube, with 15 ml of Buffer QF. The DNA was precipitated by adding 10.5 ml isopropanol, mixed and allowed to stand for five minutes. The tube was centrifuged at 8000 rpm for 15 minutes at 4°C. The supernatant was carefully decanted, and the transparent pellet washed with 1 ml 70% ethanol at room temperature and transferred to a 1.5 ml microcentrifuge tube and centrifuged at 13000 rpm for ten minutes in a benchtop microcentrifuge. After carefully removing the supernatant the pellet was air-dried and the DNA dissolved in a suitable volume of TE buffer, pH 8.0 and stored at -20°C.

2.9.4 Gel extraction

Gel extraction was done for cloning desired fragments, using QIAquick® Gel extraction kit from Qiagen. All the centrifugation steps were done at maximum speed i.e. 13000 rpm on a tabletop microcentrifuge. DNA restriction fragments separated on an agarose gel were viewed with a long wavelength UV emission transilluminator. The desired band was excised using a clean sharp scalpel and transferred to a 1.5 ml microfuge tube. The gel slice was weighed in a colourless microcentrifuge tube. 3 volumes of buffer QG was added to 1 volume gel (100 mg~100 µl). To dissolve the gel slice, the tube was incubated at 50ºC on a heat block for about 10 minutes with intermittent vortexing. 1 gel volume of isopropanol was added to the sample and mixed. QIAquick spin column was placed on a 2 ml collection tube provided in the kit. For DNA to bind, the sample was applied to the QIAquick column and centrifuged for one minute. Flow through was discarded and the QIAquick column was placed back onto the same tube. 750 µl of wash buffer PE was added to the QIAquick column and centrifuged for one min. Flow through was discarded and the column was again placed back. To remove the residual buffer the QIAquick column was centrifuged again, any flow through was discarded and the column was placed on a clean 1.5 ml microcentrifuge tube. Finally, to elute the DNA 50 µl buffer EB (10 mM Tris.HCl, pH 8.5) was added to the centre of QIAquick membrane. To increase the efficiency, after adding the buffer EB, the tube was allowed to stand for three minutes and then centrifuged for two minutes to elute the DNA.

2.9.5 DNA Quantification

DNA concentration was determined by measuring the optical density of the solution at 260 nm (OD260) using a Nanodrop 1000 (Thermo Scientific). The following equation was used to calculate the DNA concentration: 1 OD unit at 260 nm= 50 µg/ml of DNA

2.9.6 DNA Sequencing

DNA sequencing was undertaken to verify the various constructs at different stages in this study. Sequencing reactions were carried out in THERMO- FAST® non-skirted 96-well plates from Thermo Scientific. BigDye® Terminator v1.1

Cycle Sequencing Kit from Applied Biosystems was used. 1 µl plasmid DNA at a concentration of about 150 ng/µl was added.

Table 2.2 Sequencing reaction constituents

Reagents	**1x sequencing reaction**
Big Dye Mix	1 µl
Better Buffer (Microzone)	5 µl
Primer (5 µM)	0.75 µl
Betaine (Sigma Aldrich)	3 µl
ddH_2O	4.25 µl
Total volume	15 µl

Reactions were set up in accordance with the above protocol. The plate was covered and given a pulse spin. PCR reactions were run on a Biorad DNA engine Tetrad® 2 Thermal Cycler machine. Details of the PCR cycle are: Initial denaturation at 96ºC for 1 min; 25 cycles of Denaturation at 96ºC for 30 seconds, Annealing at 50ºC for 15 seconds, Extension at 60ºC for 4 minutes. After a final extension for 5 minutes, the reaction was put on hold at 4ºC for an indefinite time.

To purify extension products, the following protocol was used:

To each sequencing reaction, 3.75 µl of 0.125 M EDTA was added ensuring the solution was pipetted into the bottom of the well. 45 µl of 100% absolute ethanol was added to each reaction and mixed. After 15 minutes at room temperature, the plate was centrifuged at 3000xg for 30 minutes at 4°C. The plate was inverted on to a paper towel and spun at 185xg for one minute. After that 60 µl of 70% ethanol was added and the plate was centrifuged at 1650xg for 15 minutes at 4°C. The plate was again inverted on to a paper towel and spun at 185xg for one minute. To remove final traces of ethanol the plate was left uncovered at room temperature for 15 minutes. The plate was stored at -20°C and the sequencing reaction was run by the Human Genetics group at MRC Prion Unit on a 3730xl

DNA Analyzer (Applied Biosystems). To analyse the sequences, Applied Biosystems Sequence Scanner software v1.0 was used.

Later for sequencing, samples were outsourced to SourceBioScience (https://www.sourcebioscience.com/).

2.9.7 Gateway Recombinational Cloning

Some constructs used in this study were prepared by Prof. Parmjit Jat and to complete the list the remaining were ordered from DNASU plasmid repository as Gateway adapted Entry clones and prepared using the following protocol:

LR Clonase™ II enzyme mix from ThermoFisher Scientific was used for Gateway Recombinational Cloning of ORFs of genes into the pLX301 destination vector. The components mentioned in the table below (Table 2.3) were added to a 1.5 ml microcentrifuge tube at room temperature and mixed.

Table 2.3 Gateway Recombination Cloning constituents

Entry clone from DNASU (50-150 ng)	1-7 µl
Destination Vector pLX301 (150 ng/µl)	1 µl
TE buffer, pH 8.0	To 8 µl

The LR Clonase™ II enzyme mix was thawed on ice for about two minutes and vortexed briefly twice for about two seconds each. 2 µl of LR Clonase™ II enzyme mix was added to each reaction and mixed well again by vortexing briefly. LR Clonase™ II enzyme mix was returned to -20°C immediately after use. The reactions were incubated at 25°C overnight. 1 µl of the Proteinase K solution (2 µg/µl) was added to each sample to terminate the reaction and vortexed briefly. The samples were then incubated at 37°C for ten minutes.

1 µl of each LR reaction was used to transform 100 µl of JS4 competent cells according to the protocol described in section 2.8.3 and selected for resistance to Ampicillin.

2.9.8 Multicistronic PCR cloning

To construct the multicistronic vectors, multiple sequential PCR reactions were performed. The conditions and various different parameters for each of the primary, secondary and tertiary PCR reactions are indicated in detail in Table 2.4.

DNA Construct	Forward and Reverse Primers	PCR Cloning conditions			Additional notes
		Temperature	Time	Cycles	*MgCl₂ added* (ul)
		**98 ℃*	*30 seconds*	*1*	
LIN52	**(P)** LFBF1; LFBR1	66°C 72°C	30 seconds 30 seconds	5 25	0
FOXM1ΔNΔKEN	**(P)** LFBF2; LFBR4	60°C 72°C	30 seconds 2 minutes	5 25	0
LIN52-FOXM1ΔNΔKEN	**(S)** LFBF1; LFBR4	72°C	2 minutes	30	0, 0.5
LIN52	**(P)** LFBF1; LFBR1	66°C 72°C	30 seconds 30 seconds	5 25	0
B-MYB	**(P)** LFBF5; LFBR3	66°C 72°C	30 seconds 2 minutes	5 25	0
LIN52-B-MYB	**(S)** LFBF1; LFBR3	72°C	2 minutes	30	0, 0.5
FOXM1ΔNΔKEN	**(P)** LFBF4; LFBR2	66°C 72°C	30 seconds 2 minutes	5 25	0, 0.5
B-MYB	**(P)** LFBF3; LFBR3	72°C	2 minutes	30	0
FOXM1ΔNΔKEN-B-MYB	**(S)** LFBF4; LFBR3	72°C	3 minutes	30	0, 0.5, 1, 2.5
LIN52	**(P)** LFBF1; LFBR1	66°C 72°C	30 seconds 30 seconds	5 25	0
FOXM1ΔNΔKEN	**(P)** LFBF2; LFBR2	60°C 72°C	30 seconds 2 minutes	5 25	1
B-MYB	**(P)** LFBF3; LFBR3	72°C	2 minutes	30	0
LIN52-FOXM1ΔNΔKEN	**(S)** LFBF1; LFBR2	72°C	2 minutes	30	0.5
LIN52-FOXM1ΔNΔKEN-B-MYB	**(T)** LFBF1; LFBR3	72°C	3 minutes	30	0, 0.5
		***72 ℃* ***4 ℃*	*5 minutes* *Hold*	*1*	

Table 2.4 PCR cycling parameters and conditions to construct multi-cistronic constructs.
The table describes the different parameters and cycling conditions used for recombinant PCR. Each PCR reaction correlates to either the primary (P), secondary(S) and tertiary(T) reaction based on the construction of single, double and triple constructs respectively. PCR reactions are grouped together, and colour coded for a clear explanation of the set of reactions conducted to create each multi-cistronic construct. Additional notes present the optimisation of the different Mg++ concentrations used to amplify different constructs.
* PCR cycle used at the start of every amplification reaction.
** PCR cycle used at the end to terminate every amplification reaction

For setting up 50 µl PCR reactions, template DNA was used at 10ng per reaction. Template DNA along with the forward and reverse primers (at a final concentration of 0.5 µM) were added to the master mix. The master mix was composed of 10 mM dNTPs (at a final concentration of 200 µM), 1.5 µl DMSO, 5X Phusion HF Buffer (at a final concentration of 1X) and 0.5 µl of Phusion High-

fidelity DNA polymerase from Thermofisher Scientific. The final reaction volume was made up to 50 µl with RNase/DNase free water.

2.10 Protein Analysis

2.10.1 Preparation of total protein extracts

Fresh medium was added to the cell cultures the day prior to making lysates. For some of the constructs, there were only a few CL3^{EcoR} cells growing at the non-permissive temperature which had bypassed senescence, therefore, cells from two flasks were trypsinized, pooled and replated on a 10 cm dish. Cell cultures were harvested at about 80% confluency on the day of lysis. For lysis, cells were washed twice with cold PBS. One ml of RIPA lysis buffer (50 mM Tris-HCl, pH 8.0, with 150 mM sodium chloride, 1.0% Igepal CA-630 (NP-40), 0.5% sodium deoxycholate, and 0.1% sodium dodecyl sulfate; Sigma Aldrich) supplemented with 2 µl of Protease Inhibitor Cocktail (2 mM 4-[2-aminoethyl] benzenesulphonyl fluoride [AEBSF], 1 mM EDTA, 130 µM Bestatin, 14 µM E-64, 1 µM Leupeptin and 0.3 µM Aprotinin; Sigma Aldrich) was added, making sure that the whole surface was covered. Cells were incubated for thirty minutes on ice. Meanwhile 1.5 ml microcentrifuge tubes were labelled and pre-chilled on ice. After thirty minutes cells were scraped off and transferred to pre-chilled microcentrifuge tubes. To shear the DNA, lysates were passed three times through a 21-gauge needle and centrifuged at 10,000 rpm at 4°C for thirty minutes. The supernatant was collected and transferred to a fresh pre-chilled microcentrifuge tube and stored at -20°C.

2.10.2 Determination of Protein concentration

Protein concentrations were determined using the Bradford assay. To determine the concentration lysates were thawed on ice and diluted fivefold in PBS. To make a standard curve, BSA standards prepared in PBS were used (0 µg/ml, 125 µg/ml, 250 µg/ml, 500 µg/ml, 750 µg/ml, 1000 µg/ml, 1500 µg/ml, 2000 µg/ml). 5 µl of each of the BSA standard was pipetted in triplicate into a 96 well clear plate making sure there were no bubbles in the wells. 5 µl of the samples to be analysed were pipetted in triplicate into the rest of the plate again avoiding bubbles. The Bradford reagent was mixed by inverting the bottle and 250 µl of

the reagent was added to each well using a multichannel pipette. The plate was sealed with a plate cover evenly across and incubated at room temperature for ten minutes. The absorbance was measured at 595 nm on a Tecan plate reader and the absorbance plotted against the protein concentration of BSA standards. The regression coefficient was calculated, and the unknown sample concentrations determined.

2.10.3 Sodium-Dodecyl-Sulphate-Polyacrylamide-Gel-Electrophoresis

20 µg of each cell lysate was heated at 90°C for five minutes with 4X Sample buffer (50% glycerol, 5% lithium dodecyl sulphate, 5% Tris (hydroxymethyl) amino methane and 1% HCl; Bio-Rad Laboratories Ltd.) and fractionated by SDS-PAGE (7% for FOXM1 and B-MYB and 12% for LIN52 SDS-PAGE gels were used). Electrophoresis was done at a constant voltage of 100V in running buffer (25 mM Tris, 190 mM Glycine, 0.1% [w/v] SDS). Protein samples were fractionated alongside a Novex™ Sharp Pre-stained protein standard marker from ThermoFisher Scientific.

2.10.4 Western blotting of SDS-PAGE

After the samples were separated by SDS-PAGE, the proteins were transferred on to a nitrocellulose membrane by electrophoretic transfer in a wet tank blotting system in transfer buffer (25 mM Tris, 190 mM glycine and 20% [v/v] methanol). The transfer was done at 90V for ninety minutes. After transfer, the nitrocellulose membrane was blocked in 5% skimmed milk powder or BSA in PBS for at least one hour at room temperature. After five quick washes with 0.05% (v/v) PBST, the membrane was incubated with primary antibody diluted at 1:1000 dilution in 5% BSA overnight at 4°C. Next day the membrane was washed with 0.05% (v/v) PBST (ten minutes each at room temperature) for at least one hour. The blot was then incubated with HRP (Horseradish Peroxidase) conjugated secondary antibody at 1:2000 dilution in PBST for one hour at room temperature. The blot was washed again for one hour with 0.05% (v/v) PBST (ten minutes each at room temperature). For developing, Western Lightning Plus-ECL from PerkinElmer was used. Chemiluminescence Reagent was prepared by mixing equal volumes of Enhanced Luminol Reagent and the Oxidizing Reagent. The membrane was incubated in Chemiluminescence Reagent for one minute with gentle agitation.

Excess chemiluminescence reagent was removed. The membrane was then placed in a cassette and exposed to an auto-radiographic film for different times varying from 30 seconds to 20 minutes. Films were then developed in the dark.

2.10.5 Antibodies used

To test ectopic expression in this study the following primary antibodies were used (Table 2.5). HRP conjugated polyclonal goat Anti-rabbit (P044801-2) and Anti-mouse (P044701-2) secondary antibodies were used at 1:2000 dilution from Agilent Dako.

Table 2.5 Antibodies used

Target	Host	Clonality	Supplier	Dilution	Cat number
LIN52	Rabbit	Polyclonal	LifeSpan BioSciences	1:1000	LS-C165783
B-MYB	Mouse	Monoclonal	MerckMillipore	1:1000	MABE886
FOXM1	Rabbit	Polyclonal	Santa Cruz Biotechnology	1:1000	sc-502
β-tubulin	Rabbit	Polyclonal	Santa Cruz Biotechnology	1:1000	sc-9104

Chapter 3 Identification of upregulated and downregulated TFs, preparation of expression constructs and assessment of their functional role in senescence

3.1 Identification of up-regulated and downregulated TFs

3.1.1 Objectives

Transcription factors (TFs) are the family of distal effector proteins that regulate gene expression at different stages of embryonic development and are key to the establishment and maintenance of specific cell fate by ensuring the correct expression of specific genes at an appropriate time and place (Levine and Tijan 2003; Bustamante et al. 2005; Vaquerizas et al. 2009). They also play a central role in regulating biological processes by controlling cell function and how cells respond to various stimuli. Defining the key TFs and dissecting the underlying transcriptional networks is therefore important for defining the phenotype of a particular cell or disease state.

Even though acquisition of a limitless replicative potential has been proposed to be one of the key events required for malignant transformation, we still do not fully know the transcriptional networks that underlie entry into senescence, the signal transduction pathways and how the diverse signals that result in senescence are all integrated. Several studies have reported the involvement of two key tumour suppressor pathways namely, p53/p21^{WAF1} and p16^{INK4A}/pRB, in achieving and maintaining senescence growth arrest. However, the critical downstream TFs involved in these pathways are not known.

Hence, the objective of this section of this chapter is to identify and refine the list of upregulated and downregulated TFs that might play a key role in manifesting cellular senescence.

3.1.2 Identification of differential transcription factors that underlie cellular senescence

The present work is an extension of the previous work undertaken in my lab where microarray expression profiling studies were conducted to identify changes in gene expression upon senescence (Rovillain et al. 2011). If changes in gene expression that were identified are specific to senescence growth arrest, the changes should be reversed upon its abrogation. Genome wide expression profiling coupled with inactivation of the p53-$p21^{WAF1}$ and/or $p16^{INK4A}$-pRB pathways, in the $CL3^{EcoR}$ cells, using SV40 LT (wt_LT) antigen, HPV16/18 E7, Adenovirus E1A, GSEp53 (dominant negative p53), E2F-DB (dominant negative E2F), p53shRNA (pRS_p53) and $p21^{WAF1}$ shRNA (pRS_$p21^{WAF1}$) yielded a comprehensive catalogue of genes whose levels are altered upon senescence comprising 3059 up-regulated and 5005 down-regulated transcripts (Rovillain et al. 2011). It was also observed that expression of these differentially expressed transcripts was reversed when senescence was bypassed.

MicroRNAs(miRNA) are key regulator molecules which aid in post-transcriptional gene expression by RNA silencing. They play a crucial role in maintaining many cellular processes, for example, metastasis, cell proliferation, differentiation, cell cycle, apoptosis etc. Interestingly previous expression profiling studies conducted in the lab also investigated the involvement of microRNAs in senescence to identify senescence specific microRNA expression in $CL3^{EcoR}$ cells. Functional validation of the top 15 downregulated miRNAs by ectopic expression and senescence bypass assay in $CL3^{EcoR}$ cells revealed six miRNAs namely, miR186, miR195, miR218, miR25, miR372 and miR423, which bypassed growth arrest (Rovillain 2011).

Luscombe and colleagues have presented a high quality and comprehensive census of TFs in the human genome. Their study lists 1391 manually curated sequence specific DNA binding factors and also proposed their function, evolutionary conservation and genomic organization (Vaquerizas et al. 2009). Therefore, the starting key step in this project was to overlay the previously identified 3059 up-regulated and 5005 down-regulated transcripts with the 1391 manually curated sequence-specific DNA binding transcription factors identified

by Luscombe and colleagues (Vaquerizas et al. 2009). The purpose of this overlay was to identify DNA binding transcription factors from the list of previously identified differential genes as in this thesis we are interested in studying the functional role of transcription factors.

The results of this overlay identified a total of 462 differentially expressed candidate DNA binding transcription factors of which 124 were up-regulated and 338 were down-regulated. The top 23 up- (positive numbers for log2 fold change indicated as GA) and down-regulated (negative numbers for log2 fold change indicated as GA) TFs are shown below in Figure 3.1. The overlays showed that differential expression of the TFs was reversed when senescence was bypassed; however, the reversal is clearer for the down-regulated TFs than it is for the up-regulated TFs as depicted in Figure 3.1.

A.	GA	wt_LT	GSE_p53	E1A	E7	E2F-DB	pRS_p53	pRS_p21	mir186	mir195	mir218	mir25	mir372	mir423
BMP2	2.45	-5.05	-3.39	-4.46	-3.48	-3.08	-1.46	-1.85	-0.14	0.25	0.67	-1.20	-1.73	0.78
ARID5B	1.78	0.22	-0.27	-0.97	-0.27	-0.74	-0.77	-1.39	-2.33	-2.52	-2.39	-1.88	0.25	-2.40
GPR155	1.68	-1.27	-1.03	-0.65	-1.07	-1.30	-1.29	-1.11	-1.64	-1.66	-1.69	-1.74	-1.16	-1.81
ZMAT3	1.66	-1.60	-1.14	-0.07	-0.70	-0.24	-1.83	0.16	-2.03	-1.54	-1.46	-2.03	-0.91	-1.38
CD36	1.61	-1.08	-0.61	-1.15	-0.88	-0.90	-0.75	-1.10	-1.76	-1.59	-1.72	-2.07	-1.53	-1.96
NR3C2	1.58	-2.63	-1.84	-1.40	-0.94	0.09	-0.85	-1.04	-0.79	-0.99	-0.66	-0.45	-0.36	0.28
ZBTB1	1.52	-0.94	0.15	-2.57	-1.58	-1.73	-0.83	-1.01	-1.00	-0.69	-0.82	-0.59	-0.63	-0.48
RORA	1.31	-1.62	-0.76	-0.77	-1.09	-1.62	-0.62	-0.67	-0.58	-1.02	-1.61	-1.33	0.11	-2.26
ZNF432	1.23	-0.96	-0.85	-0.72	-0.97	-0.86	-0.61	-0.36	-2.17	-2.18	-2.92	-1.97	-1.27	-2.48
STAT1	1.23	-1.16	-1.60	-1.53	-1.14	-1.82	-0.78	-1.12	0.48	-0.57	-0.59	-0.60	-1.00	-1.63
FBN1	1.23	0.16	0.97	-1.14	-0.19	-0.88	0.06	0.03	-1.19	-1.80	-2.19	-0.97	0.09	-2.33
RUNX1	1.12	-0.84	-1.03	-1.15	-0.63	-0.71	-0.63	-0.65	-2.25	-1.98	-1.58	-1.88	-1.02	-1.51
OSR1	1.10	-0.80	-0.46	-3.54	-1.36	-2.29	-0.94	-0.75	-1.78	-2.91	-2.93	-2.92	-0.58	-4.07
AFF1	1.10	-1.03	-0.74	-1.25	-0.52	-0.30	-0.84	-0.87	-0.68	-0.67	-0.50	-0.57	-0.39	-0.22
FAM44A	1.09	-0.73	-0.56	-0.88	-0.68	-0.76	-0.85	-0.81	-0.54	-0.89	-0.43	-0.79	-0.56	-0.78
RGS7	1.08	-0.36	-0.45	-0.16	-0.08	0.12	-0.16	-0.47	-1.16	-1.67	-1.25	-1.57	0.25	-1.60
DEPDC6	1.07	0.26	1.10	-0.26	0.13	-0.41	0.53	0.26	-1.77	-2.14	-1.47	-1.89	-1.77	-2.16
CREB3	1.05	-0.84	-0.67	-0.85	-0.51	-0.47	-0.55	-0.62	-0.65	-0.68	-0.58	-0.78	-0.34	-0.79
SP110	1.04	-0.85	-1.24	-1.19	-0.67	-1.06	-0.48	-0.86	0.66	-0.42	-0.25	-0.67	-0.63	-1.19
STAT2	0.97	-0.25	-0.55	-0.89	-0.31	-0.72	-0.18	-0.21	0.41	-0.30	-0.48	-0.48	-0.34	-0.70
FAM171B	0.95	-0.61	-0.39	-0.03	-0.26	-0.36	-0.86	-0.26	-0.69	-0.90	-0.84	-0.80	-0.69	-0.66
LGR4	0.93	-0.49	0.41	-0.47	-0.59	-1.04	0.47	0.19	-1.07	-1.00	-1.00	-0.81	-0.14	-0.80
EPAS1	0.93	-1.44	-0.78	-3.25	-1.00	-0.94	-0.85	-0.52	-0.78	-0.72	-0.59	-0.79	-0.45	-0.35

B.	GA	wt_LT	GSE_p53	E1A	E7	E2F-DB	pRS_p53	pRS_p21	mir186	mir195	mir218	mir25	mir372	mir423
DEPDC1	-3.27	3.69	3.46	3.62	3.14	3.47	3.16	2.80	2.66	2.86	2.49	2.92	1.73	3.06
DEPDC1B	-3.05	3.26	2.48	4.14	2.62	3.03	2.34	2.29	2.79	2.30	2.70	2.93	1.89	2.64
E2F8	-2.85	3.07	2.70	3.63	2.24	1.52	1.76	1.14	1.66	2.06	1.31	1.86	1.55	0.90
HMGB2	-2.84	2.89	2.45	3.28	2.46	2.46	2.25	1.66	2.37	2.65	2.42	2.59	1.48	2.40
FOXM1	-2.66	2.57	2.19	2.56	2.07	2.31	2.08	1.89	2.53	2.29	2.41	2.26	1.28	2.42
EZH2	-1.88	1.73	1.38	1.51	1.36	1.15	0.97	0.92	1.65	1.68	1.43	1.66	1.06	1.47
B-MYB	-1.85	1.70	1.15	3.15	1.00	1.09	0.98	0.80	1.56	1.60	1.50	1.60	1.85	0.88
HOXA3	-1.73	0.60	1.12	1.38	0.16	0.07	0.34	0.57	0.47	0.80	1.19	0.72	-0.56	0.80
SSRP1	-1.70	1.26	1.15	1.24	1.05	0.83	0.82	0.84	1.38	1.12	1.38	1.28	0.64	1.49
ID1	-1.64	1.51	1.54	0.03	0.85	0.20	0.70	0.76	0.29	0.05	0.08	0.71	0.82	-0.66
H1FX	-1.64	1.65	0.74	2.28	0.86	0.68	0.79	1.05	1.57	1.55	1.50	1.23	0.76	1.11
TOX	-1.56	0.96	0.74	-0.12	0.51	0.91	1.55	0.49	1.30	-0.54	0.40	0.46	0.44	-0.39
BNC1	-1.56	0.81	0.33	0.85	1.58	2.05	0.86	0.68	2.32	2.99	3.22	2.59	-0.34	3.72
HMGB1	-1.54	1.10	1.15	1.17	0.64	0.95	0.90	0.72	0.59	0.81	0.60	0.97	0.64	0.75
WHSC1	-1.52	1.60	1.41	1.10	1.13	1.03	1.03	0.84	1.78	1.40	1.47	1.69	0.98	1.57
PRMT3	-1.51	0.53	0.63	1.15	0.89	1.23	0.72	0.59	0.73	1.25	1.15	0.84	0.03	1.40
H1F0	-1.50	1.16	0.73	1.66	0.34	0.01	0.65	0.34	1.28	1.17	1.03	0.92	0.45	0.27
DLX2	-1.42	-0.56	-0.77	0.44	-0.40	-0.96	-0.55	0.00	-0.15	-0.27	0.11	0.48	0.68	-0.10
YEATS4	-1.39	1.09	1.26	1.31	0.70	0.81	0.44	0.51	0.84	1.07	1.01	1.01	0.58	1.06
C14orf106	-1.38	2.27	1.79	2.32	1.28	1.29	1.45	1.01	0.68	1.06	0.25	1.38	0.87	1.24
ZNF639	-1.34	0.88	1.05	0.27	0.53	0.28	0.53	0.25	0.68	1.01	0.46	0.92	0.49	0.79
ZNF22	-1.34	0.59	0.49	1.03	-0.29	0.24	0.22	0.18	0.97	0.88	0.51	1.22	0.90	0.10
RNF138	-1.30	0.88	0.49	0.99	0.94	0.99	0.62	0.59	0.68	1.01	0.58	0.91	0.72	0.73

Figure 3.1 TFs differentially expressed upon senescence growth arrest (GA).
GA represents the log_2 fold change between CL3^{EcoR} cells at 38°C relative to CL3^{EcoR} cells at 34°C. A. The top 23 up-regulated TFs (positive numbers for log_2 fold change indicated as GA shaded in red). B. The top 23 down-regulated (negative numbers for log_2 fold change indicated as GA shaded in green) TFs are presented. Also shown is the effect on expression when senescence was bypassed using SV40 LT (wt_LT) antigen, HPV16/18 E7, Adenovirus E1A, GSEp53 (dominant negative p53), E2F-DB (dominant negative E2F), p53shRNA (pRS_p53), p21^{WAF1}shRNA (pRS_p21^{WAF1}), miR186, miR195, miR218, miR25, miR372 and miR423. Hence, the log_2 fold change from column 2 onwards indicates expression in various additionally engineered cells where senescence has been bypassed relative to CL3^{EcoR} cells at 34°C. The changes in expression was reversed upon senescence bypass as depicted by the reversal of colour. Log_2 fold change of less than 0.50 and -0.50 is indicated by light red and light green shades respectively. Data source: (Rovillain 2011).

The list of candidate TFs was further refined by performing another overlay. The aim of this second overlay study was to refine the list of identified 462 differential DNA binding factors from the first overlay, to identify TFs for which expression is not only differential when the cells undergo senescence arrest but is also reversed completely when senescence was bypassed upon inactivation of the $p16^{INK4A}$/pRB and/or p53/$p21^{WAF1}$ pathways, or by ectopic expression of miRs that can bypass senescence in $CL3^{EcoR}$ cells (Rovillain 2011).

This reduced the list of candidate TFs to 39 up- and 128 down-regulated which exhibited complete reversal after abrogation of senescence shown in Table 3.1 and Table 3.2 respectively. The overlays were done with the help of Dr. Holger Hummerich, a bioinformatician at MRC Prion Unit who routinely handles large amounts of microarray data and undertakes such analyses for members of the MRC prion unit.

Table 3.1 List of 39 shortlisted differential up-regulated TFs which showed complete reversal after senescence bypass.

	GA	wt_LT	GSE_p53	E1A	E7	E2F-DB	pRS_p53	pRS_p21	mir186	mir195	mir218	mir25	mir372	mir423
GPR155	1.68	-1.27	-1.03	-0.65	-1.07	-1.30	-1.29	-1.11	-1.64	-1.66	-1.69	-1.74	-1.16	-1.81
CD36	1.61	-1.08	-0.61	-1.15	-0.88	-0.90	-0.75	-1.10	-1.76	-1.59	-1.72	-2.07	-1.53	-1.96
ZNF432	1.23	-0.96	-0.85	-0.72	-0.97	-0.86	-0.61	-0.36	-2.17	-2.18	-2.92	-1.97	-1.27	-2.48
RUNX1	1.12	-0.84	-1.03	-1.15	-0.63	-0.71	-0.63	-0.65	-2.25	-1.98	-1.58	-1.88	-1.02	-1.51
AFF1	1.10	-1.03	-0.74	-1.25	-0.52	-0.30	-0.84	-0.87	-0.68	-0.67	-0.50	-0.57	-0.39	-0.22
OSR1	1.10	-0.80	-0.46	-3.54	-1.36	-2.29	-0.94	-0.75	-1.78	-2.91	-2.93	-2.92	-0.58	-4.07
FAM44A	1.09	-0.73	-0.56	-0.88	-0.68	-0.76	-0.85	-0.81	-0.54	-0.89	-0.43	-0.79	-0.56	-0.78
CREB3	1.05	-0.84	-0.67	-0.85	-0.51	-0.47	-0.55	-0.62	-0.65	-0.68	-0.58	-0.78	-0.34	-0.79
FAM171B	0.95	-0.61	-0.39	-0.03	-0.26	-0.36	-0.86	-0.26	-0.69	-0.90	-0.84	-0.80	-0.69	-0.66
EPAS1	0.93	-1.44	-0.78	-3.25	-1.00	-0.94	-0.85	-0.52	-0.78	-0.72	-0.59	-0.79	-0.45	-0.35
ZNF846	0.88	-0.88	-0.87	-0.91	-0.59	-0.78	-0.44	-0.26	-1.00	-0.99	-0.91	-1.22	-1.25	-0.95
LARP6	0.87	-1.37	-0.69	-1.77	-0.97	-1.02	-0.52	-0.80	-0.83	-0.98	-0.66	-0.99	-0.49	-0.84
PLXNA3	0.86	-0.61	-0.62	-0.45	-0.61	-0.62	-0.47	-0.56	-1.14	-1.53	-1.40	-1.07	-0.37	-1.38
ETV7	0.83	-1.64	-1.77	-0.63	-0.92	-1.44	-1.69	-1.85	-0.96	-1.54	-1.22	-1.82	-0.71	-1.95
SLC22A4	0.82	-2.28	-1.49	-3.80	-2.01	-1.32	-1.02	-1.13	-0.62	-0.44	-1.01	-0.56	-0.04	-0.41
ZBTB47	0.79	-0.86	-0.18	-1.12	-0.95	-0.96	-0.49	-0.63	-1.13	-0.93	-1.24	-1.14	-0.94	-1.29
ZNF226	0.72	-0.63	-0.52	-0.19	-0.76	-0.47	-0.50	-0.48	-0.91	-0.61	-0.78	-0.62	-0.84	-1.16
NR1H4	0.69	-1.05	-0.83	-1.08	-0.87	-1.05	-0.99	-1.08	-0.73	-0.95	-1.00	-1.18	-0.91	-1.10
PPARA	0.69	-1.01	-0.33	-1.18	-0.83	-0.89	-0.65	-0.64	-0.22	-0.55	-0.56	-0.61	-0.51	-0.50
C5orf41	0.68	-1.15	-0.57	-0.85	-0.96	-1.00	-0.70	-0.72	-1.05	-1.05	-1.08	-1.00	-1.19	-0.62
CUL4B	0.68	-0.87	-0.62	-1.18	-0.55	-0.66	-0.24	-0.65	-0.53	-0.69	-0.92	-0.43	-0.53	-0.49
RARB	0.67	-0.70	-0.99	-0.64	-0.27	-0.56	-0.34	-0.42	-0.04	-1.16	-0.90	-0.80	-0.93	-1.12
KIAA0415	0.65	-0.84	-0.40	-0.78	-0.56	-0.74	-0.90	-0.93	-0.58	-0.53	-0.33	-0.68	-0.67	-0.34
ZNF561	0.60	-0.52	-0.18	-0.64	-0.42	-0.61	-0.60	-0.15	-0.91	-1.28	-1.04	-1.07	-0.62	-1.24
C20orf194	0.58	-0.56	-0.31	-0.73	-0.62	-0.64	-0.43	-0.58	-1.23	-1.23	-1.48	-1.08	-0.22	-1.39
PLXNB3	0.58	-0.42	-0.82	-0.57	-0.27	-0.31	-0.44	-0.16	-1.07	-1.25	-1.00	-1.16	-0.46	-1.25
ZNF691	0.58	-0.43	-0.15	-0.05	-0.27	-0.39	-0.10	-0.05	-0.25	-0.20	-0.13	-0.20	-0.29	-0.41
ZNF557	0.56	-1.14	-0.81	-0.87	-0.65	-0.68	-0.46	-0.34	-0.94	-0.52	-0.60	-0.65	-0.30	-0.70
BCL6	0.53	-0.24	-0.31	-0.84	-0.50	-0.69	-0.33	-0.37	-0.79	-0.74	-1.01	-0.73	-0.27	-0.89
TFEC	0.53	-0.43	-0.37	-0.65	-0.20	-0.20	-0.14	-0.12	-0.56	-0.55	-0.26	-0.78	-0.69	-0.66
ZNF565	0.52	-0.25	-0.24	-0.37	-0.68	-0.88	-0.47	-0.55	-0.88	-0.92	-1.45	-0.67	-0.36	-1.46
NFAT5	0.49	-0.21	-0.12	-0.27	-0.29	-0.28	-0.45	-0.35	-0.86	-0.84	-1.01	-0.57	-0.53	-0.66
CHD6	0.45	-0.47	-0.23	-0.33	-0.48	-0.52	-0.20	-0.18	-0.50	-0.36	-0.87	-0.51	-0.14	-1.00
ZNF419	0.45	-0.62	-0.41	-0.23	-0.48	-0.52	-0.24	-0.25	-0.85	-1.09	-1.01	-0.83	-0.46	-1.41
ZNF319	0.39	-0.63	-0.31	-0.63	-0.45	-0.49	-0.65	-0.62	-0.35	-0.31	-0.17	-0.28	-0.18	-0.30
ZNF277	0.36	-0.62	-0.16	-0.11	-0.35	-0.10	-0.08	-0.44	-0.38	-0.35	-0.39	-0.39	-0.53	-0.11
ZNF627	0.36	-0.40	-0.04	-0.49	-0.40	-0.67	-0.22	-0.21	-0.35	-0.40	-0.31	-0.33	-0.18	-0.64
ZNF771	0.31	-0.33	-0.49	-0.14	-0.25	-0.26	-0.21	-0.13	-0.09	-0.03	-0.11	-0.14	-0.16	-0.15
NFE2L1	0.30	-0.48	-0.32	-0.46	-0.41	-0.37	-0.45	-0.59	-0.57	-0.63	-0.51	-0.68	-0.55	-0.58

Table 3.2 List of 128 shortlisted differential down-regulated TFs which showed complete reversal after senescence bypass.

	GA	wt_LT	GSE_p53	E1A	E7	E2F-DB	pRS_p53	pRS_p21	mir186	mir195	mir218	mir25	mir372	mir423
DEPDC1	-3.27	3.69	3.46	3.62	3.14	3.47	3.16	2.80	2.66	2.86	2.49	2.92	1.73	3.06
DEPDC1B	-3.05	3.26	2.48	4.14	2.62	3.03	2.34	2.29	2.79	2.30	2.70	2.93	1.89	2.64
E2F8	-2.85	3.07	2.70	3.63	2.24	1.52	1.76	1.14	1.66	2.06	1.31	1.86	1.55	0.90
HMGB2	-2.84	2.89	2.45	3.28	2.46	2.46	2.25	1.66	2.37	2.65	2.42	2.59	1.48	2.40
FOXM1	-2.66	2.57	2.19	2.56	2.07	2.31	2.08	1.89	2.53	2.29	2.41	2.26	1.28	2.42
EZH2	-1.88	1.73	1.38	1.51	1.36	1.15	0.97	0.92	1.65	1.68	1.43	1.66	1.06	1.47
B-MYB	-1.85	1.70	1.15	3.15	1.00	1.09	0.98	0.80	1.56	1.60	1.50	1.60	1.85	0.88
SSRP1	-1.70	1.26	1.15	1.24	1.05	0.83	0.82	0.84	1.38	1.12	1.38	1.28	0.64	1.49
H1FX	-1.64	1.65	0.74	2.28	0.86	0.68	0.79	1.05	1.57	1.55	1.50	1.23	0.76	1.11
HMGB1	-1.54	1.10	1.15	1.17	0.64	0.95	0.90	0.72	0.59	0.81	0.60	0.97	0.64	0.75
WHSC1	-1.52	1.60	1.41	1.10	1.13	1.03	1.03	0.84	1.78	1.40	1.47	1.69	0.98	1.57
PRMT3	-1.51	0.53	0.63	1.15	0.89	1.23	0.72	0.59	0.73	1.25	1.15	0.84	0.03	1.40
H1F0	-1.50	1.16	0.73	1.66	0.34	0.01	0.65	0.34	1.28	1.17	1.03	0.92	0.45	0.27
YEATS4	-1.39	1.09	1.26	1.31	0.70	0.81	0.44	0.51	0.84	1.07	1.01	1.01	0.58	1.06
C14orf106	-1.38	2.27	1.79	2.32	1.28	1.29	1.45	1.01	0.68	1.06	0.25	1.38	0.87	1.24
ZNF639	-1.34	0.88	1.05	0.27	0.53	0.28	0.53	0.25	0.68	1.01	0.46	0.92	0.49	0.79
RNF138	-1.30	0.88	0.49	0.99	0.94	0.99	0.62	0.59	0.68	1.01	0.58	0.91	0.72	0.73
KNTC1	-1.19	1.44	1.31	1.05	1.00	0.70	0.81	0.63	0.94	1.22	0.66	1.15	0.55	1.15
DUSP12	-1.16	0.27	0.49	0.34	0.11	0.23	0.28	0.19	0.56	0.48	0.47	0.53	0.41	0.39
TFAM	-1.06	0.70	0.54	0.97	0.78	0.90	0.43	0.47	0.81	0.91	0.92	1.07	0.50	1.20
TEAD4	-1.06	0.93	0.51	1.08	0.71	0.78	0.45	0.36	1.00	1.07	1.24	0.97	0.99	1.08
TCF19	-1.04	1.49	1.27	1.21	1.22	0.89	0.75	0.83	1.37	1.04	1.04	1.11	1.29	0.69
TWIST1	-1.03	1.51	1.45	0.48	0.65	0.41	0.80	0.46	1.26	0.81	0.66	0.82	0.82	0.49
HMGB3	-1.01	1.42	1.48	1.28	1.23	1.36	1.20	1.12	1.69	2.03	1.60	1.80	0.70	1.64
UNK	-1.00	0.43	0.57	0.61	0.24	0.23	0.17	0.28	0.27	0.48	0.40	0.37	0.09	0.23
PCGF6	-1.00	0.50	0.42	0.87	0.65	0.65	0.50	0.46	0.78	1.00	1.10	0.98	0.67	1.25
HMG2L1	-1.00	0.79	0.68	0.73	0.38	0.24	0.23	0.23	0.47	0.55	0.36	0.48	0.13	0.52
CTCF	-1.00	0.83	0.75	0.84	0.47	0.34	0.20	0.22	0.63	0.73	0.50	0.77	0.52	0.52
ZNF496	-0.99	0.39	0.25	0.68	0.18	0.23	0.27	0.15	0.82	0.74	0.45	0.62	0.51	0.46
NUFIP1	-0.98	0.27	0.32	0.01	0.07	0.44	0.28	0.20	0.22	0.48	0.43	0.40	0.30	0.54
HOXA9	-0.94	0.75	1.33	1.82	0.14	0.11	0.48	0.73	0.71	0.32	0.42	0.46	0.49	0.16
DEK	-0.94	1.09	1.08	1.07	0.96	0.86	0.92	0.82	0.69	0.94	0.63	0.96	0.33	1.00
HOXA7	-0.93	0.73	0.99	1.06	0.02	0.13	0.31	0.42	0.64	0.35	0.22	0.41	0.61	0.08
EWSR1	-0.93	0.44	0.54	0.59	0.30	0.24	0.42	0.40	0.56	0.52	0.41	0.66	0.40	0.48
ATF1	-0.93	0.83	1.06	0.36	0.46	0.42	0.56	0.06	0.57	0.65	0.55	0.62	0.06	0.55
ZNF511	-0.92	0.60	0.76	0.60	0.47	0.45	0.24	0.34	1.15	1.29	1.50	1.13	0.59	1.37
PSMD11	-0.91	0.57	0.37	0.65	0.61	0.49	0.22	0.29	0.90	0.90	0.93	0.72	0.25	0.86
ELK4	-0.89	0.25	0.10	0.63	0.34	0.48	0.40	0.39	0.90	1.04	0.89	1.02	0.59	1.14
TTF1	-0.86	0.60	0.59	0.83	0.56	0.73	0.45	0.33	0.64	0.82	0.66	0.78	0.28	1.08
PDS5B	-0.86	0.89	0.81	1.17	0.52	0.87	0.69	0.74	0.30	0.72	0.23	0.94	0.77	0.66
TSHZ1	-0.85	0.87	1.29	0.47	0.10	0.45	0.81	0.80	0.52	0.36	0.14	0.29	0.13	0.24
SF3A3	-0.85	0.55	0.44	0.30	0.47	0.29	0.11	0.22	0.77	0.65	0.68	0.54	0.07	0.61
U2AF1	-0.84	0.74	0.66	0.50	0.60	0.53	0.53	0.49	0.87	0.91	0.79	0.80	0.43	0.84
POGK	-0.84	0.41	0.19	1.10	0.20	0.30	0.12	0.23	0.52	0.44	0.45	0.41	0.39	0.48
HOXA2	-0.83	0.52	0.47	1.06	0.25	0.24	0.26	0.37	0.53	0.28	0.74	0.44	0.04	0.50
CIZ1	-0.83	0.61	0.53	0.44	0.33	0.51	0.33	0.35	0.49	0.43	0.55	0.39	0.06	0.68
ADNP2	-0.83	0.43	0.40	0.58	0.25	0.19	0.23	0.09	0.59	0.72	0.53	0.45	0.22	0.54
RAD51	-0.82	0.87	0.73	1.29	0.67	0.69	0.74	0.44	0.85	0.66	0.79	0.64	0.63	0.57
CBFB	-0.82	0.60	0.24	0.74	0.62	0.67	0.21	0.31	0.53	0.44	0.59	0.76	0.50	0.82
SP3	-0.81	0.43	0.51	0.59	0.34	0.29	0.30	0.22	0.04	0.15	0.07	0.38	0.04	0.19
DUS3L	-0.81	0.47	0.14	0.30	0.28	0.53	0.25	0.25	1.21	1.29	1.31	0.98	0.72	1.27
NRF1	-0.80	0.62	0.48	0.63	0.31	0.36	0.41	0.24	0.69	0.56	0.54	0.61	0.28	0.45
UBE2K	-0.78	0.36	0.54	0.14	0.20	0.12	0.17	0.10	0.27	0.09	0.07	0.44	0.27	0.26
SP1	-0.77	0.93	0.73	0.92	0.44	0.41	0.31	0.32	0.85	0.63	0.65	0.72	0.25	0.74
PHB2	-0.77	0.49	0.52	0.76	0.40	0.49	0.36	0.34	0.63	0.65	0.79	0.62	0.38	0.66
DMAP1	-0.77	0.48	0.54	0.84	0.34	0.33	0.35	0.29	0.64	0.52	0.56	0.43	0.39	0.30
FOXK2	-0.76	0.27	0.26	0.36	0.28	0.32	0.27	0.05	0.77	0.65	0.75	0.43	0.23	0.52
ZNF326	-0.75	0.36	0.80	0.19	0.20	0.33	0.35	0.24	0.45	0.73	0.59	0.66	0.28	0.93
TFDP1	-0.75	1.09	0.71	0.98	0.80	0.74	0.41	0.53	0.93	0.96	0.97	0.84	0.49	0.95
MTA1	-0.73	0.92	0.86	1.31	0.32	0.38	0.26	0.19	0.32	0.62	0.63	0.37	0.17	0.51
GTF2F1	-0.73	0.31	0.25	0.14	0.20	0.20	0.14	0.06	0.52	0.48	0.56	0.39	0.09	0.44
POLE3	-0.71	0.77	0.85	0.70	0.81	0.85	0.59	0.45	0.82	0.84	1.14	0.86	0.29	1.17
NOC4L	-0.71	0.26	0.12	0.08	0.19	0.49	0.33	0.20	0.73	0.93	0.68	0.62	0.28	0.69
GLI3	-0.71	0.59	0.29	0.29	0.21	0.13	0.22	0.12	0.88	0.91	0.60	0.69	0.45	0.66

....

....

	GA	wt_LT	GSE_p53	E1A	E7	E2F-DB	pRS_p53	pRS_p21	mir186	mir195	mir218	mir25	mir372	mir423
SLC30A9	-0.70	0.54	0.66	0.55	0.49	0.56	0.19	0.04	0.43	0.22	0.27	0.63	0.28	0.50
PPP2R3B	-0.70	0.28	0.29	0.59	0.30	0.33	0.34	0.16	1.02	1.07	1.05	0.79	0.62	1.10
PSMD12	-0.69	0.20	0.32	0.38	0.41	0.52	0.20	0.23	0.63	0.57	0.56	0.75	0.40	0.82
MRPL28	-0.69	0.36	0.47	1.00	0.41	0.45	0.24	0.34	0.58	0.53	0.78	0.60	0.28	0.57
THAP11	-0.68	0.49	0.59	0.75	0.27	0.19	0.15	0.31	0.81	0.86	0.75	0.79	0.57	0.56
RBM27	-0.68	0.50	0.60	0.59	0.30	0.35	0.26	0.15	0.08	0.23	0.10	0.46	0.06	0.51
E2F1	-0.68	0.58	0.34	0.47	0.50	0.42	0.39	0.48	0.51	0.52	0.53	0.49	0.41	0.40
SMARCE1	-0.67	0.49	0.56	0.66	0.44	0.54	0.46	0.45	0.60	0.71	0.56	0.61	0.41	0.54
IKZF4	-0.67	0.28	0.25	0.40	0.10	0.04	0.08	0.14	0.38	0.25	0.31	0.22	0.18	0.29
AHCTF1	-0.67	0.53	0.48	0.56	0.39	0.58	0.54	0.48	0.30	0.45	0.03	0.71	0.27	0.93
LARP5	-0.66	0.38	0.30	0.33	0.39	0.35	0.14	0.07	0.22	0.42	0.39	0.50	0.45	0.63
CUL1	-0.66	0.33	0.23	0.27	0.21	0.18	0.28	0.09	0.47	0.55	0.53	0.47	0.30	0.72
ZNF664	-0.65	0.44	0.44	0.94	0.35	0.35	0.11	0.18	0.02	0.27	0.34	0.27	0.13	0.44
COPS3	-0.65	0.63	0.58	0.62	0.74	0.76	0.42	0.45	0.53	0.59	0.71	0.47	0.27	0.59
ZNF530	-0.64	0.28	0.19	0.50	0.17	0.27	0.23	0.26	0.68	0.45	0.42	0.83	0.55	0.38
TCF3	-0.64	0.65	0.59	0.29	0.35	0.33	0.22	0.03	0.65	0.62	0.64	0.55	0.36	0.49
SUZ12	-0.64	0.80	0.58	0.97	0.67	0.87	0.38	0.32	0.42	0.80	0.37	0.63	0.16	0.75
SP4	-0.64	1.06	0.70	1.78	0.70	0.84	0.72	0.69	0.44	0.56	0.30	0.58	0.25	0.62
TCF7L2	-0.63	0.59	0.79	0.79	0.27	0.17	0.24	0.04	0.25	0.44	0.57	0.54	0.20	0.75
RBAK	-0.63	0.27	0.09	0.48	0.11	0.27	0.07	0.09	0.43	0.57	0.64	0.26	0.25	0.55
PRR3	-0.63	0.47	0.19	0.41	0.57	0.33	0.41	0.47	0.75	0.59	0.86	0.63	0.22	0.52
GABPB1	-0.63	0.38	0.15	0.37	0.26	0.25	0.17	0.18	0.62	0.54	0.57	0.64	0.35	0.66
E2F2	-0.63	0.44	0.25	1.01	0.36	0.30	0.26	0.07	0.84	0.83	0.74	0.74	0.27	0.35
CDC5L	-0.63	0.56	0.44	0.54	0.32	0.17	0.32	0.32	0.47	0.54	0.36	0.67	0.35	0.54
ARID2	-0.63	0.60	0.66	1.08	0.32	0.56	0.16	0.24	0.30	0.65	0.35	0.43	0.30	0.64
ZBED3	-0.62	0.70	0.26	1.78	0.54	0.36	0.30	0.08	0.14	0.49	0.50	0.22	0.23	0.01
ZNF207	-0.61	0.31	0.36	0.35	0.29	0.32	0.29	0.24	0.44	0.48	0.42	0.60	0.41	0.43
MATR3	-0.60	0.60	0.63	0.62	0.47	0.40	0.38	0.33	0.21	0.28	0.20	0.56	0.25	0.52
GTF2H2	-0.60	0.27	0.46	0.46	0.31	0.32	0.23	0.09	0.26	0.36	0.30	0.54	0.29	0.43
ZNF828	-0.58	0.61	0.28	0.66	0.25	0.18	0.06	0.05	0.05	0.28	0.04	0.09	0.29	0.13
USP39	-0.58	0.30	0.36	0.47	0.38	0.16	0.24	0.19	0.65	0.54	0.72	0.43	0.23	0.52
HP1BP3	-0.57	0.91	0.81	0.73	0.49	0.33	0.51	0.37	0.46	0.26	0.05	0.49	0.22	0.30
THAP7	-0.56	0.43	0.20	0.37	0.26	0.11	0.26	0.42	0.67	0.67	0.76	0.55	0.55	0.59
NR2C2	-0.56	0.48	0.25	0.32	0.18	0.15	0.09	0.07	0.60	0.67	0.49	0.50	0.15	0.60
NFX1	-0.56	0.38	0.53	0.59	0.41	0.28	0.17	0.35	0.28	0.14	0.16	0.43	0.32	0.39
DOT1L	-0.56	0.57	0.18	0.46	0.18	0.14	0.23	0.19	0.74	0.69	0.41	0.64	0.42	0.25
DPF1	-0.55	0.45	0.32	0.11	0.28	0.31	0.05	0.14	0.13	0.17	0.03	0.31	0.06	0.02
UBTF	-0.54	0.70	0.61	0.69	0.39	0.33	0.35	0.18	0.32	0.17	0.19	0.38	0.17	0.18
DVL2	-0.54	0.44	0.20	0.62	0.34	0.30	0.29	0.32	0.51	0.63	0.51	0.45	0.38	0.46
CHD2	-0.54	0.53	0.78	0.08	0.31	0.21	0.35	0.09	0.21	0.12	0.47	0.13	0.04	0.18
NFYC	-0.52	0.34	0.26	0.10	0.29	0.10	0.24	0.19	0.66	0.39	0.66	0.16	0.16	0.39
MBD3	-0.52	0.43	0.32	0.54	0.31	0.20	0.22	0.21	0.59	0.51	0.50	0.51	0.30	0.47
MYST2	-0.51	0.40	0.44	0.53	0.36	0.45	0.25	0.17	0.46	0.65	0.73	0.46	0.22	0.49
FARSA	-0.51	0.08	0.20	0.12	0.12	0.13	0.29	0.28	0.36	0.28	0.44	0.29	0.12	0.38
EP400	-0.51	0.42	0.43	0.29	0.35	0.45	0.22	0.17	0.57	0.48	0.34	0.42	0.27	0.50
ZFP161	-0.50	0.41	0.35	0.28	0.30	0.32	0.23	0.31	0.57	0.55	0.51	0.43	0.40	0.53
SMAD4	-0.50	0.59	0.73	0.83	0.30	0.28	0.22	0.20	0.27	0.57	0.28	0.27	0.14	0.33
TOE1	-0.49	0.39	0.09	0.23	0.36	0.11	0.34	0.28	0.77	0.72	0.79	0.51	0.25	0.65
ZNF586	-0.48	0.63	0.13	0.84	0.33	0.35	0.34	0.27	0.92	0.53	0.34	0.71	0.68	0.11
TADA2L	-0.48	0.53	0.36	0.68	0.46	0.35	0.31	0.34	0.68	0.70	0.75	0.49	0.45	0.62
MYNN	-0.48	0.68	0.68	0.43	0.48	0.23	0.45	0.31	0.23	0.51	0.12	0.60	0.28	0.49
RBM6	-0.47	0.52	0.37	0.49	0.20	0.44	0.36	0.28	0.17	0.21	0.04	0.22	0.11	0.17
RBM10	-0.47	0.55	0.55	0.61	0.24	0.25	0.21	0.27	0.69	0.67	0.63	0.54	0.38	0.47
FOXJ2	-0.47	0.27	0.49	0.02	0.20	0.14	0.09	0.04	0.31	0.29	0.36	0.26	0.26	0.20
FGD1	-0.47	0.54	0.27	0.18	0.35	0.35	0.22	0.31	0.56	0.64	0.64	0.54	0.41	0.65
ZNF830	-0.46	0.20	0.38	0.49	0.15	0.27	0.12	0.09	0.49	0.59	0.45	0.43	0.21	0.32
ZNF318	-0.46	0.55	0.15	0.55	0.11	0.09	0.19	0.25	0.40	0.29	0.29	0.36	0.39	0.33
ZNF124	-0.44	0.20	0.05	0.80	0.14	0.47	0.47	0.46	0.38	0.43	0.20	0.42	0.21	0.67
STAT3	-0.44	0.79	0.39	0.39	0.41	0.40	0.20	0.17	0.33	0.23	0.56	0.29	0.04	0.63
ZBTB26	-0.37	0.26	0.04	0.40	0.12	0.22	0.34	0.29	0.53	0.72	0.70	0.73	0.24	0.82
FARSB	-0.37	0.24	0.59	0.18	0.41	0.32	0.32	0.28	0.49	0.39	0.36	0.44	0.24	0.38
MLLT1	-0.30	0.57	0.52	0.38	0.29	0.16	0.23	0.16	0.26	0.17	0.10	0.08	0.03	0.12
ZNF839	-0.29	0.28	0.48	0.23	0.03	0.20	0.04	0.08	0.02	0.27	0.38	0.14	0.01	0.40
YBX1	-0.25	0.43	0.30	0.32	0.42	0.46	0.26	0.26	0.32	0.26	0.39	0.29	0.12	0.37

DNA microarray technology has revolutionized and generated a plethora of data related to complex gene expression patterns in cancer. Unfortunately, most of this information is not being utilized by researchers due to lack of a consolidated platform which integrates all the existing available information. This leads to underutilization of the full potential of the data from numerous gene expression profiling studies with microarrays. For this reason, Oncomine (www.oncomine.org), a cancer microarray data base and web based integrated data-mining platform, was designed to provide a unifying bioinformatics resource combining information from over 4700 microarray experiments. As a result, Oncomine contains 65 gene expression datasets comprising nearly 48 million gene expression measurements.

The list of differential TF candidates was further reduced by mining their expression in Oncomine. This is based on the hypothesis that TFs up-regulated in senescence should be down-regulated in cancer whereas those down-regulated upon senescence should be up-regulated in cancer as senescence is the flip side of cancer and needs to be bypassed in cancer (Hanahan and Weinberg 2011). Oncomine data for each of the differential TFs was obtained with the help of Dr. Otavia Caballero who at the time was based at Ludwig Institute for Cancer Research, New York, USA and had access to the Oncomine data base. On analysing the previously obtained list of differential TFs which showed complete reversal, this led to identification of 5 up-regulated and 49 down-regulated TFs, for which expression correlated inversely with cancer as well as showing complete reversal upon senescence bypass (Table 3.3).

Table 3.3 List of TFs exhibiting inverse correlation with cancer from Oncomine database that showed complete reversal upon senescence bypass previously

		Cancer vs. Normal Analysis (March,2011)			Cancer vs. Normal Analysis (November,2011)			Cancer vs. Normal Analysis (March,2014)		
	Fold Change	Upregulated	Downregulated	Number of studies	Upregulated	Downregulated	Number of studies	Upregulated	Downregulated	Number of studies
CD36	1.61	5	21	246	8	55	346	10	76	457
EPAS1	0.93	2	16	242	4	36	334	14	47	445
LARP6	0.87	6	11	203	8	16	280	8	28	391
SLC22A4	0.82	0	18	225	1	23	303	1	23	414
NR1H4	0.69	0	11	246	0	16	324	0	16	436
RBM6	-0.47	3	1	252	4	1	330	7	3	441
MYNN	-0.48	2	0	182	4	0	259	4	4	370
EP400	-0.51	3	0	241						
NFYC	-0.52	4	1	226	4	1	304	4	1	415
MATR3	-0.6	17	1	265	18	1	343	18	2	452
ZNF207	-0.61	7	2	242	10	3	320	13	3	431
PRR3	-0.63	5	3	257	7	3	335			
GABPB1	-0.63	6	2	253	6	2	331	7	2	442
TCF3	-0.64	25	4	266	33	4	344	35	7	455
SUZ12	-0.64	4	2	206	8	2	284	8	2	395
ZNF664	-0.65	2	0	124	2	0	183	2	1	284
SMARCE1	-0.67	13	1	225	15	2	303	16	7	414
E2F1	-0.68	7	2	261	15	2	339	18	4	449
PSMD12	-0.69	9	1	258						
NOC4L	-0.71	5	1	154	5	1	231	5	1	343
MTA1	-0.73	13	1	256	13	1	334	13	1	445
GTF2F1	-0.73	3	1	257	3	1	335	3	3	446
PHB2	-0.77	14	2	268	14	2	346	15	2	457
UBE2K	-0.78	10	1	258	11	2	336	13	2	447
SP3	-0.81	8	1	264	9	3	342	11	5	450
RAD51	-0.82	11	3	245	23	3	323	27	4	434
CBFB	-0.82	23	0	260	32	1	338	33	3	449
CIZ1	-0.83	5	1	232	8	1	310	8	1	421
POGK	-0.84	7	0	155	10	0	232	11	1	343
TTF1	-0.86	7	1	146	7	1	223	7	1	334
PSMD11	-0.91	8	1	254	8	1	330	9	1	441
ZNF511	-0.92	2	0	113	4	0	173	7	0	274
DEK	-0.94	15	2	257	17	3	335	19	3	446
NUFIP1	-0.98	8	1	191	13	1	268	13	1	379
HMG2L1	-1	9	1	220	9	1	298	9	1	409
HMGB3	-1.01	26	2	234	36	2	312	49	2	393
TWIST1	-1.03	15	3	222	21	6	300	22	13	411
TCF19	-1.04	5	0	138	7	0	198	8	0	299
TFAM	-1.06	10	4	263	10	4	341	11	5	452
TEAD4	-1.06	26	0	246	35	0	324	39	0	435
KNTC1	-1.19	19	3	238	43	4	330	51	4	440
C14orf106	-1.38	4	0	180	9	0	271	10	2	382
YEATS4	-1.39	6	2	192	12	3	283	13	3	394
PRMT3	-1.51	3	0	81	9	0	131	9	0	211
WHSC1	-1.52	16	7	231	26	8	323	32	8	434
HMGB1	-1.54	11	0	246	16	1	336	17	3	443
H1FX	-1.64	12	0	220	17	0	312	17	1	423
SSRP1	-1.7	9	1	232	16	1	324	18	1	435
MYBL2	-1.85	20	4	251	45	5	343	51	5	454
EZH2	-1.88	32	4	246	61	6	338	68	6	449
FOXM1	-2.66	37	1	244	61	3	344	75	3	455
HMGB2	-2.84	16	2	206	27	2	298	31	4	409
E2F8	-2.85	11	0	174	21	2	265	27	4	376
DEPDC1B	-3.05	10	0	121	26	1	195	31	1	296

In addition, on carefully analysing the Oncomine data it was observed that some TFs from the previous list of 462 differential TFs that did not show complete reversal upon senescence bypass also exhibited inverse correlation with cancer. As very strict parameters were initially used for refinement (for example only TFs that showed complete reversal for all the multiple different components used for senescence bypass were included), the TFs which did not show complete reversal but exhibited inverse correlation with cancer were also considered relevant to be studied. This led to the identification of 5 other upregulated TFs and 25 down-regulated TFs, shown in Table 3.4.

Table 3.4 List of TFs exhibiting inverse correlation with cancer from Oncomine database that did not show complete reversal upon senescence bypass

		Cancer vs. Normal Analysis (March,2011)			Cancer vs. Normal Analysis (November,2011)			Cancer vs. Normal Analysis (March,2014)		
	Fold Change	Upregulated	Downregulated	Number of studies	Upregulated	Downregulated	Number of studies	Upregulated	Downregulated	Number of studies
NR3C2	1.58	2	21	230	3	48	322	3	57	434
RORA	1.31	2	11	226	5	28	326	3	31	437
RGS7	1.08	1	10	229	2	15	321	2	16	431
DNAJC21	0.81	0	6	139	0	6	199	0	6	300
MXD1	0.65	3	17	268	3	28	346	3	34	458
CUL4A	-0.47	8	1	257	9	1	335			
TFCP2	-0.49	4	1	256	4	1	334			
ZNF280C	-0.52	6	0	107	12	0	167	12	0	238
IFI16	-0.52	43	2	266	46	5	344	54	6	455
LARP4	-0.54	7	2	250	12	2	328	18	2	439
RBM22	-0.55	5	2	209	5	2	286	5	2	397
AEBP2	-0.55	7	1	142	7	1	202	8	1	303
LARP1	-0.57	7	2	240	10	2	318	11	2	429
PRRX1	-0.6	18	1	216	20	1	294	31	5	405
GLIS2	-0.6	11	0	136	11	0	196			
SMARCA5	-0.63	9	1	236	12	1	314			
MET	-0.63	34	10	252	47	14	330			
ADNP	-0.65	15	0	229	20	0	307	20	2	418
ARNTL2	-0.68	19	0	150	26	1	227			
GATAD2B	-0.69	5	0	144	5	0	204	5	1	305
SMARCC1	-0.71	22	3	250	31	4	328	32	5	439
CEBPG	-0.71	12	3	254	14	3	332	15	3	443
ETV4	-0.77	16	2	179	22	2	239	30	2	340
PATZ1	-0.8	12	2	226	14	2	304	15	2	415
DNAJC2	-0.84	8	2	255	10	2	331	10	2	440
ZNF107	-0.9	13	1	186	14	1	263	17	1	374
MYBL1	-0.93	17	5	243	20	5	319	21	10	409
TCF4	-1.05	29	15	265	32	16	343	35	21	454
ETS1	-1.18	5	0	226	8	2	326	9	11	438
ZNF22	-1.34	7	3	250						

After considering all the above described refining strategies and combining the TFs from Table 3.3 and Table 3.4, the following up-regulated and down-regulated TFs indicated in Table 3.5 and Table 3.6 were shortlisted and prioritized to be included in this study, along with $p21^{WAF1}$, RELA, RELB and CEBPβ because of their previously known role in senescence.

Table 3.5 List of upregulated TFs shortlisted to investigate their functional role which exhibited both reversal upon senesce bypass and inverse correlation with cancer

CD36	NR1H4
DNAJC21	NR3C2
EPAS1	RGS7
LARP6	RORA
MXD1	SLC22A4

Table 3.6 List of downregulated TFs shortlisted to investigate their functional role which exhibited both reversal upon senescence bypass and inverse correlation with cancer

ADNP	ETS1	LARP1	PRR3	TEAD4
AEBP2	ETV4	LARP4	PRRX1	TFAM
ARNTL2	EZH2	MATR3	PSMD12	TFCP2
B-MYB	FOXM1ΔNΔKEN	MET	RAD51	TTF1
C14ORF106	GABPB1	MTA1	RBM22	TWIST1
CBFB	GATAD2B	MYBL1	RBM6	UBE2K
CEBPG	GLIS2	MYNN	SMARCA5	WHSC1
CIZ1	GTF2F1	NFYC	SMARCC1	YEATS4
CUL4A	H1FX	NOC4L	SMARCE1	ZNF107
DEK	HMG2L1	NUF1P1	SP3	ZNF207
DEPDC1B	HMGB1	PSMD11	SSRP1	ZNF22
DNAJC2	HMGB2	PATZ1	SUZ12	ZNF280C
E2F1	HMGB3	PHB2	TCF19	ZNF511
E2F8	IF16	POGK	TCF3	ZNF664
EP400	KNTC1	PRMT3	TCF4	

3.2 Preparation of constructs for modulating expression

3.2.1 Objectives

To study the functional role of the candidate TFs in our model system, i.e. $CL3^{EcoR}$ cells, our aim was to prepare desired lentiviral constructs. For downregulated TFs, full length lentiviral constructs were prepared. The two commonly used lentiviral vectors in this study for ectopically expressing downregulated TFs were pLX301 and pLEX-MCS. For upregulated TFs, the pGIPZ lentiviral vector has been used (Figure 2.1). The reason for specifically using these vectors is firstly because they use the CMV promoter to drive gene expression. Secondly, as $CL3^{EcoR}$ cells are G418, hygromycin and blasticidin resistant, these vectors confer puromycin resistance as the mammalian selection marker. The objective of this section was to prepare the lentiviral constructs for TFs which were studied for their biological role in this study.

3.2.2 Cloning of expression constructs

3.2.2.1 Gateway recombination cloning of the expression constructs

Some of the constructs used in this study were previously cloned by Prof. Parmjit Jat. To complete the list, the remaining constructs mentioned in the Table 3.7 below were ordered as full length Gateway entry vectors from DNASU plasmid repository https://dnasu.org/DNASU/ and were cloned into the pLX301 destination lentiviral vector using the Gateway recombination cloning technology described in methods section 2.9.7. Most of the Open Reading Frames (ORFs) of clones were ordered from DNASU plasmid repository apart from PSMD11, which was a kind gift from Dr. David Vilchez, University of Cologne, Germany and C14ORF106, Gateway entry clone that was purchased from the Human gene and protein database, Japan http://hgpd.lifesciencedb.jp/cgi/ (Goshima et al. 2008). After gateway recombination cloning, each construct was sequence verified before studying its bypass potential.

Table 3.7 List of TFs cloned by Gateway Recombination Cloning

NUF1P1	E2F8	RBM6
TCF4	RBM22	MYB
MTA1	NFYC	ZNF626
GABPB1	ZNF280C	LARP4
PRR3	TFCP2	C14ORF106
B-MYB	DNAJC2	TTF1
CUL4A	YEATS4	PRRX1
AEBP2	HMGB3	TEAD4
Full length LIN9	PSMD11	

3.2.2.2 Cloning of KNTC1

Full length ORF gateway entry clone for KNTC1 was not available from any repository but a cDNA clone in pBluescript (pBS) was kindly provided by Dr. Andrea Musacchio, Max Planck Institute of Molecular Physiology, Germany. The objective was to clone the full length ORF for KNTC1 into pLEX-MCS.

The first step was to confirm the pBS-KNTC1 provided; pBS-KNTC1 was transformed, plasmid DNA isolated and the ends of the clone were sequence verified using M13 forward and reverse primers detailed in Table 3.8. Upon sequencing, it was observed that there was an additional ATG very close to the ORF, and extra nucleotides present at the 3' end. Therefore, the 5'- and the 3'-end required trimming. Hence, PCR amplification was performed to amplify the KNTC1 ORF.

Table 3.8 M-13 Primers

Primer	**Sequence 5'→3'**
M13F	GTAAAACGACGGCCAG
M13R	GAAACAGCTATGACCATG

Initially, the PCR reaction was set up using primers mentioned in Table 3.9 with Vent DNA polymerase enzyme. Spe1 and Not1 site, were used in the forward and reverse primers (highlighted in orange) for cloning KNTC1 into pLEX-MCS (Figure 3.2) vector as they are single unique cutters and not present within the KNTC1 ORF.

Table 3.9 Primers used to amplify TF KNTC1

Primer	**Sequence 5'→3'**
KNTC1F	CGCGCACTAGTCATGTGGAATGATATTGAGCTGC
KNTC1R	CAGCGGCCGCTTACGATAATCCACTAAGAAACATCTTC

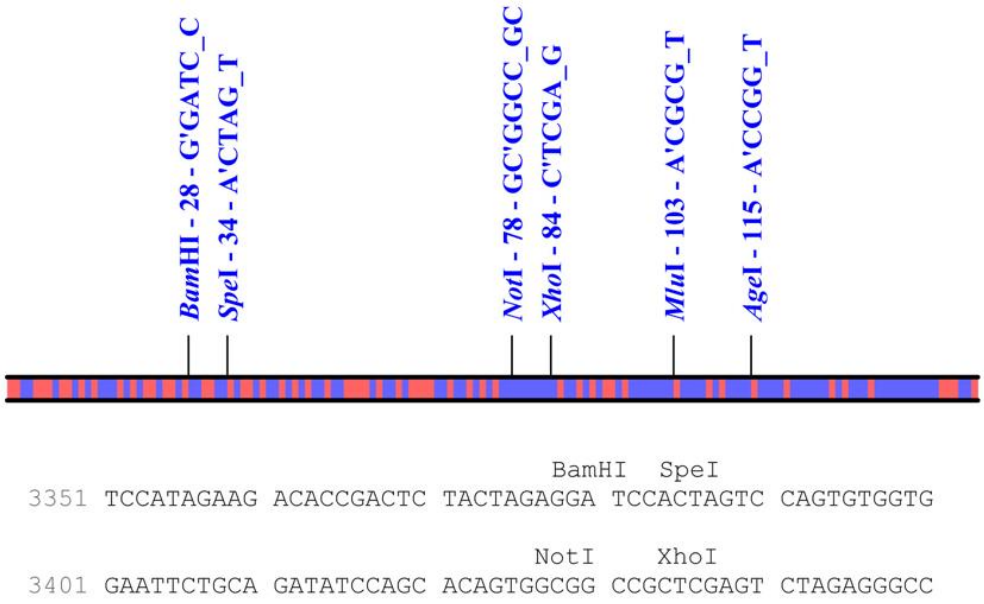

Figure 3.2 Polylinker site of pLEX-MCS lentiviral vector

Unfortunately, the PCR amplification did not work. Hence, the PCR amplification reaction was optimized using different Mg^{++} concentrations and using a different high-fidelity polymerase called, Phusion DNA polymerase. Phusion DNA polymerase was used because it can generate long amplification products with very high accuracy and speed which was previously not attainable by a single enzyme. Phusion DNA polymerase is 52 times more accurate than *Taq* DNA

polymerase and up to 6 times more accurate than *Pfu* DNA polymerase. The reason for the observed high fidelity and robust amplification by Phusion DNA polymerase lies in its unique structure in which a novel Pyrococcus like enzyme is fused with a processivity-enhancing domain. This leads to tenfold greater processivity than *Pfu* DNA polymerase and twice that of *Taq* DNA polymerase.

Melting temperatures and annealing temperatures for the primers were predicted using the Thermoscientific website (www.thermofisher.com/tmcalculator). The following PCR amplification reaction described in Table 3.10 was set up using the Phusion DNA polymerase with varying Mg++ concentrations.

Table 3.10 PCR amplification reaction to amplify TF, KNTC1

Component	**50 µl Reaction**	**Final Concentration**
Water	Add to 50 µl	
5X Phusion HF Buffer	10 µl	1X
10 mM dNTPs	1 µl	200 µM each
10 µM Forward primer	2.5 µl	0.5 µM
10 µM Reverse primer	2.5 µl	0.5 µM
Template DNA	10 ng	<250 ng
DMSO	1.5 µl	3%
Phusion DNA polymerase	0.5 µl	U/µl
50 mM $MgCl_2$	0 µl, 1 µl, 2 µl, 5 µl	

PCR cycling conditions used for the amplification are described in Table 3.11. As the annealing temperature calculated using Thermoscientific website was 72°C, it was decided first to carry out a few cycles (5 cycles), at a slightly lower annealing temperature i.e. 65.7°C as this was the annealing temperature predicted for the primer sequence that is homologous to KNTC1.

Table 3.11 PCR cycling conditions used to amplify TF KNTC1

Cycle Step		Temperature	Time	Cycles
Initial Denaturation		98°C	30 seconds	1
Shorter version	Denaturation	98°C	10 seconds	5
	Annealing	65.7°C	20 seconds	5
	Extension	72°C	3 minutes	5
Longer version	Denaturation	98°C	10 seconds	25
	Annealing and Extension	72°C	3 minutes	25
Final extension		72°C	5 minutes	1
		4°C	hold	1

Use of high fidelity Phusion DNA polymerase indeed improved the amplification of KNTC1 very efficiently. A correct sized band was obtained as indicated in the Figure 3.3 below for all Mg++ concentrations studied, the band obtained at 1 µl $MgCl_2$ (Lane 4) looked the best.

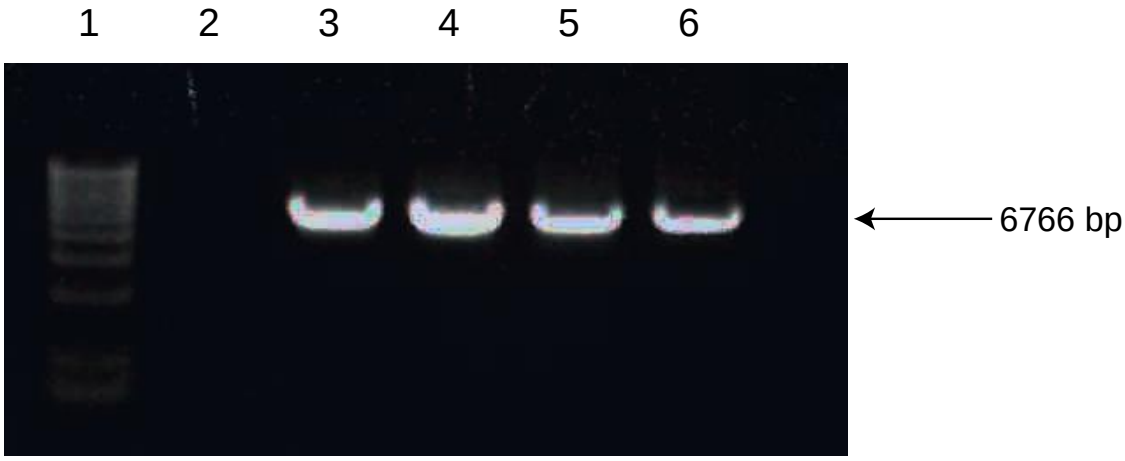

Figure 3.3 Amplification of TF KNTC1.
Amplified PCR product was run on 1.4% agarose gel. Lane 1: Ladder; Lane 2: No DNA negative control; Lane 3: 0 µl $MgCl_2$; Lane 4: 1 µl $MgCl_2$; Lane 5: 2 µl $MgCl_2$; Lane6: 5 µl $MgCl_2$

To clone the amplified KNTC1 product into the desired pLEX-MCS lentiviral vector, amplified DNA was purified and digested with Spe1 and Not1; pLEX-MCS vector was similarly digested. The digested insert and vector were purified and ligated overnight at 16°C. The ligation reaction was used to transform JS4 competent cells. Colonies obtained were picked and used to inoculate LB superbroth and plasmid DNA was isolated. To check for the presence of the correct KNTC1 insert into the pLEX-MCS vector, isolated plasmids were digested with Xho1 and also double digested with BamH1 and Not1 as KNTC1 ORF has an internal BamH1 restriction site, to confirm for the presence of correct insert.

Table 3.12 Primers used to sequence verify the KNTC1

Primer	**Sequence 5'→3'**
KNTC1SQ1	GTTCCAGCTGATAGACAA
KNTC1SQ2	GACCAGAAAAATTCAGTG
KNTC1SQ3	CAACTGGTGAAACAGCAC
KNTC1SQ4	CTGAATCTTCCTTCCATG
KNTC1SQ5	CTCAGTACTGATGCCCCAG
KNTC1SQ6	GTTCCTTCAAGATATCTG
KNTC1SQ7	CACAGCCACGAGTCCATG
KNTC1SQ8	GAAGAGACACTGAAGAGC
KNTC1SQ9	GCAGTCTAGTTTGGGCAG
KNTC1SQ10	CAGAGTGCTGAAGACAGG
KNTC1SQ11	CTCCTGTAAGCTAGCAAC
KNTC1SQ12	GCAACGTGATCAACTCTC
KNTC1SQ13	GACATCTGAGTACTAACAC
KNTC1SQ14	GAACCATCCTTCTCAATG

After carefully analysing the bands obtained after further digests most of the clones look correct but the best five were chosen for sequence verification. Sequencing for all five clones chosen was undertaken using multiple overlapping

primers that enabled the sequence to be read forward and backwards (Table 3.12). After sequence analysis, it was found that clone 1 had the correct sequence.

3.2.3 Lentiviral silencing constructs

Some shRNA constructs for upregulated TFs were already present in our lab. To be able to test each upregulated TF with multiple shRNAs more lentiviral pGIPZ shRNAmir constructs corresponding to each up-regulated TF mentioned below in Table 3.13 were obtained from UCL RNAi silencing consortium. Each of the lentiviral pGIPZ shRNA hairpin-containing bacteria was obtained as a LB agar stab culture. Bacteria from the top of the stab culture for each hairpin were streaked on a LB agar plate containing zeocin (25 µg/ml) and carbenicillin (100 µg/ml). Bacteria were allowed to grow overnight at 37°C, single colonies were picked, and plasmid DNA isolated. To confirm the clones have the correct hairpin sequence, the plasmid DNA obtained was sequence verified before packaging into lentiviruses.

Table 3.13 List of shRNA constructs

Up-regulated TF	pGIPZ shRNAmir Construct
NR1H4	V3LHS_311034 V2LHS_50021
LARP6	V3LHS_412840 V3LHS_412841
EPAS1	V2LHS_113750 V3LHS_402392 V3LHS_318637 V3LHS_318640
RGS7	V2LHS_32635 V3LHS_407580
CEBPβ	V3LHS_371451 V3LHS_371449
RELA	V3LHS_633760 V2LHS_98065

3.3 Senescence bypass potential of TFs downregulated during senescence, upon ectopic expression

3.3.1 Objectives

After successful cloning of TFs in an appropriate lentiviral vector, the next step was to study the biological effect of the shortlisted TFs in $CL3^{EcoR}$ cells. Hence, the main objective here was to determine if ectopic expression of down-regulated TFs individually, can bypass senescence.

Full length lentiviral expression constructs for each shortlisted down-regulated TF prepared either in pLX301 or pLEX-MCS lentiviral vector were used. The expression constructs were tested in the senescence bypass assay by

packaging as lentiviruses and stably transducing the CL3^{EcoR} cells. This leads to stable integration of the ectopically expressed TF into the genome of the host cell. 35,000 stably transduced cells were assayed for bypass of senescence by determining the number of densely growing colonies of cells at the high non-permissive temperature after 3 weeks in culture. As negative control, RAD51 and empty vector pLX301 were used. RAD51 was used as a negative control because previous work by other rotation students showed that it does not bypass senescence.

These studies will enable us to determine if ectopic expression of any of the down-regulated TFs, bypasses senescence, if yes, then how efficiently.

3.3.2 Preliminary experiment to test shortlisted down-regulated TFs

To identify downregulated TFs that have the potential to bypass senescence individually, a bypass assay was performed by ectopically expressing the downregulated TFs, mentioned in Table 3.14.

Table 3.14 Downregulated TFs tested in the preliminary experiment

B-MYB	FOXM1ΔNΔKEN*	MATR3	RAD51
E2F1	GTF2F1	MYNN	TWIST
ETV4	HMG2L1	NUF1P1	UBE2K
EZH2	HMGB2	PATZ1	

*FOXM1ΔNΔKEN is a constitutively active version of FOXM1 that was previously shown to be capable of bypassing senescence (Rovillain et al. 2011).

Lentiviruses were prepared by transient transfection of HEK293T cells using the three-plasmid transfection procedure. 1.5 µg of DNA was transfected for constructs mentioned in Table 3.14 along with 1 µg of packaging vectors, i.e. pMDG and p8.91, to make lentiviruses. Infections were done in duplicate for each TF, in CL3^{EcoR} cells using the 5 ml of lentiviruses made. To aid infection polybrene was used at 8 µg/ml. Successfully transduced cells were selected using puromycin at 2 µg/ml as the lentiviral vectors confer puromycin resistance as a mammalian selection marker. After allowing minimum of two days for successfully infected cells to grow, 35000 cells were counted and plated in

duplicate in T-75 flasks. The next day cells were shifted to the non-permissive temperature, i.e. 38.5°C, to assess the senescence bypass potential of each of the TF. After three weeks, flasks were stained with 2% methylene blue to count the number of densely growing blue colonies.

Unfortunately, none of the TFs studied in this preliminary experiment showed a significant bypass potential (data not shown). pLX301 and RAD51 were used as the negative controls. Ectopic expression should be further confirmed by either RT-PCR or western blotting if an antibody is available. This will be particularly important if the TF does not exhibit any bypass activity, to ensure that lack of activity was not due to lack of expression.

3.4 Optimization and refinement of different parameters to maximize efficiency of the senescence bypass assay.

As none of the downregulated TF tested in the previous preliminary experiment showed any bypass potential, it was decided to optimize and refine the different parameters of the senescence bypass assay to maximize its efficiency. Previous work in the laboratory had shown that B-MYB bypasses senescence efficiently in $CL3^{EcoR}$, whereas RAD51 was consistently negative. Although B-MYB did not show any bypass potential when tested in the previous experiment, for the different parameters discussed below, the efficiency of the senescence bypass assay was assessed and compared using B-MYB and RAD51. The number of blue spots observed on flasks after staining with methylene blue depicts healthy growing colonies of cells and therefore is a measure of the bypass potential.

3.4.1 Temperature

The model of study used in this thesis i.e. $CL3^{EcoR}$ cell line, is a conditionally immortalised stringently temperature sensitive cell line. Temperature therefore, is a crucial factor. One possibility owing to why none of TF tested in the previous experiment showed significant bypass potential can be the high non- permissive temperature. Hence, to determine the optimum temperature for the senescence bypass assay, experiments were undertaken at different temperatures.

$CL3^{EcoR}$ cells are immortal at 33-34°C but undergo growth arrest upon shift to a higher temperature where the tsSV40LT antigen (U19tsA58) is inactivated. It has been previously shown in the laboratory that irreversibility of the growth arrest is dependent upon temperature. If the non-permissive temperature to which the cells are shifted is raised quite high, nothing grows. However, if the temperature is too low, growth arrest can still occur but there is background due to some cells escaping growth arrest. At 37°C, the growth arrest is reversible whereas at temperature >38°C, it is irreversible (Rovillain et al. 2011).

Hence, in the beginning to ensure the assay would work, the temperature was reduced to as low as 37.5°C. It was found that 37.5°C gave background in the negative controls. The background was reduced significantly when the temperature was increased to 37.8°C as shown in Figure 3.4. This depicts how wonderfully the $CL3^{EcoR}$ model system is conditioned with regards to temperature. The stringency of the senescence bypass assay can be increased by raising the non-permissive temperature by as little as 0.3°C.

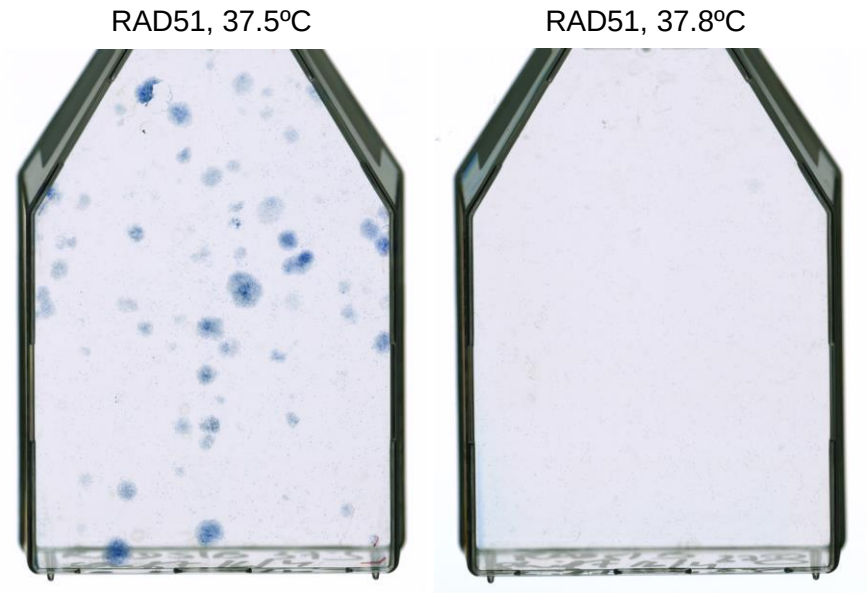

Figure 3.4 Temperature Optimization
Representative images of flasks studied to maximize efficiency of senescence bypass assay with respect to temperature for the negative control (RAD51). Bypass assay was carried out at different non-permissive temperatures i.e. 37.5°C and 38.7°C, at 5% CO_2 and 35,000 cells per T-75 flask. Flasks were stained after three weeks with 2% methylene blue. Background was observed at 37.5°C whereas increasing the temperature by 0.3°C led to a significant reduction of background.

3.4.2 Sequence verification of expression constructs

Since some of the expression constructs had been made previously, sequence verification was undertaken to ensure that they were all correct before testing them for their senescence bypass potential. They were transformed into JS4 cells and fresh plasmid DNA extracted from two independent colonies, followed by setting up the DNA sequencing reaction for all the constructs mentioned in Table 3.15 according to the protocol described in 2.9.6.

Table 3.15 List of TFs tested for sequence verification

ADNP	GLIS2	NOC4L	TCF19
ARNTL2	GTF2F1	NUF1P1	TCF3
B-MYB	H1FX	PATZ1	TEAD4
CBFB	HMG2L1	PHB2	TFAM
CEBPG	HMGB1	POGK	TWIST
CIZ1	HMGB2	PRMT3	UBE2K
DEK	HMGB3	RAD51	WHSC1
E2F1	IFI16	SMARCA5	ZNF107
E2F8	LARP1	SMARCC1	ZNF2017
EP400	MATR3	SMARCE1	ZNF22
ETS1	MET	SP3	ZNF280C
ETV4	MYBL1	SSRP1	ZNF511
EZH2	MYNN	SUZ12	

Sequences were analysed for each of the two different plasmid DNA isolated for each TF. For most of the clones, both the plasmid DNA isolated showed correct sequence, for some, one of them showed correct sequence. This enabled the preparation of a set of sequence verified expression vectors. Only one of the TFs showed incorrect sequence for both plasmid DNA preparations; this was B-MYB.

This explained the previous results for senescence bypass assay, where B-MYB did not show bypass potential.

3.4.2.1 Gateway recombination cloning of B-MYB

As the sequence for TF B-MYB was incorrect, B-MYB was constructed again from the original Gateway entry vector by Gateway Recombination Cloning. After successful recombination cloning, the sequence was verified again. The sequence obtained this time was correct. All future experiments utilised the newly cloned and sequence verified B-MYB.

3.4.3 Clean cell lines

Our senescence bypass assay utilizes two different cell lines, namely HEK293T and $CL3^{EcoR}$. Both cell lines were checked periodically to ensure that they were mycoplasma free. Mycoplasma free clean cultures were expanded and frozen in bulk. The cell lines were only used for two rounds of lentiviral production and lentiviral infection, before a fresh vial of each cell line was revived.

3.4.4 Cell number

Previously in the laboratory (Rovillain et al. 2011), in senescence bypass assays, stably transduced cells derived after puromycin selection were reseeded at 50,000 cells in T-75 flasks and then shifted to a higher non-permissive temperature. Subsequently, the cell number was reduced to 35,000 to lower the background.

To determine which of the two cell numbers produce improved results in this study, experiments were done using the two different cell numbers i.e. 35,000 and 50,000 cells per T-75 flask for both B-MYB as positive control and RAD51 as a negative control.

The fixed number of cells reseeded is crucial as it maintains constant number of cells in a flask for each construct after viral infection which allows accurate and precise quantification and hence increases reproducibility. Ensuring constant cell numbers is also very important as the viral titres vary between constructs and between experiments. This experiment also showed improved and consistent

results when the cell counting was done using C-chip haemocytometer as opposed to a Beckman Coulter Counter.

As we increased the cell number to 50,000, a clear improvement was seen in the extent of senescence bypass for the positive control B-MYB as shown in Figure 3.5. B-MYB cultures at 50,000 cells appear to be densely stained compared to B-MYB cultures at 35000 cells. Also reseeding 50,000 cells for RAD51 did not produce any colonies and no significant background was observed.

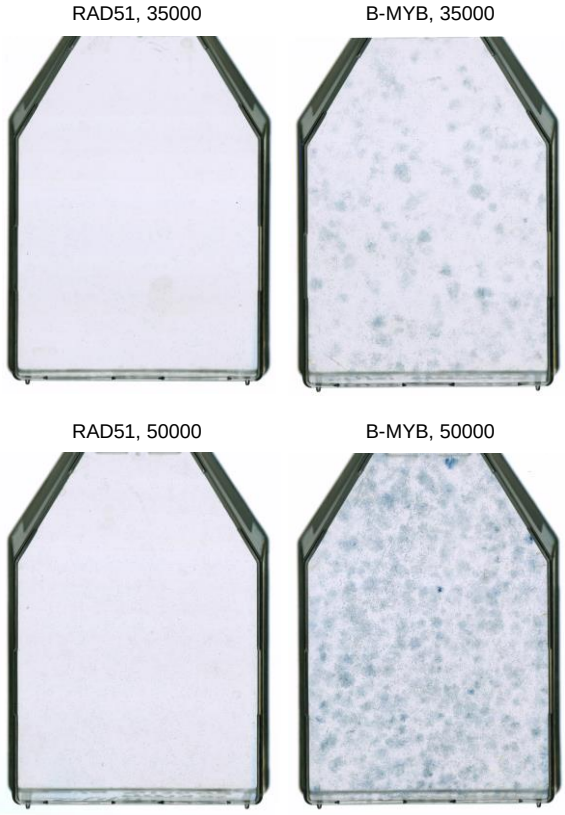

Figure 3.5 Cell number optimization
Representative images of flasks studied to maximize efficiency of senescence bypass assay for the positive control (B-MYB) and negative control (RAD51). Assay was performed by seeding different cell numbers i.e. 35,000 and 50,000 cells per T-75 flask at 5% CO_2 and at 37.8°C. Flasks were stained after three weeks with 2% methylene blue. Reseeding 50,000 cells produced stronger bypass for B-MYB with no background in negative control (RAD51).

Hence, in future experiments, where the bypass assay is required to be performed under less stringent conditions, 50,000 cells can be reseeded to study the bypass potential of TFs as no background was observed for the negative control.

3.4.5 CO_2 level

CO_2, another critical parameter for cell growth in tissue culture, was also optimized to maximize bypass efficiency. The DMEM medium used to culture cells is suitable for growth between 5-10% CO_2. Experiments were therefore undertaken at two different percentage of CO_2, 5% CO_2 and 10% CO_2.

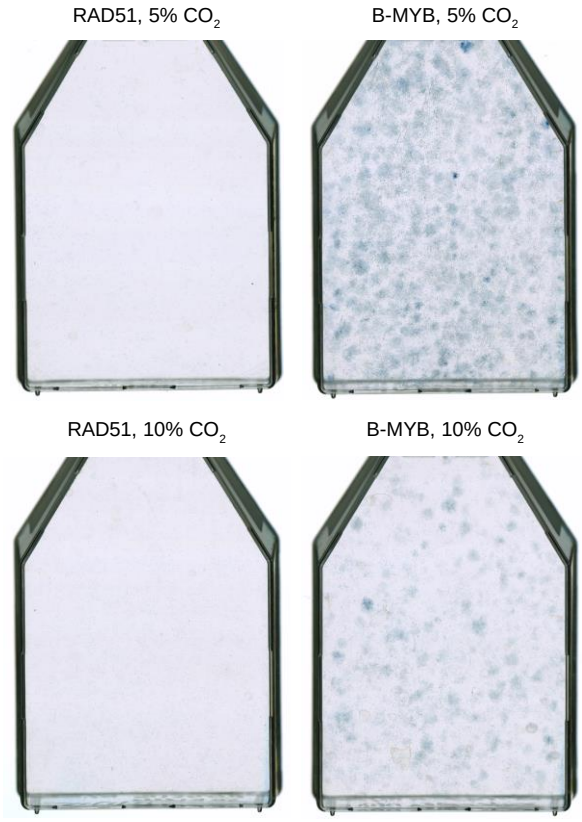

Figure 3.6 CO_2 percentage optimization
Representative images of flasks studied to maximize efficiency of senescence bypass assay for the positive control (B-MYB) and negative control (RAD51). Bypass assay was done at 5% and 10% CO_2 by reseeding 50,000 cells per T-75 flask at 37.8°C. Flasks were stained after three weeks with 2% methylene blue. No background was observed for either CO_2 percentage for RAD51, but a greater number of distinct dark densely stained colonies were observed for 5% CO_2 as opposed to 10% CO_2.

It was observed that under the non-permissive conditions, cells at 10% CO_2 for B-MYB did not appear to be happy and healthy. The cells also appeared to readily detach from the surface of the flask at 10% CO_2. Therefore, for all the future experiments cells were grown at 5% CO_2 as colonies for B-MYB at 10% CO_2 look lightly stained and were fewer in number compared to 5% CO_2 as shown in Figure 3.6.

3.4.6 Infections

To increase the bypass efficiency of the assay, it was important that the infections were highly efficient, and the virus titres were high as possible. To increase the efficiency of infection, the strategy adopted was to perform a double infection which involves infecting cells with fresh virus consecutively for 6-8 hours for a total of about 24 hours rather than a single overnight infection. It was observed that double infections greatly enhanced the efficiency of the senescence bypass assay.

The titre of the virus is very dependent on the HEK293T cells; the healthier HEK293T cells are, the higher is the titre of the virus. To produce viruses in HEK293T cells, transfections were carried out using Fugene (Promega); however, Fugene makes cells clump together. Therefore, an experiment was undertaken to determine the optimum time interval for exposing the cells to Fugene reagent (i.e. 6 hours, 12 hours or 18 hours) such that the cells would clump less. It was found that removal of Fugene 6 hours or 18 hours after addition of transfection mix was acceptable. It was also found that if Fugene containing medium was removed after 6 hours, then Round 2 (virus harvested between 24 to 48 hours) virus was as high titre as compared to Round 1(virus harvested at 24 hours) virus. On the other hand, when Fugene containing medium was removed after 18 hours then Round 1 virus was higher titre than Round 2 virus. The titre of the virus here was estimated by the number of survivors observed after puromycin selection after infecting $CL3^{EcoR}$ cells with these lentiviruses.

3.4.7 Incubation time at non-permissive temperature

To reduce the experiment duration, we also compared the senescence bypass assay results by staining the flasks with methylene blue at the end of two and three weeks. It was observed that two weeks were a little early to visualize large distinct darkly stained densely growing colonies as shown in Figure 3.7. Cultures were therefore always stained after allowing cells to grow at non-permissive temperature for three weeks.

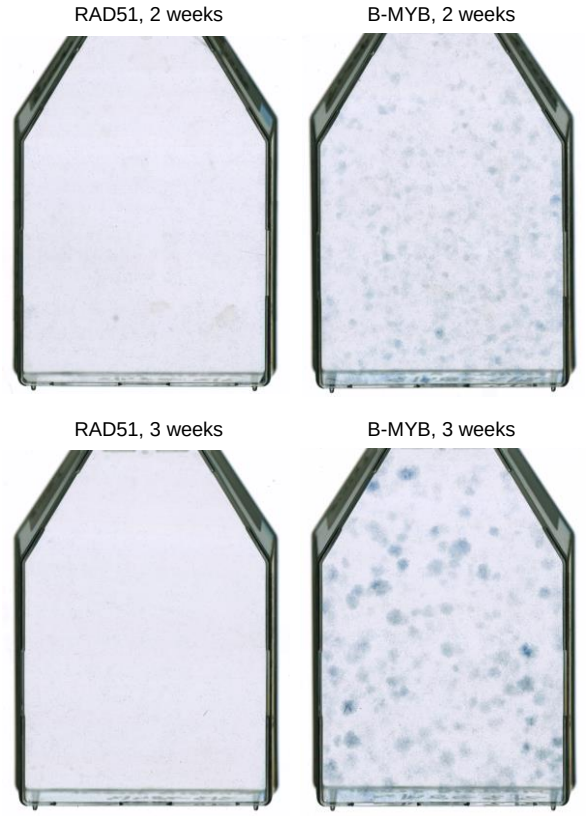

Figure 3.7 Incubation time optimization
Representative images of flasks studied to maximize efficiency of senescence bypass assay for the positive control (B-MYB) and negative control (RAD51). Bypass assay was done at 37.8°C, 5% CO2 and 50,000 cells per T-75 flask. Flasks were stained after incubating cells at 37.8°C for two weeks and three weeks with 2% methylene blue. Colonies obtained after staining the B-MYB flasks after two weeks were very lightly stained and small as compared to colonies obtained after three weeks which were densely stained, dark and large.

3.5 Assessment of senescence bypass potential after standardization of senescence bypass assay

After optimization and refinement of the various parameters of senescence bypass assay, an experiment was designed to study the bypass potential of the downregulated TF mentioned in Table 3.16. Lentiviruses were made for each of the candidate TF in HEK293T cells and used to stably transduce $CL3^{EcoR}$ cells to study the senescence bypass potential following the protocol described in section 2.6. The results obtained by staining the flasks with methylene blue after three weeks at non-permissive temperature are shown below in Figure 3.8.

Table 3.16 TFs studied after optimization of different parameters of senescence bypass assay

B-MYB	FOXM1ΔNΔKEN	MYNN	WHSC1
DEK	HMG2L1A	RAD51	
DEPDC1	HMGB2	TWIST1	
EZH2	MATR3	UBE2K	

No background was observed for the negative control i.e. RAD51. The most interesting result from this experiment is the strong bypass potential observed for B-MYB as significant number of dense dark blue stained colonies were observed. This highlighted the importance of the sequence verification which led to identification of B-MYB clone being incorrect. Spotting the incorrect clone and cloning the correct B-MYB construct, led to the identification of the strong bypass potential of B-MYB as depicted clearly in Figure 3.8. For the remaining TFs studied in this experiment, no significant number of blue colonies were observed. This suggests that these TFs (DEK, DEPDC1, EZH2, FOXM1ΔNΔKEN, HMG2L1A, HMGB2, MATR3, MYNN, RAD51, TWIST1, UBE2K and WHSC1) do not play a critical role in bypassing senescence when studied individually. Other possibility could be that these TFs were not expressed in the cells as biochemical analysis has not confirmed their expression.

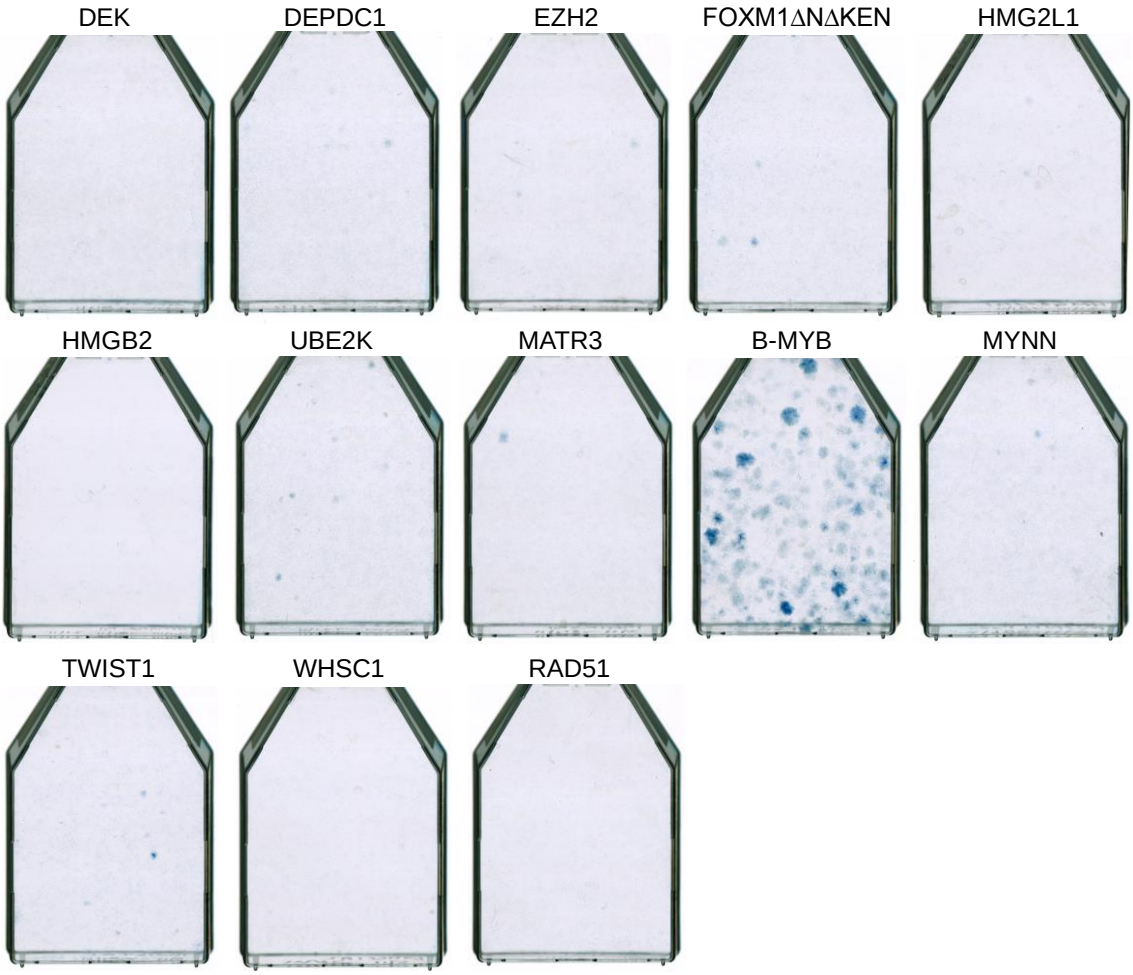

Figure 3.8 Senescence bypass assay of down-regulated TFs examined individually
Representative images of flasks of different TFs studied for their senescence bypass potential. Bypass assay was done at 37.8°C, 5% CO_2 and 50,000 cells per T-75 flask. Flasks were stained after three weeks with 2% methylene blue. RAD51 was used as a negative control. B-MYB displayed the strongest bypass potential among all the TFs studied by producing large, multiple, darkly stained colonies.

3.6 Senescence bypass potential of TFs upregulated during senescence, upon RNA silencing

3.6.1 Objective

The objective of these experiments was to determine if silencing the expression of up-regulated TFs had the potential to individually bypass senescence. Lentiviral pGIPZ shRNAmir constructs corresponding to each up-regulated TF were used to silence expression. To rule out any non-specific bystander effects which might arise due to off-target effects from vector based shRNAs, senescence bypass was studied using at least two or more different shRNAs

targeting the same upregulated TF (Echeverri et al. 2006; Birmingham et al. 2006). It is highly unlikely to be an off-target effect if two or more different shRNAs targeting the same TF, show strong senescence bypass.

Senescence bypass assay was performed to assess the bypass potential as explained in section 2.6. The senescence bypass assay involves packaging the pGIPZ shRNAmir constructs as lentiviruses, followed by infection of $CL3^{EcoR}$ cells and selection for the stably transduced cells in puromycin at 6 µg/ml. High concentration of puromycin (6 µg/ml) was used for selection to enrich for the cells which have the highest expression of the shRNA's to ensure efficient silencing. This had been determined empirically using a $p21^{WAF1}$ shRNAmiR from the pGIPZ shRNAmiR library, by Dr Kat Wanek, a previous PhD student in the laboratory (Wanek 2011). As positive control for these experiments, silencing of $p21^{WAF1}$ was used and pRS Lamin A/C was used as a negative control.

This allowed identification of up-regulated TFs which when silenced, bypass senescence. It also aided in studying the efficiency of senescence bypass and identification of the most active lentiviral pGIPZ shRNAmiR for each TF.

3.6.2 Preliminary experiment to test shortlisted up-regulated TFs

To identify which upregulated TFs have the potential to bypass senescence, preliminary senescence bypass assay was performed by silencing each shortlisted upregulated TF with at least two different shRNAmiRs. Fourteen upregulated TFs were examined once with two different shRNAmiRs, each in duplicate. As positive control for these experiments, silencing of $p21^{WAF1}$ was used and as negative control pRS Lamin A/C was used.

3.6.2.1 Development of an alternative method for analysis of bypass potential

Until now the colonies obtained after three weeks incubation at non-permissive temperature were stained with 2% methylene blue and the dark densely stained colonies were counted manually independently twice by placing the flask on a light box. To cross check the manual count and validate the results obtained, another method was devised to calculate the area of the flask stained in blue. Definiens Developer XD software was used to develop an algorithm. The algorithm was written to: first, identify the flask, exclude the top of the flask and

calculate the surface area of the flask. Additionally, the program could analyse scanned flask images to distinguish between the blue stained area of the flask and the unstained area of the flask. Development of this method required extensive thresholding to be able to specifically pick up the blue stained colonies. The result obtained by the iterative testing of the flasks using the optimised method developed, generated the total area of the flask, area stained in blue and unstained area. Hence, to assess the extent of bypass, percentage area stained in blue was calculated by dividing the area stained in blue to the total area. The program was developed by Dr. Matthew Ellis, Image analyst, Division of Neuropathology, UCL using Definiens Developer XD software.

$$\text{Percentage area stained} = \frac{\text{Area stained in blue } (\text{cm}^2)}{\text{Total flask area } (\text{cm}^2)} \times 100$$

Hence, the bypass results obtained for each experiment undertaken in this study were analysed by manual counting as well as by computational analysis. For each experiment, apart from the representative flask images obtained after staining, corresponding flask images are shown for the alternative method used, where the blue spots indicate the specific blue area included by the software to calculate the area in blue. Therefore, for each experiment, extent of senescence bypass is now verified by both manual counting as well as software analysis. Figure 3.9 shows multiple optimisation and different thresholding of the program, to develop the final version of the analysis method which can specifically pick up blue colonies and provide confirmatory evidence for the manual count.

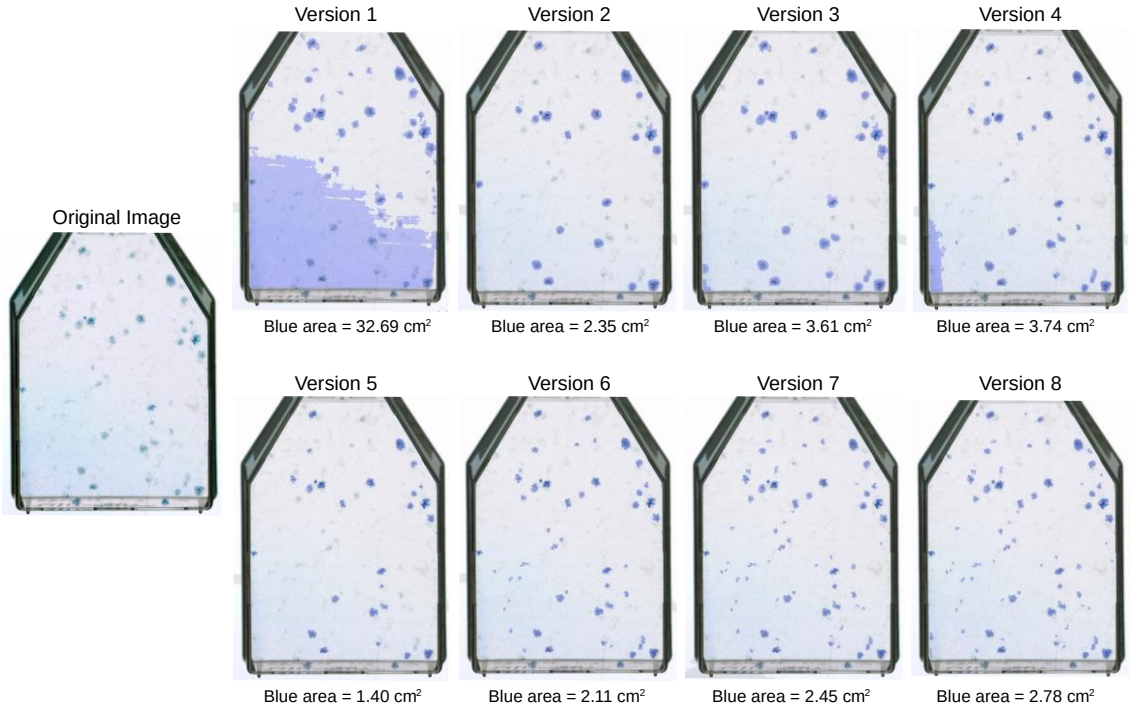

Figure 3.9 Optimisation of the software algorithm
Definiens Developer XD software was used to calculate the area of the flask covered in blue. Multiple different versions of the algorithm were developed to set the threshold to specifically pick blue colonies and to reduce the background picked up as blue. The first version of the algorithm indicated as Version 1 picked up faint shadow of blue present in the original scanned image of the flask as blue. This led to computing high area covered in blue than actual area covered in blue. Various refinements were undertaken to train the program to specifically pick up blue colonies. Area covered in blue calculated by different versions of algorithm is mentioned below each flask.

3.6.2.2 Assessment of senescence bypass potential

For studying the bypass potential of upregulated TFs, silencing of $p21^{WAF1}$ was used as a positive control for these experiments. For ease of representation $p21^{WAF1}$ is discussed here separately as it clearly shows that silencing $p21^{WAF1}$ produces a saturated flask covered with blue spots after staining the healthy growing colonies obtained after the cultures were allowed to grow for three weeks at the non-permissive temperature indicating the strong bypass potential observed after silencing $p21^{WAF1}$ (Figure 3.10). $p21^{WAF1}$ flask is too confluent to be counted manually; therefore, in the experiments discussed below when each up-regulated TF is studied individually, $p21^{WAF1}$ is excluded from analysis. Strong bypass potential would be expected upon silencing $p21^{WAF1}$ because the p53-$p21^{WAF1}$ pathway is a key pathway in manifesting senescence, indicating appropriate use of $CL3^{EcoR}$ model system for studying senescence bypass.

p21

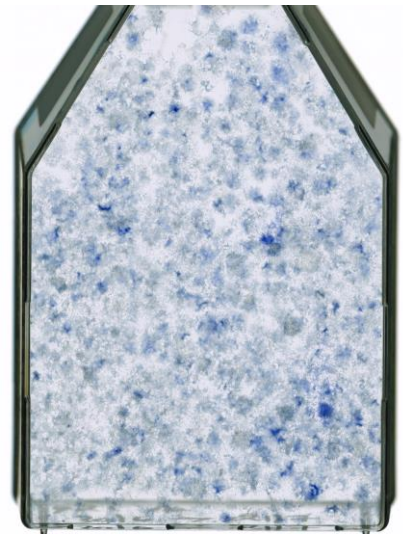

Figure 3.10 Senescence bypass assay after silencing of $p21^{WAF1}$
$p21^{WAF1}$ was silenced using shRNAmiR V2LHS_230370. $p21^{WAF1}$ has been studied multiple times in different independent experiments. Bypass assays were performed at 5% CO_2, 37.8°C and 38.9°C reseeding 35,000 cells as well as 50,000 cells per T-75 flask. Flask was stained with 2% methylene blue after three weeks. Silencing of $p21^{WAF1}$ works very efficiently both under stringent and non-stringent conditions showing the strongest bypass potential resulting in completely saturated flask making it impossible to count individual colonies manually.

RELA is known to have a role in the canonical NF-κB signalling pathway and silencing of RELA has been shown to bypass senescence in $CL3^{EcoR}$ previously (Rovillain et al. 2011). Silencing RELA showed a weak potential to bypass senescence in my experiments as shown in Figure 3.11. Out of the two shRNAmiRs studied, one of them (V2LHS_98066) showed stronger bypass relative to the other (V2LHS_98068). Interestingly, the preliminary experiment identified four other TFs apart from RELA that have for the first-time exhibited some senescence bypass potential, where the extent of bypass was greater than RELA.

Silencing EPAS1 (Endothelial PAS Domain Protein1) using two different shRNAmiRs generated a greater number of dense dark blue stained colonies shown in Figure 3.12. This exhibited the potential of EPAS1 to bypass senescence in $CL3^{EcoR}$ cells. RGS7 (Regulator of G-protein Signalling 7) and LARP6 (La Ribonucleoprotein Domain Family, Member 6) also exhibited same bypass potential which was greater than the negative control. For both RGS7 and LARP6, silencing by one shRNAmiR i.e. V2LHS_32637 for RGS7 and

V3LHS_412842 for LARP6 showed better bypass than silencing with other shRNAmiRs (Figure 3.13 and Figure 3.14). NR1H4(Nuclear receptor sub family 1, Group H, Member 4) showed marginal bypass potential with both different shRNAmiRs as shown in Figure 3.15.

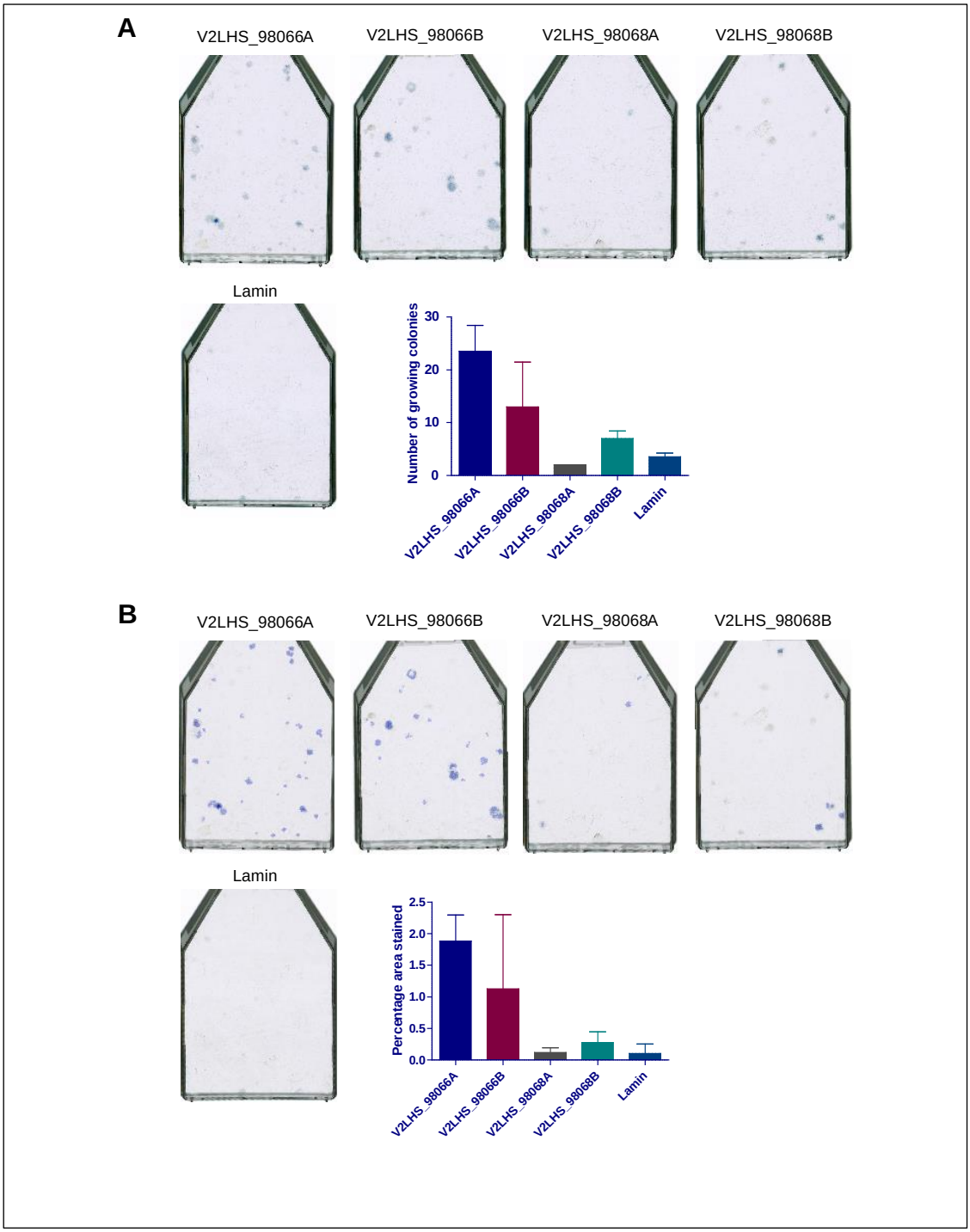

Figure 3.11 Senescence bypass assay after silencing of up-regulated TF, RELA.
RELA was silenced using shRNAmiR V2LHS_98066 and V2LHS_98068 as indicated on top of each representative flask. Assay was performed at 5% CO_2, 37.8°C and at 35,000 cells per T-75 flask. Flasks were stained with 2% methylene blue after three weeks. Silencing of $p21^{WAF1}$ was used as a positive control and silencing of Lamin A/C as a negative control. A) Manual analysis: Representative flask images obtained after staining and quantitative representation of bypass assay depicted graphically by plotting the average number of colonies (+/- SD) obtained after independently counting each replicate twice. B) Computational analysis: Corresponding flask images shown with blue spots depicting the area of the flask computed as blue areas by the computer algorithm and quantitative representation of bypass assay presented graphically by plotting the calculated percentage area (+/- SD) covered in blue by Definiens Developer XD software for each of the replicates.

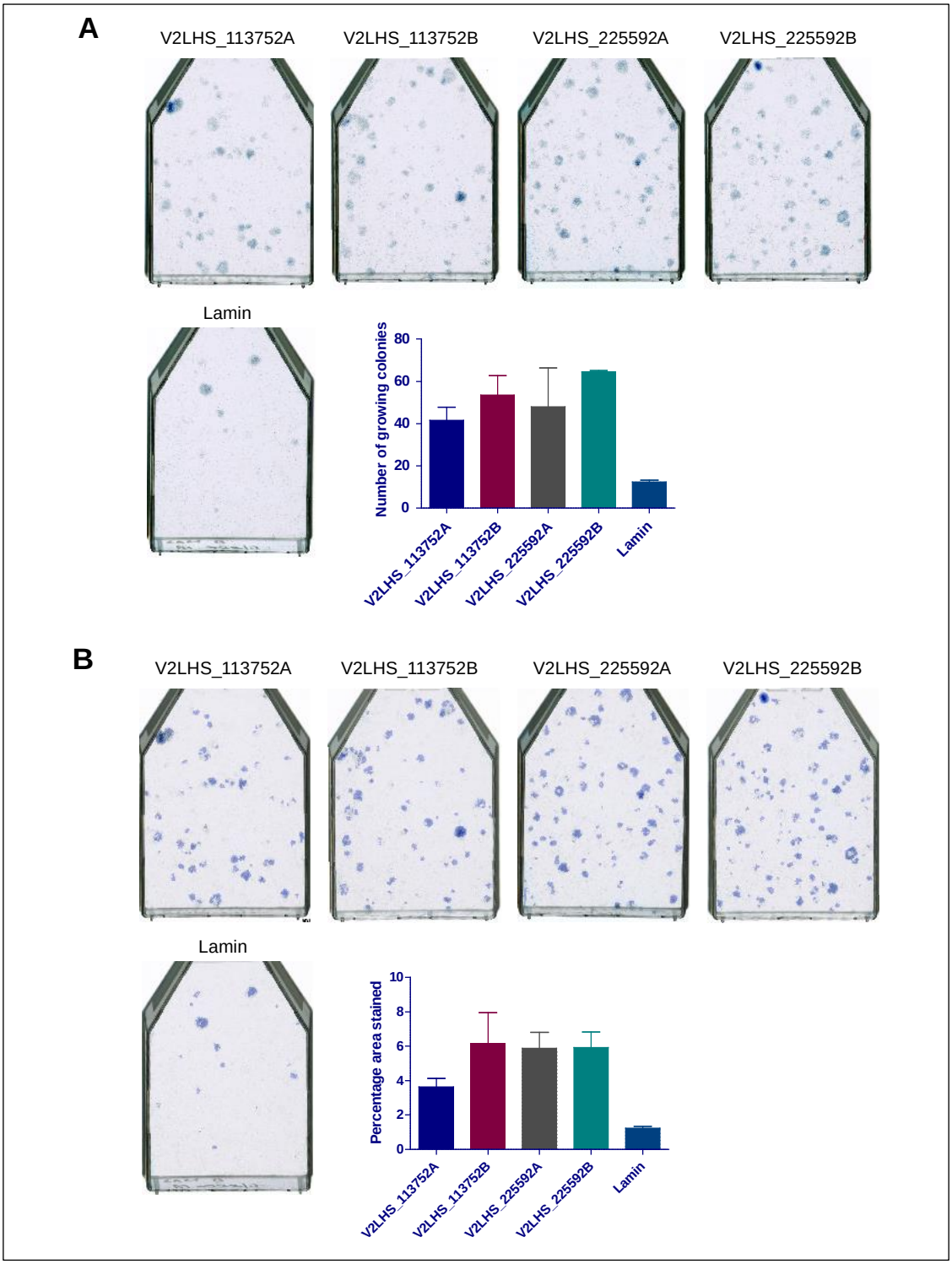

Figure 3.12 Senescence bypass assay after silencing of up-regulated TF, EPAS1.
EPAS1 was silenced using shRNAmiR V2HS_113752 and V2HS_22592 as indicated on top of each representative flask. Both shRNAs showed senescence bypass. Assay was performed as before. A) Manual analysis: Representative flask images obtained after staining and quantitative representation of bypass assay depicted graphically by plotting the average number of colonies (+/- SD) obtained after independently counting each replicate twice. B) Computational analysis: Corresponding flask images shown with blue spots depicting the area of the flask computed as blue areas by the computer algorithm and quantitative representation of bypass assay presented graphically by plotting the calculated percentage area (+/- SD) covered in blue by Definiens Developer XD software for each of the replicates.

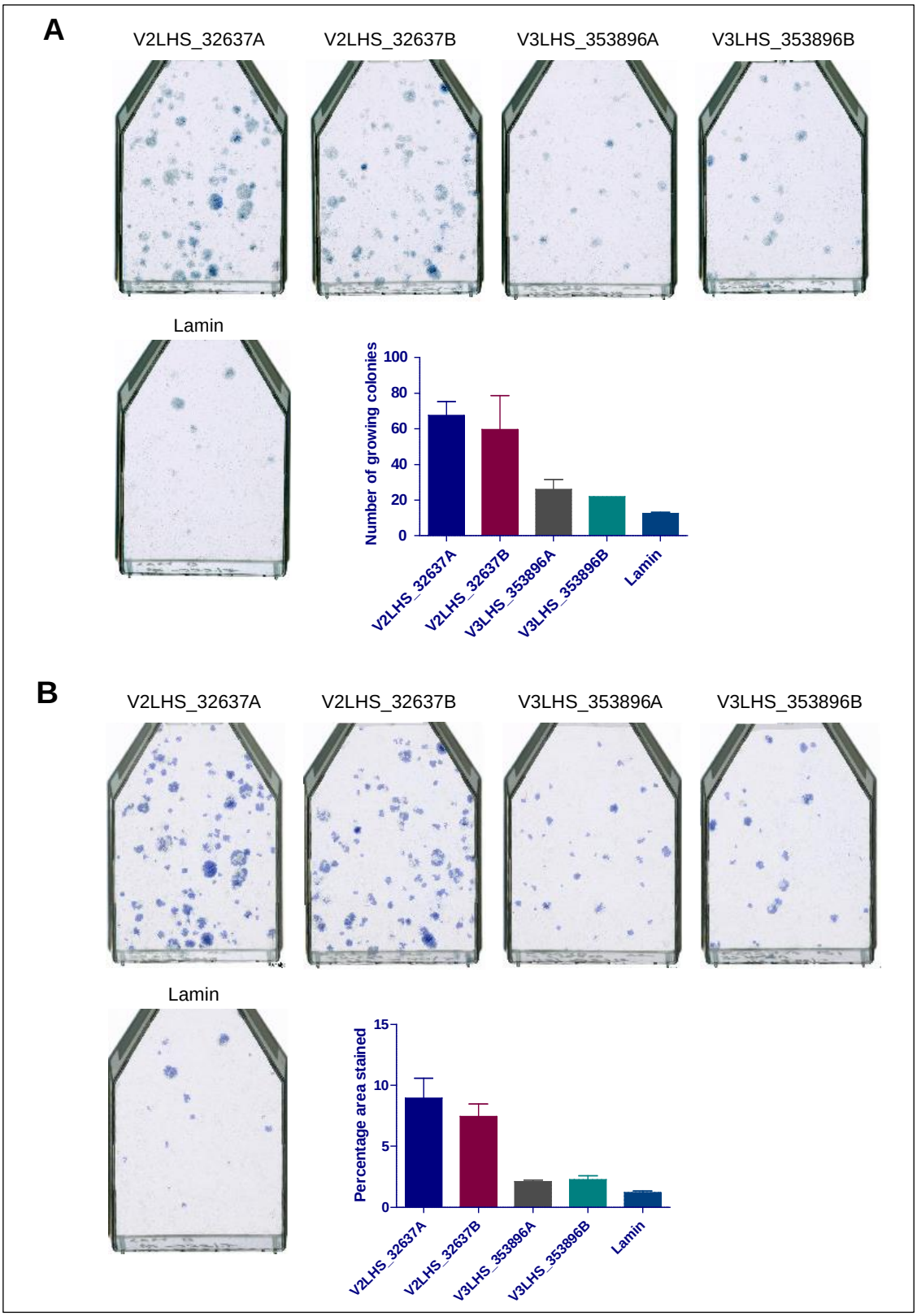

Figure 3.13 Senescence bypass assay after silencing of up-regulated TF, RGS7.
RGS7 silenced using shRNAmiR V2LHS_32637 and V3LHS_353896. Silencing of RGS7 using shRNAmiR V2LHS_32637 showed stronger bypass than V3LHS_353896. Assay was performed as before. A) Manual analysis: Qualitative and quantitative analysis B) Computational analysis: Corresponding flask images showing the blue spots which mark the area of the flask computed as blue areas by the computer algorithm and quantitative representation of bypass assay presented graphically by plotting the calculated percentage area.

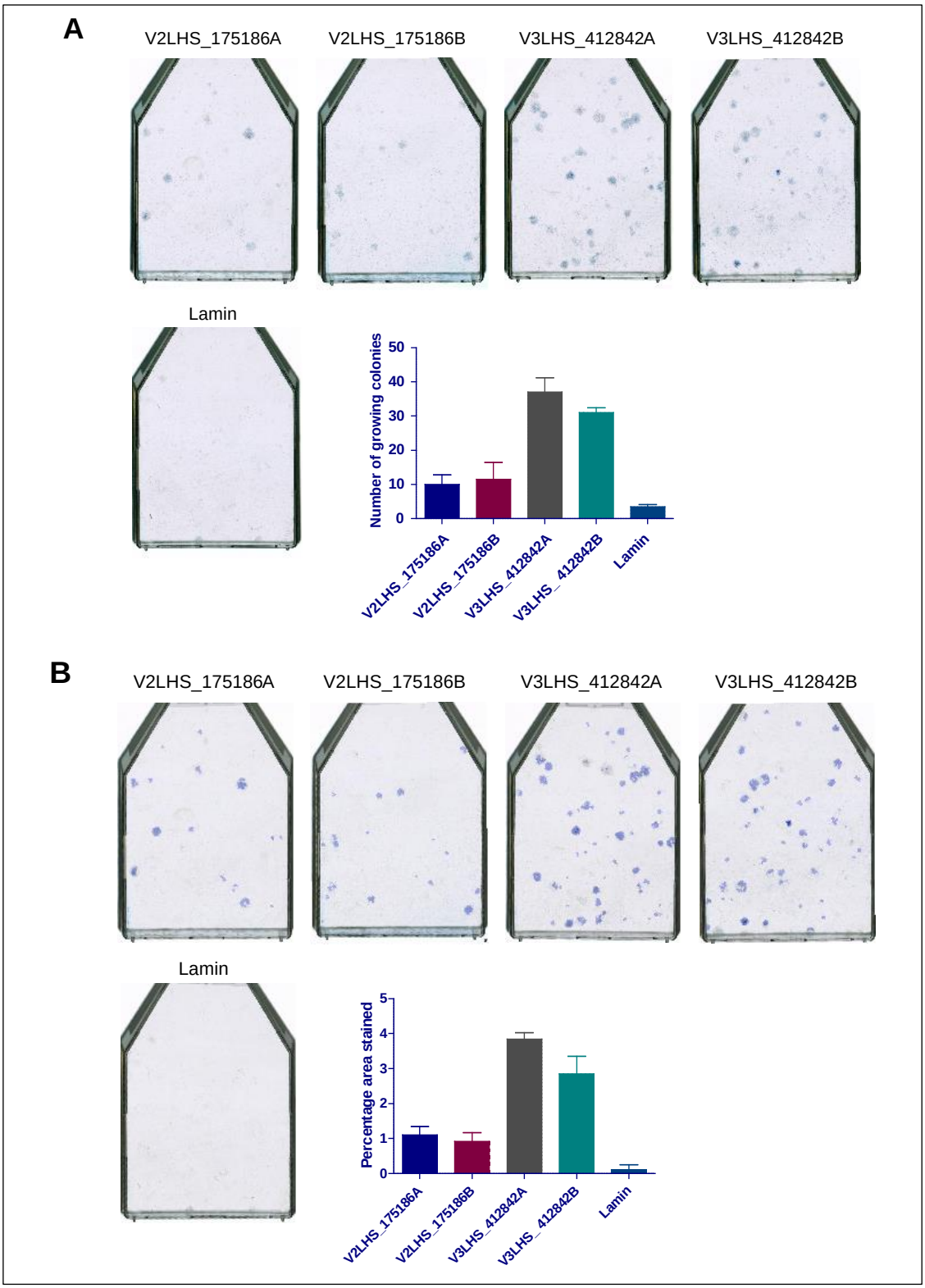

Figure 3.14 Senescence bypass assay after silencing of up-regulated TF, LARP6.
LARP6 silenced using shRNAmiR V2LHS_175186 and V3LHS_412842. Silencing of LARP6 using shRNAmiR V3LHS_412842 exhibited stronger bypass than V2LHS_175186. Bypass assay was conducted as before. A) Manual analysis: Qualitative and quantitative analysis B) Computational analysis: Corresponding flask images showing the blue spots which mark the area of the flask computed as blue areas by the computer algorithm and quantitative representation of bypass assay presented graphically by plotting the calculated percentage area.

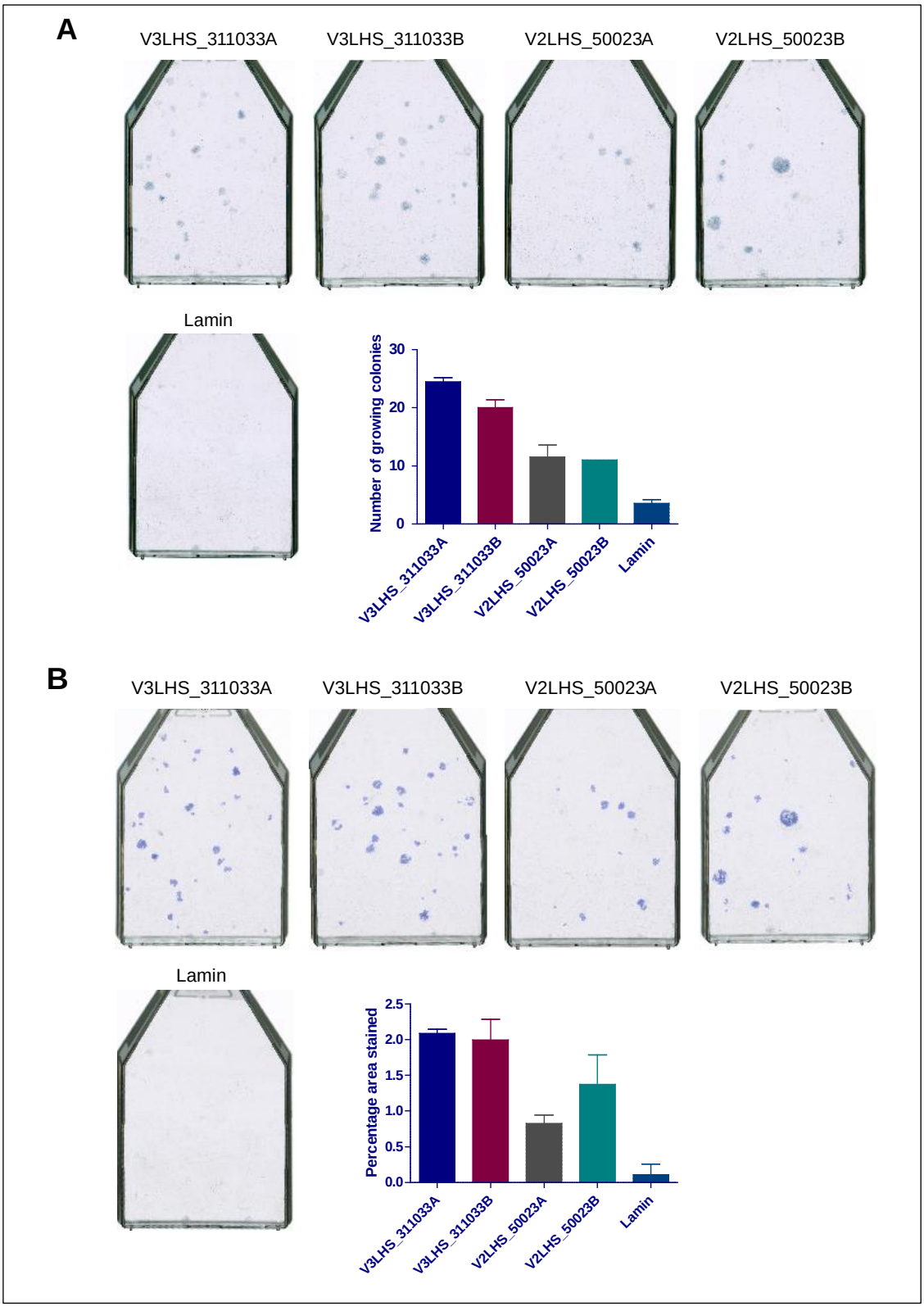

Figure 3.15 Senescence bypass assay after silencing of up-regulated TF, NR1H4.
NR1H4 silenced using shRNAmiR V3LHS_311033 and V2LHS_50023. Assay was performed as before. A) Manual analysis: Qualitative and quantitative analysis B) Computational analysis: Corresponding flask images showing the blue spots which mark the area of the flask computed as blue areas by the computer algorithm and quantitative representation of bypass assay presented graphically by plotting the calculated percentage area.

Therefore, of the 14 upregulated TFs tested in this preliminary experiment at 37.8°C, five exhibited some senescence bypass potential whereas, the remainder did not show any bypass (CD36, SLC22A4, NR3C2, MXD, RELB, CEBPβ, RORA, DNAJC21 and PMS1). Data is shown below for SLC22A4 (Figure 3.16), CEBPβ (Figure 3.17), RORA (Figure 3.18), and DNAJC21 (Figure 3.19). It is possible that either these TFs which did not show any bypass do not have a critical role in regulating senescence or they were not expressed in our model system.

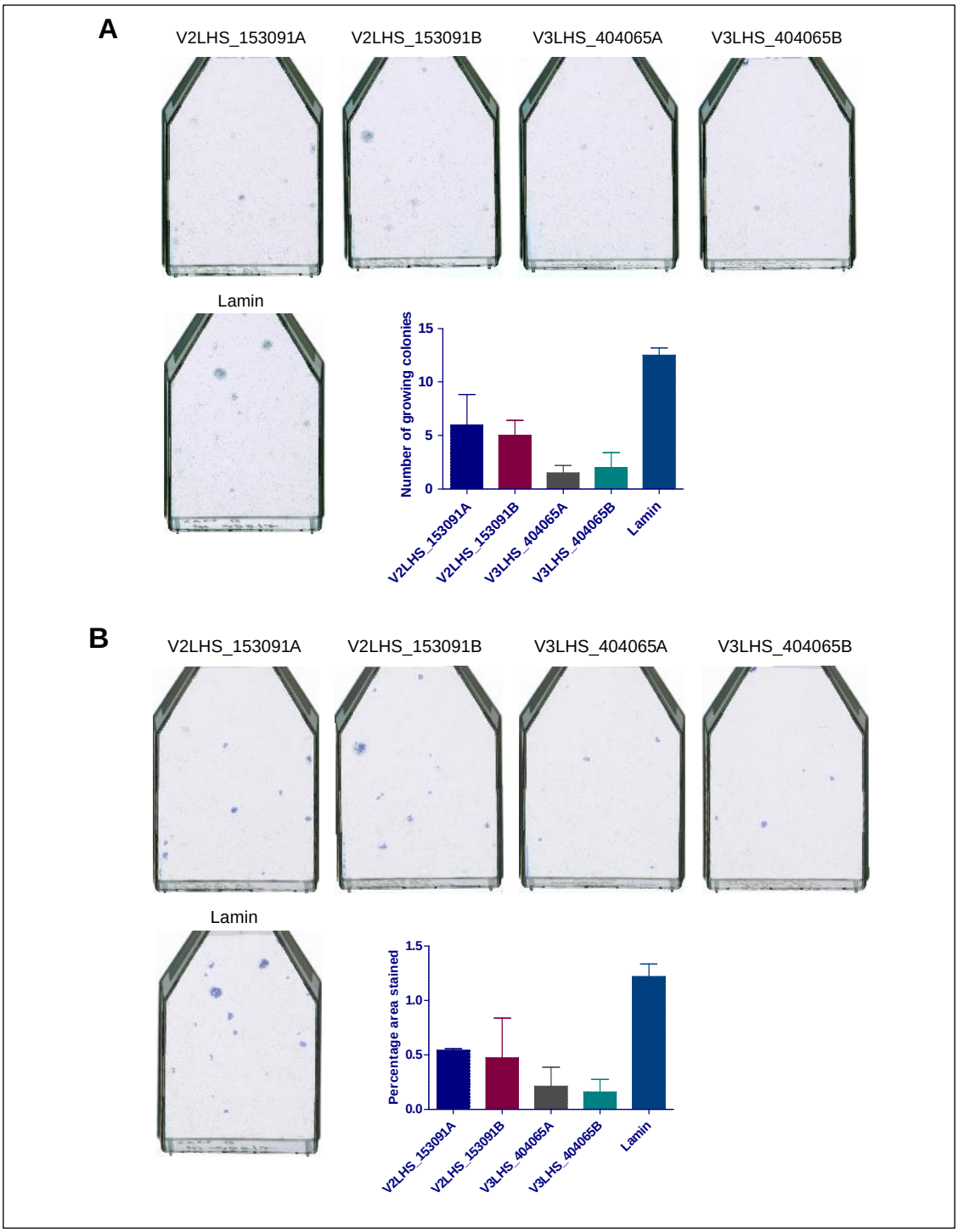

Figure 3.16 Senescence bypass assay after silencing of up-regulated TF, SLC22A4.
SLC22A4 silenced using shRNAmiR V2LHS_153091 and V2LHS_404065. Assay was performed at 5% CO_2, 37.8°C and at 35,000 cells per T-75 flask. Silencing of $p21^{WAF1}$ was used as a positive control and silencing of Lamin A/C as a negative control. A) Manual analysis: Representative flask images obtained after staining and quantitative representation of bypass assay depicted graphically by plotting the average number of colonies (+/- SD) obtained after independently counting each replicate twice. B) Computational analysis: Corresponding flask images shown with blue spots depicting the area of the flask computed as blue areas by the computer algorithm and quantitative representation of bypass assay presented graphically by plotting the calculated percentage area (+/- SD) covered in blue by Definiens Developer XD software for each of the replicates.

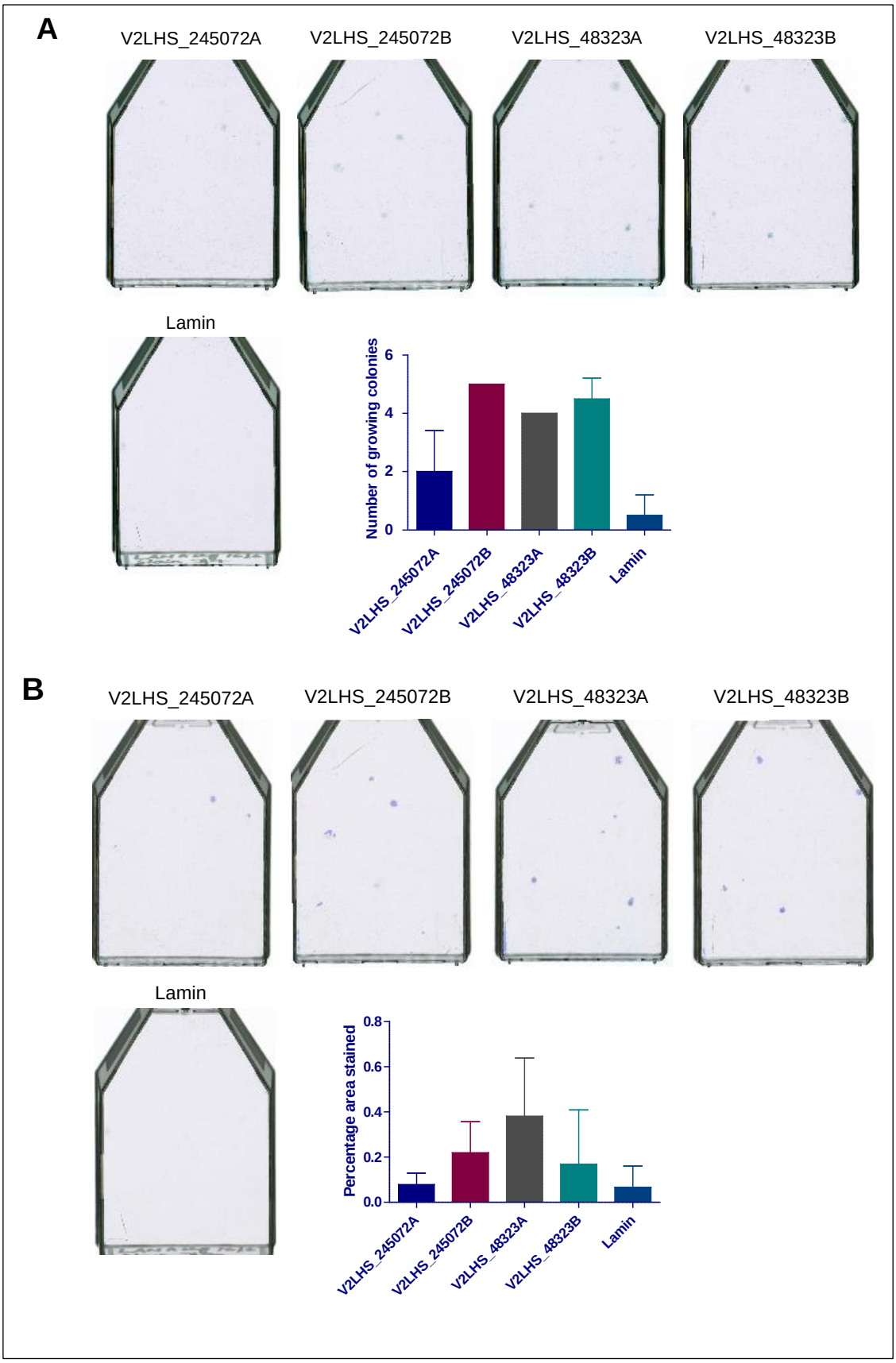

Figure 3.17 Senescence bypass assay after silencing of up-regulated TF, CEBPβ. CEBPβ silenced using shRNAmiR V2LHS_245072 and V2LHS_48323.

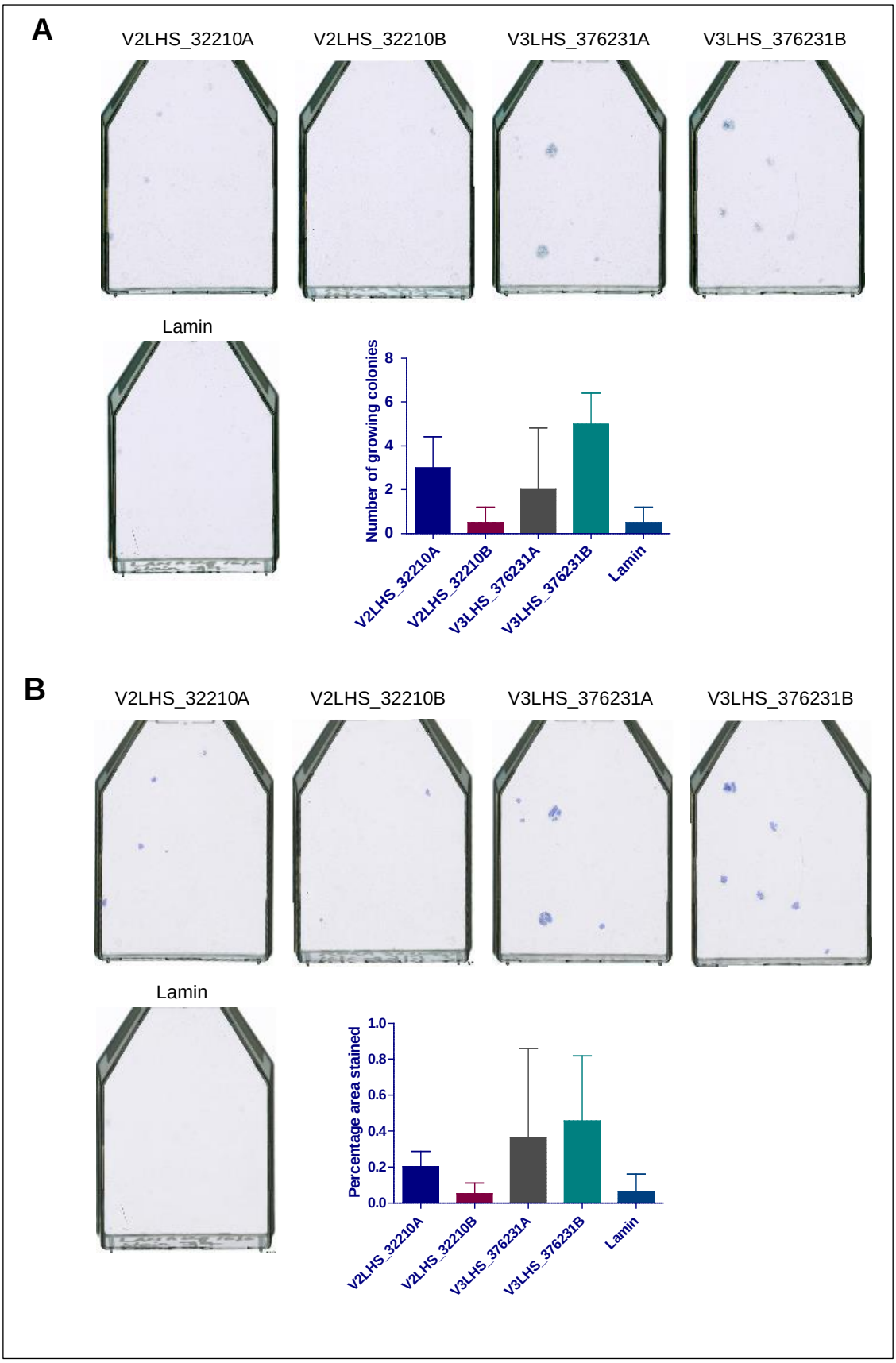

Figure 3.18 Senescence bypass assay after silencing of up-regulated TF, RORA. RORA silenced using shRNAmiR V2LHS_32210 and V3LHS_376231.

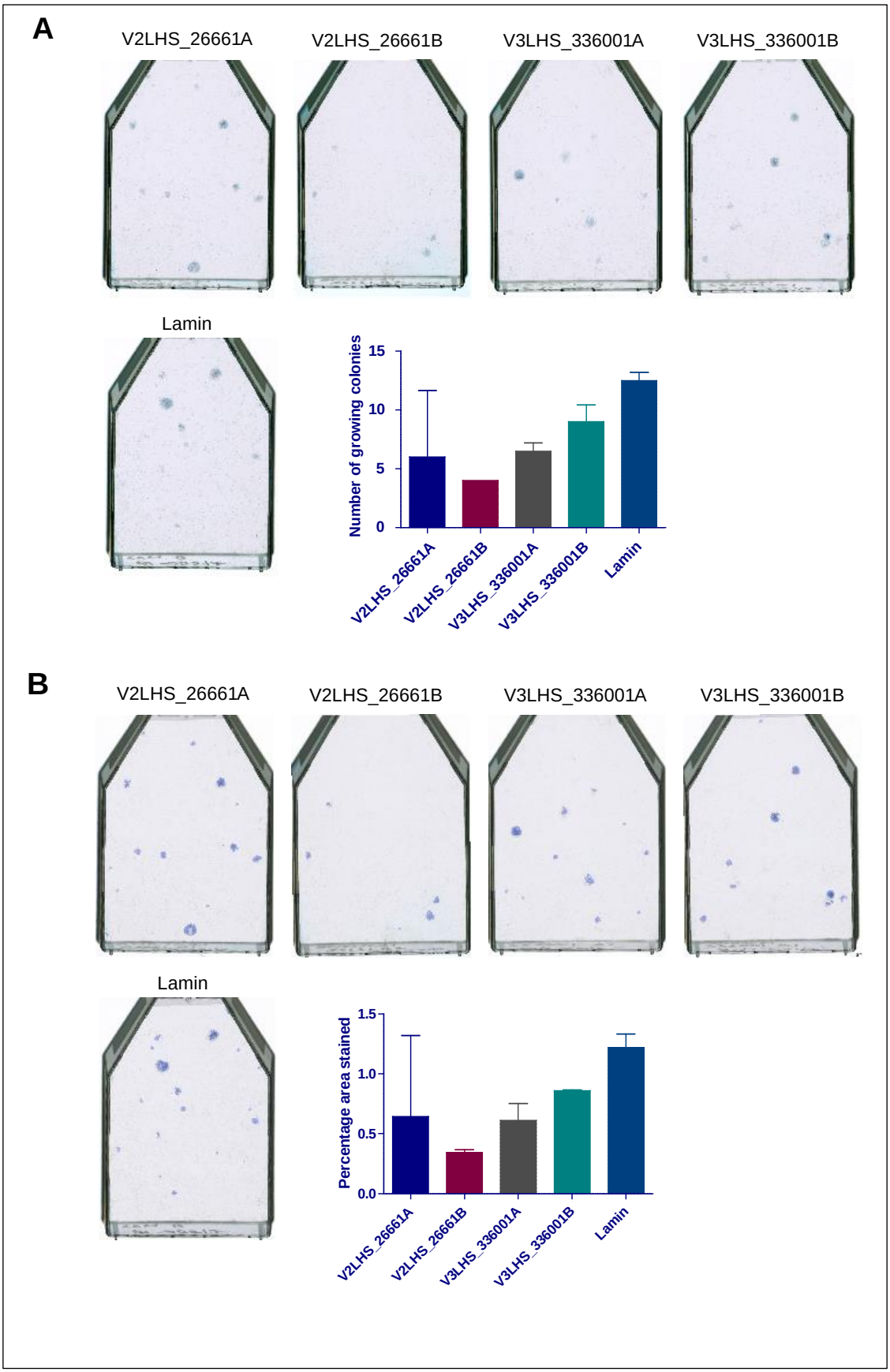

Figure 3.19 Senescence bypass assay after silencing of up-regulated TF, DNAJC21. DNAJC21 silenced using shRNAmiR V2LHS_26661 and V2LHS_336001.

3.6.3 Further assessment of senescence bypass potential of upregulated TFs identified from the preliminary experiment

The senescence bypass assay was repeated for the selected TFs which showed some bypass potential in the preliminary experiment described above. This time the assay was done under stringent temperature conditions i.e. 38.9°C and was conducted using additional shRNAmiRs for each candidate gene. Senescence bypass potential was tested for CEBPβ, EPAS1, LARP6, NR1H4, RELA and RGS7. Silencing of $p21^{WAF1}$ using shRNAmiR V2LHS_230370 was used as a positive control and silencing of Lamin A/C was used as a negative control.

For CEBPβ, the bypass potential was tested using four different shRNAmiRs. Very weak bypass potential was obtained under stringent conditions as shown in Figure 3.20. Two shRNAmiRs namely, V2LHS_48323 and V3LHS_371449 showed some bypass potential compared to the negative control. Senescence bypass potential of EPAS1 was assesed using five different shRNAmiRs. Some marginal bypass potential was observed as shown by presence of few stained colonies. However, none of the shRNAmiRs exhibited significantly stronger bypass potential than the negative control under the stringent conditions as shown in Figure 3.21. For LARP6 and NR1H4, four different shRNAmiRs were used to study its bypass potential under stringent conditions. None of the shRNAmiR showed a significantly higher bypass potential relative to negative as depicted in Figure 3.22 and Figure 3.23 respectively.

Out of the four different shRNAmiRs used to test the bypass potential of RGS7, only one shRNA called V3LHS_407580 showed stronger bypass potential compared to negative as shown in Figure 3.24. For RELA, the bypass potential was tested using four different shRNAmiRs. Only one shRNA i.e. V2LHS_98068 showed significantly higher bypass potential in comparison to the negative control as indicated in Figure 3.25.

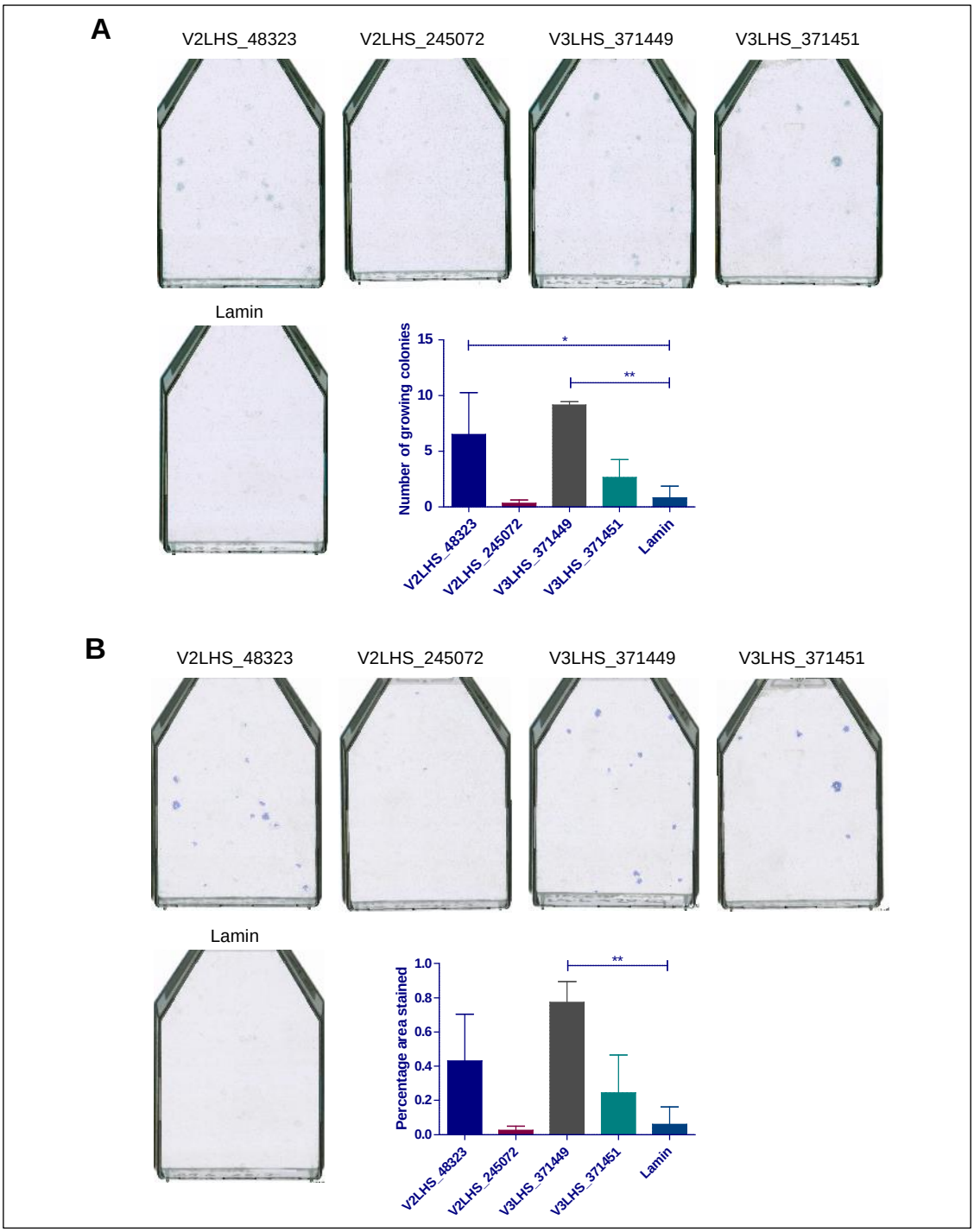

Figure 3.20 Senescence bypass assay after silencing of up-regulated TF, CEBPβ.
CEBPβ silenced using multiple different shRNAmiRs V2LHS_48323, V2LHS_245072, V3LHS_371449 and V3LHS_371451 as indicated on top of each representative flask. This time the assay was performed under stringent conditions at 5% CO_2, 38.9°C and at 35,000 cells per T-75 flask. A) Manual analysis: Representative flask images obtained after staining and quantitative representation of bypass assay depicted graphically by plotting the average number of colonies (+/- SD) obtained after independently counting each replicate twice. B) Computational analysis: Corresponding flask images shown with blue spots depicting the area of the flask computed as blue areas by the computer algorithm and quantitative representation of bypass assay presented graphically by plotting the calculated percentage area (+/- SD) covered in blue by Definiens Developer XD software for each of the replicates. Statistical analysis was conducted using One-way ANOVA, Tukey's Multiple Comparison Test (*p<0.05, **p<0.01, ***p<0.001)

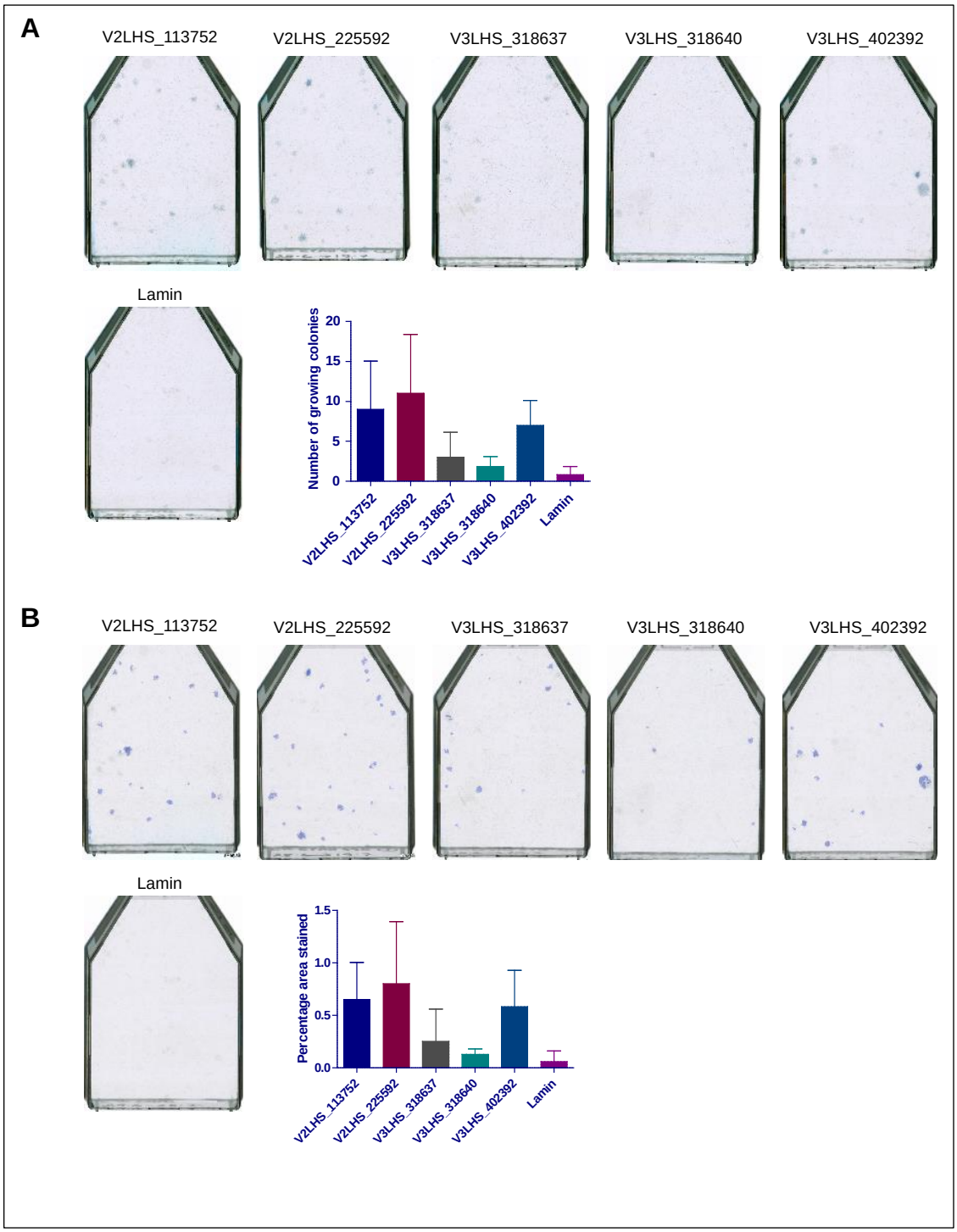

Figure 3.21 Senescence bypass assay after silencing of up-regulated TF, EPAS1.
EPAS1 silenced using multiple different shRNAmiRs V2LHS_113752, V2LHS_225592, V3LHS_318637, V3LHS_318640 and V3LHS_402392. The assay was performed under stringent conditions at 5% CO_2, 38.9°C and at 35,000 cells per T-75 flask. A) Manual analysis: Representative flask images obtained after staining and quantitative representation of bypass assay depicted graphically by plotting the average number of colonies (+/- SD) obtained after independently counting each replicate twice. B) Computational analysis: Corresponding flask images shown with blue spots depicting the area of the flask computed as blue areas by the computer algorithm and quantitative representation of bypass assay presented graphically by plotting the calculated percentage area (+/- SD) covered in blue by Definiens Developer XD software for each of the replicates. Statistical analysis was conducted using One-way ANOVA, Tukey's Multiple Comparison Test (*p<0.05, **p<0.01, ***p<0.001)

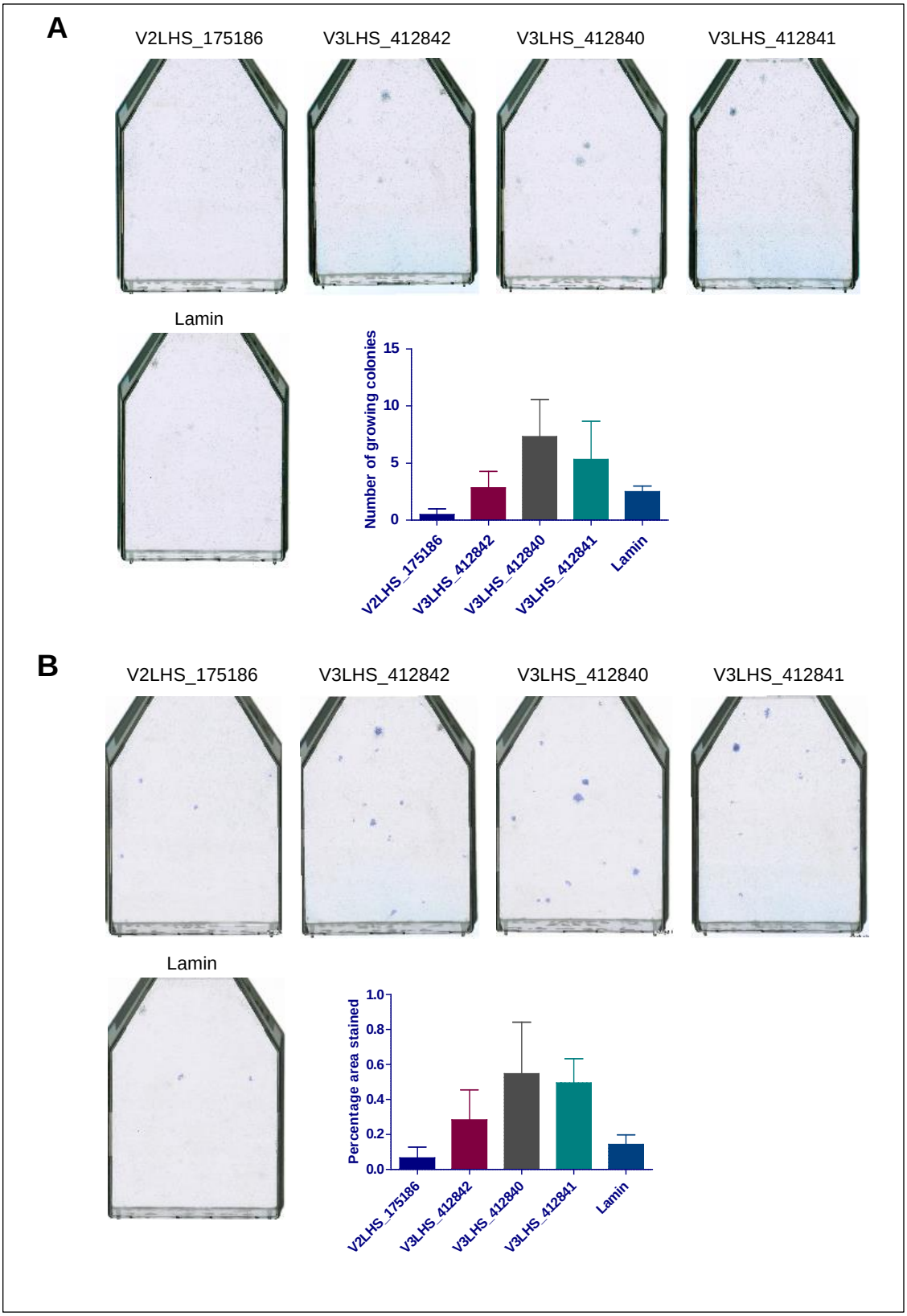

Figure 3.22 Senescence bypass assay after silencing of up-regulated TF, LARP6.
LARP6 silenced using multiple different shRNAmiRs V2LHS_175186, V3LHS_412842, V3LHS_412840 and V3LHS_412841. Bypass assay was performed under similar stringent conditions described above. A) Manual analysis B) Computational analysis Statistical analysis was conducted using One-way ANOVA, Tukey's Multiple Comparison Test (*p<0.05, **p<0.01, ***p<0.001)

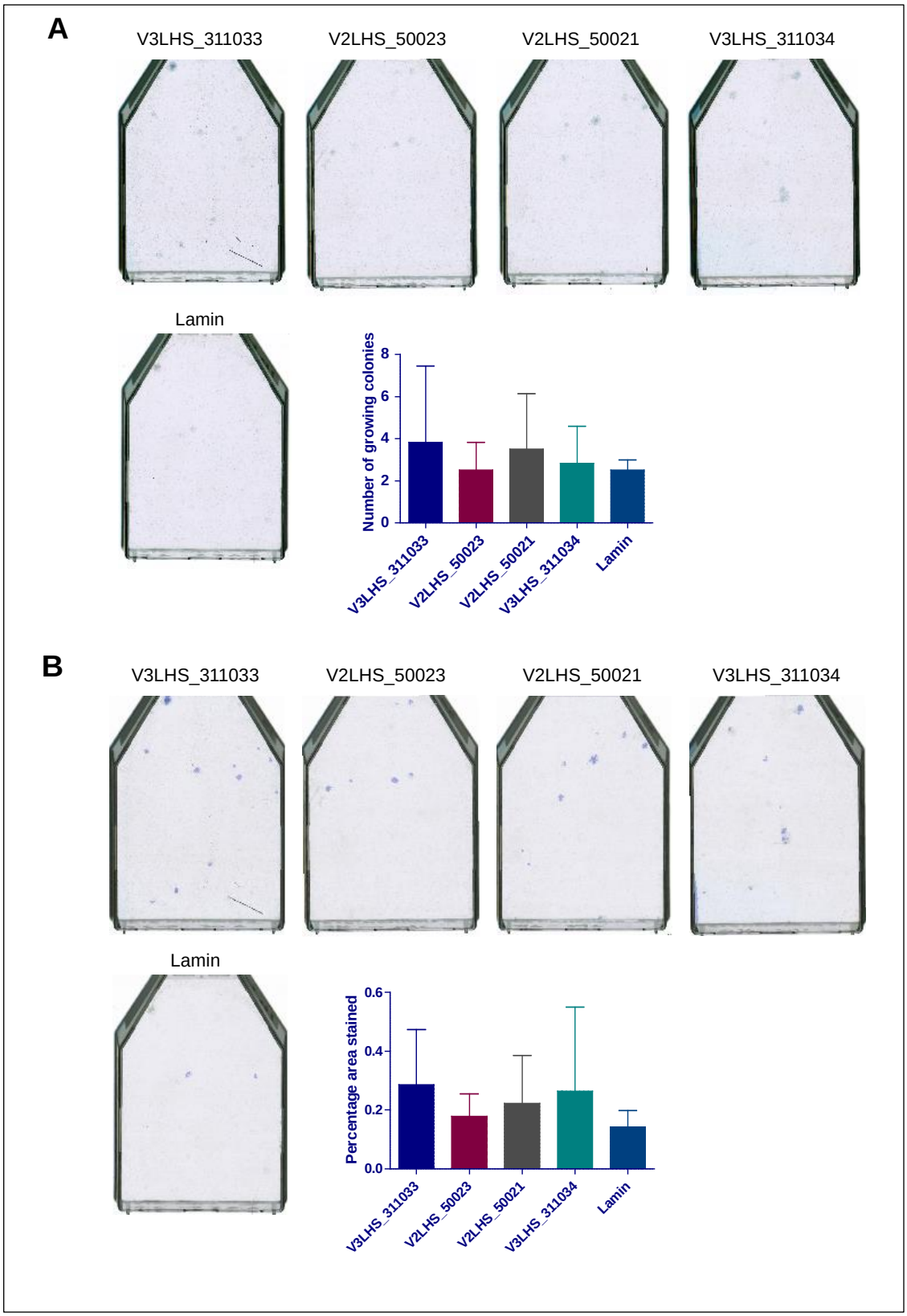

Figure 3.23 Senescence bypass assay after silencing of up-regulated TF, NR1H4.
NR1H4 silenced using multiple shRNAmiRs V3LHS_311033, V2LHS_50023, V2LHS_50021 and V3LHS_311034. Bypass assay was performed under the stringent conditions explained previously. A) Manual analysis B) Computational analysis Statistical analysis was conducted using One-way ANOVA, Tukey's Multiple Comparison Test (*p<0.05, **p<0.01, ***p<0.001)

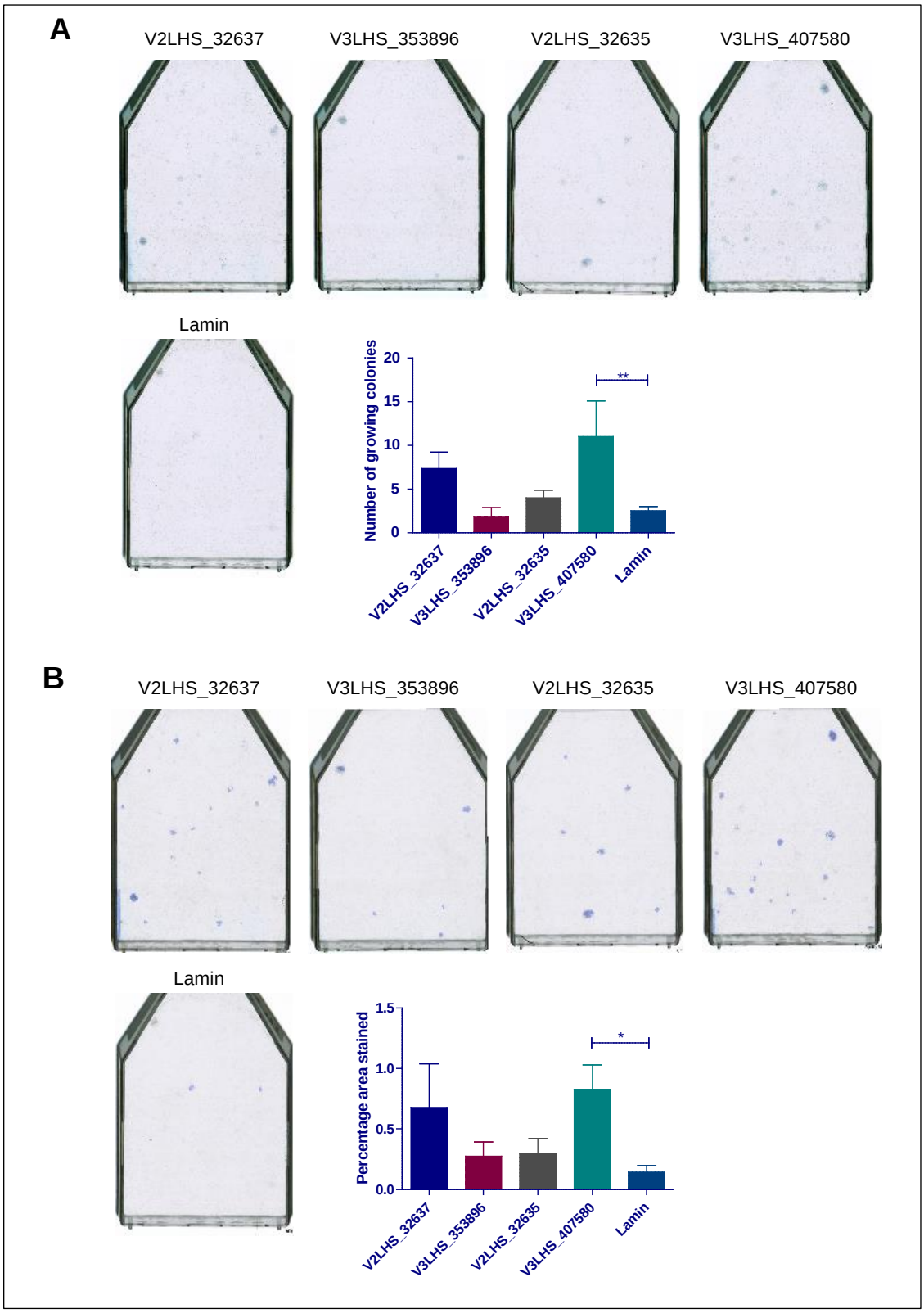

Figure 3.24 Senescence bypass assay after silencing of up-regulated TF, RGS7.
RGS7 silenced using multiple different shRNAmiRs V2LHS_32637, V3LHS_353896, V2LHS_32635 and V3LHS_407580. Bypass assay was conducted under stringent conditions as described before. A) Manual analysis B) Computational analysis Statistical analysis was conducted using One-way ANOVA, Tukey's Multiple Comparison Test (*p<0.05, **p<0.01, ***p<0.001)

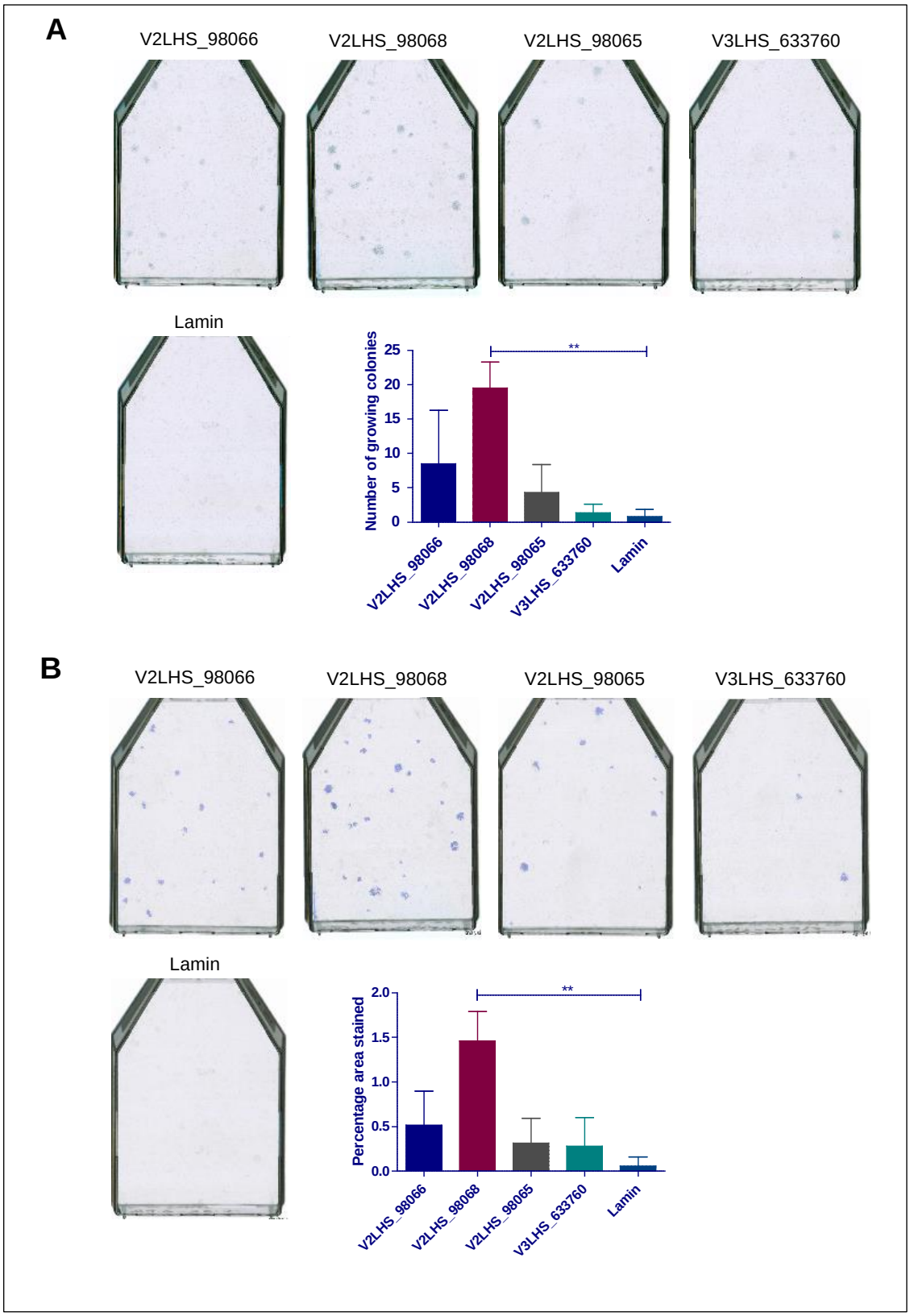

Figure 3.25 Senescence bypass assay after silencing of up-regulated TF, RELA.
RELA silenced using multiple different shRNAmiRs V2LHS_98066, V2LHS_98068, V2LHS_98065 and V3LHS_633760. Bypass assay was carried out under stringent conditions as above. A) Manual analysis B) Computational analysis Statistical analysis was conducted using One-way ANOVA, Tukey's Multiple Comparison Test (*p<0.05, **p<0.01, ***p<0.001)

Therefore, the results obtained after studying the shortlisted up-regulated TFs identified from preliminary experiments were not very encouraging. It was found that under stringent conditions with multiple shRNAmiRs none of the TFs reported significantly strong bypass potential with more than two shRNAmiRs. Silencing of expression needs to be confirmed by either q-RT PCR or western blotting to determine if there is any correlation between the degree of silencing and the bypass potential.

Chapter 4 Dissecting the role of DREAM complex associated components in cellular senescence

4.1 Reconstituting the active MMB-FOXM1 complex

4.1.1 Objectives

Recent studies by DeCaprio and colleagues have shown that in mammalian cells, the p107 and p130 RB-like pocket proteins associate with dimerization partner (DP), E2F and multi-vulval class B (MuvB) proteins to form the DREAM complex which represses most if not all gene expression in quiescence (Sadasivam and DeCaprio 2013; Litovchick et al. 2007). The MuvB core complex comprises five proteins: LIN9, LIN37, LIN52, LIN54 and RBBP4. DeCaprio and colleagues have further shown that in mammalian cells, the MuvB core complex dissociates from p130 and sequentially recruits B-MYB, during S phase, and FOXM1, in G2 phase, to activate mitotic gene expression as illustrated in Figure 4.1 (Schmit et al. 2007; Sadasivam et al. 2012).

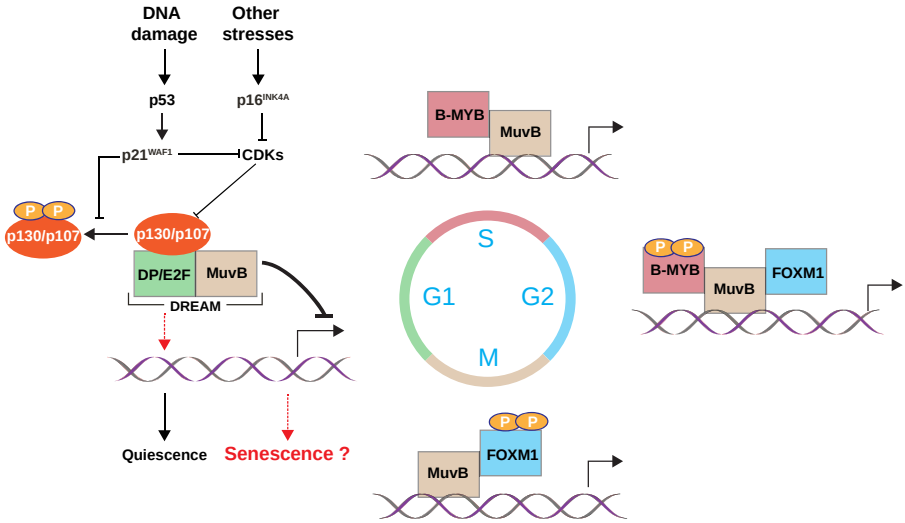

Figure 4.1 Regulation of cell cycle progression by association of MuvB with B-MYB and FOXM1. MuvB core complex comprises five proteins: LIN9, LIN37, LIN52, LIN54 and RBBP4. MuvB associates with p107/p130 RB-like pocket proteins, dimerization partner (DP) and E2F to form the repressive DREAM complex which is capable of inducing quiescence in G0. Upon appropriate signals stimulating cell cycle entry, MuvB core complex dissociates from p130, sequentially recruiting B-MYB, during S-phase and FOXM1, during G2/M phase to their respective target gene promoters activating mitotic gene expression. Upon signals stimulating repression of cell cycle progression, phosphorylation of MuvB is required for re-association of MuvB with p107/p130 RB-like pocket proteins, dimerization partner (DP) and E2F leading to re-assembly of DREAM complex which is capable of repressing cell cycle progression. Adapted from (Mowla et al. 2014; Engeland 2017)

Previous expression profiling of CL3^{EcoR} cells had shown that B-MYB and FOXM1 were highly down-regulated upon senescence growth arrest and this was reversed when it was bypassed as shown in Figure 4.2. After studying multiple different TFs that are downregulated in senescence for their bypass potential, it was found that only B-MYB showed consistently strong bypass potential. No other TFs when tested individually in senescence bypass assay exhibited significant bypass potential. Along with B-MYB and FOXM1, LIN9 and LIN52 were also found to be downregulated during senescence in the expression profiling studies done previously in the lab as shown below in Figure 4.2. LIN54 and RBBP4 were also downregulated upon senescence growth arrest but this was not significant (data not shown). In contrast LIN37 was found to be up-regulated upon senescence arrest as shown below (Figure 4.2).

	GA	wt_LT	GSE_p53	E1A	E7	E2F-DB	pRS_p53	pRS_p21
FOXM1	-2.66	2.57	2.19	2.56	2.07	2.31	2.08	1.89
B-MYB	-1.85	1.70	1.15	3.15	1.00	1.09	0.98	0.80
LIN9	-1.58	1.50	1.39	1.80	0.96	1.49	1.33	1.17
LIN9	-0.35	0.33	0.03	0.24	0.18	0.37	0.07	0.11
LIN37	0.54	-0.68	-0.37	-0.79	-0.86	-0.88	-0.66	-0.72
LIN52	-0.67	0.30	0.50	0.53	0.03	0.05	0.13	0.18
RBL1	-1.68	1.12	1.15	1.23	0.90	0.90	0.56	0.77
RBL1	-1.25	0.64	0.49	0.91	0.71	0.55	0.89	1.00
RBL1	-0.86	0.83	0.17	1.09	0.92	0.73	0.58	0.77
DYRK1A	-0.77	0.53	0.55	0.54	0.21	0.13	0.40	0.19

Figure 4.2 Log2 fold changes in expression upon senescence growth arrest (GA)
Positive numbers for GA indicate up-regulation and are shaded in red, (log2 fold change less than 0.5 are shaded in light red). Negative numbers indicating down-regulation are shaded in green (log2 fold change less than -0.5 are shaded in light green). Also shown is the effect on expression when senescence was bypassed using SV40 LT (wt_LT) antigen, HPV16/18 E7, Adenovirus E1A, GSEp53 (dominant negative p53), E2F-DB (dominant negative E2F), p53shRNA (pRS_p53) and p21^{WAF1} shRNA (pRS_p21^{WAF1}). The changes in expression were reversed upon bypass.

The role of DREAM complex in inducing quiescence is well studied. On the other hand, the role of DREAM complex in senescence growth arrest has not been studied in depth. Therefore, the objective of this section was to study the relevance of DREAM complex and associated complexes in regulating senescence growth arrest. This was studied by testing if the components of the

active form of DREAM complex i.e. (MMB-FOXM1) could bypass senescence, as they are known to promote cell cycle progression.

To study this, the approach used was motivated by the strategy used by Takahashi and Yamanaka, wherein, they introduced 24 TFs simultaneously, by retroviral infection (Takahashi and Yamanaka 2006). As none of the downregulated TFs except B-MYB, showed significant bypass potential on its own when studied individually, it was decided to mix TFs together and study them simultaneously.

Hence, in this section the functional role of the active form of DREAM complex was studied in detail in a series of experiments by reconstituting the components of active form of the DREAM complex by mixing the relevant TFs together which make up the complex. Also, the key individual components of the active complex were characterized in detail where relevant.

4.1.2 Preliminary reconstitution experiment

Since B-MYB and FOXM1 have been suggested to play a role in bypassing senescence and B-MYB, FOXM1, along with LIN9 and LIN52 are downregulated during senescence, it was very interesting to study if the components of the active form of DREAM complex (MMB-FOXM1) would have a role in bypassing senescence. As in previous experiments only B-MYB could bypass senescence in $CL3^{EcoR}$ cells, the aim here was to determine if different components synergise when expressed together and if they act in combination with the MuvB proteins.

Dr. DeCaprio had kindly provided hygromycin resistant expression constructs for LIN9, LIN37, LIN52 and LIN54. Since $CL3^{EcoR}$ cells are hygromycin resistant, each of the inserts was cloned into the pLEX-MCS puromycin resistant lentiviral vector. A preliminary reconstruction experiment was done where B-MYB, FOXM1 and MuvB components of the complex were mixed together. FOXM1ΔNΔKEN, a constitutively active form of FOXM1 cloned in pLEX-MCS was used in the experiment (Rovillain et al. 2011). Equal amounts of DNA i.e. 1ug for each TF were mixed first to make a DNA pool as described in Table 4.1. From this DNA pool, 1.5ug DNA was then used to prepare lentiviruses in

HEK293T cells following the transient packaging protocol described in section 2.5.

B-MYB studied individually was used as a positive control for the experiment as it had consistently worked previously. For negative control non-infected cells, empty vector pLX301 and RAD51 found to be consistently negative were used.

Table 4.1 DNA pools made to reconstitute active whole complex (MMB-FOXM1)

Reconstituted complex	**Constituents**
WC1	1 µg each of LIN9, LIN37, LIN52, LIN54, FOXM1ΔNΔKEN13* and B-MYB
WC2	1 µg each of LIN9, LIN37, LIN52, LIN54, FOXM1ΔNΔKEN17* and B-MYB
5+1 B-MYB	5 µg of RAD51 (five-sixth) and 1 µg of B-MYB (one sixth)

* 13 and 17 depict two different clones for FOXM1ΔNΔKEN

$CL3^{EcoR}$ cells stably transduced after infection with the different lentivirus pools and puromycin selection were reseeded at 50,000 cells per T-75 flask and studied for bypass potential. The senescence bypass for this reconstruction experiment was done under very stringent conditions of temperature as high as 38.9°C. The use of such a high temperature reduced the efficiency of B-MYB, minimized the background and allowed us to determine if there was any synergy present among the different components.

The senescence bypass results obtained from this preliminary experiment were striking. The results obtained from this preliminary experiment presented in Figure 4.3 are revealing in several ways. A large number of densely blue stained growing colonies were obtained for the reconstituted MMB-FOXM1 complex. No colonies were observed in any of the negative controls whereas B-MYB as expected presented lots of blue colonies. Interestingly the cells transduced with one sixth B-MYB, which is the amount of B-MYB present in WC1 and WC2, produced only very few colonies. However, RAD51 is not an ideal negative control for combining with B-MYB as it is possible that RAD51 might oppose the effect of B-MYB.

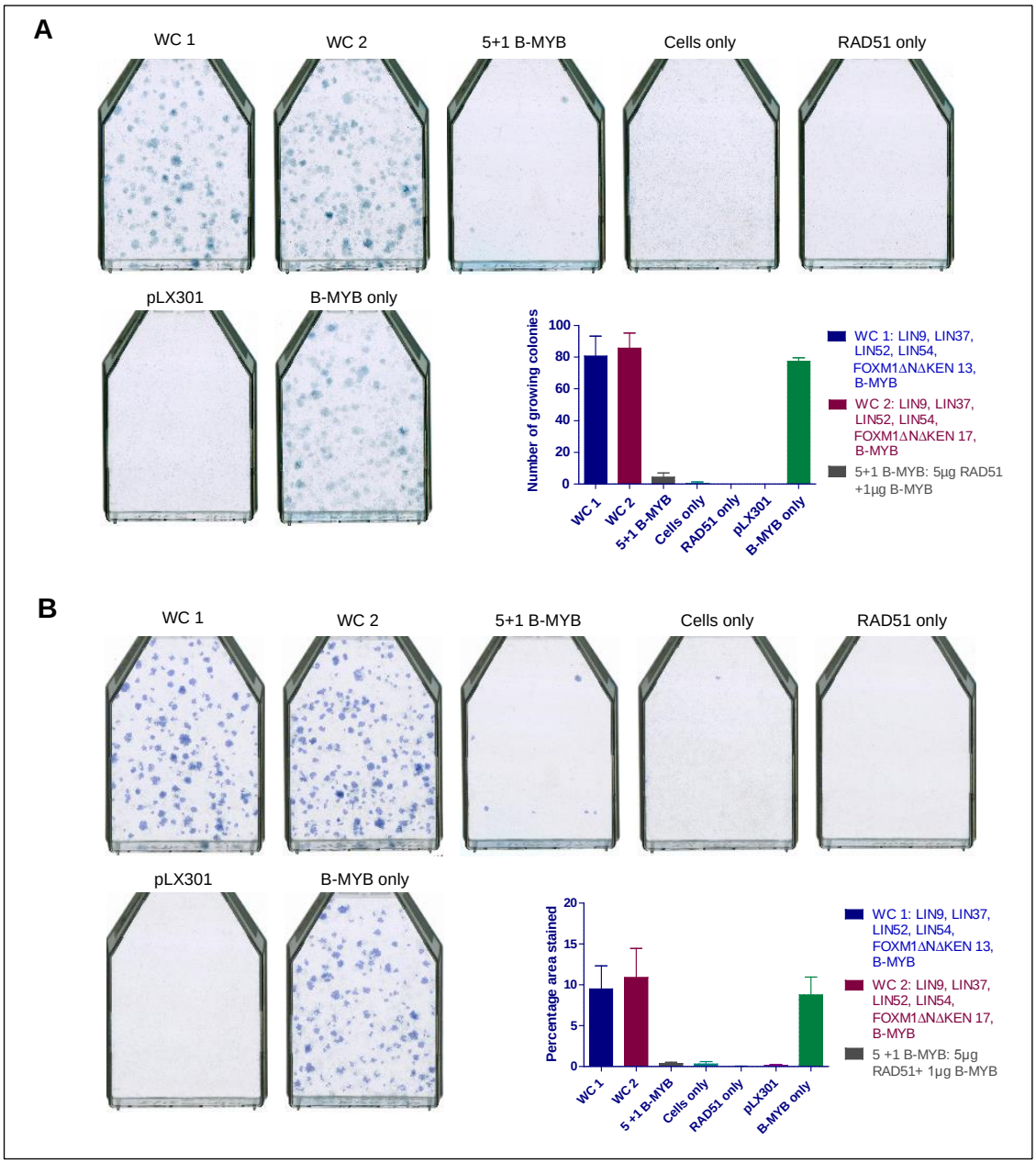

Figure 4.3 Senescence bypass assay after reconstituting active MMB-FOXM1
Bypass assay was performed at 5% CO_2 and 38.9°C with 50,000 cells per T-75 flask. Single representative flasks from the internal repeats are shown. B-MYB was used as a positive control and cells only, pLX301 empty vector and RAD51 were used as negative controls. A) Manual analysis: Representative flask images obtained after staining and quantitative representation of bypass assay depicted graphically by plotting the average number of colonies (+/- SD) obtained after independently counting each replicate twice. B) Computational analysis: Corresponding flask images shown with blue spots depicting the area of the flask computed as blue areas by the computer algorithm and quantitative representation of bypass assay presented graphically by plotting the calculated percentage area (+/- SD) covered in blue by Definiens Developer XD software for each of the replicates.

The results indicated that reconstitution of the active components of the DREAM complex (MMB-FOXM1) bypass senescence very efficiently. It was as efficient as when B-MYB was studied alone. Second, the pool of 5+1 B-MYB as shown in Figure 4.3, yielded very few densely growing colonies as this flask was infected

with only one sixth the quantity of B-MYB which is equivalent to the amount of B-MYB present in WC1 and WC2, where the whole active complex (MMB-FOXM1) is reconstituted. This suggested that B-MYB alone when present in the same ratio as in whole complex lacking other components, did not exhibit a similar level of strong bypass potential as observed with the reconstituted active MMB-FOXM1 complex. This suggests that B-MYB can be synergized by the presence of other components of MuvB and FOXM1 of the MMB-FOXM1 complex as B-MYB works better in presence of these other genes. The results obtained have been verified both by the manual analysis as well as the computational analysis.

Hence, this experiment for the first time in this study showed that mixing different TFs together to reconstitute the active DREAM complex works very efficiently. The results obtained from this experiment also suggested the presence of a synergistic effect with respect to one of the components of the active complex (MMB-FOXM1) i.e. B-MYB. However, potentially alternative explanation of the variation in senescence rescue obtained could be due to differences in relative titre of active viruses in the different packaging reactions.

4.2 Identification of the critical components of the active MMB-FOXM1 complex that are crucial for bypassing cellular senescence

4.2.1 Objective

Previous experiment demonstrated that the active (MMB-FOXM1) complex can bypass senescence strongly and consistently; the next obvious question was to determine the key components of the complex which are crucial for the strong bypass observed. Therefore, in this section the contribution of each individual component of the complex towards the strong bypass observed, was analysed.

The rationale behind performing this experiment is, if a critical component that has a role to play in synergizing the assay is omitted, its absence will reduce the bypass potential which can be analysed both qualitatively and quantitatively.

4.2.2 Bypass potential of the reconstituted complex lacking one component

A reconstruction experiment was designed in which different lentiviruses were produced from DNA pools where one component of the complex was omitted in each reconstitution as shown in Table 4.2. 1.5 µg of DNA from each of the DNA pools was packaged as lentiviruses in HEK293T cells and subsequently used to stably transduce $CL3^{EcoR}$ cells.

Table 4.2 List of DNA pools for the reconstruction experiment of the MMB-FOXM1 complex lacking one component

	RAD51	LIN9	LIN37	LIN52	LIN54	FOXM1	B-MYB
5+1 B-MYB	5 µg	X	X	X	X	X	1 µg
WC	X	1 µg	1 µg	1 µg	1 µg	1 µg	1 µg
X LIN9	1 µg	X	1 µg	1 µg	1 µg	1 µg	1 µg
X LIN37	1 µg	1 µg	X	1 µg	1 µg	1 µg	1 µg
X LIN52	1 µg	1 µg	1 µg	X	1 µg	1 µg	1 µg
X LIN54	1 µg	1 µg	1 µg	1 µg	X	1 µg	1 µg
X FOXM1ΔNΔKEN	1 µg	1 µg	1 µg	1 µg	1 µg	X	1 µg
X B-MYB	1 µg	1 µg	1 µg	1 µg	1 µg	1 µg	X
RAD51	6 µg	X	X	X	X	X	X

RAD51 was used as the negative control. The cross indicates the absence of that particular component. RAD51 was used to replace the missing component.

Results obtained from the experiment are shown in Figure 4.4. The highest numbers of densely growing colonies were observed with the whole complex "WC" and "X LIN54" in which LIN54 had been omitted. "X LIN9" and "X LIN37" produced the next highest whereas "X LIN52", "X FOXM1ΔNΔKEN" and "X B-MYB" produced the least of which "X LIN52" lacking LIN52 was the lowest. This was very interesting as it suggested that LIN52 was more, or as important as FOXM1 and B-MYB. LIN52 was not found to be highly differentially downregulated in the microarray data as opposed to LIN9 which was highly

downregulated as shown in Figure 4.2. This demonstrated the importance of undertaking functional assays to determine role of each TF rather than relying on expression profiling as protein levels might be affected or modification such as phosphorylation can alter.

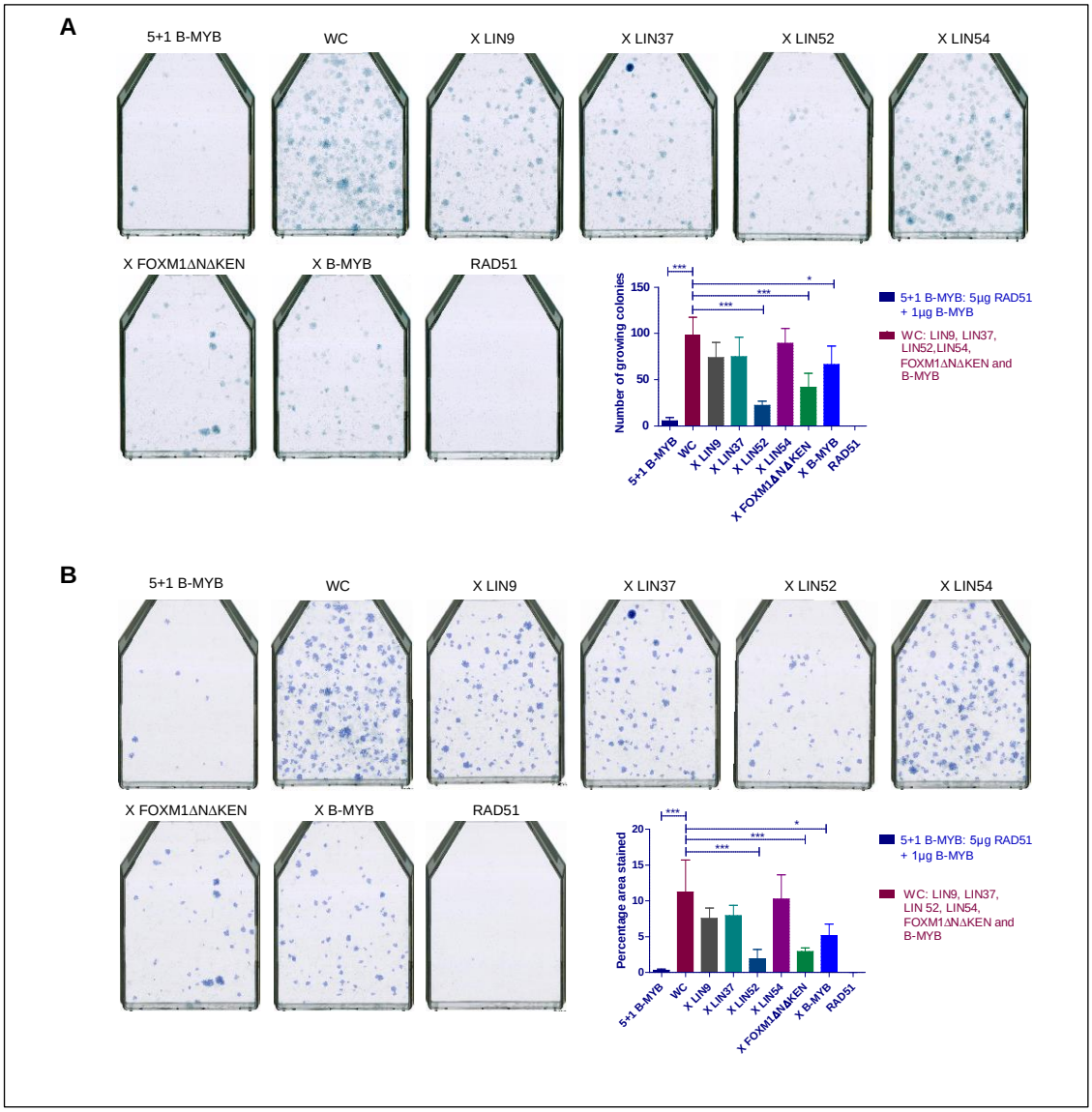

Figure 4.4 Senescence bypass assay for the reconstituted active form of DREAM complex lacking one component.
Bypass assay was performed three times independently at 5% CO_2 and 38.9°C with 50,000 cells per T-75 flask. For qualitative analysis single representative flasks from internal repeats are shown with the component absent from the reconstituted complex indicated. "X" indicated in front of a component depicts its absence in the reconstituted complex. For quantitative analysis the bar charts depict an overall average (+/- SD) of all three-independent repeat experiments. RAD51 was used as the negative control. A) Manual analysis B) Computational analysis. Statistical analysis was conducted using One-way ANOVA, Tukey's Multiple Comparison Test (*p<0.05, **p<0.01, ***p<0.001)

The key finding from this experiment after carefully analysing the results obtained both qualitatively and quantitatively was that it demonstrated that three

components out of the six components which form the MMB-FOXM1 complex were critical for the strong bypass potential. They were: LIN52, FOXM1ΔNΔKEN and B-MYB. Absence of LIN52 showed the strongest reduction followed by FOXM1ΔNΔKEN and B-MYB.

4.3 Senescence bypass potential of each of the components of the MMB-FOXM1 complex

4.3.1 Objective

Until now I have studied the bypass potential of the MMB-FOXM1 complex and have indirectly identified the crucial components to be: LIN52, FOXM1 and B-MYB. It was therefore important to study the senescence bypass potential of each of the six components on their own. Hence, in this section the bypass potential of each of the components of MMB-FOXM1 complex was examined individually.

4.3.2 Senescence bypass assay of the individual components of the active MMB-FOXM1 complex

Experiment was designed where lentiviruses were prepared for each of the individual components of the complex i.e. LIN9, LIN37, LIN52, LIN54, FOXM1ΔNΔKEN and B-MYB in HEK293T cells. They were then used to infect $CL3^{EcoR}$ cells and the bypass potential analysed after three-week incubation at the non-permissive temperature.

Senescence bypass potential observed for each of the component is shown in Figure 4.5. The most striking result was that LIN52 on its own for the first time was clearly able to bypass senescence. Until now in this study no other downregulated TF when ectopically expressed individually had shown any bypass potential apart from B-MYB. This was very encouraging as it validates the finding from the previous experiment where absence of LIN52 showed a strong reduction in bypass potential, highlighting its importance. Apart from LIN52, B-MYB as observed previously showed a strong bypass potential.

The third important component identified in the previous experiment was FOXM1ΔNΔKEN, which showed a marginal bypass potential that was similar to

that observed after ectopically expressing LIN9. The remaining components LIN37 and LIN54 did not show any bypass potential when studied individually. The reconstituted MMB-FOXM1 complex was also studied simultaneously and again showed a strong and efficient bypass as demonstrated by the representative flask (WC) in Figure 4.5.

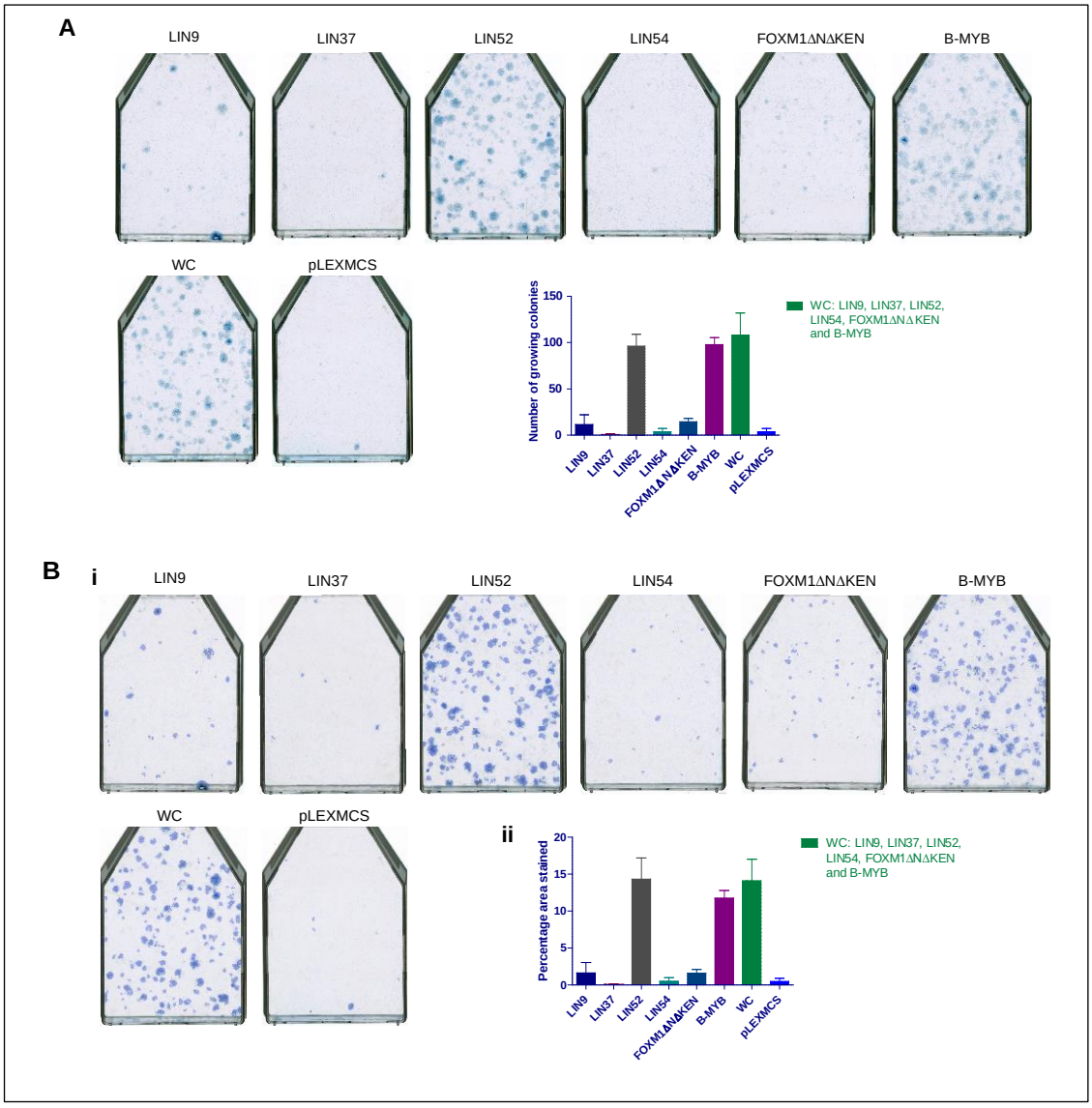

Figure 4.5 Senescence bypass assay of the individual components of the MMB-FOXM1 complex Bypass assay was performed twice independently at 5% CO_2 and 38.9°C with 35,000 cells per T-75 flask. Single representative flasks from internal repeats are shown with the ectopically expressed component name indicated. For quantitative analysis the bar charts depict an overall average (+/- SD) of the independent repeat experiments. Empty vector pLEX-MCS was used as negative control. Constitutively active form of LIN52 and FOXM1 were used. A) Manual analysis B) Computational analysis.

4.4 Further Characterization of the individual components of the active MMB-FOXM1 complex

4.4.1 LIN9

4.4.1.1 Objective

The original LIN9 clone was kindly given to us by Prof. James A. DeCaprio, Dana-Farber Cancer Institute, Boston, U.S.A. Before studying every TF functionally for its bypass potential in this thesis, they were sequence verified. After analysing the sequence of LIN9, it was observed that the LIN9 clone was in frame but lacked sixteen amino acids at its 5' end. Therefore, to rule out the possibility that the lack of observed bypass was due to the lack of the sixteen amino acids, the aim was to compare and study both the truncated and the full length LIN9 for their bypass potential. Both forms of LIN9 were studied by ectopically expressing them individually as well as part of the MMB-FOXM1 complex. This allowed us to determine any difference in bypass potential of LIN9 that might arise due to the missing amino acids, when expressed individually or as part of the reconstituted complex.

4.4.1.2 Gateway recombination cloning of Full length LIN9

A full length LIN9 clone (HsCD00515936) was obtained as a stab from the DNASU plasmid repository (https://dnasu.org/DNASU/), plated on an appropriate antibiotic plate, colonies picked, plasmid isolated and the sequence checked before cloning, to verify the sequence. Comparison of the protein coding sequence of full length and the truncated LIN9 is shown in Figure 4.6.

Gateway recombination cloning was used to clone the full length LIN9 into the puromycin resistant pLX301 destination vector. Plasmid DNA isolated from two colonies picked after successful cloning and transformation was sequenced verified for presence of full length LIN9 in pLX301 lentiviral vector.

A.

MHRGGQPLKKRRGSFKMAELDQLPDESSSAKALVSLKEGSLSNTWNEKYSSLQKTPVWKGRNTSSAVEMPFRNSKRSRL
FSDEDDRQINTRSPKRNQRVAMVPQKFTATMSTPDKKASQKIGFRLRNLLKLPKAHKWCIYEWFYSNIDKPLFEGDNDF
CVCLKESFPNLKTRKLTRVEWGKIRRLMGKPRRCSSAFFEEERSALKQKRQK
IRLLQQRKVADVSQFKDLPDENSFASGYXNESYSTITWCS

B.

```
Query  17   MAELDQLPDESSSAKALVSLKEGSLSNTWNEKYSSLQKTPVWKGRNTSSAVEMPFRNSKR  76

Sbjct  1    MAELDQLPDESSSAKALVSLKEGSLSNTWNEKYSSLQKTPVWKGRNTSSAVEMPFRNSKR  60

Query  77   SRLFSDEDDRQINTRSPKRNQRVAMVPQKFTATMSTPDKKASQKIGFRLRNLLKLPKAHK  136

Sbjct  61   SRLFSDEDDRQINTRSPKRNQRVAMVPQKFTATMSTPDKKASQKIGFRLRNLLKLPKAHK  120

Query  137  WCIYEWFYSNIDKPLFEGDNDFCVCLKESFPNLKTRKLTRVEWGKIRRLMGKPRRCSSAF  196
```

Figure 4.6 Comparison of LIN9 sequences
A. Protein sequence of LIN9 depicting the missing 16 amino-acids indicated in red box. B. After sequence verification it was found that LIN9 clone lacked sixteen amino acids at its N-terminus. On aligning the sequences of full length (Query) and truncated (Sbjct) LIN9 clone, the homology started from the seventeenth amino acid residue confirming the absence of sixteen amino acids at the N-terminus.

4.4.1.3 Comparison of bypass potential of full length and truncated LIN9

To compare the bypass potential of both full length and truncated LIN9, lentiviruses were prepared for both forms of LIN9 in HEK293T cells. Also, to study the effect of both the forms of LIN9 in the whole complex, two DNA pools were made to reconstitute the whole complex with full length and truncated LIN9 (Table 4.3). The lentiviruses were used to stably transduce $CL3^{EcoR}$ cells and assess the bypass potential.

Table 4.3 DNA pools made to reconstitute the MMB-FOXM1 complex with full length and truncated LIN9

Reconstituted complex	Constituents
WC-LIN9	LIN9, LIN37, LIN52, LIN54, FOXM1ΔNΔKEN and B-MYB
WC-FL*-LIN9	FL-LIN9, LIN37, LIN52, LIN54, FOXM1ΔNΔKEN and B-MYB

*Full length

Three weeks later after staining with methylene blue, it was observed that both the full length LIN9 and truncated LIN9 produced few colonies. On the other hand, the reconstituted MMB-FOXM1 complex generated significantly higher numbers of colonies. Moreover, the number of colonies obtained for full length and truncated LIN9 were not significantly different both when studied individually or as part of the whole complex as shown in Figure 4.7. This indicated that presence of sixteen amino acids in LIN9 did not change the bypass potential significantly compared to the truncated LIN9. Therefore, in subsequent experiments, truncated LIN9 was used when required as truncated LIN9 was in pLEX-MCS. This means that wherever possible all MMB-FOXM1 components were in same vector.

This experiment together with previous experiments suggests that although LIN9 has been known to be a key component of the MuvB complex (Schmit et al. 2007), in our model system, it was not found to be a component which was required for the observed senescence bypass.

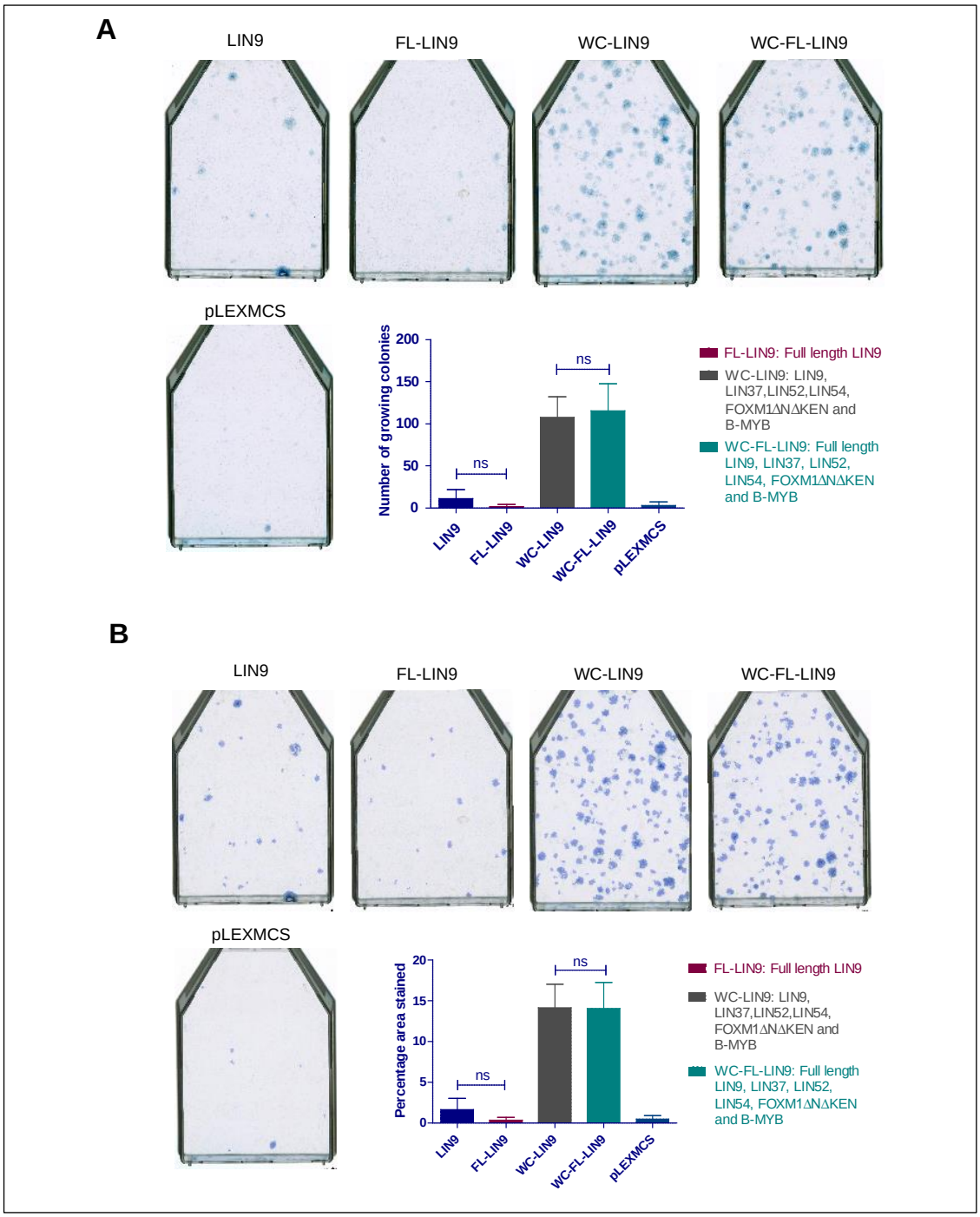

Figure 4.7 Comparison of senescence bypass assay of full length and truncated LIN9
Bypass assay was performed twice independently at 5% CO_2 and 38.9°C with 35,000 cells per T-75 flask. For quantitative analysis the bar charts depict an overall average (+/- SD) of the independent repeat experiments. Empty vector pLEX-MCS was used as negative control. A) Manual analysis B) Computational analysis Statistical analysis was conducted using One-way ANOVA, Tukey's Multiple Comparison Test (*p<0.05, **p<0.01, ***p<0.001)

4.4.2 FOXM1

4.4.2.1 Objective

In this study FOXM1 did not show a strong bypass potential when studied individually, suggesting that it might not be sufficient on its own in regulating senescence even though Rovillain et al., 2011, had previously observed some bypass activity (Rovillain et al. 2011). Moreover, this does not rule out the possibility that there may be some synergism between FOXM1 and other MMB complex associated components. Interestingly, while studying bypass after removing each component from the reconstituted complex, FOXM1 was found to be crucial as its absence led to a significant reduction in the bypass potential of the whole complex, indicating indirectly that it is a key component.

Activity of FOXM1 is kept low in the G1/S phase of cell cycle by the presence of an auto-inhibitory domain at its N-terminus. The N-terminus also contains KEN box sequences which are required for the proteolytic targeting and degradation of the FOXM1 via binding of the APC/C^{Cdh1} adaptor protein. There exists a mutant of FOXM1 where the N-terminus and KEN have been deleted called FOXM1ΔNΔKEN which is constitutively active, non-degradable and does not require cyclin-CDK activity for its activation. Park et al., 2008, presented a comprehensive study comparing wild type FOXM1 and N-terminus deleted FOXM1 (Park et al. 2008). The findings from their study showed that deletion of N-terminal 232 residues led to more than 20-fold increase in the transcriptional activity of FOXM1 compared to wild type FOXM1. N-terminal deleted mutant also showed a significant increase in transforming ability of FOXM1. This study also reported that N-terminal deleted FOXM1 mutant is maintained at constitutively at high levels throughout the cell cycle as opposed to the wild type FOXM1, which is regulated by growth factors (Park et al. 2008). Therefore, for our experiments we have utilised the constitutively active FOXM1ΔNΔKEN.

It will of course be interesting to compare the bypass potential of wild type FOXM1 and the constitutively active FOXM1ΔNΔKEN, both individually and as part of the reconstituted complex in our model system. Both the constitutively active and the wild type form of FOXM1 were provided by Prof. Rene Medema, Netherlands Cancer Institute, Amsterdam, Netherlands and recloned into pLEX-

MCS lentiviral vector for uniformity. Previously Rovillain et al., 2011, showed that FOXM1ΔNΔKEN did exhibit some bypass potential when expressed from the pLNCX2 retroviral vector (Rovillain et al. 2011).

4.4.2.2 Comparison of the bypass potential of wild type and constitutively active FOXM1

Apart from ectopically expressing wild type and the constitutively active form of FOXM1 individually, two different DNA pools were made to reconstitute the whole complex, one with WT-FOXM1 and the other with the constitutively active non-degradable FOXM1ΔNΔKEN (Table 4.4). Respective lentiviruses were made in HEK293T cells, followed by stable transduction of $CL3^{EcoR}$ cells.

Table 4.4 DNA pools made to reconstitute whole MMB-FOXM1 complex with WT and constitutively active FOXM1

Reconstituted complex	**Constituents**
WC-FOXM1-WT*	LIN9, LIN37, LIN52, LIN54, Wild type FOXM1 and B-MYB
WC-FOXM1ΔNΔKEN	LIN9, LIN37, LIN52, LIN54, FOXM1ΔNΔKEN and B-MYB

*Wild type

Similar to the previous observations, both wild type and constitutively active FOXM1 yielded only few darkly stained growing colonies as shown in Figure 4.8. This indicated a weak senescence bypass potential of FOXM1 when analysed individually. In contrast, the cells stably transduced with components of MMB-FOXM1 complex exhibited strong bypass potential as significantly higher number of blue darkly stained colonies were obtained, as shown in Figure 4.8. However, on comparing the bypass potential of the two different MMB-FOXM1 complexes, a small but significant difference was observed between the active complex reconstituted with the constitutively active form and the wild type FOXM1. The complex reconstituted with constitutively active form of FOXM1 presented a greater number of colonies than the complex reconstituted with WT FOXM1, thereby indicating that the bypass observed with the active complex reconstituted with constitutively active FOXM1 was higher than the complex containing wild

type FOXM1. Therefore, for all the experiments conducted in this study, the constitutively active form of FOXM1 i.e. FOXM1ΔNΔKEN has been used.

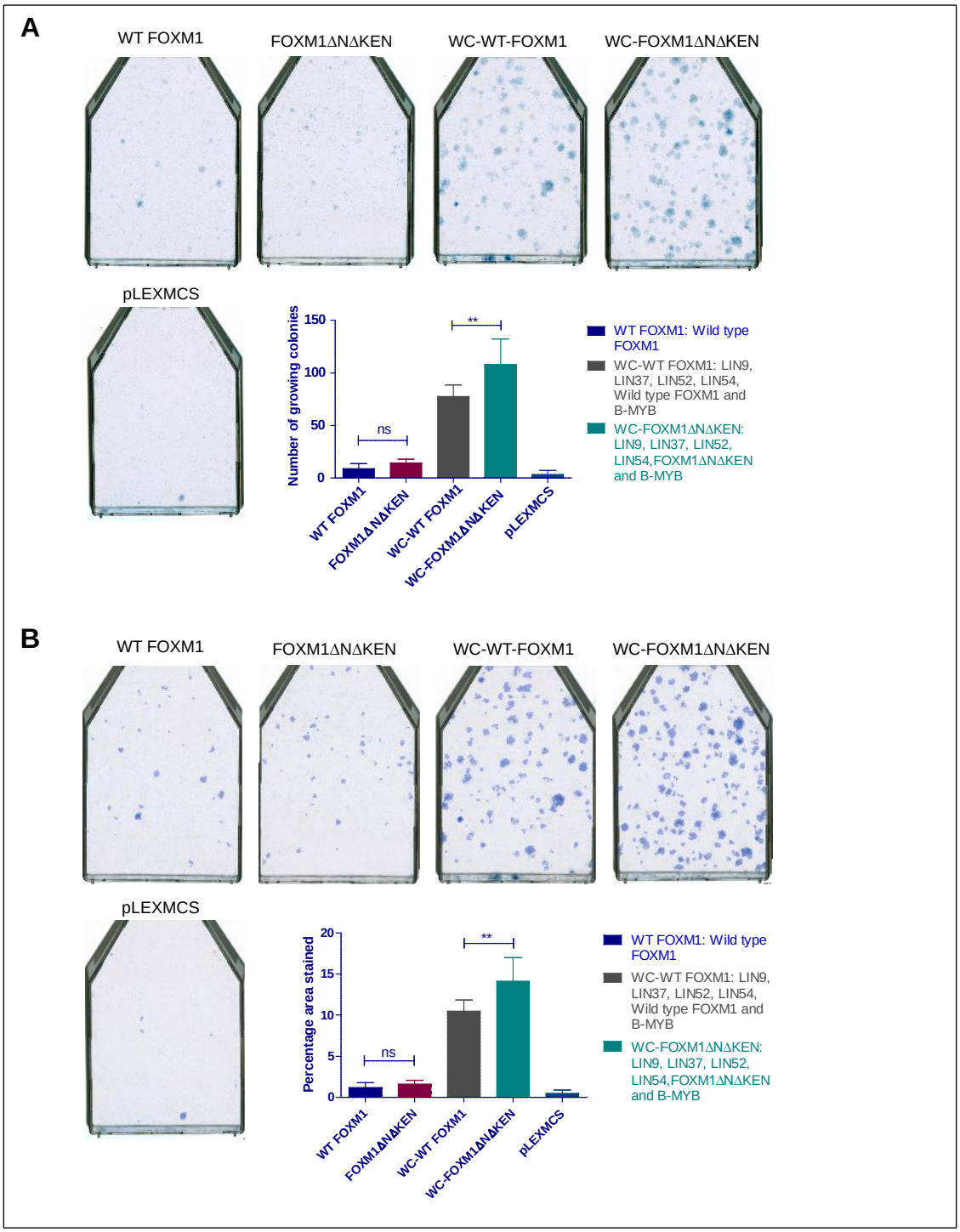

Figure 4.8 Comparison of senescence bypass assay of wild type and constitutively active form of FOXM1.

Bypass assay was performed twice independently at 5% CO_2 and 38.9°C with 35,000 cells per T-75 flask. For quantitative analysis the bar charts depict an overall average (+/- SD) of the independent repeat experiments. Empty vector pLEX-MCS was used as negative control. A) Manual analysis B) Computational analysis Statistical analysis was conducted using One-way ANOVA, Tukey's Multiple Comparison Test (*p<0.05, **p<0.01, ***p<0.001)

4.5 LIN52

4.5.1 Objective

It has recently been found that LIN52 is a key MuvB component which is essential for the switch between the repressive DREAM complex which promotes quiescence and the active MMB-FOXM1 complex which initiates cell cycle progression. Litovchick et al., 2011, have described the critical role of phosphorylation of LIN52 at serine 28 in promoting the binding of MuvB core to p130/E2F4 in quiescence (Litovchick et al. 2011). This binding leads to the assembly of the repressive DREAM complex that inhibits the progression of cell cycle and leads to quiescence. This phosphorylation is promoted by DYRK1A (dual-specific tyrosine-(Y)-phosphorylation regulated kinase 1A), that promotes entry into quiescence by promoting assembly of the DREAM complex (Litovchick et al. 2011). Rather surprisingly, DYRK1A, was found to be significantly down-regulated upon senescence growth arrest which was reversed upon senescence bypass, shown in Figure 4.2. Litovchick et al., 2011, also highlighted the importance of phosphorylation of Serine-28 by showing that inhibition of Ser-28 phosphorylation by DYRK1A results in the failure of cells to undergo growth arrest (Litovchick et al. 2011).

As phosphorylation of the LIN52 at Ser-28 is crucial, it was very important to examine the effect of phosphorylation of Ser-28 of LIN52 on senescence bypass in our model system. The rationale is that the non-phosphorylated form of LIN52 will inhibit assembly of repressive DREAM complex thereby promoting the formation of the active MMB-FOXM1 complex which promotes cell proliferation. Non-phosphorylated form can be mimicked by point substitution of Ser-28 to Ala-28. Therefore, non-phosphorylated LIN52 should show a strong bypass potential, whereas, phosphorylated LIN52, which can be mimicked by substitution of Ser-28 to Glu-28, should result in binding of p130, aiding the assembly of the repressive DREAM complex and hence should lead to a reduction in the senescence bypass potential.

4.5.2 LIN52 Alanine and Glutamic acid mutants

4.5.2.1 Cloning of LIN52 mutant forms

The 28th amino acid residue of LIN52 was mutated to alanine to mimic the non-phosphorylated form of LIN52, as alanine cannot be phosphorylated. Glutamic acid has been used in many cancer studies to mimic phosphorylated serine. Another mutant of LIN52 was designed where the 28th amino acid residue was mutated to glutamic acid to mimic phosphorylated LIN52. ORFs for both mutant forms of LIN52 were designed and ordered from GeneArt Gene Synthesis and Services [ThermoFisher Scienctific (https://www.thermofisher.com/)] (Figure 4.9). Mutant ORFs obtained were cloned into pLEX-MCS vector.

Multiple colonies were picked, plasmid DNA isolated and outsourced to SourceBioScience (https://www.sourcebioscience.com/) for sequence verification. For both mutants, LIN52 clones for which complete ORF sequence was checked for the presence of the mutation at the correct position, were chosen to study their effect on their ability to bypass senescence.

A. >LIN52-Ser

GGATCCACTAGTGACATGGGTTGGAAGATGGCGTCTCCCACAGACGGGACAGATCT
GGAAGCATCTTTGCTAAGTTTTGAAAAACTTGACCGTGCC**TCA**CCAGATCTTTGGC
CAGAACAATTACCAGGTGTTGCTGAATTTGCAGCTTCCTTCAAAAGTCCTATTACT
AGTTCTCCACCCAAATGGATGGCTGAGATAGAACGTGATGACATCGACATGTTGAA
AGAACTGGGGAGTCTCACCACGGCTAATTTGATGGAGAAGGTTCGAGGCCTACAGA
ACCTAGCCTATCAGCTGGGGCTGGATGAGTCCAGAGAGATGACACGGGGGAAATTC
CTCAATATTCTAGAGAAGCCCAAGAAGTAGGCGGCCGC

B. >LIN52-Ala aligned to LIN52-Ser

```
Query   1    GGATCCACTAGTGACATGGGTTGGAAGATGGCGTCTCCCACAGACGGGACAGATCTGGAA  60
             ||||||||||||||||||||||||||||||||||||||||||||||||||||||||||||
Sbjct   1    GGATCCACTAGTGACATGGGTTGGAAGATGGCGTCTCCCACAGACGGGACAGATCTGGAA  60

Query   61   GCATCTTTGCTAAGTTTTGAAAAACTTGACCGTGCCGCACCAGATCTTTGGCCAGAACAA  120
             ||||||||||||||||||||||||||||||||||| ||||||||||||||||||||||||
Sbjct   61   GCATCTTTGCTAAGTTTTGAAAAACTTGACCGTGCCTCACCAGATCTTTGGCCAGAACAA  120

Query   121  TTACCAGGTGTTGCTGAATTTGCAGCTTCCTTCAAAAGTCCTATTACTAGTTCTCCACCC  180
             ||||||||||||||||||||||||||||||||||||||||||||||||||||||||||||
Sbjct   121  TTACCAGGTGTTGCTGAATTTGCAGCTTCCTTCAAAAGTCCTATTACTAGTTCTCCACCC  180

Query   181  AAATGGATGGCTGAGATAGAACGTGATGACATCGACATGTTGAAAGAACTGGGGAGTCTC  240
             ||||||||||||||||||||||||||||||||||||||||||||||||||||||||||||
Sbjct   181  AAATGGATGGCTGAGATAGAACGTGATGACATCGACATGTTGAAAGAACTGGGGAGTCTC  240

Query   241  ACCACGGCTAATTTGATGGAGAAGGTTCGAGGCCTACAGAACCTAGCCTATCAGCTGGGG  300
             ||||||||||||||||||||||||||||||||||||||||||||||||||||||||||||
Sbjct   241  ACCACGGCTAATTTGATGGAGAAGGTTCGAGGCCTACAGAACCTAGCCTATCAGCTGGGG  300

Query   301  CTGGATGAGTCCAGAGAGATGACACGGGGGAAATTCCTCAATATTCTAGAGAAGCCCAAG  360
             ||||||||||||||||||||||||||||||||||||||||||||||||||||||||||||
Sbjct   301  CTGGATGAGTCCAGAGAGATGACACGGGGGAAATTCCTCAATATTCTAGAGAAGCCCAAG  360

Query   361  AAGTAGGCGGCCGC  374
             ||||||||||||||
Sbjct   361  AAGTAGGCGGCCGC  374
```

C. >LIN52-Glu aligned to LIN52-Ser

```
Query   1    GGATCCACTAGTGACATGGGTTGGAAGATGGCGTCTCCCACAGACGGGACAGATCTGGAA  60
             ||||||||||||||||||||||||||||||||||||||||||||||||||||||||||||
Sbjct   1    GGATCCACTAGTGACATGGGTTGGAAGATGGCGTCTCCCACAGACGGGACAGATCTGGAA  60

Query   61   GCATCTTTGCTAAGTTTTGAAAAACTTGACCGTGCCGAACCAGATCTTTGGCCAGAACAA  120
             ||||||||||||||||||||||||||||||||||| ||||||||||||||||||||||||
Sbjct   61   GCATCTTTGCTAAGTTTTGAAAAACTTGACCGTGCCTCACCAGATCTTTGGCCAGAACAA  120

Query   121  TTACCAGGTGTTGCTGAATTTGCAGCTTCCTTCAAAAGTCCTATTACTAGTTCTCCACCC  180
             ||||||||||||||||||||||||||||||||||||||||||||||||||||||||||||
Sbjct   121  TTACCAGGTGTTGCTGAATTTGCAGCTTCCTTCAAAAGTCCTATTACTAGTTCTCCACCC  180

Query   181  AAATGGATGGCTGAGATAGAACGTGATGACATCGACATGTTGAAAGAACTGGGGAGTCTC  240
             ||||||||||||||||||||||||||||||||||||||||||||||||||||||||||||
Sbjct   181  AAATGGATGGCTGAGATAGAACGTGATGACATCGACATGTTGAAAGAACTGGGGAGTCTC  240

Query   241  ACCACGGCTAATTTGATGGAGAAGGTTCGAGGCCTACAGAACCTAGCCTATCAGCTGGGG  300
             ||||||||||||||||||||||||||||||||||||||||||||||||||||||||||||
Sbjct   241  ACCACGGCTAATTTGATGGAGAAGGTTCGAGGCCTACAGAACCTAGCCTATCAGCTGGGG  300

Query   301  CTGGATGAGTCCAGAGAGATGACACGGGGGAAATTCCTCAATATTCTAGAGAAGCCCAAG  360
             ||||||||||||||||||||||||||||||||||||||||||||||||||||||||||||
Sbjct   301  CTGGATGAGTCCAGAGAGATGACACGGGGGAAATTCCTCAATATTCTAGAGAAGCCCAAG  360

Query   361  AAGTAGGCGGCCGC  374
             ||||||||||||||
Sbjct   361  AAGTAGGCGGCCGC  374
```

Figure 4.9 LIN52 mutants.
A) WT LIN52-Ser sequence depicting the key 28th Serine marked in red. B) LIN52-Ser aligned to LIN52-Ala where 28th residue is mutated to Alanine, indicated by red oval. C) LIN52-Ser aligned to LIN52-Glu where 28th residue is mutated to Glutamic acid, indicated by red oval.

4.5.2.2 Comparison of the bypass potential of LIN52 mutants

The bypass potential of both LIN52 mutants was studied individually as well as part of the reconstituted MMB-FOXM1 complex. Lentiviruses were prepared for both LIN52 mutants i.e. LIN52-Ala and LIN52-Glu individually in HEK293T cells. DNA pools described in Table 4.5 were prepared to reconstitute the active whole complex with LIN52 mutant forms as well as one without LIN52. Respective lentiviruses made were used to stably transduce $CL3^{EcoR}$ cells and assess the senescence bypass potential.

Table 4.5 DNA pools made to reconstitute whole complex (MMB-FOXM1) to study the effect of different LIN52 mutants

Reconstituted complex	Constituents
WC-Ala	1 µg LIN9, 1 µg LIN37, 1 µg LIN52-Ala, 1 µg LIN54, 1 µg FOXM1ΔNΔKEN and 1 µg B-MYB
WC-Glu	1 µg LIN9, 1 µg LIN37, 1 µg LIN52-Glu, 1 µg LIN54, 1 µg FOXM1ΔNΔKEN and 1 µg B-MYB
WC w/o LIN52	1 µg LIN9, 1 µg LIN37, 1 µg LIN54, 1 µg FOXM1ΔNΔKEN, 1 µg B-MYB and 1 µg pLEX-MCS

The results of the senescence bypass assay are shown in Figure 4.10. They were somewhat counterintuitive. LIN52-Ala on its own exhibited a high number of densely stained dark blue colonies. Similarly, MMB-FOXM1 complex with LIN52-Ala also generated significant number of stained colonies. This indicates that LIN52-Ala mutant which mimics the non-phosphorylated form showed a strong bypass potential as expected, both when expressed individually as well as part of the whole complex. Variant LIN52 is expected to dominantly disrupt formation of the DREAM complex and hence leading to bypass of senescence. Therefore, the strong bypass observed by LIN52-Ala is due to loss/interference with normal LIN52-Ser function.

On the other hand, the bypass observed for LIN52-Glu mutant which was supposed to mimic the phosphorylated form, did not show the expected reduction in the bypass potential as a similar number of densely blue stained colonies were

obtained for LIN52-Glu as were observed for LIN52-Ala shown in Figure 4.10. Similarly, the MMB-FOXM1 complex reconstituted with LIN52-Glu presented the unexpected high number of colonies which were comparable to the number of colonies generated by the complex consisting LIN52-Ala. Therefore, no significant reduction in the bypass potential of LIN52-Glu mutant was observed neither individually nor as a part of the complex, compared to LIN52-Ala mutant, shown graphically in Figure 4.10.

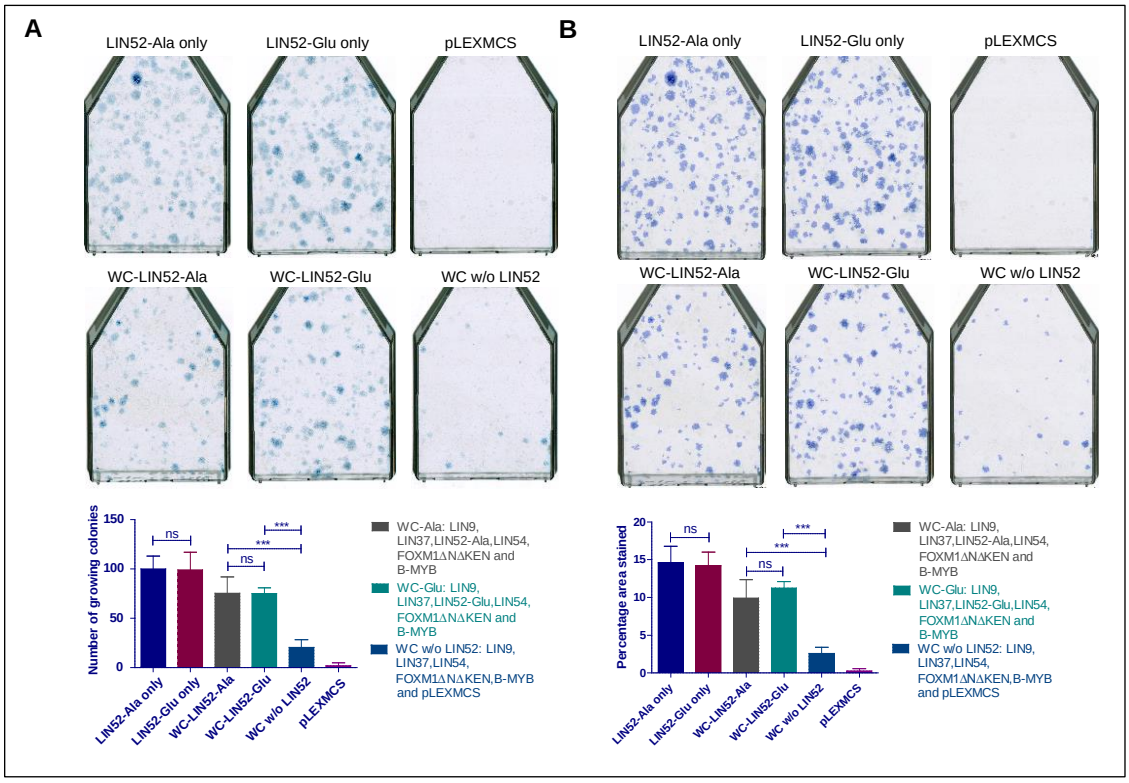

Figure 4.10 Comparison of senescence bypass assay for LIN52-Ala and LIN52-Glu mutants. Bypass assay was performed twice independently at 5% CO_2 and 38.9°C with 35,000 cells per T-75 flask. For quantitative analysis the bar charts depict an overall average (+/- SD) of the independent repeat experiments. Empty vector pLEX-MCS was used as negative control. A) Manual analysis B) Computational analysis. Statistical analysis was conducted using One-way ANOVA, Tukey's Multiple Comparison Test (*p<0.05, **p<0.01, ***p<0.001)

However, the results presented in Figure 4.10 show a marked reduction in the bypass potential of the MMB-FOXM1 complex reconstituted without LIN52. This highlights the huge importance of the role played by loss of LIN52 towards the strong senescence bypass potential observed.

4.5.3 WT LIN52-Ser 28

4.5.3.1 Cloning

Previous experiment had set out to distinguish between the bypass potential of phosphorylated and non-phosphorylated forms of LIN52 but unfortunately it failed. It has been seen in many studies that glutamic acid does not perfectly mimic the phosphorylation of serine (Chen and Cole 2015). The other possibility for not being able to detect a reduction in bypass potential could be because the phosphomimic glutamate residue binds weakly with p130, thereby enabling cell cycle progression.

As initially only the ends of the sequences were verified, during the course of previous experiment the whole sequence for all LIN52 forms was also determined. Surprisingly the whole sequence revealed that the original LIN52 clone that we had received from Prof. DeCaprio actually had alanine at the 28th amino acid residue. Hence, as the WT LIN52-Ser form had never been tested in this study, another LIN52 ORF where 28th amino acid residue was serine was designed and ordered from GeneArt Gene Synthesis and Services [ThermoFisher Scienctific (https://www.thermofisher.com/)]. WT LIN52-Ser was successfully cloned into pLEX-MCS. After successful cloning into pLEX-MCS, multiple colonies were picked to isolate plasmid DNA and outsourced for sequence verification to identify a correct clone before studying its bypass potential.

4.5.3.2 Senescence bypass potential of WT LIN52-Ser

Lentiviruses were prepared for WT LIN52-Ser individually along with the LIN52-Ala and LIN52-Glu and were used to stably transduce CL3^{EcoR} to compare the bypass potential.

The results were striking. Similar to the results obtained from the previous experiment both LIN52-Ala and LIN52-Glu showed a high number of densely stained blue colonies indicating strong bypass potential. To our surprise, CL3^{EcoR} cells transduced with WT-LIN52-Ser were unable to bypass senescence. No healthy growing colonies were obtained for WT-LIN52-Ser after staining with methylene blue after the culture was allowed to grow for three weeks. The

bypass potential of the WT LIN52-Ser was drastically reduced, shown qualitatively and quantitatively in Figure 4.11. There was a highly significant reduction in the bypass potential of WT LIN52-Ser compared to LIN52-Ala and LIN52-Glu as no colonies were obtained for WT LIN52-Ser. To draw definite conclusions from the results of this experiment, biochemical confirmatory experiment ensuring the expression of WT-LIN52-Ser is must.

The results suggest that in our model system non-phosphorylated forms of LIN52 exhibit a consistent, strong and efficient bypass potential highlighting the importance of the non-phosphorylated form of LIN52 in bypassing senescence by blocking DREAM complex assembly. Another suggestion from this experiment was the critical role played by phosphorylation of LIN52 as WT LIN52-Ser showed a strong reduction in the bypass potential. It was no higher than the empty vector control. These results suggest that phosphorylation of Serine residue of LIN52 was inhibitory towards bypassing the senescence in $CL3^{EcoR}$ cells indirectly suggesting a role for the repressive DREAM complex in regulating senescence as the phosphorylated form of LIN52 can lead to the assembly of the repressive DREAM complex, thereby preventing cell cycle progression and a reduction in the bypass of senescence.

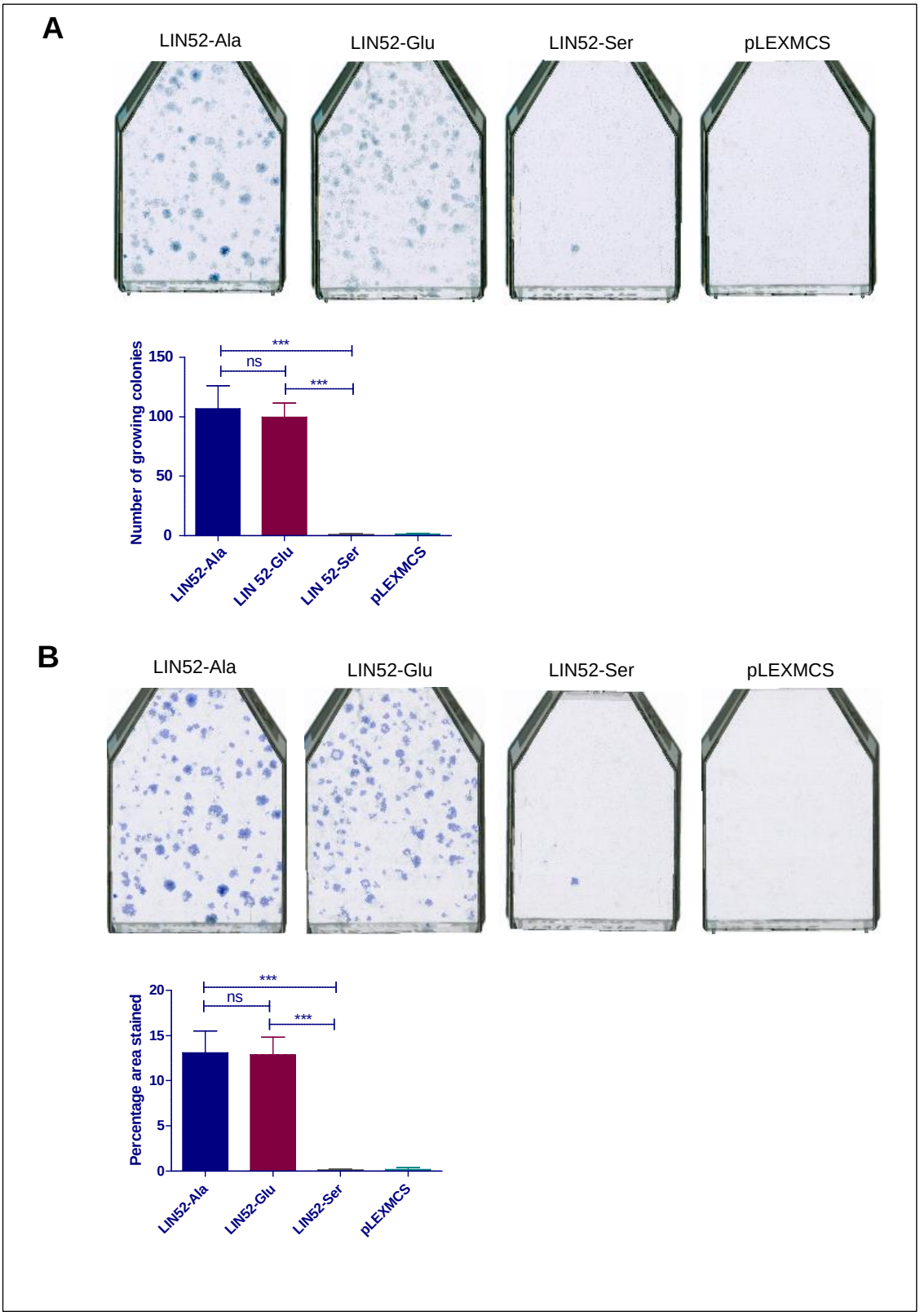

Figure 4.11 Comparison of senescence bypass assay for different LIN52 mutants.
Bypass assay was performed twice independently at 5% CO_2 and 38.9°C with 35,000 cells per T-75 flask. Both LIN52 mutants showed strong senescence bypass whereas WT-LIN52-Ser did not show any pass. For quantitative analysis the bar charts depict an overall average (+/- SD) of the independent repeat experiments. Empty vector pLEX-MCS was used as negative control. A) Manual analysis B) Computational analysis. Statistical analysis was conducted using One-way ANOVA, Tukey's Multiple Comparison Test (*p<0.05, **p<0.01, ***p<0.001)

4.5.4 Comparison of bypass potential of LIN52 mutants after dilution

4.5.4.1 Objective

As both LIN52-Ala and LIN52-Glu showed very strong bypass potential as depicted in Figure 4.11, to rule out the possibility that a difference in bypass potential was not observed due to saturation, an independent preliminary experiment was designed. The three LIN52 mutants were diluted ten times with empty vector i.e. pLEX-MCS at the lentivirus production stage. The rationale behind doing this was to reduce the total number of colonies to be able to observe any small differences.

4.5.4.2 Comparison of the bypass potential

Lentiviruses made from each of the LIN52 mutants individually as well as after diluting them ten times, shown in Table 4.6 were used to stably transduce $CL3^{EcoR}$ cells.

Table 4.6 LIN52 mutants diluted tenfold.

Reconstituted complex	Constituents
9+1 LIN52-Ala	1 µg LIN52-Ala + 9 µg pLEX-MCS
9+1 LIN52-Glu	1 µg LIN52-Glu + 9 µg pLEX-MCS
9+1 LIN52-Ser	1 µg LIN52-Ser + 9 µg pLEX-MCS

The results of this preliminary experiment are shown in Figure 4.12. For both LIN52-Ala and LIN52-Glu a high number of densely stained colonies were obtained. LIN52-Ser, similar to the results obtained previously, hardly exhibited any blue healthy growing colonies. This again confirmed the severe reduction in bypass potential with WT-LIN52-Ser, highlighting the crucial role of LIN52 phosphorylation in senescence in our model system. As expected after dilution, a clear reduction was observed in the total number of colonies obtained after diluting the DNAs. Interestingly, upon analysis of the results obtained from this preliminary dilution experiment, it was observed that the number of colonies obtained for LIN52-Glu were slightly less than LIN52-Ala. This indicated a small

reduction in the bypass potential for LIN52-Glu when compared to LIN52-Ala, which contrasted with the bypass observed for undiluted LIN52, where no significant reduction was observed here as well as previously. This dilution experiment was conducted only once and therefore needs to be repeated to clarify and establish any significant difference between the bypass potential of LIN52-Ala and LIN52-Glu.

Nevertheless, diluting the LIN52 mutants ten times did lower the total number of colonies obtained and suggested the possibility of a difference between the bypass potential of LIN52-Ala and LIN52-Glu mutants, but this needs to be further validated by carrying out more repeats.

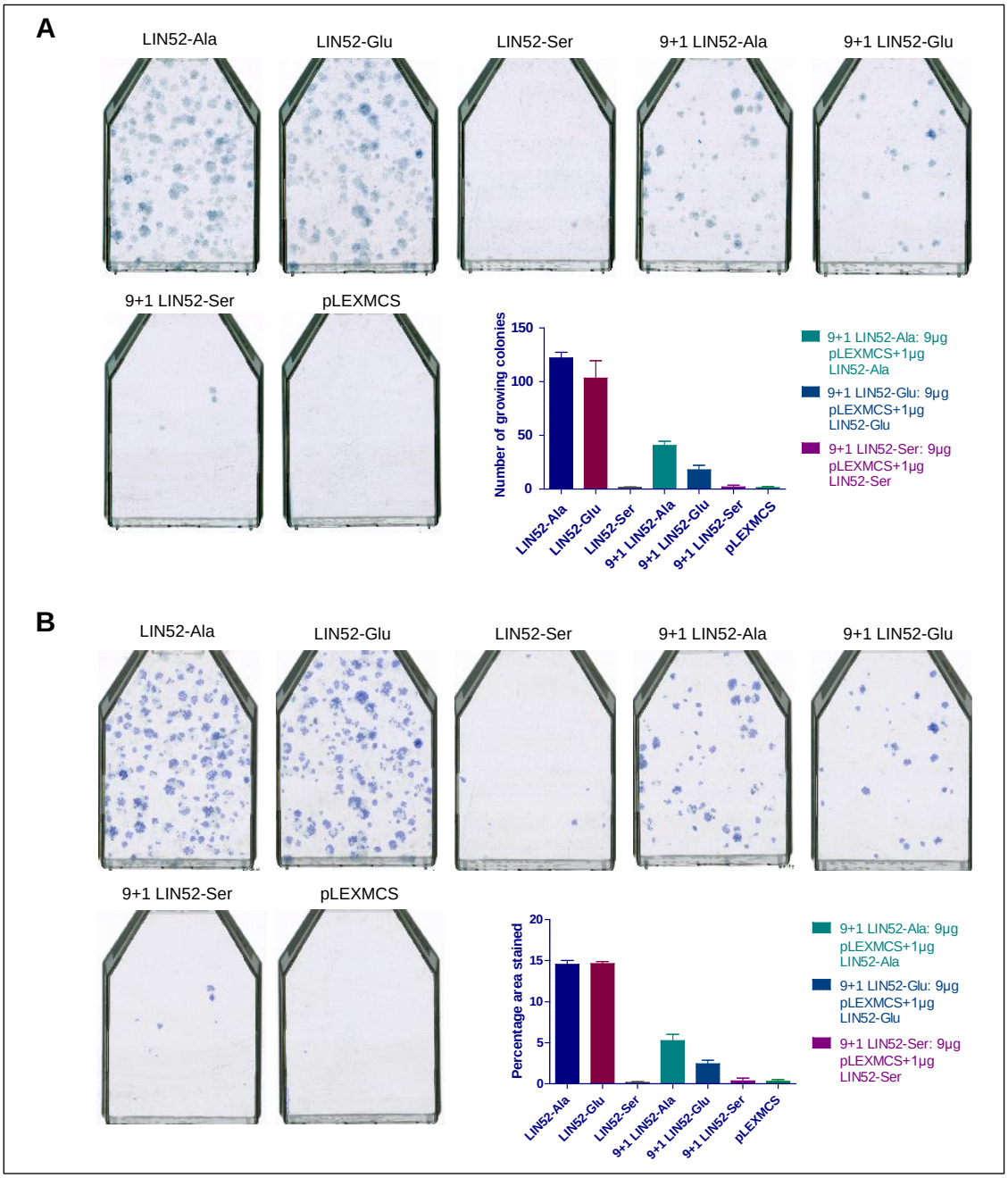

Figure 4.12 Comparison of bypass potential of different LIN52 mutants after dilution
Bypass assay was performed at 5% CO_2 and 38.9°C with 35,000 cells per T-75 flask. Empty vector pLEX-MCS was used as negative control. A) Manual analysis B) Computational analysis.

4.5.5 Comparison of the bypass potential of active whole complex reconstituted with different LIN52 mutants

4.5.5.1 Objective

As WT LIN52-Ser showed clear reduction in senescence bypass potential when assayed on its own, the next obvious question was: would WT LIN52-Ser as part of the MMB-FOXM1 complex influence the strong bypass potential observed by the complex.

4.5.5.2 Comparison of senescence bypass

To compare the bypass potential of the whole complex containing different LIN52 mutants, an experiment was designed with two different DNA pools to reconstitute the whole complex, Table 4.7. One DNA pool contained the constitutively active form of LIN52 i.e. LIN52-Ala and the other DNA pool included WT LIN52-Ser which is capable of being phosphorylated thereby potentially leading to the formation of the inhibitory DREAM complex. Lentiviruses from both these DNA pools were packaged in HEK 293T cells and used to stably transduce $CL3^{EcoR}$ cells.

Table 4.7 DNA pools made to study the effect of WT LIN52-Ser in reconstituted MMB-FOXM1 complex

Reconstituted complex	Constituents
WC	1 µg LIN9, 1 µg LIN37, 1 µg LIN52-Ala, 1 µg LIN54, 1 µg FOXM1ΔNΔKEN and 1 µg B-MYB
WC-Ser	1 µg LIN9, 1 µg LIN37, 1 µg LIN52-Ser, 1 µg LIN54, 1 µg FOXM1ΔNΔKEN and 1 µg B-MYB

Figure 4.13 shows the results obtained after staining the flasks after three weeks. Sufficient number of stained growing colonies were obtained for the cells transduced with DNA pool consisting of MMB-FOXM1 complex containing the LIN52-Ala. Fewer stained colonies were obtained upon stable transduction with DNA pool of MMB-FOXM1 complex consisting of WT-LIN52-Ser. Upon analysis

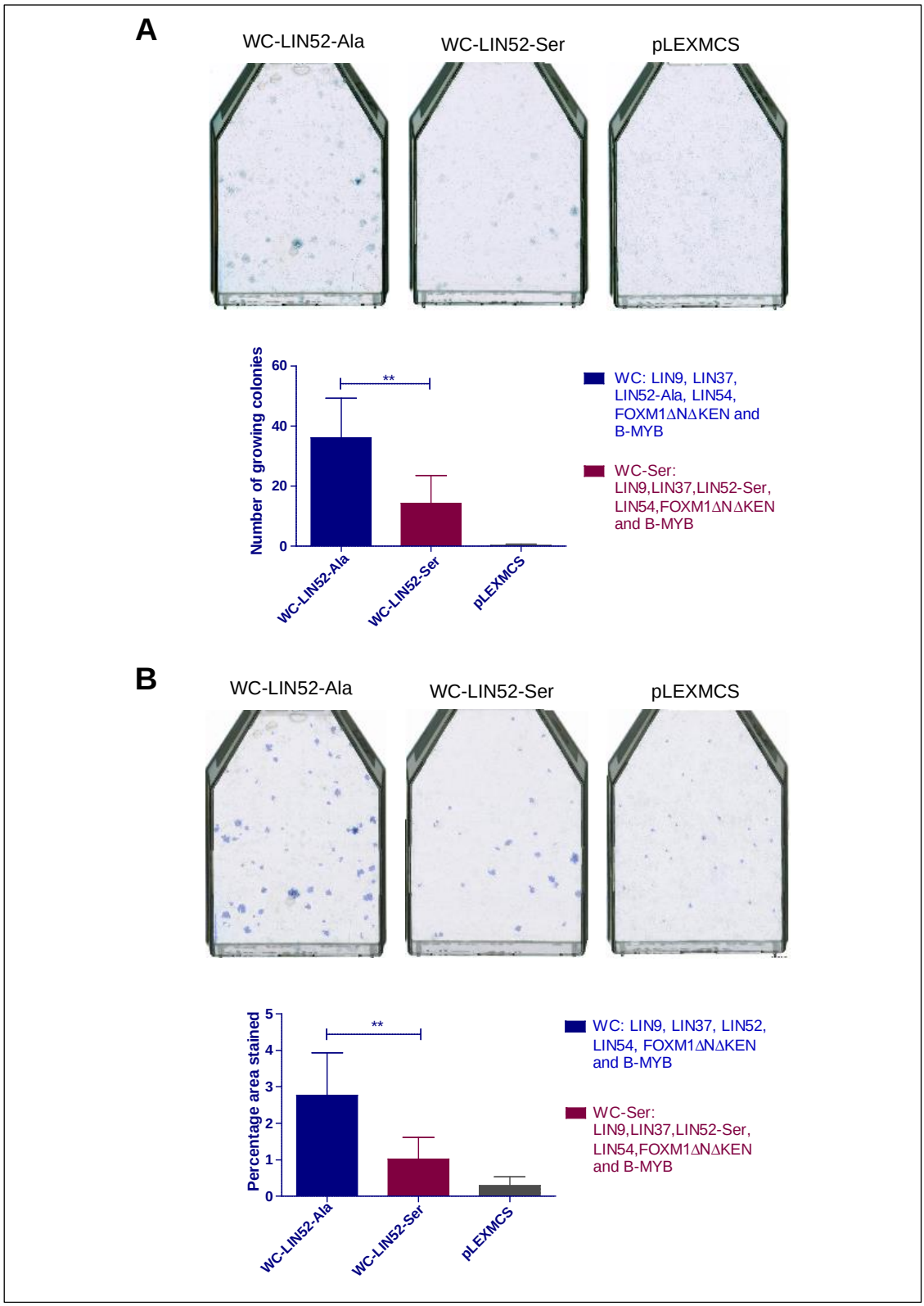

Figure 4.13 Comparison of the bypass potential of active whole complex reconstituted with different LIN52 mutant forms.

Bypass assay was performed twice independently at 5% CO_2 and 38.9°C with 35,000 cells per T-75 flask. For quantitative analysis the bar charts depict an overall average (+/- SD) of the independent repeat experiments. Empty vector pLEX-MCS was used as negative control. A) Manual analysis B) Computational analysis. Statistical analysis was conducted using One-way ANOVA, Tukey's Multiple Comparison Test (*p<0.05, **p<0.01, ***p<0.001)

the data indicated a reduction in the bypass potential when WT LIN52-Ser was present in the MMB-FOXM1complex compared to when LIN52-Ala was present as part of the MMB-FOXM1 complex. This highlighted the importance of the non-phosphorylated form of LIN52 for the strong bypass observed by MMB-FOXM1 complex in $CL3^{EcoR}$ cells. It also demonstrated the ability of the WT LIN52-Ser to significantly reduce the bypass potential not only when expressed individually but also as part of the MMB-FOXM1 complex.

4.6 Examination of synergy between the three identified critical components of the active MMB-FOXM1 complex

4.6.1 Objective

The previous series of experiments conducted in this study showed that three most important components for the bypass potential observed by active whole complex were: LIN52, FOXM1 and B-MYB. When studied individually both LIN52 and B-MYB have shown a strong bypass potential whereas FOXM1 exhibited marginal bypass. Interestingly in the previous experiments' synergy was established with respect to B-MYB as described in section 4.1.2. Therefore, it was important to study if there was any synergy present with respect to the remaining two key components, LIN52 and FOXM1.

The rationale of this experiment was to rule out the possibility that the strong bypass potential observed for the whole complex was solely due to the presence of any one of the critical components. This would also help to establish if there was any synergy between the components of the active complex i.e. is the bypass observed simply a sum of the activity of the three critical components or is the effect greater?

4.6.2 Study of bypass potential to check for synergy

To establish any synergy present with respect to the three key components, experiment was designed where the extent of bypass of each of the relevant component was assessed with the same amount of DNA as was present in the reconstituted MMB-FOXM1 complex. This was then compared to the bypass of the whole MMB-FOXM1 complex to identify synergy. Lentiviruses for the DNA pools in Table 4.8 were made in HEK293T cells followed by stable transduction of $CL3^{EcoR}$ cells.

Table 4.8 DNA pools prepared to check for synergy

Reconstituted complex	Constituents
WC	1 µg LIN9, 1 µg LIN37, 1 µg LIN52, 1 µg LIN54, 1 µg FOXM1ΔNΔKEN and 1 µg B-MYB
5+1 LIN52	1 µg LIN52+ 5 µg pLEX-MCS
5+1 FOXM1ΔNΔKEN	1 µg FOXM1ΔNΔKEN+ 5 µg pLEX-MCS
5+1 B-MYB	1 µg B-MYB+ 5 µg pLEX-MCS

Qualitative and quantitative results obtained after staining the flasks from this experiment are presented in Figure 4.14. The highest number of densely stained colonies were observed with the reconstituted MMB-FOXM1 complex. Comparatively a smaller number of stained colonies were obtained for cells transduced with one-sixth of each of LIN52, FOXM1 and B-MYB component of the complex. Quantitative analysis revealed that the number of colonies obtained with one sixth LIN52 were significantly lower than the number of colonies obtained with whole complex. This indicated that even though LIN52 is capable of strongly bypassing senescence on its own, bypass on its own was less efficient than when all the components of the complex were present together. The number of colonies obtained when one sixth of B-MYB and FOXM1 were present were even lower and comparable to the negative control indicating presence of clear synergy among the different components of MMB-FOXM1 complex.

There was a clear reduction in the bypass potential observed for LIN52, FOXM1 and B-MYB when they were present in the same amount as in the complex i.e. one sixth. Taken together, these results suggest that none of the three critical components show similar extent of bypass when studied individually in the same ratio, as shown when all the components of the complex were present together. Therefore, these experiments clearly indicate synergy between the components of the whole complex.

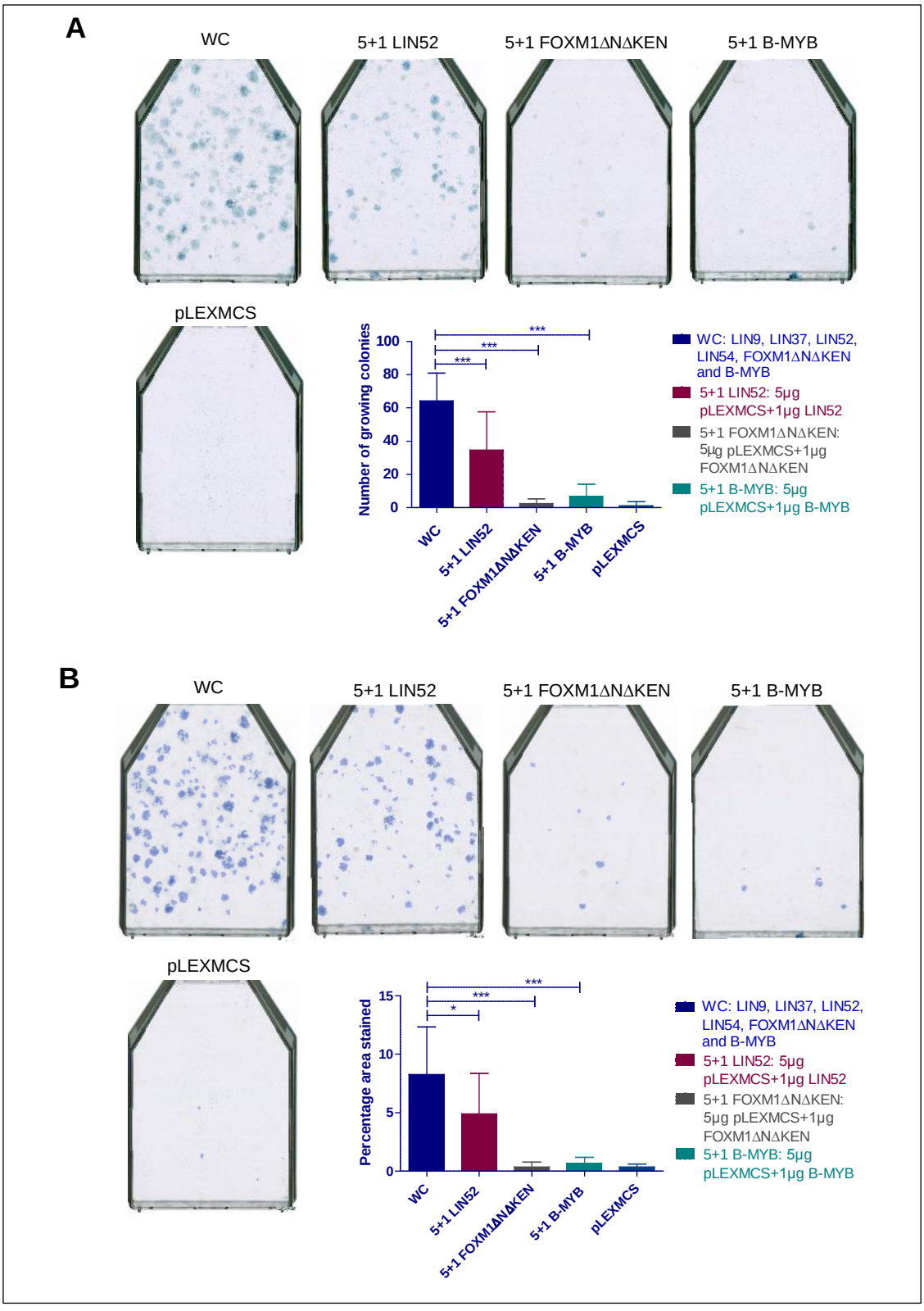

Figure 4.14 Study of bypass for presence of synergy with respect to the three identified critical components of the MMB-FOXM1 complex.

Bypass assay was performed thrice independently at 5% CO_2 and 38.9°C with 35,000 cells per T-75 flask. For quantitative analysis the bar charts depict an overall average (+/- SD) of all three-independent repeat experiments. Empty vector pLEX-MCS was used as a negative control. A) Manual analysis B) Computational analysis. Statistical analysis was conducted using One-way ANOVA, Tukey's Multiple Comparison Test (*p<0.05, **p<0.01, ***p<0.001)

4.7 Comparison of the bypass potential of the active whole complex (MMB-FOXM1) to the combination of the three critical components

4.7.1 Objective

This experiment was motivated by the finding that there was synergy when three critical components were present as part of the whole complex. Therefore, it was interesting to study the bypass potential of the three critical components when present together and compare it to the bypass potential of the whole complex containing all six components. This will also allow us to determine if a combination of the three key components identified in this study would work as well as the whole MMB-FOXM1 complex in the senescence bypass assay.

4.7.2 Comparison of bypass potential

Following DNA pools were made to compare the bypass potential of reconstituted MMB-FOXM1 whole complex to a combination of the three critical components, described in Table 4.9. Lentiviruses for the DNA pools were prepared in HEK293T cells along with the negative vector control (pLEX-MCS). The lentiviruses were used to stably transduce CL3^{EcoR} cells and assayed for senescence bypass.

Table 4.9 DNA pools made to compare bypass of whole complex (MMB-FOXM1) to three critical components

Reconstituted complex	Constituents
WC	1 µg LIN9, 1 µg LIN37, 1 µg LIN52, 1 µg LIN54, 1 µg FOXM1ΔNΔKEN and 1 µg B-MYB
3+3	3 µg pLEX-MCS, 1 µg LIN52, 1 µg FOXM1ΔNΔKEN and 1 µg B-MYB

Results obtained are displayed in Figure 4.15. Staining with methylene blue after three weeks resulted in growing blue colonies for both the whole MMB-FOXM1

complex as well as for three components (LIN52, FOXM1ΔNΔKEN and B-MYB) present together.

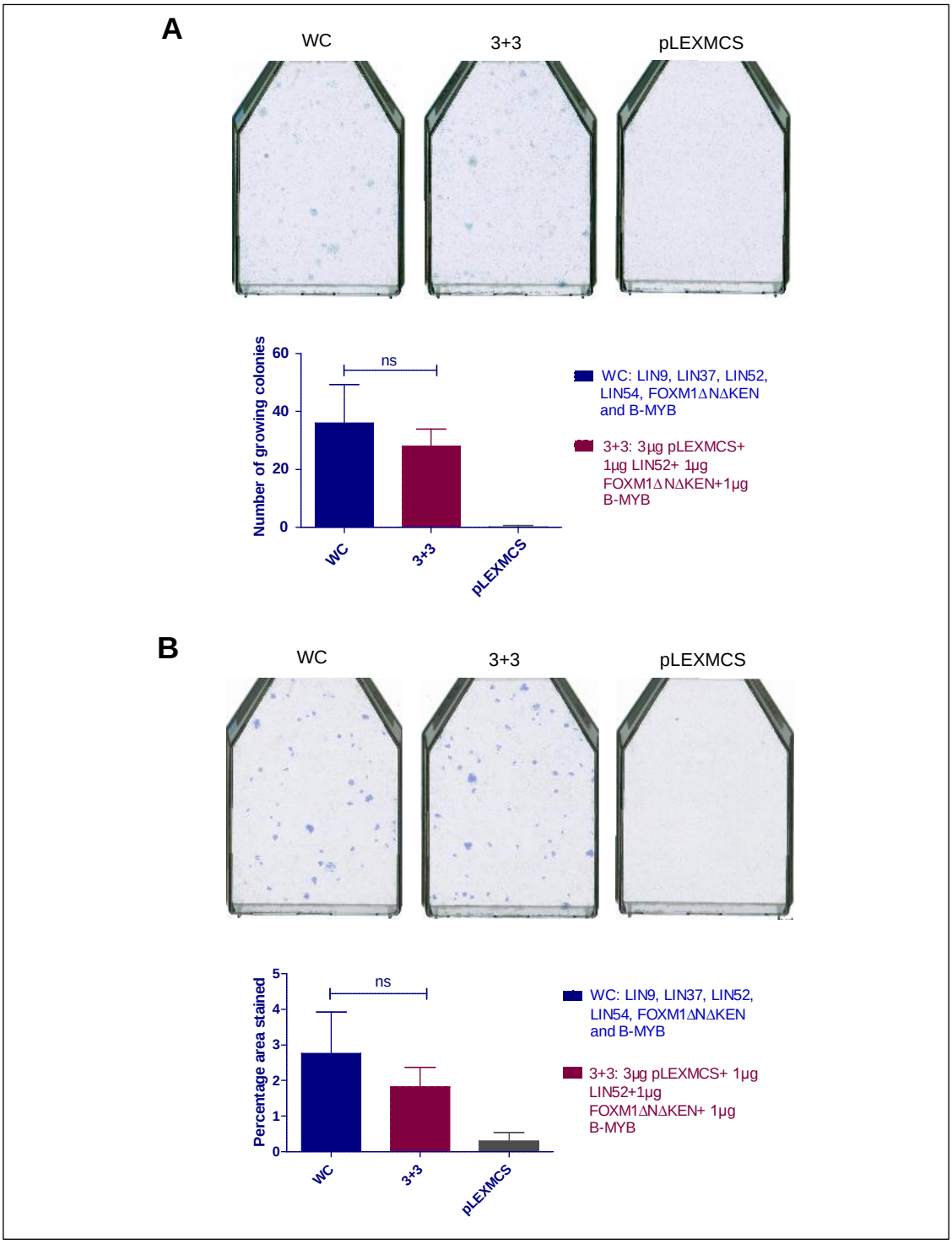

Figure 4.15 Comparison of the bypass potential of the whole MMB-FOXM1 complex to three components together

Bypass assay was performed twice independently at 5% CO_2 and 38.9°C with 35,000 cells per T-75 flask. For quantitative analysis the bar charts depict an overall average (+/- SD) of the independent repeat experiments. Empty vector pLEX-MCS was used as negative control. A) Manual analysis B) Computational analysis. Statistical analysis was conducted using One-way ANOVA, Tukey's Multiple Comparison Test (*p<0.05, **p<0.01, ***p<0.001)

Quantitative analysis of the results showed that a combination of the three components demonstrated weaker bypass potential when compared to the bypass of the whole MMB-FOXM1 complex, but the reduction was not significant as shown in Figure 4.15.

This was a very important finding that demonstrated for the first time the bypass potential of the combination of LIN52, FOXM1 and B-MYB. They further demonstrated that the strong bypass potential observed by the whole complex observed in our model system is mainly because of the combined synergistic actions of the three key components namely: LIN52, FOXM1 and B-MYB.

4.8 Construction of multi-cistronic vectors expressing LIN52, FOXM1 and B-MYB using 2A-self cleaving peptides

4.8.1 Objective

Previous experiments clearly established that LIN52, FOXM1 and B-MYB were the key components for the bypass observed by the MMB-FOXM1 complex in $CL3^{EcoR}$ cells. Moreover, the bypass observed for three components together was comparable to the whole MMB-FOXM1 complex.

Until now all the experiments were undertaken by preparing pools of different constructs and packaging them in lentiviruses and using these pools to infect cells. Even more importantly they relied on cells being infected by multiple viruses. We therefore decided it would be very informative to prepare multi-cistronic constructs to directly compare the bypass potential of these critical components. Multi-cistronic vectors constructed using 2A- self cleaving peptides can express multiple proteins from the same mRNA as opposed to traditional approach of using different vectors or cistrons to co-express multiple genes.

The rationale behind designing multi-cistronic constructs is to ensure that all genes are transduced and expressed simultaneously in each cell after successful infection. In contrast, when the infections are done with lentiviruses made from mixed pool of TFs, there is a possibility that an infected cell could be infected by any one, two or multiple lentiviruses. Hence, to rule out this possibility and to investigate the functional role of the key identified components in detail, varying

combinations of multi-cistronic viral vectors were designed and successfully constructed using the 2A 'self-cleaving' peptide strategy (Szymczak et al. 2004). Cloning experiments were performed with the help of Ms. Marta Benedekova, a UCL MSci rotation student.

Self-cleaving 2A peptides offer many advantages over other strategies for co-expressing genes. Firstly, 2A peptides are short peptides about 20 amino acids long as opposed to IRES elements which are quite big; the short size of 2A peptides therefore allows room to clone larger gene sequence as there is a restriction on the size of insert that can be packaged. This is relevant in this study as we were interested in cloning large fragments like B-MYB which is 4284 bp long. Secondly, no external factors are required to initiate the cleavage of polyproteins due to their self-cleaving because of ribosome skipping. Thirdly, as opposed to IRES elements where the second gene is expressed at a lower level compared to the first one, 2A peptides produce equimolar amounts of protein from the multiple genes from the same mRNA, irrespective of being present upstream or downstream of 2A peptide.

Kim et.al., 2011, studied the cleavage efficiency of four different 2A peptides derived from foot-and-mouth disease virus (F2A), Thosea asigna virus (T2A), porcine teschovirus-1 (P2A) and equine rhinitis virus (E2A) in widely used human cell lines, adult mice and zebra fish embryos (Kim et al. 2011a). Detailed experimental investigations from this study reported that P2A peptide has the highest cleavage efficiency among the four 2A peptides followed by T2A, E2A and F2A (Kim et al. 2011a). Based on these results, in this study P2A and T2A peptides were used to generate different combinations of multi-cistronic vectors shown in Figure 4.16A. It has been suggested that addition of Gly-Ser-Gly nucleotide sequence at the N-terminus of 2A peptides leads to a further increase in cleavage efficiency. The cleavage occurs between the glycine and proline residue as indicated in Figure 4.16B (Ryan et al. 1991).

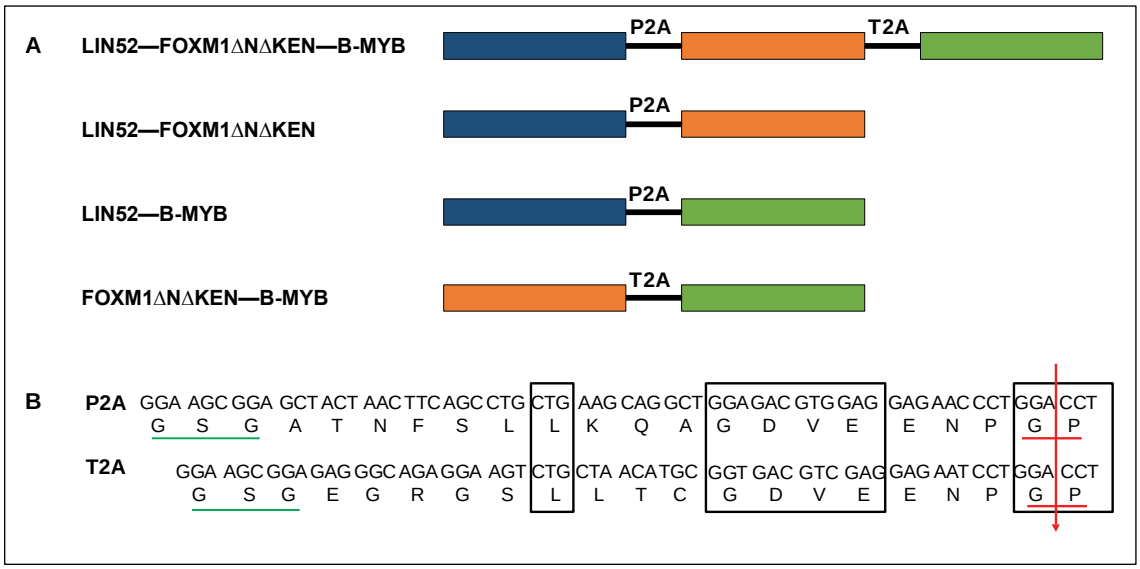

Figure 4.16 2A 'self-cleaving' peptides used to generate different multi cistronic constructs
A. Diagrammatic representation of different multi-cistronic constructs designed in this study and 2A peptides used to connect the genes in each construct. B. P2A: Porcine teschovirus-1 (66 bp) and T2A: Thosea asigna virus (63 bp), sequences of the two peptides. Boxed areas indicate conserved residues. Green underlined GSG sequence, depict residues added to improve the cleavage efficiency. Red arrow shows the cleavage point of 2A peptides between Glycine and Proline residue. Constitutively active forms for both LIN52 and FOXM1 i.e. LIN52-Ala and FOXM1 Δ N Δ KEN respectively were used.

4.8.2 Design and construction of multi-cistronic vectors using 2A 'self-cleaving' peptides

To construct the bi-cistronic and multi-cistronic cassettes, P2A and T2A peptides were used. It was ensured that all the internal gene constructs in the multi-cistronic vector did not have a terminator codon as the cleavage of 2A peptides occurs post translationally. A detailed schematic illustration of the cloning approach used is presented in Figure 4.17. It describes the position and direction of corresponding primers and specifies their sequences.

A.

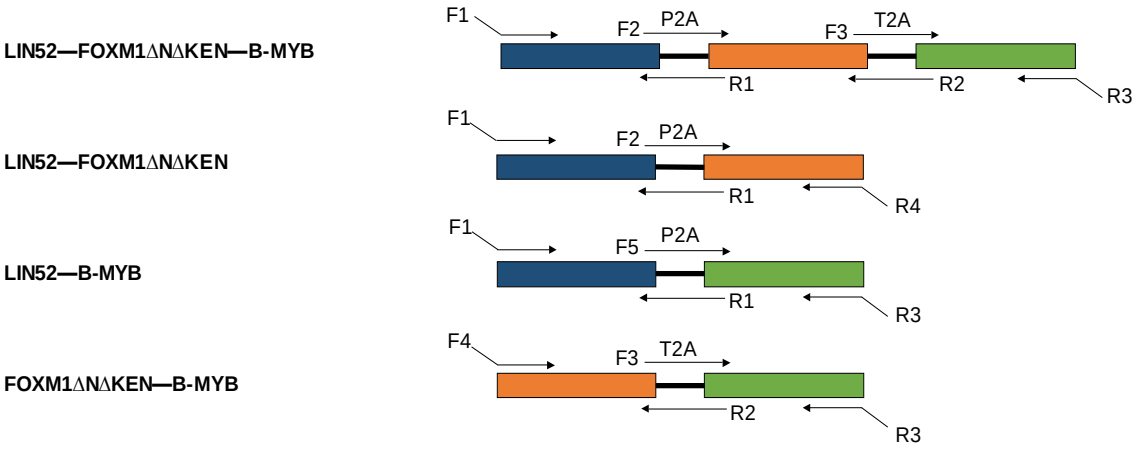

B.

Primer Code	Sequence (5'→3')
F1: ((LIN52))	CCATAGAAGACACCGACTCTACTAGA**GGATCC**ACTAGTGGAC**((**ATGGGTTGGAAGATGGCG**))**
F2:**P2A**((FOXM1))	**CTACTAACTTCAGCCTGCTGAAGCAGGCTGGAGACGTGGAGGAGAACCCTGGACCT((**ATGGATTACAAGGATGACGAC**))**
F3: **T2A**((B-MYB))	**CGGAGAGGGCAGAGGAAGTCTGCTAACATGCGGTGACTCGAGGAGAATCCTGGACCT((**ATGTCTCGGCGGACGCGCTGC**))**
F4: ((FOXM1))	CCATAGAAGACACCGACTCTACTAGA**GGATCC**ACTAGTGAC**((**ATGGATTACAAGGATGACGACGATAAG**))**
F5: **P2A**((B-MYB))	**CTACTAACTTCAGCCTGCTGAAGCAGGCTGGAGACGTGGAGGAGAACCCTGGACCT((**ATGTCTCGGCGGACGCGCTGC**))**
R1: **P2A**((LIN52))	**CTCCACGTCTCCAGCCTGCTTCAGCAGGCTGAAGTTAGTAGCTCCGCTTCC((**CTTCTTGGGCTTCTCTAGAATATTGAGG**))**
R2:**T2A**((FOXM1))	**CAGGATTCTCCTCGACGTCACCGCATGTTAGCAGACTTCCTCTGCCCTCTCCGCTTCC((**CTGTAGCTCAGGAATAAACTGGGACCAGTTGATGTTG**))**
R3: ((B-MYB))	GACGCGTCGGGCCCTCTAGACTCGA**GCGGCCGC**TCACTATACTGTAGC**((**TCAGGACAAGATGAGGGTC**))**
R4: ((FOXM1))	CGCGTCGGGCCCTCTAGACTCGA**GCGGCCGC((**TCACTACTGTAGCTCAGGAATAAACTGGGACCAGTTGATGTTG**))**

Figure 4.17 Cloning strategy used to create 2A peptide linked multi-cistronic constructs.
To construct the desired multi-cistronic constructs recombinant PCR was used. A. Diagrammatic representation of the different primers used to set up relevant PCR reactions F: Forward primer; R: Reverse primer) B. The oligonucleotide sequences of the different primers used in 5'→3' direction. Different regions of the sequence are colour coded. To clone multi-cistronic constructs created into the desired pLEX-MCS lentiviral vector, BamHI (red coloured sequences) and NotI (blue coloured sequences) restriction sites were used. The regions within brackets correspond to the sequence of either LIN52, FOXM1ΔNΔKEN or B-MYB genes as indicated in the Primer Code and the bold regions depict the relevant 2A peptide used to link different genes as indicated in the Primer Code.

Additionally, Figure 4.18 demonstrates the step-wise construction of different multi-cistronic vectors generated. Primary PCR reactions were setup to amplify the single construct with desired overhangs. Secondary PCRs were conducted to combine and amplify respective bi-cistronic constructs. The tertiary PCR reaction finally combined B-MYB amplified in the primary PCR with LIN52 and FOXM1 from the secondary reaction. The amplification products were inserted into pLEX-MCS after digestion with BamHI and NotI, shown in Figure 4.19. Sequencing was carried out after cloning the amplified fragments into pLEX-MCS before studying its biological activity.

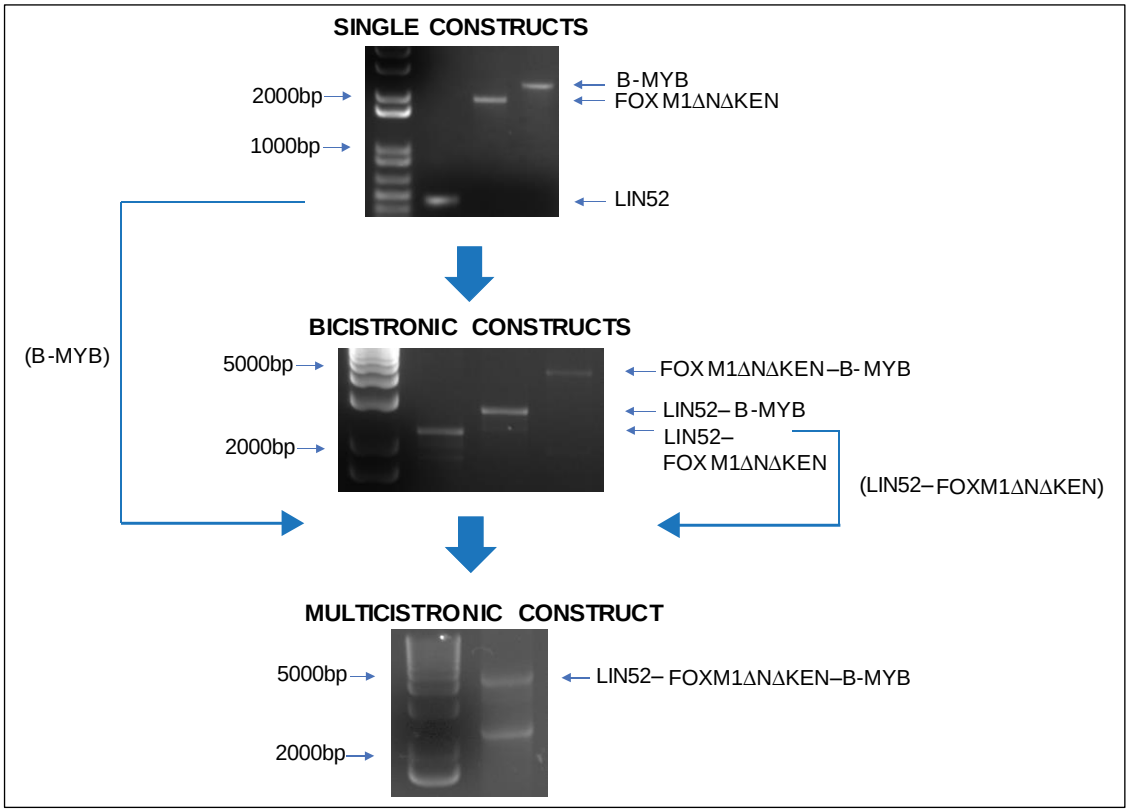

Figure 4.18 Schematic flow diagram depicting sequential generation of PCR products
First gel picture shows the amplification of single constructs using primers with overhangs. Second gel picture shows the construction of bi-cistronic cassettes made by PCR annealing different combination of previously amplified single constructs. The final gel picture presents the construction of LFM by annealing B-MYB from the first amplification together with the LF from the second amplification.

A. >LIN52—FOXM1ΔNΔKEN

CCATAGAAGACACCGACTCTACTAGAGGATCCACTAGTGACATGGGTTGGAAGATGGCGTCTCCCACAGACGGGACAGATCTGGAAGCATCTTTGCTA
AGTTTTGAAAAACTTGACCGTGCCGCACCAGATCTTTGGCCAGAACAATTACCAGGTGTTGCTGAATTTGCAGCTTCCTTCAAAAGTCCTATTACTAGT
TCTCCACCCAAATGGATGGCTGAGATAGAACGTGATGACATCGACATGTTGAAAGAACTGGGGAGTCTCACCACGGCTAATTTGATGGAGAAGGTTCG
AGGCCTACAGAACCTAGCCTATCAGCTGGGGCTGGATGAGTCCAGAGAGATGACACGGGGGAAATTCCTCAATATTCTAGAGAAGCCCAAGAAGGGA
AGCGGAGCTACTAACTTCAGCCTGCTGAAGCAGGCTGGAGACGTGGAGGAGAACCCTGGACCTATGGATTACAAGGATGACGACGATAAGTGTCACC
TGGAGCAGCGACAGGTTAAGGTTGAGGAGCCTTCGAGACCATCAGCGTCCTGGCAGAACTCTGTGTCTGAGCGGCCACCCTACTCTTACATGGCCAT
GATACAATTCGCCATCAACAGCACTGAGAGGAAGCGCATGACTTTGAAAGACATCTATACGTGGATTGAGGACCACTTTCCCTACTTTAAGCACATTGC
CAAGCCAGGCTGGAAGAACTCCATCCGCCACAACCTTTCCCTGCACGACATGTTTGTCCGGGAGACGTCTGCCAATGGCAAGGTCTCCTTCTGGACC
ATTCACCCCAGTGCCAACCGCTACTTGACATTGGACCAGGTGTTTAAGCCACTGGACCCAGGGTCTCCACAATTGCCCGAGCACTTGGAATCACAGC
AGAAACGACCGAATCCAGAGCTCCGCCGGAACATGACCATCAAAACCGAACTCCCCCTGGGCGCACGGCGGAAGATGAAGCCACTGCTACCACGGG
TCAGCTCATACCTGGTACCTATCCAGTTCCCGGTGAACCAGTCACTGGTGTTGCAGCCCTCGGTGAAGGTGCCATTGCCCCTGGCGGCTTCCCTCAT
GAGCTCAGAGCTTGCCCGCCATAGCAAGCGAGTCCGCATTGCCCCCAAGGTGCTGCTAGCTGAGGAGGGGATAGCTCCTCTTTCTTCTGCAGGACC
AGGGAAAGAGGAGAAACTCCTGTTTGGAGAAGGGTTTTCTCCTTTGCTTCCAGTTCAGACTATCAAGGAGGAAGAAATCCAGCCTGGGGAGGAAATG
CCACACTTAGCGAGACCCATCAAAGTGGAGAGCCCTCCCTTGGAAGAGTGGCCCTCCCCGGCCCCATCTTTCAAAGAGGAATCATCTCACTCCTGGG
AGGATTCGTCCCAATCTCCCACCCCAAGACCCAAGAAGTCCTACAGTGGGCTTAGGTCCCCAACCCGGTGTGTCTCGGAAATGCTTGTGATTCAACA
CAGGGAGAGGAGGGAGAGGAGCCGGTCTCGGAGGAAACAGCATCTACTGCCTCCCTGTGTGGATGAGCCGGAGCTGCTCTTCTCAGAGGGGCCCA
GTACTTCCCGCTGGGCCGCAGAGCTCCCGTTCCCAGCAGACTCCTCTGACCCTGCCTCCCAGCTCAGCTACTCCCAGGAAGTGGGAGGACCTTTTA
AGACACCCATTAAGGAAACGCTGCCCATCTCCTCCACCCCGAGCAAATCTGTCCTCCCCAGAACCCCTGAATCCTGGAGGCTCACGCCCCCAGCCAA
AGTAGGGGGACTGGATTTCAGCCCAGTACAAACCTCCCAGGGTGCCTCTGACCCCTTGCCTGACCCCCTGGGGCTGATGGATCTCAGCACCACTCC
CTTGCAAAGTGCTCCCCCCCCTTGAATCACCGCAAAGGCTCCTCAGTTCAGAACCCTTAGACCTCATCTCCGTCCCCTTTGGCAACTCTTCTCCCTCAG
ATATAGACGTCCCCAAGCCAGGCTCCCCGGAGCCACAGGTTTCTGGCCTTGCAGCCAATCGTTCTCTGACAGAAGGCCTGGTCCTGGACACAATGAA
TGACAGCCTCAGCAAGATCCTGCTGGACATCAGCTTTCCTGGCCTGGACGAGGACCCACTGGGCCCTGACAACATCAACTGGTCCCAGTTTATTCCT
GAGCTACAGTAGTGAGCGGCCGCTCGAGTCTAGAGGGCCCGACGCGTC

B. >LIN52—B-MYB

CCATAGAAGACACCGACTCTACTAGAGGATCCACTAGTGACATGGGTTGGAAGATGGCGTCTCCCACAGACGGGACAGATCTGGAAGCATCTTTGCTAAGT
TTTGAAAAACTTGACCGTGCCGCACCAGATCTTTGGCCAGAACAATTACCAGGTGTTGCTGAATTTGCAGCTTCCTTCAAAAGTCCTATTACTAGTTCTCAC
CCAAATGGATGGCTGAGATAGAACGTGATGACATCGACATGTTGAAAGAACTGGGGAGTCTCACCACGGCTAATTTGATGGAGAAGGTTCGAGGCCTACAG
AACCTAGCCTATCAGCTGGGGCTGGATGAGTCCAGAGAGATGACACGGGGGAAATTCCTCAATATTCTAGAGAAGCCCAAGAAGGGAAGCGGAGCTACTAA
CTTCAGCCTGCTGAAGCAGGCTGGAGACGTGGAGGAGAACCCTGGACCTATGTCTCGGCGGACGCGCTGCGAGGATCTGGATGAGCTGCACTACCAGGA
CACAGATTCAGATGTGCCGGAGCAGAGGGATAGCAAGTGCAAGGTCAAATGGACCCATGAGGAGGACGAGCAGCTGAGGGCCCTGGTGAGGCAGTTTGG
ACAGCAGGACTGGAAGTTCCTGGCCAGCCACTTCCCTAACCGCACTGACCAGCAATGCCAGTACAGGTGGCTGAGAGTTTTGAATCCAGACCTTGTCAAG
GGGCCATGGACCAAAGAGGAAGACCAAAAAGTCATCGAGCTGGTTAAGAAGTATGGCACAAAGCAGTGGACACTGATTGCCAAGCACCTGAAGGGCCGG
CTGGGGAAGCAGTGCCGTGAACGCTGGCACAACCACCTCAACCCTGAGGTGAAGAAGTCTTGCTGGACCGAGGGCCGTGAGGCCCTGGTGAGGCAGTTTGG
CCACAAGGTGCTGGGCAACCGCTGGGCCGAGATCGCCAAGATGTTGCCAGGGAGGACAGACAATGCTGTGAAGAATCACTGGAACTCTACCATCAAAAG
GAAGGTGGACACAGGAGGCTTCTTGAGCGAGTCCAAAGACTGCAAGCCCCCAGTGTACTTGCTGCTGGAGCTCGAGGACAAGGACGGCCTCCAGAGTG
CCCAGCCCACGGAAGGCCAGGGAAGTCTTCTGACCAACTGGCCCTCCGTCCCTCCTACCATAAAGGAGGAGGAAAACAGTGAGGAGGAACTTGCAGCAG
CCACCACATCGAAGGAACAGGAGCCCATCGGTACAGATCTGGACGCAGTGCGAACACCAGAGCCCTTGGAGGAATTCCCGAAGCGTGAGGACCAGGAAG
GCTCCCCACCAGAAACGAGCCTGCCTTACAAGTGGGTGGTGGAGGCAGCTAACCTCCTCATCCCCGCTGTGGGTTCTAGCCTCTCTGAAGCCCTGGACTT
GATCGAGTCGGACCCTGATGCTTGGTGTGACCTGAGTAAATTTGACCTCCCTGAGGAACCATCTGCAGAGGACAGTATCAACAACAGCCTAGTGCAGCTGC
AAGCGTCACATCAGCAGCAAGTCCTGCCACCCCGCCAGCCTTCCGCCCTGGTGCCCAGTGTGACCGAGTACCGCCTGGATGGCCACACCATCTCAGACC
TGAGCCGGAGCAGCCGGGGCGAGCTGATCCCCATCTCCCCCAGCACTGAAGTCGGGGGCTCTGGCATTGGCACACCGCCCTCTGTGCTCAAGCGGCAG
AGGAAGAGGCGTGTGGCTCTGTCCCCTGTCACTGAGAATAGCACCAGTCGTCCTTCCTGGATTCCTGTAACAGCCTCACGCCCAAGAGCACCTGTTA
AGACCCTGCCCTTCTCGCCCTCCCAGTTTCTGAACTTCTGGAACAAACAGGACACATTGGAGCTGGAGAGCCCCTCGCTGACATCCACCCCAGTGTGCAG
CCAGAAGGTGGTGGTCACCACACCACTGCACCGGGACAAGACACCCCTGCACCAGAAACATGCTGCGTTTGTAACCCCAGATCAGAAGTACTCCATGGAC
AACACTCCCCACACGCCAACCCCGTTCAAGAACGCCCTGGAGAAGTACGGACCCCTGAAGCCCCTGCCACAGACCCCGCACCTGGAGGAGGACTTGAAG
GAGGTGCTGCGTTCTGAGGCTGGCATCGAACTCATCATCGAGGACGACATCAGGCCCGAGAAGCAGAAGAGGAAGCCTGGGCTGCGGCGGAGCCCCAT
CAAGAAAGTCCGGAAGTCTCTGGCTCTTGACATTGTGGATGAGGATGTGAAGCTGATGATGTCCACACTGCCCAAGTCTCTATCCTTGCCGACAACTGCCC
CTTCAAACTCTTCCAGCCTCACCCTGTCAGGTATCAAAGAAGACAACAGCTTGCTCAACCAGGGCTTCTTGCAGGCCAAGCCCGAGAAGGCAGCAGTGGC
CCAGAAGCCCCGAAGCCACTTCACGACACCTGCCCCTATGTCCAGTGCCTGGAAGACGGTGGCCTGCGGGGGGACCAGGGACCAGCTTTTCATGCAGG
AGAAAGCCCGGCAGCTCCTGGGCCGCCTGAAGCCCAGCCACACATCTCGGACCCTCATCTTGTCCTGAGCTACAGTATAGTGAGCGGCCGCTCGAGTCTA
GAGGGCCCGACGCGTC

C. >FOXM1ΔNΔKEN—B-MYB

CCATAGAAGACACCGACTCTACTAGAGGATCCACTAGTGACATGGATTACAAGGATGACGACGATAAGTGTCACCTGGAGCAGCGACAGGTTAAGGTTGAGGAGCCTTCGAG
ACCATCAGCGTCCTGGCAGAACTCTGTGTCTGAGCGGCCACCCTACTCTTACATGGCCATGATACAATTCGCCATCAACAGCACTGAGAGGAAGCGCATGACTTTGAAAGAC
ATCTATACGTGGATTGAGGACCACTTTCCCTACTTTAAGCACATTGCCAAGCCAGGCTGGAAGAACTCCATCCGCCACAACCTTTCCCTGCACGACATGTTTGTCCGGGAGAC
GTCTGCCAATGGCAAGGTCTCCTTCTGGACCATTCACCCCAGTGCCAACCGCTACTTGACATTGGACCAGGTGTTTAAGCCACTGGACCCAGGGTCTCCACAATTGCCCGA
GCACTTGGAATCACAGCAGAAACGACCGAATCCAGAGCTCCGCCGGAACATGACCATCAAAACCGAACTCCCCCTGGGCGCACGGCGGAAGATGAAGCCACTGCTACCAC
GGGTCAGCTCATACCTGGTACCTATCCAGTTCCCGGTGAACCAGTCACTGGTGTTGCAGCCCTCGGTGAAGGTGCCATTGCCCCTGGCGGCTTCCCTCATGAGCTCAGAGC
TTGCCCGCCATAGCAAGCGAGTCCGCATTGCCCCCAAGGTGCTGCTAGCTGAGGAGGGGATAGCTCCTCTTTCTTCTGCAGGACCAGGGAAAGAGGAGAAACTCCTGTTTG
GAGAAGGGTTTTCTCCTTTGCTTCCAGTTCAGACTATCAAGGAGGAAGAAATCCAGCCTGGGGAGGAAATGCCACACTTAGCGAGACCCATCAAAGTGGAGAGCCCTCCCT
TGGAAGAGTGGCCCTCCCCGGCCCCATCTTTCAAAGAGGAATCATCTCACTCCTGGGAGGATTCGTCCCAATCTCCCACCCCAAGACCCAAGAAGTCCTACAGTGGGCTTA
GGTCCCCAACCCGGTGTGTCTCGGAAATGCTTGTGATTCAACACAGGGAGAGGAGGGAGAGGAGCCGGTCTCGGAGGAAACAGCATCTACTGCCTCCCTGTGTGGATGAG
CCGGAGCTGCTCTTCTCAGAGGGGCCCAGTACTTCCCGCTGGGCCGCAGAGCTCCGTTCCCAGCAGACTCCTCTGACCCTGCCTCCCAGCTCAGCTACTCCCAGGAAGT
GGGAGGACCTTTTAAGACACCCATTAAGGAAACGCTGCCCATCTCCTCCACCCCGAGCAAATCTGTCCTCCCCAGAACCCCTGAATCCTGGAGGCTCACGCCCCCAGCCAA
AGTAGGGGGACTGGATTTCAGCCCAGTACAAACCTCCCAGGGTGCCTCTGACCCCTTGCCTGACCCCCTGGGGCTGATGGATCTCAGCACCACTCCCTTGCAAAGTGCTC
CCCCCCTTGAATCACCGCAAAGGCTCCTCAGTTCAGAACCCTTAGACCTCATCTCCGTCCCCTTTGGCAACTCTTCTCCCTCAGATATAGACGTCCCCAAGCCAGGCTCCCC
GGAGCCACAGGTTTCTGGCCTTGCAGCCAATCGTTCTCTGACAGAAGGCCTGGTCCTGGACACAATGAATGACAGCCTCAGCAAGATCCTGCTGGACATCAGCTTTCCTGG
CCTGGACGAGGACCCACTGGGCCCTGACAACATCAACTGGTCCCAGTTTATTCCTGAGCTACAGGGAAGCGGAGAGGGCAGAGGAAGTCTGCTAACATGCGGTGACGTCG
AGGAGAATCCTGGACCTATGTCTCGGCGGACGCGCTGCGAGGATCTGGATGAGCTGCACTACCAGGACACAGATTCAGATGTGCCGGAGCAGAGGGATAGCAAGTGCAAG
GTCAAATGGACCCATGAGGAGGACGAGCAGCTGAGGGCCCTGGTGAGGCAGTTTGGACAGCAGGACTGGAAGTTCCTGGCCAGCCACTTCCCTAACCGCACTGACCAGC
AATGCCAGTACAGGTGGCTGAGAGTTTTGAATCCAGACCTTGTCAAGGGGCCATGGACCAAAGAGGAAGACCAAAAAGTCATCGAGCTGGTTAAGAAGTATGGCACAAAGC
AGTGGACACTGATTGCCAAGCACCTGAAGGGCCGGCTGGGGAAGCAGTGCCGTGAACGCTGGCACAACCACCTCAACCCTGAGGTGAAGAAGTCTTGCTGGACCGAGGA
GGAGGACCGCATCATCTGCGAGGCCCACAAGGTGCTGGGCAACCGCTGGGCCGAGATCGCCAAGATGTTGCCAGGGAGGACAGACAATGCTGTGAAGAATCACTGGAAC
TCTACCATCAAAAGGAAGGTGGACACAGGAGGCTTCTTGAGCGAGTCCAAAGACTGCAAGCCCCCAGTGTACTTGCTGCTGGAGCTCGAGGACAAGGACGGCCTCCAGAG
TGCCCAGCCCACGGAAGGCCAGGGAAGTCTTCTGACCAACTGGCCCTCCGTCCCTCCTACCATAAAGGAGGAGGAAAACAGTGAGGAGGAACTTGCAGCAAGCCACCAT
CGAAGGAACAGGAGCCCATCGGTACAGATCTGGACGCAGTGCGAACACCAGAGCCCTTGGAGGAATTCCCGAAGCGTGAGGACCAGGAAGGCTCCCCACCAGAAACGAG
CCTGCCTTACAAGTGGGTGGTGGAGGCAGCTAACCTCCTCATCCCCGCTGTGGGTTCTAGCCTCTCTGAAGCCCTGGACTTGATCGAGTCGGACCCTGATGCTTGGTGTGA
CCTGAGTAAATTTGACCTCCCTGAGGAACCATCTGCAGAGGACAGTATCAACAACAGCCTAGTGCAGCTGCAAGCGTCACATCAGCAGCAAGTCCTGCCACCCCGCCAGCC
TTCCGCCCTGGTGCCCAGTGTGACCGAGTACCGCCTGGATGGCCACACCATCTCAGACCTGAGCCGGAGCAGCCGGGGCGAGCTGATCCCCATCTCCCCCAGCACTGAA
GTCGGGGGCTCTGGCATTGGCACACCGCCCTCTGTGCTCAAGCGGCAGAGGAAGAGGCGTGTGGCTCTGTCCCCTGTCACTGAGAATAGCACCAGTCTGTCCTTCCTGGA
TTCCTGTAACAGCCTCACGCCCAAGAGCACACCTGTTAAGACCCTGCCCTTCTCGCCCTCCCAGTTTCTGAACTTCTGGAACAAACAGGACACATTGGAGCTGGAGAGCCC
CTCGCTGACATCCACCCCAGTGTGCAGCCAGAAGGTGGTGGTCACCACACCACTGCACCGGGACAAGACACCCCTGCACCAGAAACATGCTGCGTTTGTAACCCCAGATC
AGAAGTACTCCATGGACAACACTCCCCACACGCCAACCCCGTTCAAGAACGCCCTGGAGAAGTACGGACCCCTGAAGCCCCTGCCACAGACCCCGCACCTGGAGGAGGAC
TTGAAGGAGGTGCTGCGTTCTGAGGCTGGCATCGAACTCATCATCGAGGACGACATCAGGCCCGAGAAGCAGAAGAGGAAGCCTGGGCTGCGGCGGAGCCCCATCAAGA
AAGTCCGGAAGTCTCTGGCTCTTGACATTGTGGATGAGGATGTGAAGCTGATGATGTCCACACTGCCCAAGTCTCTATCCTTGCCGACAACTGCCCCTTCAAACTCTTCCAG
CCTCACCCTGTCAGGTATCAAAGAAGACAACAGCTTGCTCAACCAGGGCTTCTTGCAGGCCAAGCCCGAGAAGGCAGCAGTGGCCCAGAAGCCCCGAAGCCACTTCACGA
CACCTGCCCCTATGTCCAGTGCCTGGAAGACGGTGGCCTGCGGGGGGACCAGGGACCAGCTTTTCATGCAGGAGAAAGCCCGGCAGCTCCTGGGCCGCCTGAAGCCCA
GCCACACATCTCGGACCCTCATCTTGTCCTGAGCTACAGTATAGTGAGCGGCCGCTCGAGTCTAGAGGGCCCGACGCGTC

D. >LIN52—FOXM1ΔNΔKEN—B-MYB

CCATAGAAGACACCGACTCTACTAGAGGATCCACTAGTGACATGGGTTGGAAGATGGCGTCTCCCACAGACGGGACAGATCTGGAAGCATCTTTGCTAAGTTTTGAAAAACTTG
ACCGTGCCGCACCAGATCTTTGGCCAGAACAATTACCAGGTGTTGCTGAATTTGCAGCTTCCTTCAAAAGTCCTATTACTAGTTCTCCACCCAAATGGATGGCTGAGATAGAACG
TGATGACATCGACATGTTGAAAGAACTGGGGAGTCTCACCACGGCTAATTTGATGGAGAAGGTTCGAGGCCTACAGAACCTAGCCTATCAGCTGGGGCTGGATGAGTCCAGAG
AGATGACACGGGGGAAATTCCTCAATATTCTAGAGAAGCCCAAGAAGGGAAGCGGAGCTACTAACTTCAGCCTGCTGAAGCAGGCTGGAGACGTGGAGGAGAACCCTGGACC
TATGGATTACAAGGATGACGACGATAAGTGTCACCTGGAGCAGCGACAGGTTAAGGTTGAGGAGCCTTCGAGACCATCAGCGTCCTGGCAGAACTCTGTGTCTGAGCGGCCA
CCCTACTCTTACATGGCCATGATACAATTCGCCATCAACAGCACTGAGAGGAAGCGCATGACTTTGAAAGACATCTATACGTGGATTGAGGACCACTTTCCCTACTTTAAGCACAT
TGCCAAGCCAGGCTGGAAGAACTCCATCCGCCACAACCTTTCCCTGCACGACATGTTTGTCCGGGAGACGTCTGCCAATGGCAAGGTCTCCTTCTGGACCATTCACCCCAGT
GCCAACCGCTACTTGACATTGGACCAGGTGTTTAAGCCACTGGACCCAGGGTCTCCACAATTGCCCGAGCACTTGGAATCACAGCAGAAACGACCGAATCCAGAGCTCCGCC
GGAACATGACCATCAAAACCGAACTCCCCCTGGGCGCACGGCGGAAGATGAAGCCACTGCTACCACGGGTCAGCTCATACCTGGTACCTATCCAGTTCCCGGTGAACCAGTC
ACTGGTGTTGCAGCCCTCGGTGAAGGTGCCATTGCCCCTGGCGGCTTCCCTCATGAGCTCAGAGCTTGCCCGCCATAGCAAGCGAGTCCGCATTGCCCCCAAGGTGCTGCTA
GCTGAGGAGGGGATAGCTCCTCTTTCTTCTGCAGGACCAGGGAAAGAGGAGAAACTCCTGTTTGGAGAAGGGTTTTCTCCTTTGCTTCCAGTTCAGACTATCAAGGAGGAAGA
AATCCAGCCTGGGGAGGAAATGCCACACTTAGCGAGACCCATCAAAGTGGAGAGCCCTCCCTTGGAAGAGTGGCCCTCCCCGGCCCCATCTTTCAAAGAGGAATCATCTCACT
CCTGGGAGGATTCGTCCCAATCTCCCACCCCAAGACCCAAGAAGTCCTACAGTGGGCTTAGGTCCCCAACCCGGTGTGTCTCGGAAATGCTTGTGATTCAACACAGGGAGAG
GAGGGAGAGGAGCCGGTCTCGGAGGAAACAGCATCTACTGCCTCCCTGTGTGGATGAGCCGGAGCTGCTCTTCTCAGAGGGGCCCAGTACTTCCCGCTGGGCCGCAGAGC
TCCCGTTCCCAGCAGACTCCTCTGACCCTGCCTCCCAGCTCAGCTACTCCCAGGAAGTGGGAGGACCTTTTAAGACACCCATTAAGGAAACGCTGCCCATCTCCTCCACCCCG
AGCAAATCTGTCCTCCCCAGAACCCCTGAATCCTGGAGGCTCACGCCCCCAGCCAAAGTAGGGGGACTGGATTTCAGCCCAGTACAAACCTCCCAGGGTGCCTCTGACCCCT
TGCCTGACCCCCTGGGGCTGATGGATCTCAGCACCACTCCCTTGCAAAGTGCTCCCCCCCTTGAATCACCGCAAAGGCTCCTCAGTTCAGAACCCTTAGACCTCATCTCCGTC
CCCTTTGGCAACTCTTCTCCCTCAGATATAGACGTCCCCAAGCCAGGCTCCCCGGAGCCACAGGTTTCTGGCCTTGCAGCCAATCGTTCTCTGACAGAAGGCCTGGTCCTGGA
CACAATGAATGACAGCCTCAGCAAGATCCTGCTGGACATCAGCTTTCCTGGCCTGGACGAGGACCCACTGGGCCCTGACAACATCAACTGGTCCCAGTTTATTCCTGAGCTAC
AGGGAAGCGGAGAGGGCAGAGGAAGTCTGCTAACATGCGGTGACGTCGAGGAGAATCCTGGACCTATGTCTCGGCGGACGCGCTGCGAGGATCTGGATGAGCTGCACTACC
AGGACACAGATTCAGATGTGCCGGAGCAGAGGGATAGCAAGTGCAAGGTCAAATGGACCCATGAGGAGGACGAGCAGCTGAGGGCCCTGGTGAGGCAGTTTGGACAGCAG
GACTGGAAGTTCCTGGCCAGCCACTTCCCTAACCGCACTGACCAGCAATGCCAGTACAGGTGGCTGAGAGTTTTGAATCCAGACCTTGTCAAGGGGCCATGGACCAAAGAGG
AAGACCAAAAAGTCATCGAGCTGGTTAAGAAGTATGGCACAAAGCAGTGGACACTGATTGCCAAGCACCTGAAGGGCCGGCTGGGGAAGCAGTGCCGTGAACGCTGGCACAA
CCACCTCAACCCTGAGGTGAAGAAGTCTTGCTGGACCGAGGAGGAGGACCGCATCATCTGCGAGGCCCACAAGGTGCTGGGCAACCGCTGGGCCGAGATCGCCAAGATGTT
GCCAGGGAGGACAGACAATGCTGTGAAGAATCACTGGAACTCTACCATCAAAAGGAAGGTGGACACAGGAGGCTTCTTGAGCGAGTCCAAAGACTGCAAGCCCCCAGTGTAC
TTGCTGCTGGAGCTCGAGGACAAGGACGGCCTCCAGAGTGCCCAGCCCACGGAAGGCCAGGGAAGTCTTCTGACCAACTGGCCCTCCGTCCCTCCTACCATAAAGGAGGAG
GAAAACAGTGAGGAGGAACTTGCAGCAGCCACCACATCGAAGGAACAGGAGCCCATCGGTACAGATCTGGACGCAGTGCGAACACCAGAGCCCTTGGAGGAATTCCCGAAG
CGTGAGGACCAGGAAGGCTCCCCACCAGAAACGAGCCTGCCTTACAAGTGGGTGGTGGAGGCAGCTAACCTCCTCATCCCCGCTGTGGGTTCTAGCCTCTCTGAAGCCCTG
GACTTGATCGAGTCGGACCCTGATGCTTGGTGTGACCTGAGTAAATTTGACCTCCCTGAGGAACCATCTGCAGAGGACAGTATCAACAACAGCCTAGTGCAGCTGCAAGCGTC
ACATCAGCAGCAAGTCCTGCCACCCCGCCAGCCTTCCGCCCTGGTGCCCAGTGTGACCGAGTACCGCCTGGATGGCCACACCATCTCAGACCTGAGCCGGAGCAGCCGGGG
CGAGCTGATCCCCATCTCCCCCAGCACTGAAGTCGGGGGCTCTGGCATTGGCACACCGCCCTCTGTGCTCAAGCGGCAGAGGAAGAGGCGTGTGGCTCTGTCCCCTGTCAC
TGAGAATAGCACCAGTCTGTCCTTCCTGGATTCCTGTAACAGCCTCACGCCCAAGAGCACACCTGTTAAGACCCTGCCCTTCTCGCCCTCCCAGTTTCTGAACTTCTGGAACAA
ACAGGACACATTGGAGCTGGAGAGCCCCTCGCTGACATCCACCCCAGTGTGCAGCCAGAAGGTGGTGGTCACCACACCACTGCACCGGGACAAGACACCCCTGCACCAGAA
ACATGCTGCGTTTGTAACCCCAGATCAGAAGTACTCCATGGACAACACTCCCCACACGCCAACCCCGTTCAAGAACGCCCTGGAGAAGTACGGACCCCTGAAGCCCCTGCCAC
AGACCCCGCACCTGGAGGAGGACTTGAAGGAGGTGCTGCGTTCTGAGGCTGGCATCGAACTCATCATCGAGGACGACATCAGGCCCGAGAAGCAGAAGAGGAAGCCTGGG
CTGCGGCGGAGCCCCATCAAGAAAGTCCGGAAGTCTCTGGCTCTTGACATTGTGGATGAGGATGTGAAGCTGATGATGTCCACACTGCCCAAGTCTCTATCCTTGCCGACAAC
TGCCCCTTCAAACTCTTCCAGCCTCACCCTGTCAGGTATCAAAGAAGACAACAGCTTGCTCAACCAGGGCTTCTTGCAGGCCAAGCCCGAGAAGGCAGCAGTGGCCCAGAAG
CCCCGAAGCCACTTCACGACACCTGCCCCTATGTCCAGTGCCTGGAAGACGGTGGCCTGCGGGGGGACCAGGGACCAGCTTTTCATGCAGGAGAAAGCCCGGCAGCTCCTG
GGCCGCCTGAAGCCCAGCCACACATCTCGGACCCTCATCTTGTCCTGAGCTACAGTATAGTGAGCGGCCGCTCGAGTCTAGAGGGCCCGACGCGTC

Figure 4.19 Sequences of the bi-cistronic and multi-cistronic expression cassette.
Start and terminator codons are depicted in orange. Only the final cistron in each multi-cistronic construct has a terminator codon. P2A peptide is shown in red and T2A in blue. BamHI and NotI restriction sites used to clone in pLEX-MCS vector are shown in green. A-C. DNA sequences of bi-cistronic constructs namely: A. LIN52-FOXM1ΔNΔKEN (total size=2109 bp) B. LIN52-B-MYB (total size=2532 bp) C. FOXM1ΔNΔKEN-B-MYB (total size=3870 bp) D.DNA sequence of multi-cistronic LIN52-FOXM1ΔNΔKEN-B-MYB construct (total size=4284 bp).

4.9 Bypass potential of the multi-cistronic constructs

4.9.1 Objective

To allow a deeper insight into the functional activity of multi-cistronic constructs, bypass potential of the varying combinations of the multi-cistronic constructs was compared in CL3^{EcoR} cells. The rationale was first to determine if the multi-cistronic constructs would bypass senescence in CL3^{EcoR} cells and second, to determine if any synergy was present amongst the three key identified components i.e. LIN52, FOXM1ΔNΔKEN and B-MYB.

4.9.2 Comparison of senescence bypass activity

Lentiviruses were prepared by transient transfection of HEK293T cells for the multi-cistronic constructs and used to stably transduce CL3^{EcoR} cells (Table 4.10).

Table 4.10 List of Multi-cistronic constructs studied for bypass potential

Multi-cistronic constructs	Constituents
LFM	LIN52, FOXM1ΔNΔKEN and B-MYB in a single construct
LF	LIN52 and FOXM1ΔNΔKEN in a single construct
LM	LIN52 and B-MYB in a single construct
FM	FOXM1ΔNΔKEN and B-MYB in a single construct
LFMS	LIN52, FOXM1ΔNΔKEN and B-MYB in separate constructs

Senescence bypass assay for this experiment was performed under very stringent conditions to be able to see any differences in bypass potential and spot any synergy that might exist. The non-permissive temperature used was as high as 39.5°C. 35,000 cells were reseeded after successful infection to lower the background and keep flasks less saturated. After three weeks, flasks were stained with methylene blue and the densely growing blue colonies were counted and the bypass potential analysed. pLEX-MCS empty vector was used as a negative control to determine the background level of bypass.

Senescence bypass potential of the multi-cistronic LFM construct was compared to the bypass of varying combinations of bi-cistronic constructs (LF, LM and FM), individual components alone and to the separately reconstituted mix of three components as shown in Figure 4.20.

From the results obtained shown in Figure 4.20, it was apparent that the multi-cistronic constructs functioned very well in $CL3^{EcoR}$ cells as large number of blue dense healthy growing colonies were visible after staining the flasks after three weeks. It was observed that all the multi-cistronic constructs, reconstituted mix of three components and the individual components except FOXM1 showed a strong senescence bypass activity. This experiment for the first time showed the functional ability of multi-cistronic constructs to bypass senescence in $CL3^{EcoR}$ cells. For the purpose of clear understanding of the different comparisons done

in this experiment the data have been extracted from the same experiment (Figure 4.20) and compared separately in Figure 4.21.

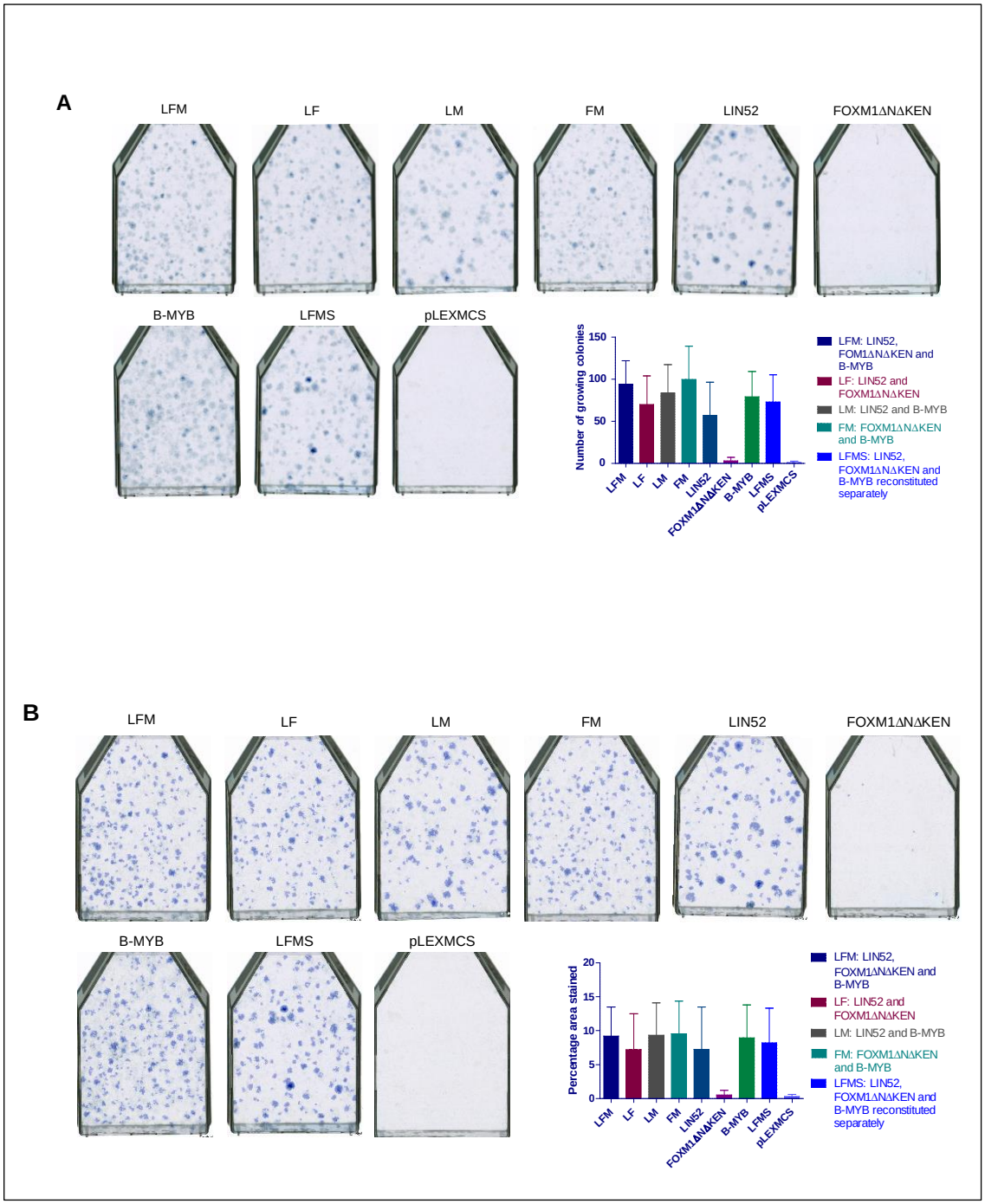

Figure 4.20 Study of senescence bypass potential of different multi-cistronic constructs. Bypass assay was performed thrice independently at 5% CO_2 and 39.5°C with 35,000 cells per T-75 flask. Flasks were stained with 2% methylene blue after three weeks. Single representative flasks from internal repeats are shown. For quantitative analysis the bar charts depict an overall average (+/- SD) of all three-independent repeat experiments. Empty vector pLEX-MCS was used as a negative control. A) Manual analysis B) Computational analysis. Statistical analysis was conducted using One-way ANOVA, Tukey's Multiple Comparison Test (*p<0.05, **p<0.01, ***p<0.001)

The first comparison undertaken was to study if it is more efficient to express different TFs from one construct rather than mixing them separately. On analysing the results obtained it was found that there was no numerical difference between the extent of bypass observed when the three constructs were expressed either from the same vector as in multi-cistronic construct or reconstituted separately. In both cases a similar strong bypass potential was observed as shown in Figure 4.21A. Results from this experiment further showed how well mixing of different TFs works, as the bypass obtained by multi-cistronic single LFM construct was comparable to the bypass observed by LFMS, where the constructs were mixed separately.

Next, to study if the three components together were better at bypassing senescence than the individual components alone, bypass potential of single multi-cistronic LFM construct was compared to LIN52, FOXM1ΔNΔKEN and B-MYB when expressed individually. Similar to the results obtained in previous experiments, both LIN52 and B-MYB exhibited strong bypass whereas FOXM1 showed marginal bypass when assayed individually as observed by the presence of large number of stained colonies. Comparing the bypass observed with the multicistronic construct consisting of all three components to the bypass of individual components, no numerical difference was observed with regards to LIN52 and B-MYB alone. However, a highly significant difference was seen with FOXM1ΔNΔKEN as shown quantitatively in Figure 4.21B.

Finally, comparing the bypass potential of multi-cistronic construct to the bypass of varying combinations of bi-cistronic constructs, it was found that there was no numerical difference between the bypass potential of any of the bi-cistronic constructs and the multi-cistronic LFM construct as shown in Figure 4.21C. This indicated that presence of any two components out of the three showed similar levels of bypass as when three components were present together confirming that there is no synergy between three components.

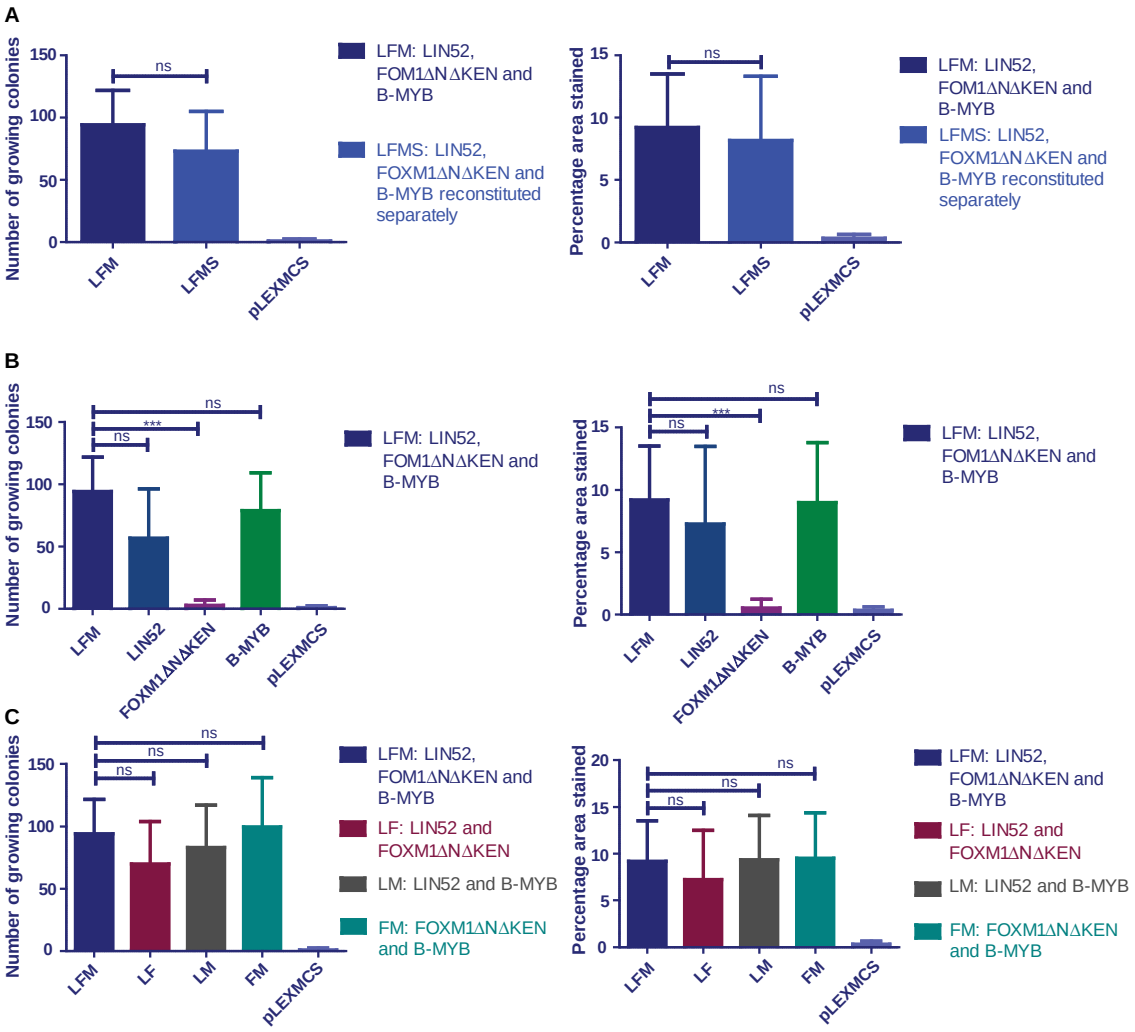

Figure 4.21 Different comparisons of multicistronic constructs.
A) LFM vs LFMS B) LFM vs Individual components C) LFM vs Bicistronic constructs. For each comparison both manual and computational analysis are shown. Statistical analysis was conducted using One-way ANOVA, Tukey's Multiple Comparison Test (*p<0.05, **p<0.01, ***p<0.001)

4.10 Bypass potential of multi-cistronic constructs after dilution

4.10.1 Objective

After analysing the results from the previous experiment, one possibility why no difference was observed between different constructs studied could be due to saturation as most of them worked efficiently to bypass senescence in our model system. It suggests that the higher densities somehow reduce the detection of rescued cells through cell overcrowding. Therefore, to identify any differences in the bypass potential that might exist between the different constructs, an independent experiment was performed, where the experiment was repeated

under stringent conditions as before and was also performed after diluting. The rationale behind diluting was to lower the total number of colonies obtained proportionately for every construct to be able to spot any small differences that might be present among the different constructs.

There are two potential ways of diluting to reduce the efficiency of the bypass. First by diluting DNA at the transfection stage and the other is the classical approach of mixing the stably transduced cells with non-transduced cells. Here, the classical approach was taken. Dilutions were therefore done by mixing the successfully infected $CL3^{EcoR}$ cells selected after puromycin selection with non-infected $CL3^{EcoR}$ cells as we also wanted to maintain a uniform cell density. This will reduce the large number of growing colonies observed as non-infected cells will not be able to grow at the non-permissive temperature. To optimize the dilution experiment, two different dilutions were used i.e. fivefold dilution and tenfold dilution. For fivefold dilution, to reseed a total of 35000 cells, 7000 successfully infected cells were mixed with 28,000 non-infected $CL3^{EcoR}$ before reseeding in T-75 flasks. Similarly, for tenfold dilution, 3500 infected cells were mixed with 31,500 non-infected $CL3^{EcoR}$ cells. The assay was performed under the same stringent high temperature conditions to minimize the background.

4.10.2 Comparison of the bypass potential of each construct upon dilution

Here, the bypass potential of each of the construct used in this study is compared individually, when its undiluted and diluted. There was a clear trend of gradual proportionate reduction in the total number of colonies obtained for each of the construct as the fold dilution increased, apart from FOXM1ΔNΔKEN and pLEX-MCS empty vector as shown in Figure 4.22, neither of which bypass senescence. This showed that the dilution approach used to reduce the total number of colonies worked successfully.

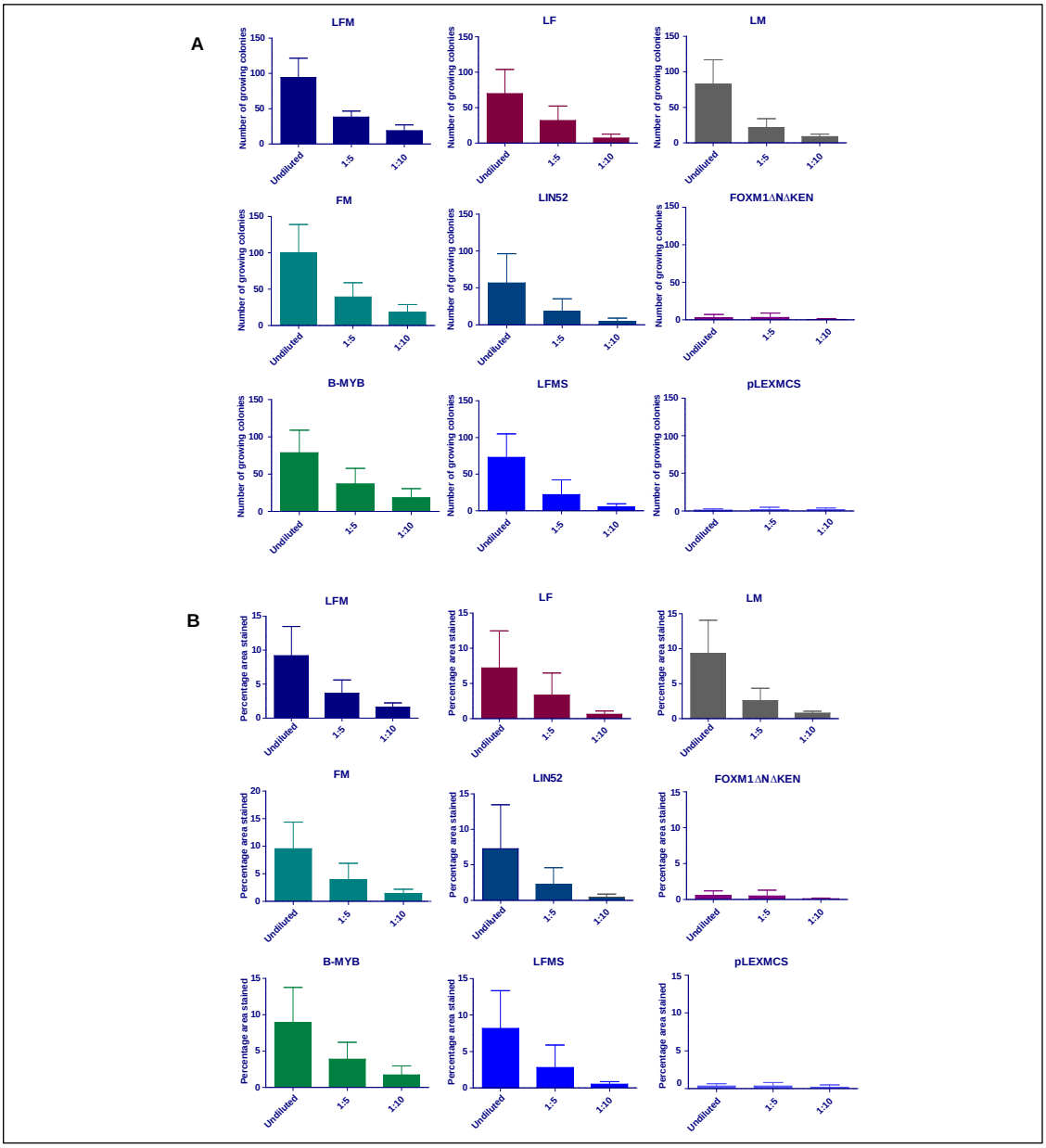

Figure 4.22 Study of bypass potential of each construct compared upon dilution
Bypass assay was performed thrice independently at 5% CO_2 and 39.5°C with 35,000 cells per T-75 flask. Bar charts depict an overall average (+/- SD) of all three-independent repeat experiments for each dilution. Empty vector pLEX-MCS was used as negative control. A) Manual

4.10.3 Fivefold dilution

After five-fold dilution, all the multi-cistronic constructs, reconstituted mix of three components and all individual components except FOXM1 were able to bypass senescence as shown in the Figure 4.23. Similar comparisons were done here as previously for the undiluted constructs. The combined results for bypass potential after fivefold dilution are shown in Figure 4.23. Separate comparisons are discussed separately for easier understanding after extracting the data from the same experiment.

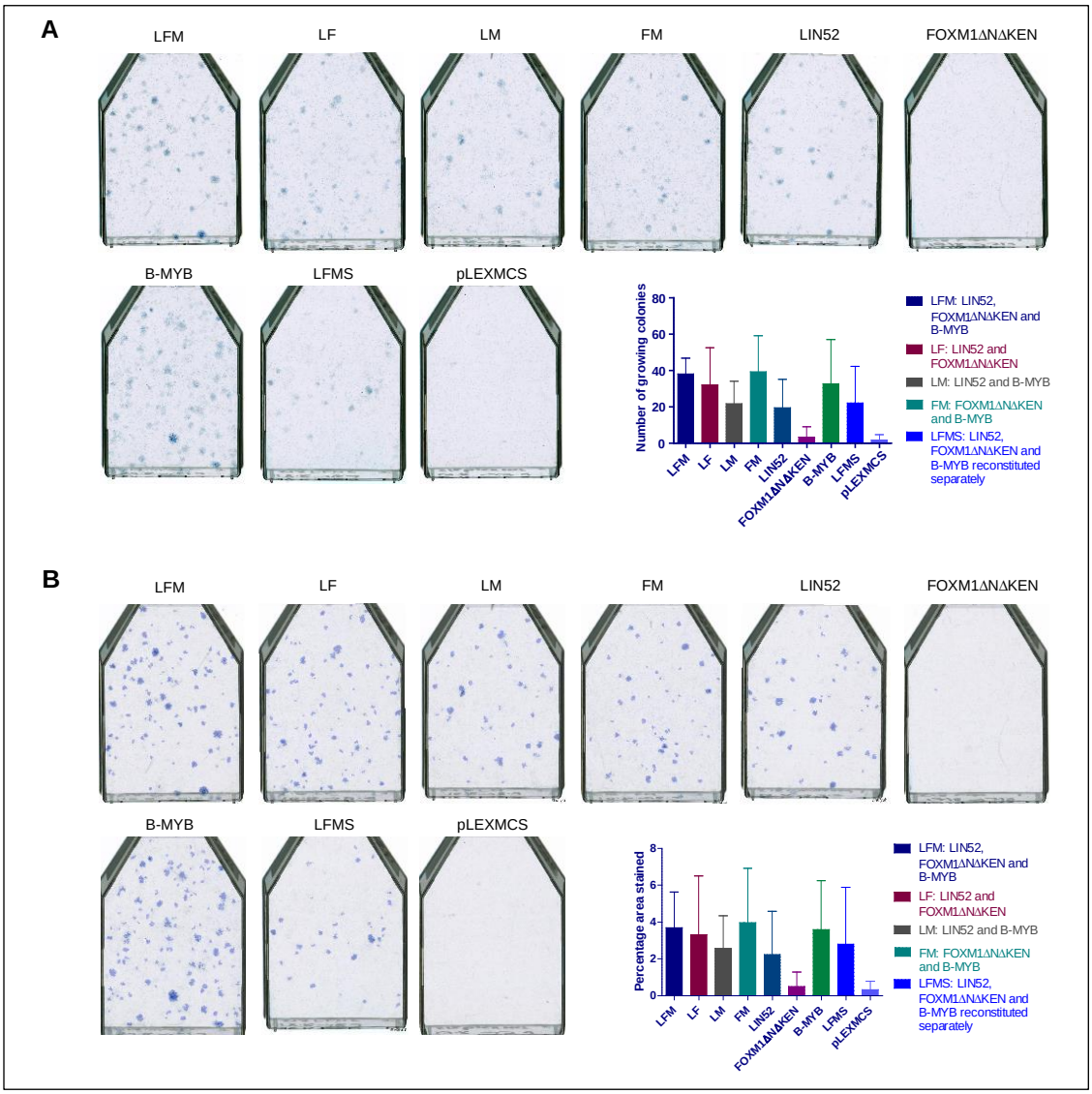

Figure 4.23 Study of the bypass potential of different multi-cistronic (LFM) constructs after fivefold dilution

Bypass assay was performed thrice independently at 5% CO_2 and 38.9°C with 35,000 cells per T-75 flask. Empty vector pLEX-MCS was used as a negative control. For quantitative analysis the bar charts depict an overall average (+/- SD) of all three-independent repeat experiments. A) Manual analysis B) Computational analysis. Statistical analysis was conducted using One-way ANOVA, Tukey's Multiple Comparison Test (*p<0.05, **p<0.01, ***p<0.001)

No numerical difference was observed between the multi-cistronic single LFM construct and the separately reconstituted LFMS mix as depicted in Figure 4.24A. This reconfirmed that reconstitution works very well in our model system. Although no numerical difference was observed, closer inspection of the colonies obtained after staining suggests that having all three constructs from one vector tends to work better than mixing them separately.

Multi-cistronic LFM construct and the single LIN52 and B-MYB constructs showed higher bypass potential than the negative control pLEX-MCS and FOXM1, after five-fold dilution. On comparing the bypass potential of LFM with the individual constructs, no numerical difference was observed between LFM and LIN52 or LFM and B-MYB whereas with respect to FOXM1 there was a highly significant difference Figure 4.24B.

After five-fold dilution, similar to undiluted, multi-cistronic construct LFM and the three different bi-cistronic constructs (LF, LM and FM) showed bypass potential higher than the negative control, pLEX-MCS. When compared all of them worked equally well and showed similar level of bypass potential. Hence, no numerical difference was observed in the bypass potential of LFM and any of the bi-cistronic construct as shown in Figure 4.24C. This indicates that presence of any two out of three identified critical components works as efficiently as all three components present together. Even after diluting five times, no numerical differences were detected between the multi-cistronic construct and different bi-cistronic constructs.

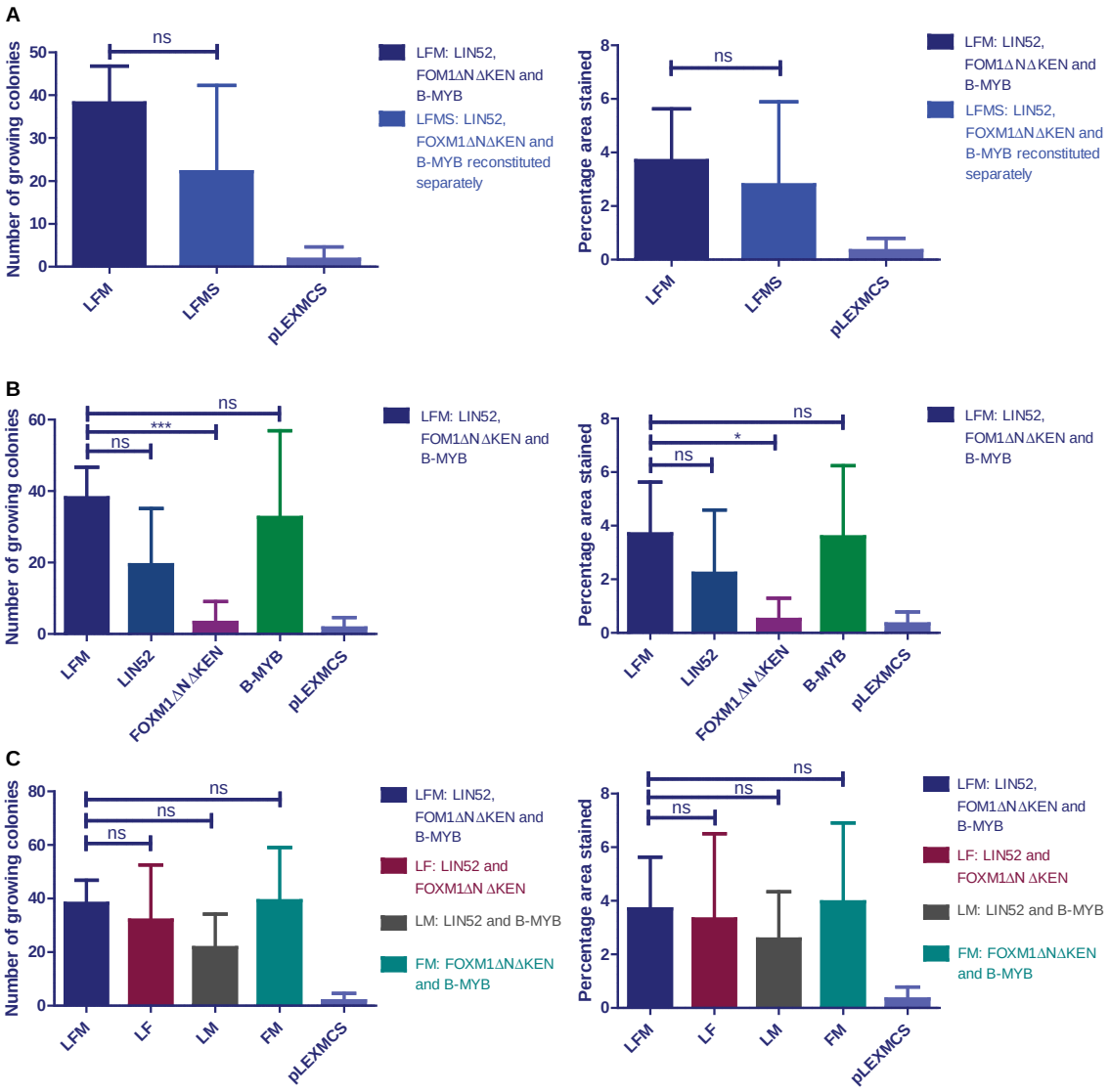

Figure 4.24 Different comparisons of multi-cistronic constructs after five-fold dilution.
A) LFM vs LFMS B) LFM vs Individual components C) LFM vs Bicistronic constructs. For each comparison both manual and computational analysis are shown. Statistical analysis was conducted using One-way ANOVA, Tukey's Multiple Comparison Test (*p<0.05, **p<0.01, ***p<0.001)

4.10.4 Tenfold dilution

Next, comparisons were done after tenfold dilutions to identify any difference in bypass that might exist. The combined results for bypass potential obtained after diluting ten times are shown in Figure 4.25. Strong reduction in the total number of colonies obtained was observed for all the constructs after dilution. Separate comparisons for a clearer understanding are discussed below after extracting the data.

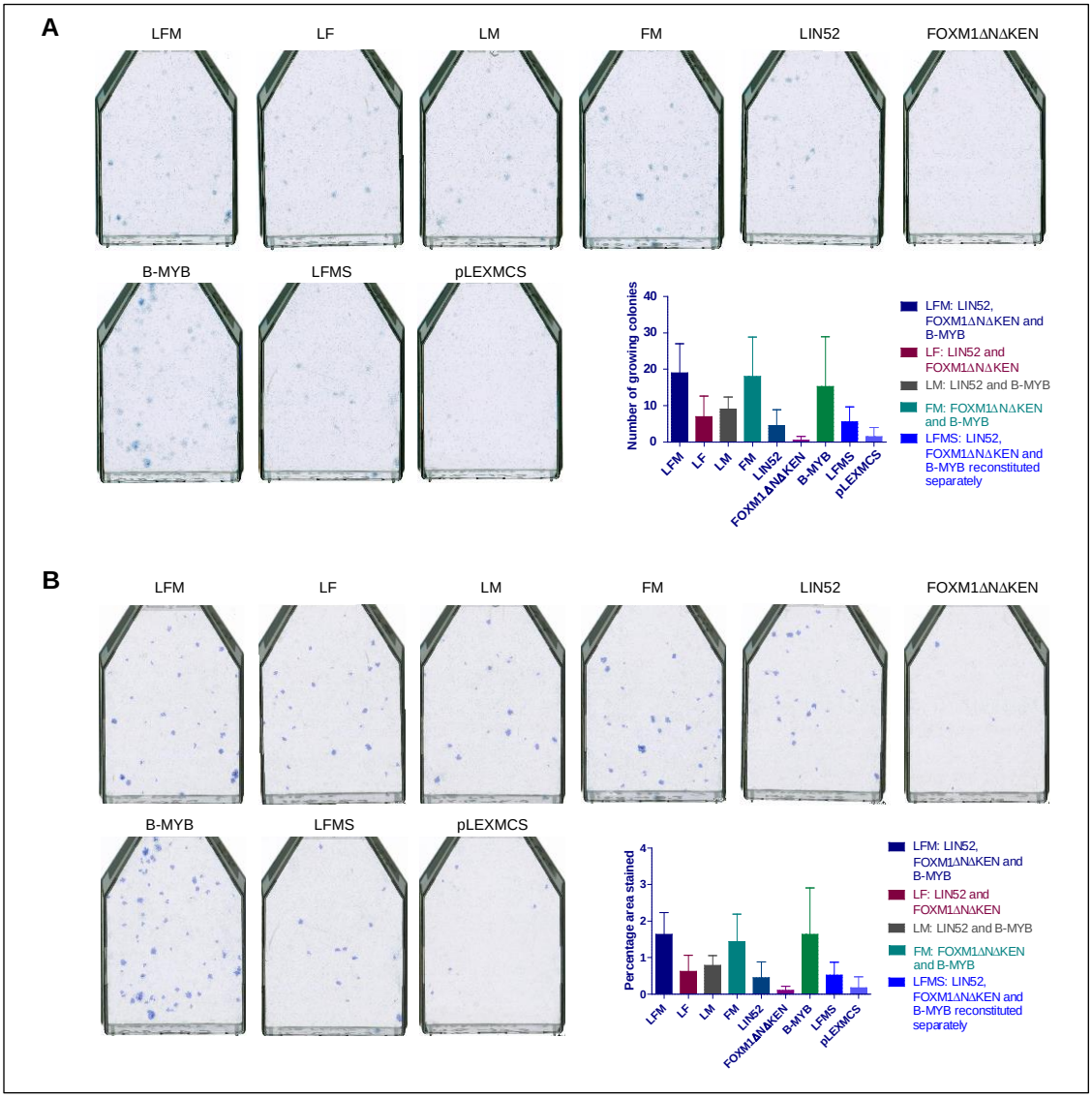

Figure 4.25 Comparison of the bypass potential of different multi-cistronic constructs designed after tenfold dilution

Bypass assay was performed thrice independently at 5% CO_2 and 39.5°C with 35,000 cells per T-75 flask. Empty vector pLEX-MCS was used as a negative control. For quantitative analysis the bar charts depict an overall average (+/- SD) of all three-independent repeat experiments. A) Manual analysis B) Computational analysis. Statistical analysis was conducted using One-way ANOVA, Tukey's Multiple Comparison Test (*p<0.05, **p<0.01, ***p<0.001)

This comparison between multi-cistronic (LFM) construct and the reconstituted mix (LFMS) after tenfold dilution is interesting, as this time a statistically significant difference was observed, as shown in Figure 4.26A. This indicates that although reconstitution does work very well, using a single multi-cistronic construct was far more efficient. The greater reduction observed upon tenfold dilution enabled us to identify the significant difference.

As observed previously the multi-cistronic LFM construct, individual constructs LIN52 and B-MYB showed higher bypass potential than the negative control pLEX-MCS and FOXM1 as shown in Figure 4.26B. The most interesting aspect of the results obtained from this experiment was that when the bypass potential of the multi-cistronic LFM construct was compared to bypass of individual constructs, a significant difference was observed not only with respect to FOXM1 but also with LIN52 for the first time. This indicated the presence of potential synergy with respect to FOXM1 and LIN52. No numerical difference was detected with regards to B-MYB, as B-MYB works extremely well and showed a very strong bypass potential on its own. B-MYB was affected the least after dilution.

Interesting results were obtained while comparing the multi-cistronic LFM construct to the different combination of bi-cistronic constructs after tenfold dilution. For the first time, we noticed a significant difference between the bypass of multi-cistronic LFM construct and bi-cistronic LF construct as shown in Figure 4.26C. No numerical difference was observed when other two bi-cistronic i.e. LM and FM were compared as depicted, even though LM presented bypass similar to LF. These results obtained after tenfold dilution indicate towards the presence of potential synergy between two and three components when present together. Another key aspect of the results obtained from this experiment was that it helps to establish the importance of the dilution approach used, in detecting small differences in efficiencies among the different key TFs.

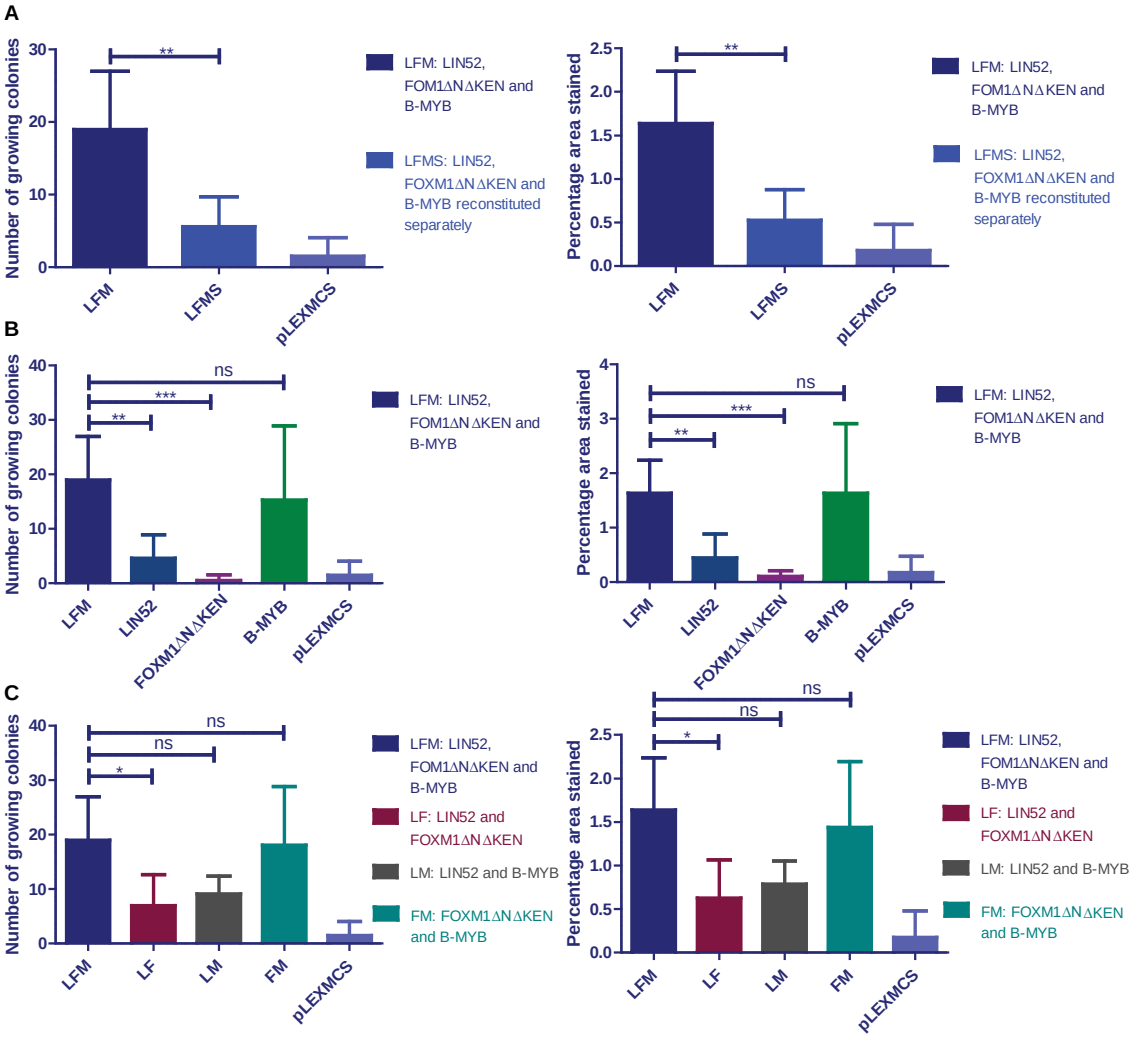

Figure 4.26 Different comparisons of multicistronic constructs after ten-fold dilution.
A) LFM vs LFMS B) LFM vs Individual components C) LFM vs Bicistronic constructs. For each comparison both manual and computational analysis are shown. Statistical analysis was conducted using One-way ANOVA, Tukey's Multiple Comparison Test (*p<0.05, **p<0.01, ***p<0.001)

4.11 Protein analysis

4.11.1 Objective

Western blot analysis was undertaken to validate the results obtained from the senescence bypass assays. It is important to verify the protein expression to ensure that the senescence bypass potential observed is due to overexpression or downregulation of a protein.

4.11.2 Western blot analysis

Due to time constraints and lack of specific antibodies, every TF tested in this study to assess its functional role in senescence could not be verified by protein analysis. As LIN52, FOXM1 and B-MYB turned out to be key TFs which have shown to play crucial role in senescence bypass, it was decided to test the expression of these proteins first. Cell lysates were prepared from stably transduced $CL3^{EcoR}$ cells with the desired constructs and grown for at least seven days at the non-permissive temperature i.e. 38.9°C. To compare protein expression of desired proteins in non-infected senescent cells and proliferating cells, cell lysates were made from non-infected $CL3^{EcoR}$ cells grown for at least five days at 38.9°C and 33°C respectively. In this study silencing $p21^{WAF1}$ has consistently worked very efficiently resulting in saturated flask as shown in Figure 3.9. Hence, cell lysates were also prepared from $CL3^{EcoR}$ cells stably transduced with $p21^{WAF1}$ shRNA after allowing them to grow for seven days at the non-permissive temperature. To study basal level of proteins, control cell lysates were prepared from healthy growing HEK293T cells at 37°C.

Western blots were performed to investigate protein expression for LIN52, FOXM1 and B-MYB. The details of the antibodies used are provided in section 2.10.5. The results obtained from western blots were rather disappointing as western blots for all three proteins after developing resulted in appearance of multiple non-specific bands as shown in Figure 4.27. This could be due to poor antibody specificity. Due to multiple non-specific bands, the results obtained for protein analysis are therefore uninterpretable.

Hence, western blot analysis needs to be optimized with different antibodies with further standardization of experimental conditions as well as antibody calibrations.

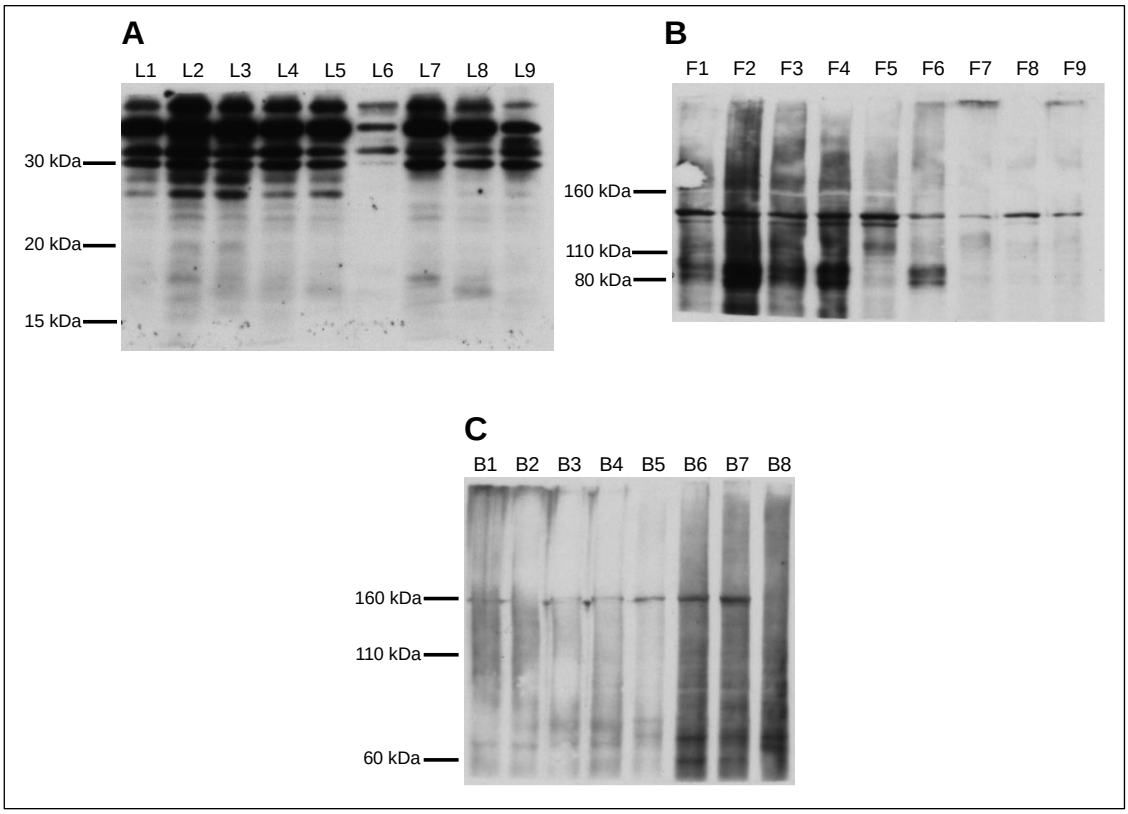

Figure 4.27 Western blot analysis to test expression of A) LIN52, B) FOXM1ΔNΔKEN and C) B-MYB.

Cell lysates were prepared from CL3^{EcoR} cells transduced with desired respective constructs after growing them at 38.9°C for at least seven days. As control to study basal level of expression lysates were prepared from HEK293T cells after 5 days at 37°C (HEK293T cells). To study how protein levels, change after silencing, p21^{WAF1} lysates were prepared from CL3^{EcoR} cells where p21^{WAF1} is silenced (p21^{WAF1}). Additionally, to study the contrast between growing cells and senescent cells lysates were prepared from non-infected CL3^{EcoR} cells after growing them for five days at 33°C and 38.9°C respectively (33°C and 38.9°C). No specific bands corresponding to the desired proteins were observed. All three western blots showed number of non-specific bands indicating that antibody used was not very specific and as a result could not detect the specific protein.

A) L1: LF, L2: LM, L3: LIN52, L4: LFMS, L5: p21^{WAF1}, L6: WC, L7: 33°C, L8: 38.9°C and L9: HEK293T cells

B) F1: LFM, F2: LF, F3: FM, F4: LFMS, F5: p21^{WAF1}, F6: WC, F7: 33°C, F8: 38.9°C and F9: HEK293T cells

C) B1: LM, B2: B-MYB, B3: LFMS, B4: p21^{WAF1}, B5: WC, B6: 33°C, B7: 39°C and B8: HEK293Tcells

*LFM: LIN52, FOXM1ΔNΔKEN and B-MYB, LF: LIN52, FOXM1ΔNΔKEN, LM: LIN52 and B-MYB, FM: FOXM1ΔNΔKEN and B-MYB and LFMS: LIN52, FOXM1ΔNΔKEN and B-MYB reconstituted separately.

Chapter 5 Assaying the bypass potential of different identified TFs after simultaneous modulation of expression

5.1 Comparison of bypass potential of $p21^{WAF1}$ with the reconstituted active whole complex

5.1.1 Objective

In this study so far, the strongest bypass potential was observed by silencing $p21^{WAF1}$. One of the most striking findings from this study was that it has shown how efficiently reconstituting the active whole complex i.e. (MMB-FOXM1) works in bypassing senescence in $CL3^{EcoR}$ cells. It was therefore interesting to compare the bypass induced by $p21^{WAF1}$ silencing to that with the reconstituted MMB-FOXM1 complex.

5.1.2 Comparison of bypass

Densely dark blue stained colonies were obtained after silencing $p21^{WAF1}$ as well as expressing the components of the MMB-FOXM1 complex. On comparing the bypass potential of $CL3^{EcoR}$ where $p21^{WAF1}$ had been silenced to $CL3^{EcoR}$ cells which had been transduced with reconstituted whole MMB-FOXM1 complex, it was observed that even though reconstituting the whole complex bypasses senescence strongly it is less efficient in comparison to the extent of bypass observed by silencing $p21^{WAF1}$. This is shown both qualitatively and quantitatively in Figure 5.1. This comparison was only possible by using the software analysis algorithm as it was not possible to count the colonies obtained manually after silencing $p21^{WAF1}$ due to a completely saturated flask. The result in Figure 5.1, show that silencing of $p21^{WAF1}$ reported a significantly high bypass potential than that observed by reconstituting the whole active complex (MMB-FOXM1). Although computational analysis suggests that about 24% of the area of the flask was stained blue indicating presence of healthy growing colonies, I believe this is an underestimation as on close examination it appears that at least 60-70% of the flask was stained blue. This is possible as the computer algorithm was not

developed for completely saturated flasks, it was developed to identify blue spots against transparent background.

This comparison suggested the possible involvement of other factors and/or signalling pathways apart from DREAM in regulating senescence. If the DREAM complex is all there is downstream of $p21^{WAF1}$, then the efficiency of bypass should be the same, but it is not. This suggests that $p21^{WAF1}$ causes senescence by acting on a multitude of effectors, one of which could be the DREAM complex.

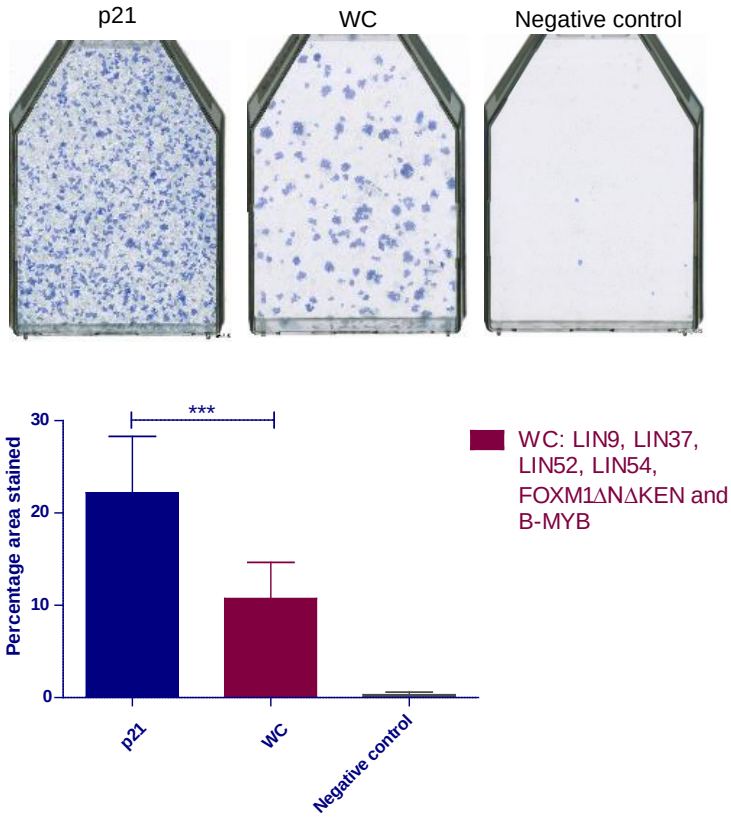

Figure 5.1 Comparison of bypass potential of silencing $p21^{WAF1}$ to MMB-FOXM1 complex
Bypass assays were performed at 5% CO_2 and 38.9°C with 35,000 cells per T-75 flask. Flasks were stained with 2% methylene blue after three weeks. Single representative flasks when $p21^{WAF1}$ was silenced and when the MMB-FOXM1 complex was reconstituted and ectopically expressed are shown. Due to completely saturated flask obtained after silencing $p21^{WAF1}$ only the software analysis was feasible. Hence, flask images shown with blue spots depict the area of the flask computed as blue areas by the computer algorithm. Quantitative representation of bypass potential is also presented graphically by plotting the calculated percentage area (+/- SD) covered in blue by Definiens Developer XD software for each of the replicates. Statistical analysis was conducted using One-way ANOVA, Tukey's Multiple Comparison Test (***p<0.001)

5.2 Identifying additional downstream mediators involved in bypassing senescence

5.2.1 Objective

An initial objective of this thesis was to identify, if there is a cocktail of TFs that can bypass senescence as efficiently as silencing of $p21^{WAF1}$ in $CL3^{EcoR}$ cells. In the previous section it is described how efficiently silencing of $p21^{WAF1}$ bypasses senescence. The bypass obtained after reconstituting the MMB-FOXM1 complex is approximately five-fold reduced in comparison to the bypass obtained after $p21^{WAF1}$ silencing. This significant difference raised the question as to what silencing of $p21^{WAF1}$ is doing? Hence, our objective was to try and identify other mediators that might be involved in addition to the components of MMB-FOXM1 complex which synergize when present together. We were particularly encouraged by the remarkable strategy used by Takahashi and Yamanaka who initially selected 24 TFs as candidates for reprogramming adult fibroblasts into iPS cells based on them playing pivotal roles in the maintenance of ES cell identity. They introduced all 24 TFs simultaneously, by retroviral infection, into adult fibroblasts and selected for cells which had been reprogrammed into iPS cells. They then left out one TF in turn until they were able to identify a cocktail of four TFs that can reprogram adult fibroblasts into iPS cells (Takahashi et al. 2007; Takahashi and Yamanaka 2006). This procedure relied on multiple viruses infecting the same cell and a very stringent assay which could detect a very small number of iPS cells in a background of non-programmed cells.

The experimental approach in this section is based on a similar strategy wherein, we have used a combination of high titre lentiviruses transducing all candidate TFs shortlisted in this study, as our starting point. Our aim was to identify a combination of TFs, which enhance the efficiency of bypassing senescence under very stringent conditions and if possible, improve it to the levels obtained after silencing $p21^{WAF1}$. This will allow us to determine if there is any potential synergism between the TFs that individually were not capable of bypassing senescence.

Hence, in this section silencing of the shortlisted up-regulated TFs was tested in conjunction with ectopic expression of the shortlisted down-regulated TFs to identify a cocktail that bypasses senescence efficiently.

5.2.2 Studying the bypass potential after mixing 73 TFs together

Firstly, a candidate list of TFs was assembled based on the initial list of up- and down-regulated TFs depending on availability of constructs. To this list some additional TFs were also added such as LIN52 which exhibited strong bypass potential in this study as discussed in the previous chapter. Also RELA, RELB and CEBPβ were included to the Pool (73) as they had shown some bypass activity upon silencing in previous studies conducted in the lab (Rovillain et al. 2011). Table 5.1 presents the list of 13 upregulated and 60 downregulated TFs. Some of these TFs were studied individually for their bypass potential as described in Chapter 3; due to time constraints all of them were not studied individually. In the previous experiments, mixing of six TFs to reconstitute the MMB-FOXM1 complex worked efficiently and produced strong bypass. Takahashi and Yamanaka's remarkable experiment where they studied 24 factors together, provided the motivation to try something far-fetched wherein, I tested the bypass potential after mixing 73 TFs together listed in Table 5.1 (Takahashi and Yamanaka 2006).

After assembling a candidate list, a DNA pool containing the most effective lentivirus shRNAmiRs for silencing up-regulated TFs were mixed together with lentiviral expression constructs for the down-regulated TFs (Table 5.2). As by now in this study we had established that LIN52, FOXM1ΔNΔKEN and B-MYB show a very strong bypass potential when present together therefore, another DNA pool called 'Pool Control' was made containing only LIN52, FOXM1ΔNΔKEN and B-MYB. This was undertaken to estimate the basal level of bypass observed because these three components that were present in the Pool in addition to 70 other TFs.

The aim of this experiment was to assess the efficiency of bypass of the other TFs, when present together and identify if there was any synergy. It was hypothesised that if we detected a stronger bypass activity in Pool (73) as

compared to Pool Control, this will suggest that there are TFs apart from LIN52, FOXM1ΔNΔKEN and B-MYB which might have an additional role to play in regulating senescence.

Table 5.1 List of 73 TFs which make up the pool of 73 TFs

ADNP	GABPB1	MYNN	SSRP1	CD36
ARNTL2	GLIS2	NOC4L	SUZ12	CEBPβ
B-MYB	H1FX	NUF1P1	TCF19	DNAJC21
C14ORF106	HMG2L1	PATZ1	TCF3	EPAS1
CBFB	HMGB1	PHB2	TCF4	LARP6
CEBPG	HMGB2	POGK	TEAD4	MXD1
CIZ1	HMGB3	PRMT3	TFAM	NR1H4
DEK	IF16	PRRX1	TWIST1	NR3C2
DEPDC1	LARP1	PSMD11	UBE2K	RELA
E2F1	LARP4	RAD51	WHSC1	RELB
E2F8	LIN52	ROD	YEATS4	RGS7
EP400	MATR3	SMARCA5	ZNF107	RORA
ETV4	MET	SMARCC1	ZNF207	SLC22A4
EZH2	MTA1	SMARCE1	ZNF280C	
FOXM1ΔNΔKEN	MYBL1	SP3	ZNF511	

*Genes listed in green were ectopically expressed whereas genes listed in red were silenced.

Lentiviruses were prepared for both Pool (73) and Pool Control to infect $CL3^{EcoR}$ cells. Freshly collected viruses were used to maximize viral titre and double infections were conducted to allow multiple infections of the same cell and stably transduced cells were assayed for bypass of senescence. pLEX-MCS was used as a negative control. The flasks were stained with methylene blue after three weeks to assess and compare the bypass potential.

Table 5.2 DNA pools made to study 73 TFs together

Reconstituted complex	Constituents
Pool (73)	1 µg of each of 73 TFs
Pool Control	70 µg pLEX-MCS+1 µg LIN52+1 µg FOXM1ΔNΔKEN and 1 µg B-MYB

Striking results were obtained. Dark blue stained colonies were obtained for both Pool (73) as well as the Pool Control. However, a greater number of densely stained colonies were obtained for Pool (73) compared to Pool Control. Pool Control had fewer faintly stained colonies. Quantitative analysis revealed a highly significant increase in the bypass potential when all 73 TFs were present together compared to Pool Control as shown in Figure 5.2. These results were independently verified in three different biological experiments. This indicated that there were other TFs present apart from LIN52, FOXM1ΔNΔKEN and B-MYB which may have a role in regulating senescence or can synergize with other TFs when expressed together.

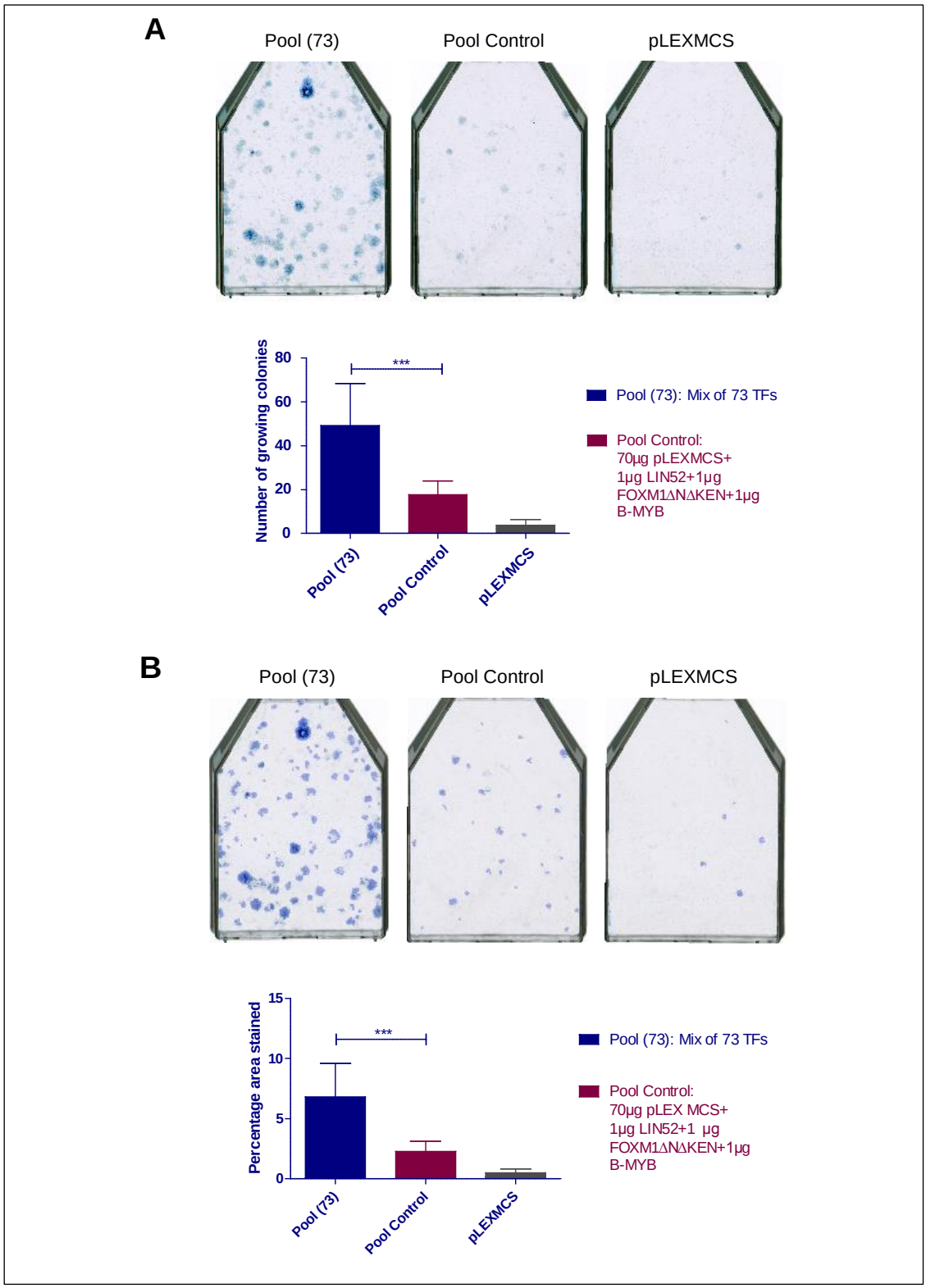

Figure 5.2 Study of bypass potential of 73 TFs when present together

Bypass assay was performed thrice independently at 5% CO_2 and 38.9°C with 35,000 cells per T-75 flask. Single representative flasks from internal repeats are shown. Bypass potential of 73 TFs was tested against Pool Control containing LIN52, FOXM1ΔNΔKEN and B-MYB. Empty vector pLEX-MCS was used as negative control. A) Manual analysis B) Computational analysis. Statistical analysis was conducted using One-way ANOVA, Tukey's Multiple Comparison Test (*p<0.05, **p<0.01, ***p<0.001)

5.3 Identification of TFs that were enriched in senescence bypassed cells stably transduced with Pool of 73 TFs

5.3.1 Objective

The results obtained from previous experiments were very encouraging as it showed that bypass potential of 73 shortlisted TFs was greater than bypass observed with Pool Control. It was possible therefore that other TFs are present within 73 TFs which have the potential to synergize or play a role in regulating senescence growth arrest.

To narrow down the candidate TFs to find out the minimum number of key TFs that have a role in senescence two approaches could be used. First approach can be similar to the one used by Takahashi and Yamanaka (Takahashi and Yamanaka 2006). This would involve repeating the bypass assays and leaving out one TF per assay. The hypothesis for this approach is that if the TF that is removed is critical, a reduction in bypass potential will be observed. A second approach that can be used is to identify the TFs which have been enriched in $CL3^{EcoR}$ cells in which senescence has been bypassed by Deep sequencing.

The first approach would require setting up 73 senescence bypass assays removing one TF per assay. As we do long term senescence bypass growth assays this approach would require a lot of time. Therefore, due to time constraints the second approach was taken in this study. This should allow us to narrow down the TFs that may be enabling senescence to be bypassed.

5.3.2 Deep sequencing

Three independent experiments were performed to test the bypass potential of Pool (73) over Pool Control. The results obtained from these experiments established that Pool (73) works better than Pool Control. The next aim was to identify from the pool of 73 exogenously introduced TFs which have been enriched in the bypassed cells. It was hypothesized that if a TF is important, it should be enriched within the cells in which senescence has been bypassed and contribute towards the observed bypass.

Deep sequencing was undertaken on genomic DNA extracted from $CL3^{EcoR}$ cells which had bypassed senescence after being stably transduced with DNA Pool (73) from three independent biological experiments. Isolated genomic DNA was amplified using P7-tagged primers specific for the three different types of vectors present in the pool: pLX301, pLEX-MCS and pGIPZ shRNAmiR. Amplified DNA was outsourced to UCL Genomics Services based at Institute of Child Health for MiSeq Micro 300 Cycle Sequencing. The results after deep sequencing were obtained as a count table that indicated how many times each sequence was uniquely identified by a sequencing read. In addition to the isolated genomic DNA from $CL3^{EcoR}$ cells, the starting mixture of DNA Pool (73) was similarly amplified followed by deep sequencing. This was done to determine the baseline count for sequencing reads when all TFs are added in similar amount in Pool (73) as the efficiency of amplification may vary between different constructs; it is possible that some TFs may amplify better than others. Hence, for every TF if the sequencing reads obtained in experimental samples of genomic DNA was significantly higher than the reads obtained for DNA pool, that TF was considered to be enriched. Analysed results are presented in Figure 5.3 for all the 73 TFs, which are an average of all the six samples. This led to identification of 18 down-regulated TFs and 5 up-regulated TFs which were found to be enriched.

The findings reported here suggest that overall 23 TFs were enriched in $CL3^{EcoR}$ cells in which senescence had been bypassed after being stably transduced with the Pool of 73 TFs.

A.

Down-regulated TFs	Length of sequence (bp)	Percentage of DNA amplified from DNA Pool (73)	Average percentage enrichment in bypassed CL3^{EcoR} cells	Ratio
ADNP	3426	0.68	0.04	0.06
ARNTL2	1849	1.76	0.96	0.54
B-MYB	2154	1.63	3.84	2.36
C14ORF106	3461	0.52	0.04	0.08
CBFB	609	3.18	9.06	2.85
CEBPG	505	3.07	6.08	1.98
CIZ1	2446	0.03	0.01	0.34
DEK	1174	0.39	1.24	3.21
DEPDC1	1722	0.58	0.26	0.45
E2F1	1477	0.00	0.00	0.00
E2F8	2651	0.48	0.08	0.17
EP400*	3002	0.00	0.00	0.00
ETV4	1504	0.06	0.01	0.10
EZH2	2302	1.32	0.46	0.35
FOXM1ΔNΔKEN	475	0.36	0.11	0.29
GABPB1	1128	19.63	4.20	0.21
GLIS2	1639	0.09	0.00	0.03
H1FX	1665	3.61	4.86	1.35
HMG2L1	1855	1.70	1.46	0.86
HMGB1	694	3.38	5.81	1.72
HMGB2	679	2.04	3.95	1.93
HMGB3	646	1.80	0.64	0.36
IFI16*	2222	0.00	0.00	0.00
KNTC1	6766	0.03	0.00	0.00
LARP1	3104	0.30	0.00	0.00
LARP4	1169	2.59	1.26	0.49
LIN52	668	1.62	2.02	1.24
MATR3	2586	0.60	0.13	0.22
MET	4276	0.39	0.00	0.01
MTA1	812	0.21	0.07	0.35
MYBL1	2125	1.53	0.29	0.19
MYNN	1885	2.15	0.44	0.21
NOC4L	1600	1.67	1.05	0.63
NUF1P1	896	2.59	5.45	2.10
PATZ1	1661	0.16	0.01	0.03
pLEXMCS	334	5.19	3.87	0.75
POGK	1877	0.11	0.00	0.00
PRMT3	1648	2.10	3.16	1.51
PRRX1	787	0.61	1.48	2.40
PSMD11	1379	0.01	0.41	68.29
RAD51	1069	6.53	4.76	0.73
SMARCA5	3203	0.48	0.10	0.22
SMARCC1	3370	0.32	0.01	0.03
SMARCE1	1285	1.67	2.08	1.25
SP3	2393	0.54	0.06	0.10
SSRP1	2178	1.64	0.82	0.50
SUZ12*	2264	0.00	0.00	0.00
TCF19	1090	1.38	1.46	1.06
TCF3	805	2.14	1.39	0.65
TCF4	2104	1.43	0.59	0.41
TEAD4	1336	1.33	3.07	2.31
TFAM	787	3.34	7.30	2.19
TWIST1*	654	0.00	0.01	0.00
UBE2K	652	3.73	5.92	1.59
WHSC1	4162	0.28	0.00	0.01
YEATS4	749	2.36	5.28	2.24
ZNF107	2897	0.22	0.00	0.01
ZNF207	1231	0.63	0.09	0.14
ZNF280C	2222	1.51	0.70	0.47
ZNF511	803	2.31	3.60	1.55

B.

Up-regulated TFs	Length of sequence (bp)	Percentage of DNA amplified from DNA Pool (73)	Average percentage enrichment in bypassed CL3^{EcoR} cells	Ratio
CD36	520	6.28	6.95	1.11
CEBP	520	7.44	15.16	2.04
DNAJC21	520	13.38	10.88	0.81
EPAS1	520	9.70	4.02	0.41
LARP6	520	3.22	5.55	1.72
MXD	520	11.74	9.39	0.80
NR1H4	520	11.98	9.94	0.83
NR3C2	520	10.16	11.97	1.18
RELA	520	2.50	4.48	1.80
RELB	520	5.58	7.15	1.28
RGS7	520	6.25	5.43	0.87
RORA	520	11.78	9.07	0.77
SLC22A4	520	0.00	0.00	0.00

Figure 5.3 Identification of enriched TFs from 73 TFs.
A) Down-regulated TFs B) Up-regulated TFs. Ratio was calculated after dividing the average percentage enrichment obtained from the genomic DNA samples of three independent biological experiments to the Percentage of reads obtained for TFs amplified from Pool DNA. TFs for which the ratio was greater than 1 (highlighted in yellow) were considered to be enriched and shortlisted for further study. '*' marked are the ones which did not amplify from DNA Pool (73).

5.3.3 Studying the bypass potential after mixing together the identified 23 TFs

Deep sequencing identified 23 TFs which were found be enriched in CL3^{EcoR} cells transduced with 73 TFs over other TFs. The next step was to analyse the bypass potential of the 23 TFs when studied together. Surprisingly FOXM1ΔNΔKEN was not found to be highly enriched in CL3^{EcoR} cells transduced with pool of 73 TFs. Therefore, FOXM1ΔNΔKEN was excluded from the Pool of 23 TFs and the pool control designed for this experiment did not contain FOXM1ΔNΔKEN as shown in Table 5.3.

To compare the bypass of Pool (23) to Pool Control, respective lentiviruses were made, and infections performed in CL3^{EcoR} cells. After three weeks bypass potential was analysed by staining the flasks with 2% methylene blue.

Table 5.3 DNA pools made to study 23 TFs that were found to be enriched together

Reconstituted complex	Constituents
Pool (23)	1 µg of each of 23 TFs
Pool Control	21 µg pLEX-MCS+1 µg LIN52 and 1 µg B-MYB

Interestingly, the Pool (23) exhibited large number of stained growing colonies. Pool control also presented some growing colonies, but they were much less than the number of colonies obtained for Pool (23). Quantitative analysis showed that the bypass potential obtained for Pool (23) was significantly higher than Pool Control as illustrated in Figure 5.4. This is very interesting as it suggests the presence of other key TFs within the identified 23 TFs which might have a role in regulating senescence growth arrest.

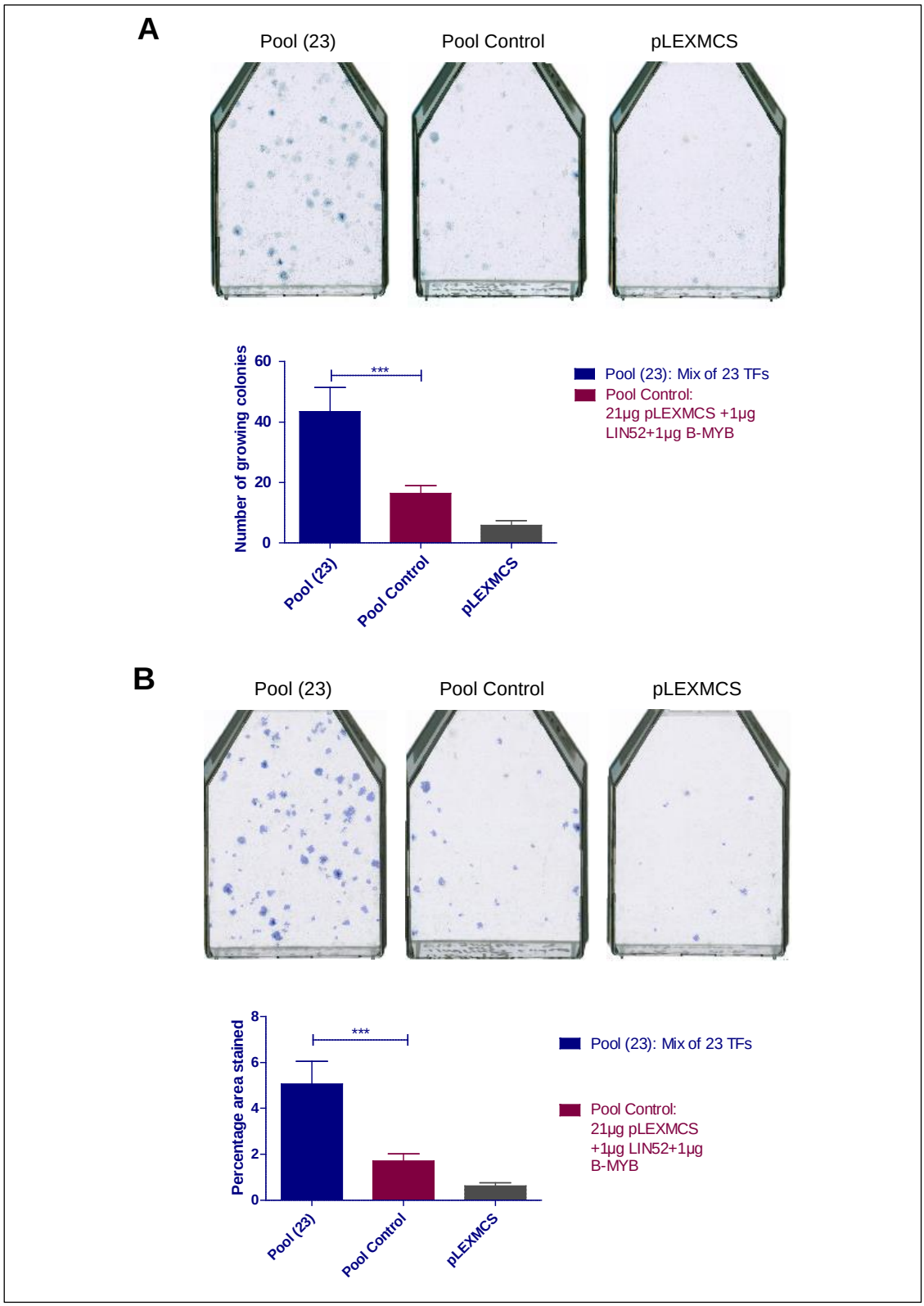

Figure 5.4 Study of bypass potential of 23 TFs when present together
Bypass assay was performed thrice independently at 5% CO_2 and 38.9°C with 35,000 cells per T-75 flask. Single representative flasks from internal repeats are shown. Bypass potential of 23 TFs was tested against Pool Control containing LIN52 and B-MYB. Empty vector pLEX-MCS was used as negative control. A) Manual analysis B) Computational analysis. Statistical analysis was conducted using One-way ANOVA, Tukey's Multiple Comparison Test (*p<0.05, **p<0.01, ***p<0.001)

5.4 Comparison of bypass potential of 73 TFs to 23 TFs

Previously, we have tested the bypass potential of 73 TFs as well as 23 TFs. However, it was important to compare and analyse the bypass potential for both pools together. Our aim was to test the hypothesis that the bypass potential for Pool (23) should be more than Pool (73) as Pool (23) only contains the TFs which were enriched and should therefore present a stronger bypass.

Lentiviruses were successfully made for both the pools (Table 5.4) and assayed for their ability to bypass senescence in $CL3^{EcoR}$ cells.

Table 5.4 DNA pools made to compare bypass potential of 73 TFs to 23 TFs

Reconstituted complex	Constituents
Pool (73)	1 µg of each of 73 TFs
Pool (23)	1 µg of each of 23 TFs

Unfortunately, the results obtained were not as expected. Staining with methylene blue after the stably transduced cultures of $CL3^{EcoR}$ cells were allowed to grow for three weeks generated healthy growing colonies for both Pool (23) as well as Pool (73). The bypass potential observed by both DNA pools of 23 and 73 TFs together were similar as shown by the representative flask images for each pool in Figure 5.5.

Also, an anomaly was present between the quantitative analysis of the results obtained when analysed by the two different methods. Quantitative analysis done by manual method showed that there was no numerical difference between the bypass potential of Pool (23) and Pool (73). On the other hand, analysis using software revealed a small significant difference between the bypass. Computational analysis showed that the extent of bypass obtained by Pool (73) was slightly higher than the bypass of Pool (23). To be able to understand this result thoroughly, further experimental investigations are required.

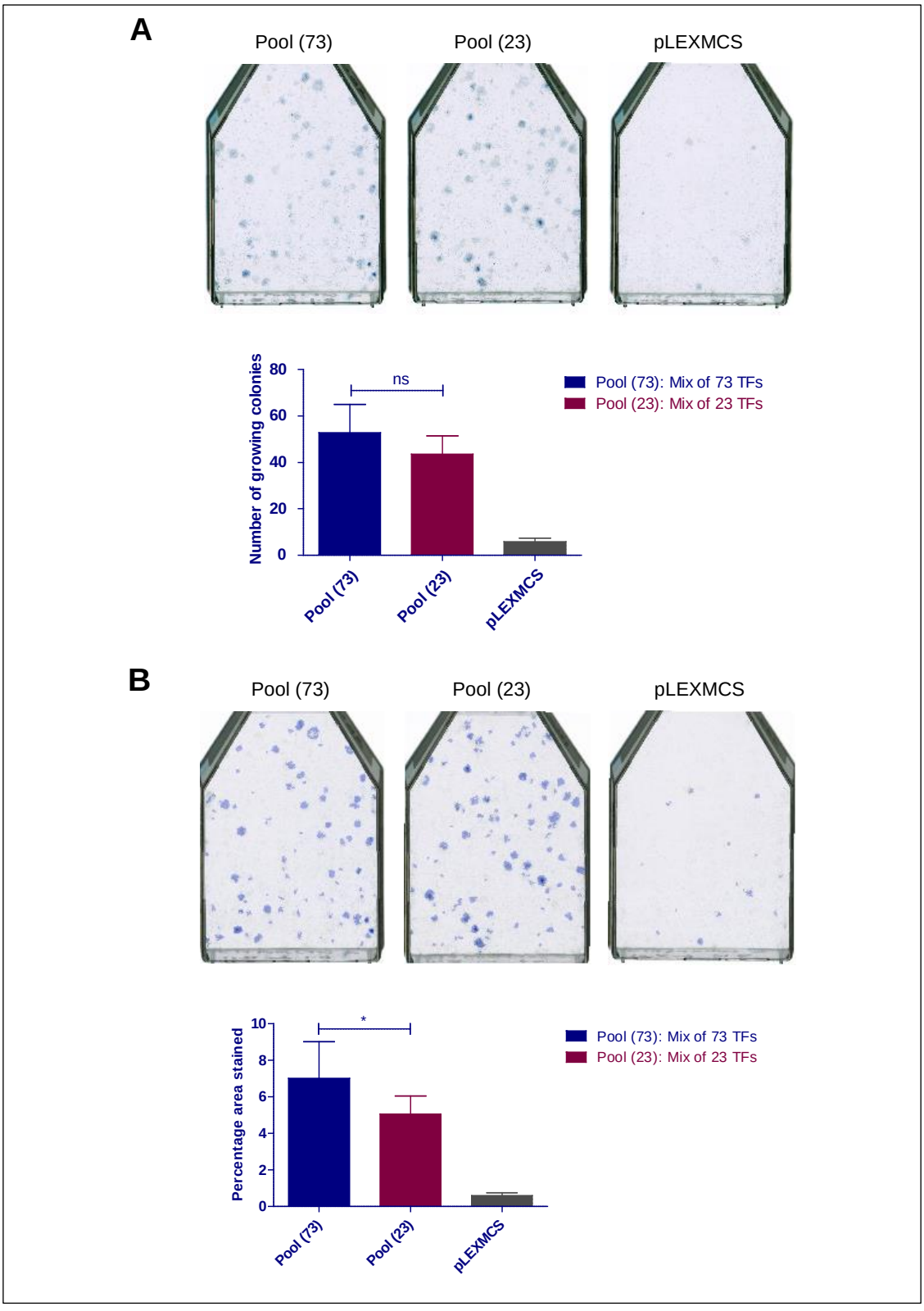

Figure 5.5 Comparison of the bypass potential of pool of 73 TFs to pool of 23 TFs.
Bypass assay was performed thrice independently under the similar stringent conditions described above. Single representative flasks from internal repeats are shown. Empty vector pLEX-MCS was used as negative control. A) Manual analysis B) Computational analysis. Statistical analysis was conducted using One-way ANOVA, Tukey's Multiple Comparison Test (*p<0.05, **p<0.01, ***p<0.001)

Chapter 6 Discussion

Cellular senescence is a stable growth arrest that normal cells undergo after a finite number of divisions, the Hayflick limit (Hayflick and Moorhead 1961). Senescence is triggered in response to a variety of intrinsic and extrinsic stimuli, for example, progressive telomere shortening; changes in telomeric structure, or other forms of genotoxic stress resulting in a DNA damage response; and growth arrest mainly via activation of p53 (Adams 2009). Other forms of stress lead to senescence via activation of the pRB pathway (Adams 2009).

Senescence can compromise tissue repair and regeneration and contribute to tissue and organismal ageing due to accumulation of senescent cells, depletion of stem/progenitor cell compartments and secretion of SASP proteins. Removal of senescent cells can prevent or delay age-related tissue dysfunction and extend healthspan (Baker et al. 2011, 2016). Senescence can also lead to the removal of defective and potentially cancerous cells from the proliferating pool, thereby limiting tumour development and acting as a potent tumour suppressor mechanism (Campisi 2005). A greater understanding of the molecular events that lead to cellular senescence is therefore essential if we are to prevent tissue dysfunction without increasing the risk of cancer.

To facilitate the study of senescence, the Jat laboratory has used a thermolabile mutant of SV40 LT antigen, in conjunction with hTERT, to develop unique conditionally immortalised human mammary $CL3^{EcoR}$ fibroblasts that are stringently temperature sensitive (O'Hare et al. 2001). These cells are immortal if grown at 34°C, but upon inactivation of thermolabile LT antigen at 38°C, resulting in activation of p53 and pRB, they undergo a stable growth arrest within 7 days, induce senescence-associated (SA)-β-galactosidase and have morphological features and express genes in common with senescent cells (Rovillain et al. 2011).

Many studies in addition to those undertaken by Rovillain et al., 2011, have shown that mechanisms underlying senescence growth arrest primarily involve $p53/p21^{WAF1}$ and $p16^{INK4A}$/pRB tumour suppressor pathways (Rovillain et al. 2011; Adams 2009; Campisi and D'Adda Di Fagagna 2007; Ben-Porath and

Weinberg 2005). But it is not known what makes the growth arrest stable; what the critical targets are; and what downstream TFs are involved, as they are likely to be the key for the establishment and maintenance of senescent state. Hence, the aim of this thesis was to identify transcription factors that act downstream of the p53/p21^{WAF1} and p16^{INK4A}/pRB pathways and assess their functional role in regulating senescence growth arrest.

Genome-wide expression profiling, coupled with inactivation of p16^{INK4A}/pRB and p53/p21^{WAF1} pathways in human mammary fibroblasts cells (CL3^{EcoR}), previously conducted in the laboratory had derived a comprehensive catalogue of genes whose levels are altered upon senescence but then reversed when senescence was bypassed (Rovillain et al. 2011).

As TFs regulate gene expression at different stages of embryonic development and are key to the establishment and maintenance of specific cell fates (Vaquerizas et al. 2009), in this thesis I undertook an overlay of the differential gene set with 1391 manually curated sequence-specific DNA binding factors. This gene list was then further refined using Oncomine, a cancer microarray database, hypothesising that gene expression in senescence and cancer should be opposite i.e. genes ‘turned on’ in cancer should be ‘turned off’ in senescence and vice versa. Once the list of differential TFs was assembled, the next step was functional validation to determine if the candidate TFs had a role in senescence by stably silencing expression of genes that were ‘turned on' and ectopically expressing genes that were ‘turned off'. Although other investigators have successfully utilised short-term senescence bypass assays, we have chosen to undertake a long-term senescence bypass assay as described by Rovillain and colleagues (Rovillain et al. 2011).

Long term senescence bypass assay involves stably transducing cells at 34ºC and then plating a fixed number of cells (35,000 or 50,000) per T-75 flask and shifting the cells to the non-permissive temperature and cultivating them for three weeks. Plating a fixed number of cells ensures that the cell density is same across the experiment. Moreover, culturing the cells for 3 weeks ensures that the cells that are growing are those in which senescence has been stably bypassed especially since in cultured cells onset of stable senescence growth arrest

requires a prolonged period (>4 days) to become fully arrested (Chen et al. 2002; Dai and Enders 2000; He and Sharpless 2017). The CL3^{EcoR} cells only become fully growth arrested after 5 to 7 days. Therefore, this protocol measures a much more stringent bypass than the short-term transient expression and silencing assays.

To determine, if the up-regulated TFs can bypass senescence individually, senescence bypass assays were conducted by silencing the upregulated TFs using different pGIPZ shRNAmiRs. To determine if ectopic expression of downregulated TFs can individually bypass senescence, senescence bypass assays were performed by ectopically expressing full-length ORFs. To study synergistic effects, reconstruction experiments were undertaken, where lentiviruses were prepared from pools of DNAs consisting of different TFs to be tested simultaneously.

6.1 Summary and Discussion of Results

6.1.1 Assessment of the functional role of differentially regulated TFs in senescence.

Use of the refining approaches which included the overlapping with DNA binding factors and Oncomine database, discussed in Chapter 3, led to the identification of 10 upregulated TFs and 74 downregulated TFs. Interestingly six differential candidate TF genes identified in this study i.e. ARID2, PATZ1, PDS5B, PLXNA3, ZBTB7A and ZC3H4 were amongst the senescence transcriptome signature genes identified in a recent study by Hernandez-Segura et al., 2017, (Hernandez-Segura et al. 2017). They incorporated datasets from whole-transcriptome profiles from six different strains of fibroblasts (BJ, HCA-2, HFF, IMR90, MRC5, WI-38) that were subjected to three different senescence inducing stimuli, replicative senescence, oncogene-induced senescence and ionizing radiation-induced senescence (Hernandez-Segura et al. 2017).

ARID2 is a transcriptional regulator which is a subunit of SWI/SNF multi-protein chromatin remodelling complex. Inactivating mutations in AT-rich Interaction domain 2 (ARID2) has been shown to be involved in non-small cell lung carcinoma, liver cancer related to Hepatitis C virus (HCV) infection and in

melanoma (Manceau et al. 2013; Li et al. 2011b). These findings predict the tumour suppressive role of ARID2.

POZ/BTB and AT-hook-containing zinc finger protein 1 (PATZ1) acts as a transcriptional repressor and plays an important role in chromatin remodelling and transcription regulation (Cho et al. 2012). Study by Cho et al., 2012, has reported PATZ1 to be downregulated in endothelial cell senescence (Cho et al. 2012). This study demonstrated that knockdown of PATZ1 in young human umbilical vascular endothelial cells accelerated premature endothelial cell senescence whereas overexpression of PATZ1 led to the reversal of a senescent phenotype. Additionally, results from this study suggested that PATZ1-induced senescence is mediated by a ROS-mediated p53-dependent DDR pathway (Cho et al. 2012). However, the role of PATZ1 as an oncogene or tumour suppressor gene is still debatable.

For PDS5 Cohesin Associated Factor B (PDS5B) and Plexin A3 (PLXNA3), no direct known links to senescence are known. However, PLXNA3 has been suggested to be involved in tumour progression (Hernandez-Segura et al. 2017).

Zinc Finger and BTB Domain containing 7A (ZBTB7A) is a member of POK (POZ/BTB and Kruppel) TF family. It has been identified as a potential proto-oncogene by multiple different studies to be involved in different types of cancer such as ovarian cancer, breast cancer, non-small cell lung carcinoma and chondrosarcoma (Jiang et al. 2010; Aggarwal et al. 2010; Qu et al. 2010; Vredeveld et al. 2010; Zhao et al. 2008; Maeda et al. 2005; Kumari et al. 2012). Study by Kumari et al., 2012, has demonstrated the use of ZBTB7A in chondrosarcomas, both as a therapeutic target as well as a diagnostic marker (Kumari et al. 2012). ZBTB7A has recently been identified as a context-dependent cancer gene which in addition to acting as a key proto-oncogene in multiple tissues, can also act as a tumour suppressor (Wang et al. 2013). It was demonstrated that inactivation of ZBTB7A greatly enhanced the progression of Pten-loss driven prostate cancer by overcoming Pten loss induced cellular senescence. Furthermore, a concomitant loss of ZBTB7A expression at both mRNA and protein level is reported in a subset of advanced human prostate cancers (Wang et al. 2013).

ZC3H4 (Zinc Finger CCCH-Type Containing 4) was recently reported to be among the top candidate genes that were downregulated upon silencing of Endogenous bornavirus-like nucleoprotein 1 (EBLN1) expression in infected oligodendroglial cells. Silencing of EBLN1 induces G2/M phase growth arrest, promotes apoptosis and inhibits cell proliferation (He et al. 2016).

The ability of the prioritized TFs to directly bypass senescence was examined in the conditionally immortalized fibroblasts by lentivirus-mediated RNA silencing or ectopic expression. Testing of all the 10 shortlisted up-regulated TFs along with other key up-regulated TFs that are known to play a crucial role in senescence i.e. $p21^{WAF1}$, RELA, RELB and CEBPβ for their bypass potential led to identification of four TFs (EPAS1, RGS7, LARP6 and NR1H4) in addition to RELA (Rovillain et al. 2011) that were able to bypass senescence to certain extent. The remainder were inactive. The strongest bypass was observed after silencing $p21^{WAF1}$, which generated a completely saturated flask of healthy growing colonies. To further confirm these findings, the bypass assay was repeated with multiple pGIPZ shRNAmiRs for each candidate TF and the assay was conducted under more stringent conditions. Unfortunately, this time none of the TFs reported significant bypass potential. Close examination of the results indicated that the only TF which showed any bypass activity under the very stringent conditions was RELA. This is in accordance with multiple previous studies indicating a role for RELA activation in senescence (Rovillain et al. 2011; Korc 2016; Lesina et al. 2016; Wang et al. 2009b; Adler et al. 2007; Penzo et al. 2009; Osorio et al. 2016; Salminen et al. 2012, 2008; Kriete and Mayo 2009). Recently ROS-activated NF-κB signalling has been reported to be involved in senescence bystander effect seen in human fibroblasts (Nelson et al. 2018).

Functional validation of the down-regulated TFs in the senescence bypass assay by their ectopic expression found that none of the TFs examined, exhibited any bypass potential. This was very surprising since previous work in the laboratory had shown that B-MYB, EZH2 and DEK, for example, were able to bypass senescence. Therefore, conditions and different parameters for the assay were optimized. In addition, all lentiviral expression clones were sequence verified. While sequence verifying TFs, it was found that some of the clones were

rearranged and none of the B-MYB clones were correct. We have found lentiviral vectors transformed into super competent DH5α cells were highly prone to recombination often leading to rearrangements and deletions. In contrast, it was found that all lentiviral constructs transformed into JS4 cells, a recA derivative of MC1061 (Sedivy et al. 1987), were highly stable and did not exhibit rearrangements.

After optimization, ectopic expression of full-length verified B-MYB was found to bypass senescence very efficiently in the $CL3^{EcoR}$ cells (Figure 3.8). However, rather surprisingly no bypass was observed upon ectopic expression of constitutively active FOXM1 that lacks the amino-terminal and the KEN box i.e. FOXM1(ΔNΔKEN) as observed previously (Rovillain et al. 2011). One possibility for this difference could be due to the lentiviral pLEX-MCS vector in this study whereas previously a retroviral pLNCX2 was used even though the CMV promoter was used to drive FOXM1 expression in both vectors. Apart from B-MYB, no other downregulated TF when studied individually exhibited strong bypass activity. This could be due to many reasons. First, the TF does not have a direct causal role in senescence. Second, ectopic expression of the TF is not able to bypass senescence due to inappropriate cellular localization or acts in conjunction with other components. Third, the construct used for expressing the TF did not express or did not express at sufficiently high levels in $CL3^{EcoR}$ cells under the experimental conditions.

For most of the experiments it was observed that on plating 35,000 cells, around 20-100 colonies were obtained after successful senescence bypass apart from with $p21^{WAF1}$. One plausible explanation for this could be that even though 35000 cells are infected, it is impossible to say that every infected cell is expressing the gene at the correct level for bypassing senescence. We do not know what that correct level is, so we can only score the positive and compare it to our best possible controls. Also, every insertion site does not give the same level of expression. Therefore, it is all a question of how well the test gene works relative to the positive control.

6.1.2 Role of DREAM complex associated components in cellular senescence

Microarray analysis of the conditionally immortal CL3^{EcoR} fibroblasts (Rovillain et al. 2011) indicated that B-MYB, FOXM1, LIN9 and LIN52 were all significantly down-regulated upon senescence and the down-regulation was reversed when senescence was bypassed upon inactivation of the p16^{INK4A}/pRB and p53/p21^{WAF1} pathways, shown in Figure 4.2. LIN54 and RBBP4 were also down-regulated upon senescence arrest but this was not significant (data not shown). In contrast, LIN37 was significantly up-regulated upon senescence arrest, shown in Figure 4.2. All the above-mentioned components are the members of the MMB-FOXM1 complex (Sadasivam and DeCaprio 2013).

As most of the components of the MMB-FOXM1 complex were downregulated in the microarray analysis (Rovillain et al. 2011), a reconstruction experiment was undertaken by preparing a DNA pool comprising B-MYB, FOXM1, LIN9, LIN37, LIN52, LIN54, to determine if these components would act in conjunction to bypass senescence under stringent conditions. This led to one of the most striking observations in this thesis; the components of the MMB-FOXM1 complex together bypassed senescence efficiently in the CL3^{EcoR} cells.

To identify the critical components within the MMB-FOXM1 complex, further reconstruction experiments were undertaken similar to Yamanaka approach where the complex was reconstituted but lacked one component. This revealed that LIN52, FOXM1 and B-MYB were the crucial components for the strong bypass observed by the whole MMB-FOXM1 complex; their omission resulted in a strong reduction in the bypass activity. Rather surprisingly the strongest effect was observed when LIN52 was omitted. Moreover, the results from this experiment clearly demonstrated a role for FOXM1 in bypassing senescence. This suggested a key role of these three components in regulating senescence growth arrest.

Next, the extent of bypass of the three critical components identified was compared individually to the bypass potential of the whole complex containing six components. It was found that none of the three components exhibited very strong bypass when present on their own in the same amount as in the whole

complex thus demonstrating a clear synergy and showed that for the strong bypass observed for the complex, these three components must be present together. The results obtained from this experiment also validated the results from the indirect approach taken in the previous experiment where the complex was reconstituted but lacking one component at a time.

An alternative experiment design where the mixing of individually packaged and titered viruses is used to assess component synergy within the MMB-FOXM1 complex, as opposed to co-packaging viral backbones. This alternative strategy should mitigate the risk that differences in rescue reflect differences in packaging preference of specific backbones in different contexts.

Furthermore, when the bypass potential of each of the components of the MMB-FOXM1 complex was tested individually, surprising results were obtained. LIN52, a 116 aa protein, found to be the critical component of the MMB-FOXM1 complex, exhibited a strong bypass potential. This was the first time in this study, that any TF apart from B-MYB, exhibited strong bypass when expressed individually. Like previous experiments B-MYB showed a strong bypass potential whereas FOXM1 exhibited marginal bypass potential along with the other components of the complex i.e. LIN9, LIN37 and LIN54. This clearly demonstrated a role for mutant LIN52 in bypassing senescence. This is in accordance with the study by Litovchick et al., 2011, where they showed that point mutations in LIN52 disrupt the DREAM assembly and significantly reduced the ability of human fibroblasts to undergo oncogenic RAS-induced senescence (Litovchick et al. 2011).

FOXM1 and B-MYB were highly down-regulated upon senescence arrest; they were the 5th and 7th most highly down-regulated transcription factors. FOXM1 is also down-regulated upon replicative senescence in primary human fibroblasts (Hardy et al. 2005) and markedly reduced in cells from elderly patients and patients with progeria (Ly et al. 2000). It regulates the G2-specific gene expression signature genes which were all down-regulated upon senescence arrest in our CL3^{EcoR} fibroblasts (Rovillain et al. 2011).

FOXM1 is widely known to promote cell proliferation and hence contribute to tumour progression. FOXM1 is one of the genes in the subset of 69 genes identified by Rhodes et al., 2004, which comprises the meta-signatures of genes commonly overexpressed in various types of undifferentiated cancer (Rhodes et al. 2004). FOXM1 has also been linked to melanoma, the most lethal form of skin cancer. It is reported to be elevated and activated in metastatic melanoma (Kruiswijk et al. 2016; Ito et al. 2016; Miyashita et al. 2015).

Recently, many studies have suggested the therapeutic use of targeting FOXM1 to treat advanced melanoma. Recent encouraging results have shown that inhibition of FOXM1 expression using siRNA or inhibitors such as thiostrepton and siomycinA, significantly suppressed the proliferation of the melanoma cells (Miyashita et al. 2015; Ito et al. 2016). Another study by Kruiswijk et al., 2016 has suggested the therapeutic use of Pin1-FOXM1 inhibitors in metastatic melanoma treatment (Kruiswijk et al. 2016). Pin1 is an enzyme that has shown to be a key regulator of FOXM1 activity mediated by MEK-dependent regulation during the cell cycle (Kruiswijk et al. 2016).

B-MYB is a member of the Myb family of genes that is ubiquitously expressed in proliferating somatic cells and represses transcription of $p16^{INK4A}$ (Huang et al. 2011). Silencing of B-MYB expression in primary human foreskin fibroblasts induces senescence (Johung et al. 2007), whereas ectopic expression rescues Ras-induced premature senescence in primary rodent cells (Masselink et al. 2001). B-MYB is known to be a key physiological regulator of cell survival, cell cycle progression and cell differentiation in tumorigenesis (Musa et al. 2017). Initially, it was believed that B-MYB promotes expression of cell cycle genes by binding to Myb sites in the promoters of target genes (Zhu et al. 2004; Knight et al. 2009). However, recent studies have now demonstrated that B-MYB, after interacting with MuvB, binds to CHR elements present in the promoter region of G2/M cell cycle genes (Müller et al. 2012, 2016, 2014). Furthermore, these studies have shown that Myb sites were not enriched in the promoters of G2/M genes (Müller et al. 2014).

Evidence in the literature suggests that there may be a potential link between B-MYB and FOXM1. They have common downstream targets such as CCNB1,

PLK1 and AURK1, which are required for progression into mitosis. Their levels are also repressed during G0 and their activities are regulated by cell cycle-dependent phosphorylation. They also undergo cell cycle-dependent ubiquitin-mediated proteasome degradation as shown in Figure 1.5.

It has been shown that LIN52 plays a crucial role in DREAM complex assembly (Litovchick et al. 2011). Phosphorylation of LIN52 at serine 28 by DYRK1A (dual-specificity tyrosine-(Y)-phosphorylation regulated kinase 1A) is central/crucial to regulating the switch in the binding of MuvB complex from B-MYB to DREAM (Litovchick et al. 2011). Rather surprisingly, Rovillain et al., 2011, found that DYRK1A which promotes entry into quiescence by promoting assembly of the DREAM complex was also significantly down-regulated upon senescence arrest and this was reversed upon senescence bypass (Rovillain et al. 2011) (Figure 4.2).

The other major finding was that LIN52 was found to be the most critical component out of LIN52, FOXM1 and B-MYB as the removal of LIN52 led to the highest reduction in bypass potential. Results obtained from experiments conducted with different LIN52 isoforms i.e. LIN52 with Ala, Glu or Ser at the 28th amino acid residue, showed that LIN52-Ala that cannot be phosphorylated exhibited a strong bypass potential whereas LIN52-Ser was unable to bypass senescence. LIN52-Ser showed bypass activity similar to the negative control as shown in Figure 4.11 indicating that under physiological conditions Ser-28 was most likely to be constitutively phosphorylated thereby promoting assembly of the inhibitory DREAM complex. A similar reduction in bypass was obtained when the MMB-FOXM1 complex was reconstituted with WT-LIN52-Ser. Rather surprisingly LIN52-Glu which was expected to mimic constitutively phosphorylated LIN52, showed a similar bypass potential to LIN52-Ala. The LIN52-Ala results show that non-phosphorylated LIN52 was required for the strong bypass potential exhibited by LIN52 when studied individually or as part of the reconstituted MMB-FOXM1 complex, indicating a role for phosphorylated LIN52 and the DREAM complex in inducing senescence.

As the subunit composition of DREAM complex is different from repressive RB-E2F complex, it is likely that the DREAM complex containing MuvB represses

genes required for cell cycle progression by mechanisms that are partially different from the repressive RB-E2F complexes. A recent study has suggested that the DREAM complex downregulates expression of cell cycle genes by nucleosome positioning (Marceau et al. 2016).

Recently, studies have examined the structural basis for DREAM assembly to understand the biochemical mechanisms behind DREAM function. Guiley et al., 2015, highlighted the importance of phosphorylation of Ser-28 by DYRK1A as they identified the LxSxExL sequence in LIN52 which binds directly with LxCxE in the pocket domain of p107 and p130 thereby promoting the assembly of the DREAM complex (Guiley et al. 2015). This highlighted the critical role of phosphorylation of nearby Ser-28 residue which provided specific binding of MuvB to only p107/p130 and not to RB protein as the binding pocket of RB is not able to bind to phosphorylated LIN52. They also studied DREAM complex assembly upon cell cycle entry as MuvB complex is capable of binding to both p107/p130 pocket proteins to facilitate DREAM assembly whereas it can also bind to B-MYB to promote cell cycle progression. It was found that upon cell cycle entry, phosphorylation of p130 by CDKs weakens its association with MuvB. Therefore, phosphorylation of LIN52 Ser-28 by DYRK1A promotes DREAM assembly whereas phosphorylation of sites in p107/p130 by CDKs facilitates DREAM disassembly to promote cell cycle progression (Guiley et al. 2015). LIN52 therefore plays dual role in recruiting components for assembly of repressive DREAM complex as well as assembling the activating MMB-FOXM1 complex, since it is essential for binding of B-MYB with MuvB which is then required for the recruitment of FOXM1(Fischer and Müller 2017; Guiley et al. 2015).

The microarray expression profiling study conducted in the laboratory found miRNA146a was the most highly up-regulated miRNA with a log2 fold change of 4.33 upon senescence (Rovillain 2011). Promoter analysis studies by Taganov et al., 2006, showed that miR-146a was an NF-κB dependent gene (Taganov et al. 2006). According to biological prediction, miR146a regulates the expression of LIN52 by binding to 3’ UTR of LIN52. A recent study (Luo et al. 2017) has interestingly evaluated the negative correlation between the expression of

miR146a and LIN52 in different clinicopathological parameters of gastric cancer, a malignancy which affects the gastrointestinal system. Therefore, miR146a mediated LIN52 inhibition is associated with improved treatment efficiency and high chemotherapeutic sensitivity in patients with gastric cancer (Luo et al. 2017). Also, it was observed that in comparison to normal non-cancerous tissue, LIN52 was distributed predominantly in the cytoplasm of advanced gastric cancer tissues (Luo et al. 2017). Inhibition of LIN52 expression in Gastrointestinal stromal tumours (GIST) has been demonstrated to be involved in tumour suppression due to imatinib-induced apoptosis (Boichuk et al. 2013).

Poor efficiency is observed for several chemotherapeutic drugs against tumour cells which are in G0 phase of cell cycle suggesting this may be one of the major reasons for resistance to chemotherapeutic drugs (Shah and Schwartz 2001). This explains the possible mechanism behind the improved chemotherapeutic sensitivity observed in advanced gastric cancer patients where high levels of miR146a driven LIN52 inhibition decreases the number of cells in G0 phase as low levels of LIN52 prevent DREAM assembly thereby reducing the number of cells in G0 resting phase (Luo et al. 2017).

None of the MuvB components apart from LIN52 exhibited strong senescence bypass activity upon ectopic expression nor did they affect the activity of the MMB-FOXM1 reconstituted complex when they were absent when assayed in $CL3^{EcoR}$ cells. LIN37 was the only MuvB component found to be upregulated (Figure 4.2) in senescent cells suggesting a role in cell cycle growth arrest. This is in accordance with a recent study (Mages et al. 2017) where knockout of LIN37 led to complete loss of DREAM repressor function whereas activation of cell cycle gene expression was not affected, as mouse myoblasts or fibroblasts continued to proliferate normally. Thus, demonstrating a role for LIN37 as an essential factor for DREAM repressor functions but dispensable for the activating MuvB related activator functions (Fischer and Müller 2017; Mages et al. 2017). Unlike LIN9, LIN52 and LIN54 which play a crucial role in both repressor and activator functions of the MuvB complex, LIN37 is important only for the repressor functions.

To enable simultaneous expression of the three key TFs, LIN52, B-MYB, and FOXM1, different multi-cistronic constructs were prepared using 2A-peptides that allow expression of multiple genes from same mRNA (Szymczak et al. 2004; Kim et al. 2011a). The results obtained were very encouraging as all the bi-cistronic and the multi-cistronic constructs worked very efficiently in our system of $CL3^{EcoR}$ cells and exhibited a very strong bypass potential. These multi-cistronic constructs will be highly relevant for studying the role of these TFs in primary human cells which are not as highly infectable as the immortalized $CL3^{EcoR}$ cells.

As the multi-cistronic constructs worked very efficiently, to detect any differences that might exist between LIN52, B-MYB and FOXM1, the bypass assay was conducted under very stringent conditions in addition to lowering the bypass potential by two following approaches. In the first approach, the amount of expression construct was reduced prior to lentiviral packaging whereas, in the second approach, stably transduced cells obtained after puromycin selection were mixed with non-transduced cells. On comparing the results obtained from both the approaches, it was found that the second classical approach produced a consistent gradual decrease in bypass potential as opposed to the dilution at DNA level which produced inconsistent results. This might be due to the different size of the constructs being tested. Constructs with large inserts tend to generate lower viral titres in comparison to those with smaller inserts.

Comparison of the extent of senescence bypass observed after silencing $p21^{WAF1}$ and RELA and ectopic expression of the reconstituted MMB-FOXM1 complex, shown in Figure 6.1, indicated that silencing of $p21^{WAF1}$ was the most efficient. It would have been interesting to check the percent rescue obtained by $p21^{WAF1}$ for which cells would have needed to be plated more sparsely to obtain countable colonies. The rescue obtained by $p21^{WAF1}$ is a lot higher than B-MYB which is rescuing of the order of 1/1000. It is important to understand what happens with the remaining 999/1000. One possibility might be the small fraction of rescued cells already possess some further required genetic change before the addition of B-MYB. Furthermore, reconstitution of the MMB-FOXM1 complex was more active at bypassing senescence than silencing RELA and therefore

inactivation of the canonical NF-κB signalling pathway. It suggested that silencing $p21^{WAF1}$ must be affecting other pathways in addition to RELA mediated NFκB signalling and MMB-FOXM1 related DREAM pathway.

Also, examination of the results obtained from experiments indicated that there was a lot of experimental variation. This variability is mainly due to the variation from individual experiment to experiment arising from different batches of cells, virus titre and fluctuations in the incubator temperature. This was also the cause of the high error bars for the quantitative analysis because there was variation between independent experiments rather than within an experiment. Results within experiments were reproducible.

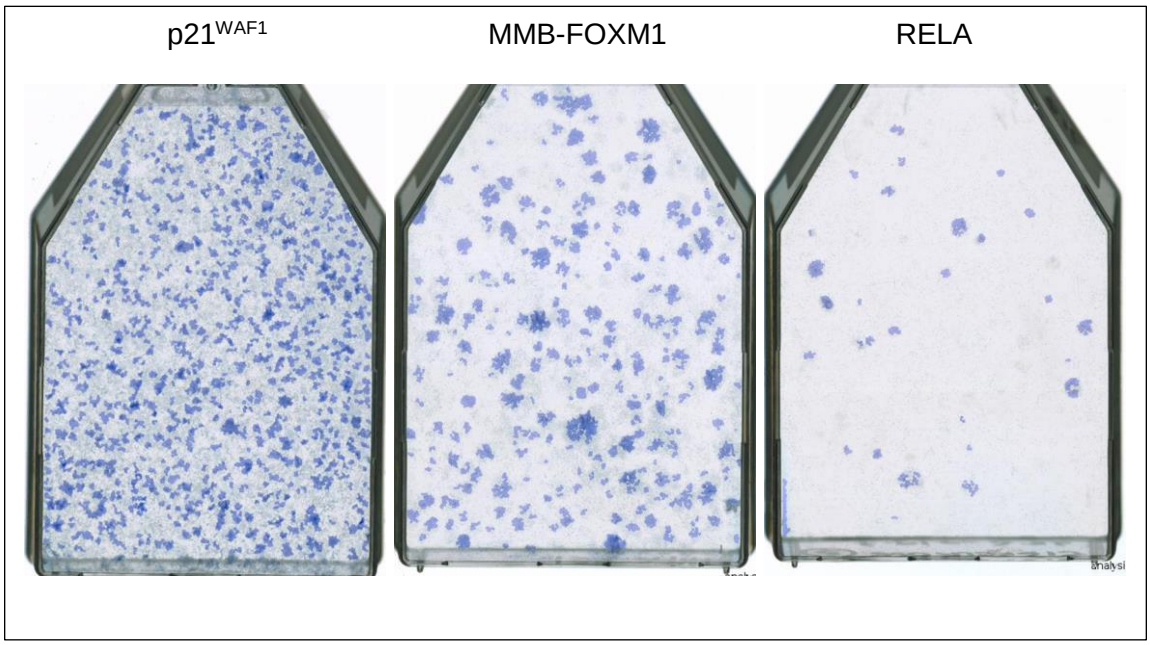

Figure 6.1 Comparison of bypass potential after silencing $p21^{WAF1}$ and RELA and ectopically expressing MMB-FOXM1 complex

6.1.3 Analysis of the bypass potential of different TFs after simultaneous modulation of expression

It was found that many TFs from the identified list did not show bypass potential when studied on their own. FOXM1, for example, did not show strong bypass when studied alone whereas it was a very important component of the MMB-FOXM1 complex. Reconstructing MMB-FOXM1 exhibited strong bypass potential and showed that a complex can work better than single factors. Therefore, it was decided to undertake an experiment wherein multiple different

TFs were pooled together as TFs may not work or work poorly when alone but may work in combination.

The question was: Is it feasible to pool a large number of factors together? Previously this was considered impossible. Takahashi and Yamanaka set the precedent by demonstrating that this can be done. They showed that it was possible to pool 24 factors together to convert somatic cells to induced pluripotent stem cells. Then they were able to leave one factor out at a time until they identified a combination of four factors which can reprogram somatic cells into induced pluripotent stem cells, one of the biggest advances in the field. Their study suggested using constitutively active factors wherever possible and also high titre viruses as high efficiency is required to ensure multiple hits which cannot be easily achieved by transfection (Takahashi and Yamanaka 2006). Their strategy relied on the requirement for multiple simultaneous infection events which can be readily achieved by using lentiviruses.

Hence, the aim was to pool together the 73 transcription factors comprising ectopic expression constructs for the downregulated TFs, shRNAmiRs for the upregulated TFs and shRNAmiRs for RELA, RELB and CEBPβ. There was a clear requirement for high stringency for this experiment to minimise the background as it was not possible to know how efficiently the pool (73) would work. It may work poorly and therefore the use of correct controls was absolutely critical to be able to discern a positive result above background even if the efficiency was low.

As many of the factors were constructs prepared in pLX301 by gateway recombination cloning, the control we used initially was a pool comprising 70 µg pLX301 with 1 µg each of LIN52, FOXM1 and B-MYB, as these factors were present within the pool of 73 factors. Since we know that both LIN52 and B-MYB exhibit senescence bypass on their own and combine with FOXM1 to reconstitute the MMB-FOXM1 complex, it was important that our pool of 73 factors should bypass more efficiently than the ‘Pool Control’. Moreover, as we thought that this was likely to be very inefficient, ten independent biological replicates for the pool (73) were prepared. The results obtained are shown in Figure 6.2. We were very surprised to find that all five replicates of the

experiment worked very efficiently; a lot of growing colonies of cells were obtained. In contrast, the pLX301 vector alone yielded no colonies, so none of the growing colonies were due to the background. However, the ‘Pool control' containing the 1 µg of LIN52, B-MYB and FOXM1 also produced lots of growing colonies which were only slightly reduced in number compared to the Pool (73). This was very discouraging and suggested that perhaps most of the bypass observed in the experimental pool was due to the presence of LIN52, B-MYB and FOXM1.

However, while undertaking further bypass experiments with the multi-cistronic constructs prepared in the pLEX-MCS lentiviral vector and undertaking controls the pLX301 and pLEX-MCS vectors side by side, it was observed that puromycin resistant cells obtained after transduction with pLX301 grew very slowly in comparison to those with pLEX-MCS. The pLEX-MCS cultures were ready to be reseeded within 4-5 days maximum whereas the pLX301 cultures required at least ten days.

Since LIN52 and FOXM1 had been cloned into pLEX-MCS, we hypothesised that in the pool of these factors with pLX301, it was likely that cells that had been transduced with LIN52, FOXM1 and B-MYB were likely to be overrepresented in comparison to cells that only contained pLX301 as cells derived with pLEX-MCS vector grow more rapidly. This could easily explain the high number of growing colonies obtained with the ‘Pool Control’ in Figure 6.2.

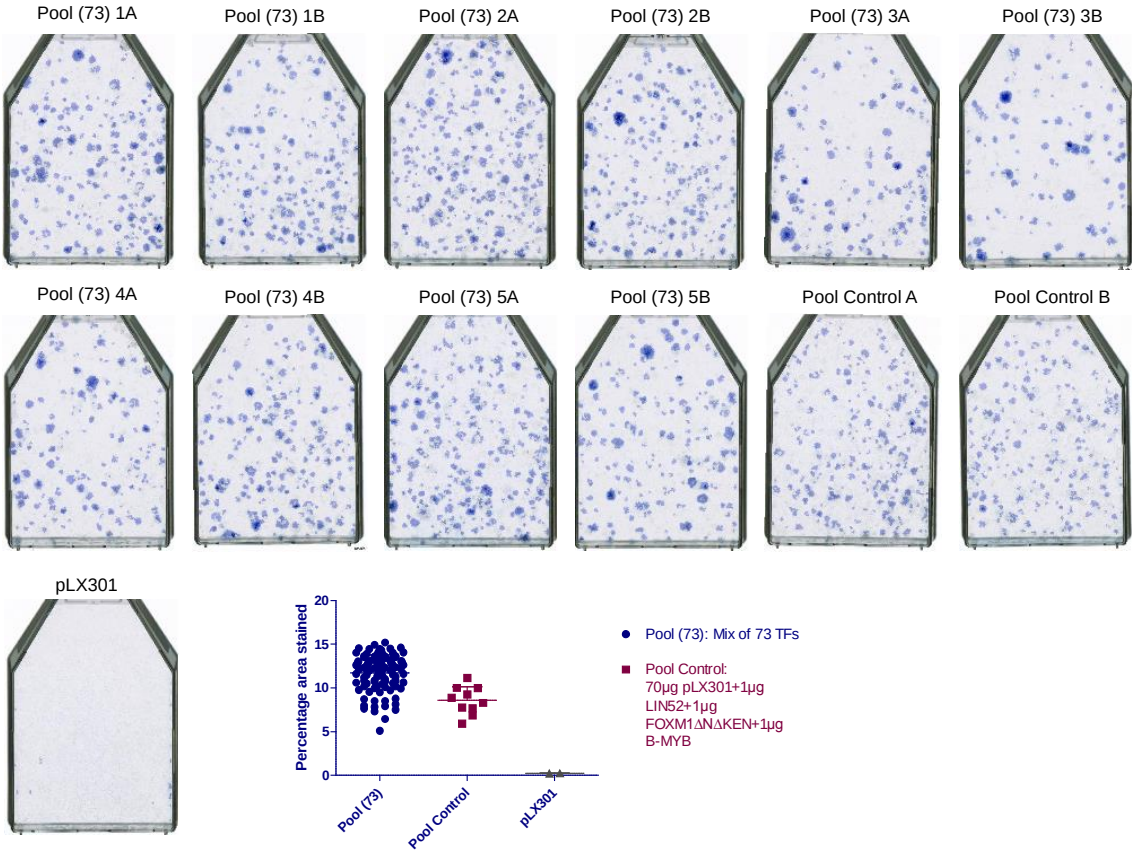

Figure 6.2 Comparison of bypass activity of Pool (73) to the bypass of Pool control reconstituted with the pLX301 vector.
The bypass assay was performed under stringent conditions at a large scale with ten technical replicates for each infection. The pool control was reconstituted with the pLX301 vector. Empty pLX301 vector was used as a negative control.

Therefore, we compared the 'Pool Control' prepared using pLX301 and pLEX-MCS and found that there was a significant difference in the number of growing colonies obtained. The bypass potential of Pool Control reconstituted with pLX301 was significantly higher than pLEX-MCS Pool Control, as shown in Figure 6.3. The empty vector did not exhibit any strong bypass potential when studied on its own (Figure 6.3). This highlighted the utmost importance of using the correct controls in an experiment.

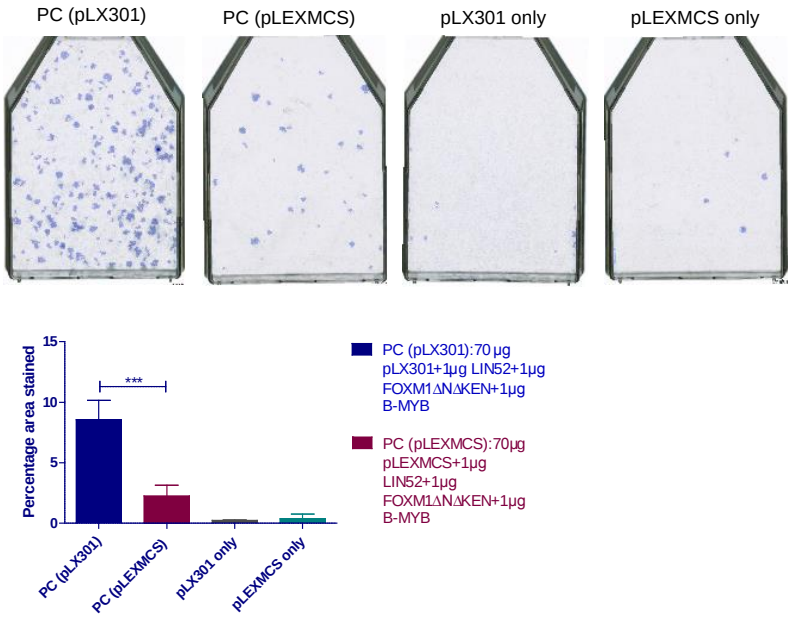

Figure 6.3 Comparison of the bypass activity of Pool Control reconstituted with pLX301 and pLEX-MCS.
Bypass assay was conducted under stringent conditions. Bypass activity of both the empty vector i.e. pLX301 and pLEX-MCS is shown.

When the 73 TF pool experiment was repeated using the pLEX-MCS vector pool control, the results obtained were very encouraging. It showed that the pool of 73 TFs exhibited a significantly higher bypass potential than the 'Pool Control' shown in Figure 5.2 both qualitatively and quantitatively. Although Yamanaka and colleagues identified the critical factors for generating iPS cells by simply leaving out one factor at a time, we hypothesised that if a factor was important for senescence bypass, it should be enriched in cells in which senescence has been bypassed. Therefore, deep sequencing was undertaken in genomic DNA extracted from multiple independent pools of cells derived from three bypass experiments, looking for factors that were enriched. This identified 23 factors that showed some enrichment after senescence bypass in cells infected with pool of 73 TFs.

Due to time limitations, a pool of these 23 factors was prepared and shown to be able to bypass senescence. Although we had hypothesised that this pool should be more efficient at bypassing senescence than the pool of 73 TFs, this was not found to be the case. Unfortunately, due to the lack of time, it was not possible to resolve why there was no increase in efficiency and which of these 23 factors

are crucial for the senescence bypass. It is, of course, possible that factors may work by a hit and run mechanism and may not be enriched. Therefore, it may be necessary to go back to 73 factors and leave out the 50 factors that were not enriched one at a time to identify if there is a factor which acts in this way.

Experiments involving Pool 73 and Pool 23 TFs but lacking B-MYB and LIN52 should also be looked at. Alternative experiments should also be designed and conducted where lentiviruses for these known active components are mixed in as opposed to co-packaged, again to mitigate the risk that these active components are present at differential titres in control and test infections.

6.2 Future directions

Based on the exciting results obtained from the reconstruction experiments conducted to study the effect of MMB-FOXM1 complex or upon combining all the prioritized TFs, this study has thrown up many questions in need of further investigation.

As shown in Figure 6.1, silencing $p21^{WAF1}$ bypasses senescence very efficiently whereas none of the TFs tested so far individually, as part of the MMB–FOXM1 complex or as multi-cistronic constructs have shown equivalent bypass potential. Even though reconstituting the MMB-FOXM1 complex exhibited strong bypass potential, the extent of the bypass was still not comparable to the level of bypass obtained after silencing $p21^{WAF1}$. This suggests that $p21^{WAF1}$ silencing involves other pathways in addition to the DREAM and NF-κB signalling pathways. Since the TF list was put together using expression profiling data from cells in which senescence had been bypassed by $p21^{WAF1}$ silencing, there is the possibility that the additional pathways may involve TFs that are components of our list of 73 critical TFs. Experiments should be conducted to study if the bypass potential of Pool (73) is affected after removing B-MYB, FOXM1ΔNΔKEN, and LIN52. Similarly, bypass of Pool (23) should be assessed after removal of B-MYB and LIN52. Future experiments should be conducted to refine the 23 TFs to develop a cocktail of TFs that can bypass senescence efficiently and study if it is as effective as silencing $p21^{WAF1}$. If not, investigate what is missing? To undertake

this, it may be necessary to go back to the list of TFs to identify any that act by a 'hit and run mechanism'.

Another important experiment which needs to be done is to measure the proliferative potential and the growth characteristics of cells which have bypassed senescence as we have not examined the biology and/or the biochemistry of these rescued cells. As the main focus in this study relied upon looking at the functional aspects of the role played by different TFs in the senescence bypass assay, it is highly relevant to confirm the findings at multiple levels such as an in-depth biochemical analysis. It will be important to demonstrate at the RNA and/or protein level that the bypass of senescence is associated with silencing or ectopic expression of up-regulated and down-regulated TFs respectively. Since expression at the level of RNA does not always correlate with protein levels, expression at the protein level can be determined by western blotting, if suitable antibodies are available commercially or from another source.

Very importantly, it is essential to establish and reproduce the findings from the current model system of conditionally immortal $CL3^{EcoR}$ cells that was developed to facilitate studies on senescence in a range of other cellular senescence systems including primary human fibroblasts such as BJ, WI-38, IMR90 cells or adult mammary fibroblasts. We will also aim to determine if the key TFs play a similar role in replicative senescence in primary human fibroblasts. These studies will enable us to refine our list of candidate TFs to those that are differentially expressed both, upon the cell, and replicative senescence. The stably transduced human fibroblasts will be serially cultivated to determine if they are immortal. Since this will involve serial passaging for many generations taking many months, the cells can also be challenged with activated Ras since expression of an activated oncogene results in premature senescence due to a DNA damage response if the cells are not immortal. Cells derived with hTERT alone undergo premature senescence upon challenge with an activated Ras oncogene. This will enable a better understanding of the genes and their function in different physiological contexts.

It will be important to assay the cocktail of TFs directly in primary human cells to determine if they are able to immortalise them. Also, check if our factors work in other human cells such as epithelial cells or neural cells or are they fibroblast specific. Also, important to assay MMB-FOXM1 complex in these other primary cells to see if they can immortalise and if they bypass other forms of senescence.

$CL3^{EcoR}$ cells are highly infectable which enabled the reconstruction experiments to work very efficiently. Primary cells, on the other hand, will not exhibit a similar level of infectivity and hence expressing different ORFs from a single vector will prove highly beneficial to enable polycistronic expression driven from a single promoter. Hence, the multi-cistronic constructs designed in this study will be highly useful in studying the role MMB-FOXM1 complex and other TFs in primary cells. It may be necessary to prepare multi-cistronic constructs for the TF cocktail.

Expression profiling of RNA extracted from independent cultures of $CL3^{EcoR}$ cells, in which senescence has been bypassed by ectopic expression of constitutively active LIN52, FOXM1 and B-MYB, should be undertaken. As the MMB-FOXM1 complex bypasses senescence very efficiently, cultures of these cells should be established, and RNA should be extracted for expression profiling. The expression data should be analysed to identify genes that are differentially expressed upon senescence arrest but whose expression is reversed upon senescence bypass. If the ectopic expression of constitutively active LIN52, FOXM1 or B-MYB bypasses senescence in IMR90 (with silencing of p53) or BJ fibroblasts, they should also be profiled. The expression profiling data sets should be overlapped to identify common downstream targets of B-MYB, MuvB and FOXM1 in $CL3^{EcoR}$, IMR90 and BJ fibroblasts.

To identify direct downstream targets of these genes, chromatin immunoprecipitation (ChIP) can be performed, in proliferating $CL3^{EcoR}$ fibroblasts as well as primary human IMR90 and BJ fibroblasts. The ChIP-Seq data can be overlapped with the expression profiling data to identify downstream targets of B-MYB, MuvB and FOXM1. These targets should be validated by carrying out ChIP on $CL3^{EcoR}$ cells in which senescence has been bypassed by B-MYB, MuvB or FOXM1 and analysing the immunoprecipitated DNA by q-PCR.

Overlap of the ChIP-Seq data, with the expression profiling data, from both $CL3^{EcoR}$ and human IMR90/BJ fibroblasts, as well as cells in which senescence has been bypassed, followed by ontological analysis, should identify direct targets of B-MYB-MuvB-FOXM1 for further analysis as mediators of senescence bypass by ectopic expression or shRNA silencing. Identification of critical downstream targets of the transcription factor complexes in primary proliferating cells and whether they are the same in cells where senescence has been bypassed should also be looked at. After confirming that changes in expression in $CL3^{EcoR}$ cells are also observed in primary fibroblasts, reciprocal co-immunoprecipitation experiments could be undertaken. These experiments will enable us to determine if B-MYB and FOXM1 are in a complex with MuvB proteins in growing versus senescent cells. More importantly, they will enable us to determine if B-MYB and FOXM1 are present in the same MuvB complex, or in different complexes; and what happens to these complexes upon senescence arrest, both in $CL3^{EcoR}$ and primary (IMR90 and BJ) fibroblasts. It will also be relevant to test if the same complexes are present in cells in which senescence has been bypassed. They will also enable us to determine if DREAM complexes are present and if they change upon senescence arrest. Also, bypass of senescence in IMR90 cells will require silencing of p53 in addition. We can also determine if they can immortalise primary human fibroblasts in conjunction with reconstitution of telomerase activity.

Mostly all the in vitro studies of cellular senescence are performed using a single senescence inducing stimulus such as oncogenes or high dose of radiations whereas within an organism individual cells experience various cellular stresses like mitotic, genotoxic and proteotoxic stresses at the same time. Therefore, our long-term focus should be to examine how combinations of different senescence-inducing stimulus affect the downstream effector pathways and resulting senescent phenotypes. This will enable a better understanding of the multifunctional nature of cellular senescence and provide a clear picture of whether fundamentally different senescence mechanisms underlie the diverse biological roles performed by senescence which are being discovered recently.

6.3 Concluding Remarks

Together this study enabled us to identify 10 upregulated and 74 downregulated TFs that are differentially expressed upon entry into cellular senescence in $CL3^{EcoR}$ cells and has highlighted the causal role played by DREAM complex and associated (MMB-FOXM1) complex in senescence. One of the most significant findings to emerge from this study is that it very clearly illustrated the role of components of the DREAM complex and associated components in bypassing senescence. Reconstitution of MMB-FOXM1 complex demonstrated that it can bypass senescence under very stringent conditions and that LIN52, FOXM1 and B-MYB were the crucial components. Furthermore, this required non-phosphorylated LIN52, suggesting a role for phosphorylated LIN52 and the DREAM complex in inducing senescence. This study has gone some way towards enhancing our understanding of the role of DREAM complex and associated components in senescence as very little is known about the role of DREAM complex in senescence. Much is known about the importance of DREAM complex in quiescence and its role in repressing cell cycle-dependent gene expression. Additional reconstitution experiments wherein all the prioritized TFs were combined, revealed the presence of synergy amongst the TFs implying the presence of other potential pathways for regulating senescence; these remain to be identified and studied further.

Chapter 7 Bibliography

Abbas T, Dutta A. 2009. P21 in cancer: Intricate networks and multiple activities. *Nat Rev Cancer* **9**: 400–414.

Ablasser A, Goldeck M, Cavlar T, Deimling T, Witte G, Röhl I, Hopfner KP, Ludwig J, Hornung V. 2013. CGAS produces a 2′-5′-linked cyclic dinucleotide second messenger that activates STING. *Nature* **498**: 380–384.

Ablasser A, Gulen MF. 2016. The role of cGAS in innate immunity and beyond. *J Mol Med* **94**: 1085–1093.

Acosta JC, Banito A, Wuestefeld T, Georgilis A, Janich P, Morton JP, Athineos D, Kang TW, Lasitschka F, Andrulis M, et al. 2013. A complex secretory program orchestrated by the inflammasome controls paracrine senescence. *Nat Cell Biol* **15**: 978–990.

Acosta JC, O'Loghlen A, Banito A, Guijarro M V., Augert A, Raguz S, Fumagalli M, Da Costa M, Brown C, Popov N, et al. 2008. Chemokine Signaling via the CXCR2 Receptor Reinforces Senescence. *Cell* **133**: 1006–1018.

Adams PD. 2009. Healing and Hurting: Molecular Mechanisms, Functions, and Pathologies of Cellular Senescence. *Mol Cell* **36**: 2–14.

Adams PD, Ivanov A, Pawlikowski J, Manoharan I, Tuyn J Van, Nelson DM, Singh Rai T, Shah PP, Hewitt G, Korolchuk VI, et al. 2013. Lysosome-mediated processing of chromatin in senescence. *J Cell Biol* **202**: 129–143.

Adler AS, Sinha S, Kawahara TLA, Zhang JY, Segal E, Chang HY. 2007. Motif module map reveals enforcement of aging by continual NF-κB activity. *Genes Dev* **21**: 3244–3257.

Aggarwal A, Hunter WJ, Aggarwal H, Silva ED, Davey MS, Murphy RF, Agrawal DK. 2010. Expression of leukemia/lymphoma-related factor (LRF/POKEMON) in human breast carcinoma and other cancers. *Exp Mol Pathol* **89**: 140–148.

Ahmad T, Sundar IK, Lerner CA, Gerloff J, Tormos AM, Yao H, Rahman I. 2015. Impaired mitophagy leads to cigarette smoke stress-induced cellular senescence: Implications for chronic obstructive pulmonary disease. *FASEB J* **29**: 2912–2929.

Aird KM, Zhang R. 2014. Metabolic alterations accompanying oncogene-induced senescence. *Mol Cell Oncol* **1**: e963481.

Ali SH, DeCaprio JA. 2001. Cellular transformation by SV40 large T antigen: Interaction with host proteins. *Semin Cancer Biol* **11**: 15–22.

Allavena P, Sica A, Solinas G, Porta C, Mantovani A. 2008. The inflammatory micro-environment in tumor progression: The role of tumor-associated macrophages. *Crit Rev Oncol Hematol* **66**: 1–9.

Althubiti M, Lezina L, Carrera S, Jukes-Jones R, Giblett SM, Antonov A, Barlev N, Saldanha GS, Pritchard CA, Cain K, et al. 2014. Characterization of novel markers of senescence and their prognostic potential in cancer. *Cell Death Dis* **5**: e1528–e1528.

Aravinthan A. 2015. Cellular senescence: a hitchhiker's guide. *Hum Cell* **28**: 51–64.

Ayrapetov MK, Gursoy-Yuzugullu O, Xu C, Xu Y, Price BD. 2014. DNA double-strand breaks promote methylation of histone H3 on lysine 9 and transient formation of repressive chromatin. *Proc Natl Acad Sci* **111**: 9169–9174.

Baker DJ, Childs BG, Durik M, Wijers ME, Sieben CJ, Zhong J, A. Saltness R, Jeganathan KB, Verzosa GC, Pezeshki A, et al. 2016. Naturally occurring p16 Ink4a-positive cells shorten healthy lifespan. *Nature* **530**: 184–189.

Baker DJ, Wijshake T, Tchkonia T, Lebrasseur NK, Childs BG, Van De Sluis B, Kirkland JL, Van Deursen JM. 2011. Clearance of p16 Ink4a-positive senescent cells delays ageing-associated disorders. *Nature* **479**: 232–236.

Bandyopadhyay D, Okan NA, Bales E, Nascimento L, Cole PA, Medrano EE. 2002. Down-regulation of p300/CBP histone acetyltransferase activates a senescence checkpoint in

human melanocytes. *Cancer Res* **62**: 6231–6239.

Barascu A, Le Chalony C, Pennarun G, Genet D, Imam N, Lopez B, Bertrand P. 2012. Oxidative stress induces an ATM-independent senescence pathway through p38 MAPK-mediated lamin B1 accumulation. *EMBO J* **31**: 1080–1094.

Barber GN. 2015. STING: infection, inflammation and cancer. *Nat Publ Gr* **15**: 760–770.

Ben-Porath I, Weinberg RA. 2005. The signals and pathways activating cellular senescence. *Int J Biochem Cell Biol* **37**: 961–976.

Bennett DC. 2016. Genetics of melanoma progression: The rise and fall of cell senescence. *Pigment Cell Melanoma Res* **29**: 122–140.

Bent EH, Gilbert LA, Hemann MT. 2016. A senescence secretory switch mediated by PI3K/AKT/mTOR activation controls chemoprotective endothelial secretory responses. *Genes Dev* **30**: 1811–1821.

Birmingham A, Anderson EM, Reynolds A, Ilsley-Tyree D, Leake D, Fedorov Y, Baskerville S, Maksimova E, Robinson K, Karpilow J, et al. 2006. 3' UTR seed matches, but not overall identity, are associated with RNAi off-targets. *Nat Methods* **3**: 199–204.

Blagosklonny M V. 2013. Aging is not programmed: Genetic pseudo-program is a shadow of developmental growth. *Cell Cycle* **12**: 3736–3742.

Blagosklonny M V. 2012. Cell cycle arrest is not yet senescence, which is not just cell cycle arrest: Terminology for TOR-driven aging. *Aging (Albany NY)* **4**: 159–165.

Blagosklonny M V. 2003. Cell senescence and hypermitogenic arrest. *EMBO Rep* **4**: 358–362.

Bodnar AG, Ouellette M, Frolkis M, Holt SE, Chiu CP, Morin GB, Harley CB, Shay JW, Lichtsteiner S, Wright WE. 1998. Extension of life-span by introduction of telomerase into normal human cells. *Science (80-)* **279**: 349–352.

Boichuk S, Parry JA, Makielski KR, Litovchick L, Baron JL, Zewe JP, Wozniak A, Mehalek KR, Korzeniewski N, Seneviratne DS, et al. 2013. The DREAM complex mediates GIST cell quiescence and is a novel therapeutic target to enhance imatinib-induced apoptosis. *Cancer Res* **73**: 5120–5129.

Booth LN, Brunet A. 2016. The Aging Epigenome. *Mol Cell* **62**: 728–744.

Bracken AP, Kleine-Kohlbrecher D, Dietrich N, Pasini D, Gargiulo G, Beekman C, Theilgaard-Mönch K, Minucci S, Porse BT, Marine JC, et al. 2007. The Polycomb group proteins bind throughout the INK4A-ARF locus and are disassociated in senescent cells. *Genes Dev* **21**: 525–530.

Burd CE, Sorrentino JA, Clark KS, Darr DB, Krishnamurthy J, Deal AM, Bardeesy N, Castrillon DH, Beach DH, Sharpless NE. 2013. Monitoring tumorigenesis and senescence in vivo with a p16 INK4a-luciferase model. *Cell* **152**: 340–351.

Bustamante CD, Fledel-Alon A, Williamson S, Nielsen R, Hubisz MT, Glanowski S, Tanenbaum DM, White TJ, Sninsky JJ, Hernandez RD, et al. 2005. Natural selection on protein-coding genes in the human genome. *Nature* **437**: 1153–1157.

Campisi J. 2013. Aging, Cellular Senescence, and Cancer. *Annu Rev Physiol* **75**: 685–705.

Campisi J. 2003. Cancer and ageing: Rival demons? *Nat Rev Cancer* **3**: 339–349.

Campisi J. 2001. Cellular senescence as a tumor-suppressor mechanism. *Trends Cell Biol* **11**.

Campisi J. 2005. Senescent cells, tumor suppression, and organismal aging: Good citizens, bad neighbors. *Cell* **120**: 513–522.

Campisi J, Andersen JK, Kapahi P, Melov S. 2011. Cellular senescence: A link between cancer and age-related degenerative disease? *Semin Cancer Biol* **21**: 354–359.

Campisi J, D'Adda Di Fagagna F. 2007. Cellular senescence: When bad things happen to good cells. *Nat Rev Mol Cell Biol* **8**: 729–740.

Carrel A, Ebeling AH. 1921. Age and Multiplication of Fibroblasts. *J Exp Med* **34**: 599–623.

Chang B-D, Swift ME, Shen M, Fang J, Broude E V, Roninson IB. 2002. Molecular determinants of terminal growth arrest induced in tumor cells by a chemotherapeutic agent. *Proc Natl Acad Sci U S A* **99**: 389–94.

Charrasse S, Carena I, Brondani V, Klempnauer KH, Ferrari S. 2000. Degradation of B-Myb by ubiquitin-mediated proteolysis: Involvement of the CdC34-SCF(p45Skp2) pathway. *Oncogene* **19**: 2986–2995.

Chau BN, Wang JYJ. 2003. Coordinated regulation of life and death by RB. *Nat Rev Cancer* **3**: 130–138.

Chehab NH, Malikzay A, Stavridi ES, Halazonetis TD. 1999. Phosphorylation of Ser-20 mediates stabilization of human p53 in response to DNA damage. *Proc Natl Acad Sci U S A* **96**: 13777–82.

Chen H, Ruiz PD, McKimpson WM, Novikov L, Kitsis RN, Gamble MJ. 2015. MacroH2A1 and ATM Play Opposing Roles in Paracrine Senescence and the Senescence-Associated Secretory Phenotype. *Mol Cell* **59**: 719–731.

Chen J, Saha P, Kornbluth S, Dynlacht BD, Dutta A. 1996. Cyclin-binding motifs are essential for the function of p21CIP1. *Mol Cell Biol* **16**: 4673–4682.

Chen Q, Sun L, Chen ZJ. 2016. Regulation and function of the cGAS-STING pathway of cytosolic DNA sensing. *Nat Immunol* **17**: 1142–1149.

Chen X, Muller GA, Quaas M, Fischer M, Han N, Stutchbury B, Sharrocks AD, Engeland K. 2013. The Forkhead Transcription Factor FOXM1 Controls Cell Cycle-Dependent Gene Expression through an Atypical Chromatin Binding Mechanism. *Mol Cell Biol* **33**: 227–236.

Chen X, Zhang W, Gao YF, Su XQ, Zhai ZH. 2002. Senescence-like changes induced by expression of p21(waf1/Cip1) in NIH3T3 cell line. *Cell Res* **12**: 229–233.

Chen Z, Cole PA. 2015. Synthetic approaches to protein phosphorylation. *Curr Opin Chem Biol* **28**: 115–122.

Chen Z, Trotman LC, Shaffer D, Lin HK, Dotan ZA, Niki M, Koutcher JA, Scher HI, Ludwig T, Gerald W, et al. 2005. Crucial role of p53-dependent cellular senescence in suppression of Pten-deficient tumorigenesis. *Nature* **436**: 725–730.

Child ES, Mann DJ. 2006. The intricacies of p21 phosphorylation: Protein/protein interactions, subcellular localization and stability. *Cell Cycle* **5**: 1313–1319.

Childs BG, Baker DJ, Kirkland JL, Campisi J, van Deursen JM. 2014. Senescence and apoptosis: dueling or complementary cell fates? *EMBO Rep* **15**: 1139–1153.

Cho JH, Kim MJ, Kim KJ, Kim JR. 2012. POZ/BTB and AT-hook-containing zinc finger protein 1 (PATZ1) inhibits endothelial cell senescence through a p53 dependent pathway. *Cell Death Differ* **19**: 703–712.

Cho KA, Ryu SJ, Park JS, Jang IS, Ahn JS, Kim KT, Park SC. 2003. Senescent phenotype can be reversed by reduction of caveolin status. *J Biol Chem* **278**: 27789–27795.

Cho KA, Sung JR, Yoon SO, Ji HP, Jung WL, Kim HP, Kyung TK, Ik SJ, Sang CP. 2004. Morphological adjustment of senescent cells by modulating caveolin-1 status. *J Biol Chem* **279**: 42270–42278.

Christensen J, Cloos P, Toftegaard U, Klinkenberg D, Bracken AP, Trinh E, Heeran M, Di Stefano L, Helin K. 2005. Characterization of E2F8, a novel E2F-like cell-cycle regulated repressor of E2F-activated transcription. *Nucleic Acids Res* **33**: 5458–5470.

Chung HY, Cesari M, Anton S, Marzetti E, Giovannini S, Seo AY, Carter C, Yu BP, Leeuwenburgh C. 2009. Molecular inflammation: Underpinnings of aging and age-related diseases. *Ageing Res Rev* **8**: 18–30.

Collado M, Blasco MA, Serrano M. 2007. Cellular Senescence in Cancer and Aging. *Cell* **130**: 223–233.

Collado M, Serrano M. 2010. Senescence in tumours: Evidence from mice and humans. *Nat Rev Cancer* **10**: 51–57.

Cook R, Zoumpoulidou G, Luczynski MT, Rieger S, Moquet J, Spanswick VJ, Hartley JA, Rothkamm K, Huang PH, Mittnacht S. 2015. Direct involvement of retinoblastoma family proteins in DNA repair by non-homologous end-joining. *Cell Rep* **10**: 2007–2019.

Coppé J-P, Desprez P-Y, Krtolica A, Campisi J. 2010a. The Senescence-Associated Secretory Phenotype: The Dark Side of Tumor Suppression. *Annu Rev Pathol Mech Dis* **5**: 99–118.

Coppé J-P, Kauser K, Campisi J, Beauséjour CM. 2006. Secretion of Vascular Endothelial Growth Factor by Primary Human Fibroblasts at Senescence. *J Biol Chem* **281**: 29568–29574.

Coppé JP, Patil CK, Rodier F, Krtolica A, Beauséjour CM, Parrinello S, Hodgson JG, Chin K, Desprez PY, Campisi J. 2010b. A human-like senescence-associated secretory phenotype is conserved in mouse cells dependent on physiological oxygen. *PLoS One* **5**.

Coppé JP, Patil CK, Rodier F, Sun Y, Muñoz DP, Goldstein J, Nelson PS, Desprez PY, Campisi J. 2008. Senescence-associated secretory phenotypes reveal cell-nonautonomous functions of oncogenic RAS and the p53 tumor suppressor. *PLoS Biol* **6**: 2853–68.

Coppé JP, Rodier F, Patil CK, Freund A, Desprez PY, Campisi J. 2011. Tumor suppressor and aging biomarker p16 INK4a induces cellular senescence without the associated inflammatory secretory phenotype. *J Biol Chem* **286**: 36396–36403.

Cormenier J, Martin N, Deslé J, Salazar-Cardozo C, Pourtier A, Abbadie C, Pluquet O. 2018. The ATF6α arm of the Unfolded Protein Response mediates replicative senescence in human fibroblasts through a COX2/prostaglandin E2intracrine pathway. *Mech Ageing Dev* **170**: 82–91.

Correia-Melo C, Marques FD, Anderson R, Hewitt G, Hewitt R, Cole J, Carroll BM, Miwa S, Birch J, Merz A, et al. 2016. Mitochondria are required for pro-ageing features of the senescent phenotype. *EMBO J* **35**: 724–742.

Counter CM, Hahn WC, Wei W, Caddle SD, Beijersbergen RL, Lansdorp PM, Sedivy JM, Weinberg RA. 1998. Dissociation among in vitro telomerase activity, telomere maintenance, and cellular immortalization. *Proc Natl Acad Sci* **95**: 14723–14728.

D'Adda Di Fagagna F. 2008. Living on a break: Cellular senescence as a DNA-damage response. *Nat Rev Cancer* **8**: 512–522.

Dai CY, Enders GH. 2000. p16(INK4a) can initiate an autonomous senescence program. *Oncogene* **19**: 1613–1622.

Dalle Pezze P, Nelson G, Otten EG, Korolchuk VI, Kirkwood TBL, von Zglinicki T, Shanley DP. 2014. Dynamic Modelling of Pathways to Cellular Senescence Reveals Strategies for Targeted Interventions ed. A. Rzhetsky. *PLoS Comput Biol* **10**: e1003728.

Davaapil H, Brockes JP, Yun MH. 2017. Conserved and novel functions of programmed cellular senescence during vertebrate development. *Development* **144**: 106–114.

De Keizer PLJ. 2017. Series: Current Trends in Aging and Age-Related Diseases The Fountain of Youth by Targeting Senescent Cells? *Trends Mol Med* **23**: 6–17.

De Lange T. 2010. How shelterin solves the telomere end-protection problem. *Cold Spring Harb Symp Quant Biol* **75**: 167–177.

Deas E, Wood NW, Plun-Favreau H. 2011. Mitophagy and Parkinson's disease: The PINK1-parkin link. *Biochim Biophys Acta - Mol Cell Res* **1813**: 623–633.

Demaria M, O'Leary MN, Chang J, Shao L, Liu S, Alimirah F, Koenig K, Le C, Mitin N, Deal AM, et al. 2017. Cellular senescence promotes adverse effects of chemotherapy and cancer relapse. *Cancer Discov* **7**: 165–176.

Demaria M, Ohtani N, Youssef SA, Rodier F, Toussaint W, Mitchell JR, Laberge RM, Vijg J, VanSteeg H, Dollé MET, et al. 2014. An essential role for senescent cells in optimal wound healing through secretion of PDGF-AA. *Dev Cell* **31**: 722–733.

Di Leonardo A, Linke SP, Clarkin K, Wahl GM. 1994. DNA damage triggers a prolonged p53-dependent G1arrest and long-term induction of Cip1 in normal human fibroblasts. *Genes Dev* **8**: 2540–2551.

Di Micco R, Fumagalli M, Cicalese A, Piccinin S, Gasparini P, Luise C, Schurra C, Garré M, Giovanni Nuciforo P, Bensimon A, et al. 2006. Oncogene-induced senescence is a DNA damage response triggered by DNA hyper-replication. *Nature* **444**: 638–642.

Di Stefano L, Jensen MR, Helin K. 2003. E2F7, a novel E2F featuring DP-independent repression of a subset of E2F-regulated genes. *EMBO J* **22**: 6289–6298.

Dimri GP, Lee X, Basile G, Acosta M, Scott G, Roskelley C, Medrano EE, Linskens M, Rubelj I, Pereira-Smith O. 1995. A biomarker that identifies senescent human cells in culture and in aging skin in vivo. *Proc Natl Acad Sci U S A* **92**: 9363–7.

Diner EJ, Burdette DL, Wilson SC, Monroe KM, Kellenberger CA, Hyodo M, Hayakawa Y, Hammond MC, Vance RE. 2013. The Innate Immune DNA Sensor cGAS Produces a Noncanonical Cyclic Dinucleotide that Activates Human STING. *Cell Rep* **3**: 1355–1361.

Dou Z, Ghosh K, Vizioli MG, Zhu J, Sen P, Wangensteen KJ, Simithy J, Lan Y, Lin Y, Zhou Z, et al. 2017. Cytoplasmic chromatin triggers inflammation in senescence and cancer. *Nature* **550**.

Draetta G, Brizuela L, Potashkin J, Beach D. 1987. Identification of p34 and p13, human homologs of the cell cycle regulators of fission yeast encoded by cdc2+ and suc1+. *Cell* **50**: 319–325.

Dreesen O, Chojnowski A, Ong PF, Zhao TY, Common JE, Lunny D, Lane EB, Lee SJ, Vardy LA, Stewart CL, et al. 2013. Lamin B1 fluctuations have differential effects on cellular proliferation and senescence. *J Cell Biol* **200**: 605–617.

Druelle C, Drullion C, Desle J, Martin N, Saas L, Cormenier J, Malaquin N, Huot L, Slomianny C, Bouali F, et al. 2016. ATF6a regulates morphological changes associated with senescence in human fibroblasts. *Oncotarget* **7**: 67699–67715.

Drummond-Barbosa D. 2008. Stem cells, their niches and the systemic environment: An aging network. *Genetics* **180**: 1787–1797.

Dyson N. 1998. The regulation of E2F by pRB-family proteins. *Genes Dev* **12**: 2245–2262.

Dyson N, Howley P, Munger K, Harlow E. 1989. The human papilloma virus-16 E7 oncoprotein is able to bind to the retinoblastoma gene product. *Science (80-)* **243**: 934–937.

Dyson NJ. 2016. RB1: A prototype tumor suppressor and an enigma. *Genes Dev* **30**: 1492–1502.

Echeverri CJ, Beachy PA, Baum B, Boutros M, Buchholz F, Chanda SK, Downward J, Ellenberg J, Fraser AG, Hacohen N, et al. 2006. Minimizing the risk of reporting false positives in large-scale RNAi screens. *Nat Methods* **3**: 777–779.

Effenberger T, Von Der Heyde J, Bartsch K, Garbers C, Schulze-Osthoff K, Chalaris A, Murphy G, Rose-John S, Rabe B. 2014. Senescence-associated release of transmembrane proteins involves proteolytic processing by ADAM17 and microvesicle shedding. *FASEB J* **28**: 4847–4856.

El-Deiry WS, Tokino T, Velculescu VE, Levy DB, Parsons R, Trent JM, Lin D, Mercer WE, Kinzler KW, Vogelstein ' B. 1993. WAF1, a Potential Mediator of ~53 Tumor Suppression. *Cell* **75**: 817–825.

Engeland K. 2017. Cell cycle arrest through indirect transcriptional repression by p53: I have a DREAM. *Cell Death Differ* **25**: 114–132.

Evangelou K, Lougiakis N, Rizou S V., Kotsinas A, Kletsas D, Muñoz-Espín D, Kastrinakis NG, Pouli N, Marakos P, Townsend P, et al. 2017. Robust, universal biomarker assay to detect senescent cells in biological specimens. *Aging Cell* **16**: 192–197.

Evans T, Rosenthal ET, Youngblom J, Distel D, Hunt T. 1983. Cyclin: A protein specified by maternal mRNA in sea urchin eggs that is destroyed at each cleavage division. *Cell* **33**: 389–396.

Ferguson EL, Sternberg PW, Horvitz HR. 1987. A genetic pathway for the specification of the vulval cell lineages of Caenorhabditis elegans. *Nature* **326**: 259–267.

Fischer M, Müller GA. 2017. Cell cycle transcription control: DREAM/MuvB and RB-E2F

complexes. *Crit Rev Biochem Mol Biol* **52**: 638–662.

Fischer M, Steiner L, Engeland K. 2014. The transcription factor p53: Not a repressor, solely an activator. *Cell Cycle* **13**: 3037–3058.

Franceschi C, Campisi J. 2014. Chronic inflammation (Inflammaging) and its potential contribution to age-associated diseases. *Journals Gerontol - Ser A Biol Sci Med Sci* **69**: S4–S9.

Franceschi C, Capri M, Monti D, Giunta S, Olivieri F, Sevini F, Panourgia MP, Invidia L, Celani L, Scurti M, et al. 2007. Inflammaging and anti-inflammaging: A systemic perspective on aging and longevity emerged from studies in humans. *Mech Ageing Dev* **128**: 92–105.

Frescas D, Roux CM, Aygun-Sunar S, Gleiberman AS, Krasnov P, Kurnasov O V., Strom E, Virtuoso LP, Wrobel M, Osterman AL, et al. 2017. Senescent cells expose and secrete an oxidized form of membrane-bound vimentin as revealed by a natural polyreactive antibody. *Proc Natl Acad Sci* **114**: E1668–E1677.

Freund A, Laberge R-M, Demaria M, Campisi J. 2012. Lamin B1 loss is a senescence-associated biomarker ed. T.M. Magin. *Mol Biol Cell* **23**: 2066–2075.

Freund A, Orjalo A V., Desprez PY, Campisi J. 2010. Inflammatory networks during cellular senescence: causes and consequences. *Trends Mol Med* **16**: 238–246.

Fuhrmann-Stroissnigg H, Ling YY, Zhao J, McGowan SJ, Zhu Y, Brooks RW, Grassi D, Gregg SQ, Stripay JL, Dorronsoro A, et al. 2017. Identification of HSP90 inhibitors as a novel class of senolytics. *Nat Commun* **8**.

Fumagalli M, Rossiello F, Clerici M, Barozzi S, Cittaro D, Kaplunov JM, Bucci G, Dobreva M, Matti V, Beausejour CM, et al. 2012. Telomeric DNA damage is irreparable and causes persistent DNA-damage-response activation. *Nat Cell Biol* **14**: 355–365.

Gao P, Ascano M, Wu Y, Barchet W, Gaffney BL, Zillinger T, Serganov AA, Liu Y, Jones RA, Hartmann G, et al. 2013. Cyclic [G(2′,5′)pA(3′,5′)p] is the metazoan second messenger produced by DNA-activated cyclic GMP-AMP synthase. *Cell* **153**: 1094–1107.

García-Prat L, Martínez-Vicente M, Perdiguero E, Ortet L, Rodríguez-Ubreva J, Rebollo E, Ruiz-Bonilla V, Gutarra S, Ballestar E, Serrano AL, et al. 2016. Autophagy maintains stemness by preventing senescence. *Nature* **529**: 37–42.

Gaubatz S, Lindeman GJ, Ishida S, Jakoi L, Nevins JR, Livingston DM, Rempel RE. 2000. E2F4 and E2F5 play an essential role in pocket protein-mediated G1 control. *Mol Cell* **6**: 729–735.

Georgakilas AG, Martin OA, Bonner WM. 2017. p21: A Two-Faced Genome Guardian. *Trends Mol Med* **23**: 310–319.

Georgakopoulou EA, Tsimaratou K, Evangelou K, Fernandez-Marcos PJ, Zoumpourlis V, Trougakos IP, Kletsas D, Bartek J, Serrano M, Gorgoulis VG. 2013. Specific lipofuscin staining as a novel biomarker to detect replicative and stress-induced senescence. A method applicable in cryo-preserved and archival tissues. *Aging (Albany NY)* **5**: 37–50.

Gil J, Peters G. 2006. Regulation of the INK4b-ARF-INK4a tumour suppressor locus: All for one or one for all. *Nat Rev Mol Cell Biol* **7**: 667–677.

Glück S, Guey B, Gulen MF, Wolter K, Kang TW, Schmacke NA, Bridgeman A, Rehwinkel J, Zender L, Ablasser A. 2017. Innate immune sensing of cytosolic chromatin fragments through cGAS promotes senescence. *Nat Cell Biol* **19**: 1061–1070.

Gonzalo S, Kreienkamp R, Askjaer P. 2017. Hutchinson-Gilford Progeria Syndrome: A premature aging disease caused by LMNA gene mutations. *Ageing Res Rev* **33**: 18–29.

Gorgoulis VG, Halazonetis TD. 2010. Oncogene-induced senescence: The bright and dark side of the response. *Curr Opin Cell Biol* **22**: 816–827.

Goshima N, Kawamura Y, Fukumoto A, Miura A, Honma R, Satoh R, Wakamatsu A, Yamamoto JI, Kimura K, Nishikawa T, et al. 2008. Human protein factory for converting the transcriptome into an in vitro-expressed proteome. *Nat Methods* **5**: 1011–1017.

Grivennikov SI, Greten FR, Karin M. 2010. Immunity, Inflammation, and Cancer. *Cell* **140**: 883–899.

Guiley KZ, Liban TJ, Felthousen JG, Ramanan P, Litovchick L, Rubin SM. 2015. Structural mechanisms of DREAM complex assembly and regulation. *Genes Dev* **29**: 961–974.

Gülow K, Bienert D, Haas IG. 2002. BiP is feed-back regulated by control of protein translation efficiency. *J Cell Sci* **115**: 2443–52.

Guney I, Wu S, Sedivy JM. 2006. Reduced c-Myc signaling triggers telomere-independent senescence by regulating Bmi-1 and p16INK4a. *Proc Natl Acad Sci* **103**: 3645–3650.

Hampel B, Malisan F, Niederegger H, Testi R, Jansen-Dürr P. 2004. Differential regulation of apoptotic cell death in senescent human cells. In *Experimental Gerontology*, Vol. 39 of, pp. 1713–1721.

Hampel B, Wagner M, Teis D, Zwerschke W, Huber LA, Jansen-Dürr P. 2005. Apoptosis resistance of senescent human fibroblasts is correlated with the absence of nuclear IGFBP-3. *Aging Cell* **4**: 325–330.

Hanahan D, Weinberg RA. 2011. Leading Edge Review Hallmarks of Cancer: The Next Generation. *Cell*.

Hanks SK. 1987. Homology probing: identification of cDNA clones encoding members of the protein-serine kinase family. *Proc Natl Acad Sci U S A* **84**: 388–392.

Hara E, Smith R, Parry D, Tahara H, Stone S, Peters G. 1996. Regulation of p16CDKN2 expression and its implications for cell immortalization and senescence. *Mol Cell Biol* **16**: 859–867.

Hardy K, Mansfield L, Mackay A, Benvenuti S, Ismail S, Arora P, O'Hare MJ, Jat PS. 2005. Transcriptional networks and cellular senescence in human mammary fibroblasts. *Mol Biol Cell* **16**: 943–53.

Harley CB, Futcher AB, Greider CW. 1990. Telomeres shorten during ageing of human fibroblasts. *Nature* **345**: 458–460.

Harrison MM, Ceol CJ, Lu X, Horvitz HR. 2006. Some C. elegans class B synthetic multivulva proteins encode a conserved LIN-35 Rb-containing complex distinct from a NuRD-like complex. *Proc Natl Acad Sci U S A* **103**: 16782–7.

Harrison MM, Lu X, Horvitz HR. 2007. LIN-61, one of two Caenorhabditis elegans malignant-brain-tumor-repeat- containing proteins, acts with the DRM and NuRD-like protein complexes in vulval development but not in certain other biological processes. *Genetics* **176**: 255–271.

Hartwell LH, Culotti J, Reid B. 1970. Genetic Control of the Cell-Division Cycle in Yeast, I. Detection of Mutants. *Proc Natl Acad Sci* **66**: 352–359.

Hartwell LH, Weinert TA. 1989. Checkpoints : control that ensure the order of cell cycles events. *Science (80-)* **246**: 629–633.

Hayashi MT, Cesare AJ, Rivera T, Karlseder J. 2015. Cell death during crisis is mediated by mitotic telomere deprotection. *Nature* **522**: 492–496.

Hayflick L. 1965. The limited in vitro lifetime of human diploid cell strains. *Exp Cell Res* **37**: 614–636.

Hayflick L. 1974. The Longevity of Cultured Human Cells. *J Am Geriatr Soc* **22**: 1–12.

Hayflick L, Moorhead PS. 1961. The serial cultivation of human diploid cell strains. *Exp Cell Res* **25**: 585–621.

He P, Sun L, Zhu D, Zhang H, Zhang L, Guo Y, Liu S, Zhou J, Xu X, Xie P. 2016. Knock-down of endogenous bornavirus-like nucleoprotein 1 inhibits cell growth and induces apoptosis in human oligodendroglia cells. *Int J Mol Sci* **17**.

He S, Sharpless NE. 2017. Senescence in Health and Disease. *Cell* **169**: 1000–1011.

Helin K. 1998. Regulation of cell proliferation by the E2F transcription factors. *Curr Opin Genet*

Dev **8**: 28–35.

Herbig U, Ferreira M, Condel L, Carey D, Sedivy JM. 2006. Cellular senescence in aging primates. *Science (80-)* **311**: 1257.

Hernandez-Segura A, de Jong T V., Melov S, Guryev V, Campisi J, Demaria M. 2017. Unmasking Transcriptional Heterogeneity in Senescent Cells. *Curr Biol* **27**: 2652–2660.e4.

Hernandez-Segura A, Nehme J, Demaria M. 2018. Hallmarks of Cellular Senescence. *Trends Cell Biol* **28**: 436–453.

Herranz N, Gallage S, Mellone M, Wuestefeld T, Klotz S, Hanley CJ, Raguz S, Acosta JC, Innes AJ, Banito A, et al. 2015. mTOR regulates MAPKAPK2 translation to control the senescence-associated secretory phenotype. *Nat Cell Biol* **17**: 1205–1217.

Hoare M, Ito Y, Kang TW, Weekes MP, Matheson NJ, Patten DA, Shetty S, Parry AJ, Menon S, Salama R, et al. 2016. NOTCH1 mediates a switch between two distinct secretomes during senescence. *Nat Cell Biol* **18**: 979–992.

Horn HF, Vousden KH. 2007. Coping with stress: Multiple ways to activate p53. *Oncogene* **26**: 1306–1316.

Hoshino A, Mita Y, Okawa Y, Ariyoshi M, Iwai-Kanai E, Ueyama T, Ikeda K, Ogata T, Matoba S. 2013. Cytosolic p53 inhibits Parkin-mediated mitophagy and promotes mitochondrial dysfunction in the mouse heart. *Nat Commun* **4**: 2308.

Hu QJ, Dyson N, Harlow E. 1990. The regions of the retinoblastoma protein needed for binding to adenovirus E1A or SV40 large T antigen are common sites for mutations. *EMBO J* **9**: 1147–55.

Huang PH, Cook R, Zoumpoulidou G, Luczynski MT, Mittnacht S. 2016. Retinoblastoma family proteins: New players in DNA repair by non-homologous end-joining. *Mol Cell Oncol* **3**: e1053596.

Huang S, Wang NP, Tseng BY, Lee WH, Lee EH. 1990. Two distinct and frequently mutated regions of retinoblastoma protein are required for binding to SV40 T antigen. *EMBO J* **9**: 1815–1822.

Huang Y, Wu J, Li R, Wang P, Han L, Zhang Z, Tong T. 2011. B-MYB delays cell aging by repressing p16INK4αtranscription. *Cell Mol Life Sci* **68**: 893–901.

Hwang ES, Yoon G, Kang HT. 2009. A comparative analysis of the cell biology of senescence and aging. *Cell Mol Life Sci* **66**: 2503–2524.

Iannello A, Thompson TW, Ardolino M, Lowe SW, Raulet DH. 2013. p53-dependent chemokine production by senescent tumor cells supports NKG2D-dependent tumor elimination by natural killer cells. *J Exp Med* **210**: 2057–2069.

Inomata M, Shimada Y, Hayashi M, Kondo H, Ohno-Iwashita Y. 2006. Detachment-associated changes in lipid rafts of senescent human fibroblasts. *Biochem Biophys Res Commun* **343**: 489–495.

Irwin MS, Kaelin WG. 2001a. P53 Family Update: P73 and P63 Develop Their Own Identities. *Cell Growth Differ* **12**: 337–49.

Irwin MS, Kaelin WG. 2001b. Role of the newer p53 family proteins in malignancy. *Apoptosis* **6**: 17–29.

Ito T, Kohashi K, Yamada Y, Iwasaki T, Maekawa A, Kuda M, Hoshina D, Abe R, Furue M, Oda Y. 2016. Prognostic significance of Forkhead box M1 (FOXM1) expression and antitumor effect of FOXM1 inhibition in melanoma. *J Cancer* **7**: 63–71.

Ito Y, Hoare M, Narita M. 2017. Spatial and Temporal Control of Senescence. *Trends Cell Biol* **27**: 820–832.

Jackson JG, Pereira-Smith OM. 2006. p53 is preferentially recruited to the promoters of growth arrest genes p21 and GADD45 during replicative senescence of normal human fibroblasts. *Cancer Res* **66**: 8356–8360.

Jacobs JL, Kieboom K, Marino S, DePinho RA, Van Lohuizen M. 1999. The oncogene and

Polycombgroup gene bmi-1 regulates cell proliferation and senescence through the ink4a locus. *Nature* **397**: 164–168.

James EL, Michalek RD, Pitiyage GN, De Castro AM, Vignola KS, Jones J, Mohney RP, Karoly ED, Prime SS, Parkinson EK. 2015. Senescent human fibroblasts show increased glycolysis and redox homeostasis with extracellular metabolomes that overlap with those of irreparable DNA damage, aging, and disease. *J Proteome Res* **14**: 1854–1871.

Jascur T, Brickner H, Salles-Passador I, Barbier V, El Khissiin A, Smith B, Fotedar R, Fotedar A. 2005. Regulation of p21WAF1/CIP1stability by WISp39, a Hsp90 binding TPR protein. *Mol Cell* **17**: 237–249.

Jeyapalan JC, Ferreira M, Sedivy JM, Herbig U. 2007. Accumulation of senescent cells in mitotic tissue of aging primates. *Mech Ageing Dev* **128**: 36–44.

Jiang LL, Siu MK, Wong OGW, Tam KF, Lam EWF, Ngan HY, Le XF, Wong ES, Chan HY, Cheung AN. 2010. Overexpression of proto-oncogene FBI-1 activates membrane type 1-matrix metalloproteinase in association with adverse outcome in ovarian cancers. *Mol Cancer* **9**: 318.

Johung K, Goodwin EC, DiMaio D. 2007. Human Papillomavirus E7 Repression in Cervical Carcinoma Cells Initiates a Transcriptional Cascade Driven by the Retinoblastoma Family, Resulting in Senescence. *J Virol* **81**: 2102–2116.

Jun J Il, Lau LF. 2011. Taking aim at the extracellular matrix: CCN proteins as emerging therapeutic targets. *Nat Rev Drug Discov* **10**: 945–963.

Karimian A, Ahmadi Y, Yousefi B. 2016. Multiple functions of p21 in cell cycle, apoptosis and transcriptional regulation after DNA damage. *DNA Repair (Amst)* **42**: 63–71.

Kastenhuber ER, Lowe SW. 2017. Putting p53 in Context. *Cell* **170**: 1062–1078.

Kim I, Rodriguez-Enriquez S, Lemasters JJ. 2007. Selective degradation of mitochondria by mitophagy. *Arch Biochem Biophys* **462**: 245–253.

Kim JH, Lee SR, Li LH, Park HJ, Park JH, Lee KY, Kim MK, Shin BA, Choi SY. 2011a. High cleavage efficiency of a 2A peptide derived from porcine teschovirus-1 in human cell lines, zebrafish and mice. *PLoS One* **6**: e18556.

Kim JS, Kim EJ, Kim HJ, Yang JY, Hwang GS, Kim CW. 2011b. Proteomic and metabolomic analysis of H2O2-induced premature senescent human mesenchymal stem cells. *Exp Gerontol* **46**: 500–510.

Kim KM, Noh JH, Bodogai M, Martindale JL, Yang X, Indig FE, Basu SK, Ohnuma K, Morimoto C, Johnson PF, et al. 2017. Identification of senescent cell surface targetable protein DPP4. *Genes Dev* **31**: 1529–1534.

Kim WY, Sharpless NE. 2006. The Regulation of INK4/ARF in Cancer and Aging. *Cell* **127**: 265–275.

Kirkwood TBL, Austad SN. 2000. Why do we age? *Nature* **408**: 233–238.

Kiyono T, Foster SA, Koop JI, McDougall JK, Galloway DA, Klingelhutz AJ. 1998. Both Rb/p16(INK4a) inactivation and telomerase activity are required to immortalize human epithelial cells. *Nature* **396**: 84–88.

Knight AS, Notaridou M, Watson RJ. 2009. A Lin-9 complex is recruited by B-Myb to activate transcription of G 2 /M genes in undifferentiated embryonal carcinoma cells. *Oncogene* **28**: 1737–1747.

Knudson AG. 1971. Mutation and Cancer: Statistical Study of Retinoblastoma. *Proc Natl Acad Sci* **68**: 820–823.

Kobayashi K, Suzuki T, Iwata E, Nakamichi N, Suzuki T, Chen P, Ohtani M, Ishida T, Hosoya H, Muller S, et al. 2015. Transcriptional repression by MYB3R proteins regulates plant organ growth. *EMBO J* **34**: 1992–2007.

Kolupaeva V, Janssens V. 2013. PP1 and PP2A phosphatases - Cooperating partners in modulating retinoblastoma protein activation. *FEBS J* **280**: 627–643.

Kopp HG, Hooper AT, Shmelkov S V., Rafii S. 2007. β-galactosidase staining on bone marrow. The osteoclast pitfall. *Histol Histopathol* **22**: 971–976.

Korc M. 2016. RelA: A tale of a stitch in time. *J Clin Invest* **126**: 2799–2801.

Korotchkina LG, Leontieva O V., Bukreeva EI, Demidenko ZN, Gudkov A V., Blagosklonny M V. 2010. The choice between p53-induced senescence and quiescence is determined in part by the mTOR pathway. *Aging (Albany NY)* **2**: 344–352.

Kovesdi lmre, Reichel R, Ft Nevins J. 1986. *Identification of a Cellular Transcription Factor Involved in E1A Transactivation*.

Kriete A, Mayo KL. 2009. Atypical pathways of NF-κB activation and aging. *Exp Gerontol* **44**: 250–255.

Krishnamurthy J, Torrice C, Ramsey MR, Kovalev GI, Al-Regaiey K, Su L, Sharpless NE. 2004. Ink4a/Arf expression is a biomarker of aging. *J Clin Invest* **114**: 1299–1307.

Kruiswijk F, Hasenfuss SC, Sivapatham R, Baar MP, Putavet D, Naipal KAT, Van Den Broek NJF, Kruit W, Van Der Spek PJ, Van Gent DC, et al. 2016. Targeted inhibition of metastatic melanoma through interference with Pin1-FOXM1 signaling. *Oncogene* **35**: 2166–2177.

Kruse JP, Gu W. 2009. Modes of p53 Regulation. *Cell* **137**: 609–622.

Kuilman T, Michaloglou C, Vredeveld LCW, Douma S, van Doorn R, Desmet CJ, Aarden LA, Mooi WJ, Peeper DS. 2008. Oncogene-Induced Senescence Relayed by an Interleukin-Dependent Inflammatory Network. *Cell* **133**: 1019–1031.

Kumari R, Li H, Haudenschild DR, Fierro F, Carlson CS, Overn P, Gupta L, Gupta K, Nolta J, Yik JHN, et al. 2012. The oncogene LRF is a survival factor in chondrosarcoma and contributes to tumor malignancy and drug resistance. *Carcinogenesis* **33**: 2076–2083.

Kurimchak A, Grana X. 2015. PP2A: More than a reset switch to activate pRB proteins during the cell cycle and in response to signaling cues http://www.tandfonline.com/doi/pdf/10.4161/15384101.2014.985069. *Cell Cycle* **14**: 18–30.

Kurz DJ, Decary S, Hong Y, Erusalimsky JD. 2000. Senescence-associated (beta)-galactosidase reflects an increase in lysosomal mass during replicative ageing of human endothelial cells. *J Cell Sci* **113 (Pt 2**: 3613–22.

Laberge RM, Awad P, Campisi J, Desprez PY. 2012. Epithelial-mesenchymal transition induced by senescent fibroblasts. *Cancer Microenviron* **5**: 39–44.

Laberge RM, Sun Y, Orjalo A V., Patil CK, Freund A, Zhou L, Curran SC, Davalos AR, Wilson-Edell KA, Liu S, et al. 2015. MTOR regulates the pro-tumorigenic senescence-associated secretory phenotype by promoting IL1A translation. *Nat Cell Biol* **17**: 1049–1061.

Lane DP. 1992. Cancer. p53, guardian of the genome. *Nature* **358**: 15–16.

Lane DP, Crawford L V. 1979. T antigen is bound to a host protein in SV40-transformed cells. *Nature* **278**: 261–263.

Laoukili J, Alvarez-Fernandez M, Stahl M, Medema RH. 2008. FoxM1 is degraded at mitotic exit in a Cdh1-dependent manner. *Cell Cycle* **7**: 2720–2726.

Lecot P, Alimirah F, Desprez P-Y, Campisi J, Wiley C. 2016. Context-dependent effects of cellular senescence in cancer development. *Br J Cancer* **114**: 1180–1184.

Lee AC, Fenster BE, Ito H, Takeda K, Bae NS, Hirai T, Yu Z, Ferrans VJ, Howard BH, Chem JB, et al. 1999. CELL BIOLOGY AND METABOLISM : Ras Proteins Induce Senescence by Altering the Intracellular Levels of Reactive Oxygen Species Ras Proteins Induce Senescence by Altering the Intracellular Levels of Reactive Oxygen Species *. *J Biol Chem* **274**: 7936–7940.

Lee MG, Nurse P. 1987. Complementation used to clone a human homologue of the fission yeast cell cycle control gene cdc2. *Nature* **327**: 31–5.

Leone G, DeGregori J, Yan Z, Jakoi L, Ishida S, Williams RS, Nevins JR. 1998. E2F3 activity is regulated during the cell cycle and is required for the induction of S phase. *Genes Dev* **12**: 2120–2130.

Leone G, Nuckolls F, Ishida S, Adams M, Sears R, Jakoi L, Miron A, Nevins JR. 2000. Identification of a novel E2F3 product suggests a mechanism for determining specificity of repression by Rb proteins. *Mol Cell Biol* **20**: 3626–3632.

Lesina M, Wörmann SM, Morton J, Diakopoulos KN, Korneeva O, Wimmer M, Einwächter H, Sperveslage J, Demir IE, Kehl T, et al. 2016. RelA regulates CXCL1/CXCR2-dependent oncogene-induced senescence in murine Kras-driven pancreatic carcinogenesis. *J Clin Invest* **126**: 2919–2932.

Levine AJ, Oren M. 2009. The first 30 years of p53: Growing ever more complex. *Nat Rev Cancer* **9**: 749–758.

Levine M, Tijan R. 2003. Transcription regulation and animal diversity. *Nature* **424**: 147–151.

Lewis PW, Beall EL, Fleischer TC, Georlette D, Link AJ, Botchan MR. 2004. Identification of a Drosophila Myb-E2F2/RBF transcriptional repressor complex. *Genes Dev* **18**: 2929–2940.

Li J, Poi MJ, Tsai MD. 2011a. Regulatory mechanisms of tumor suppressor P16INK4A and their relevance to cancer. *Biochemistry* **50**: 5566–5582.

Li M, Zhao H, Zhang X, Wood LD, Anders RA, Choti MA, Pawlik TM, Daniel HD, Kannangai R, Offerhaus GJA, et al. 2011b. Inactivating mutations of the chromatin remodeling gene ARID2 in hepatocellular carcinoma. *Nat Genet* **43**: 828–829.

Linzer DIH, Levine AJ. 1979. Characterization Tumor Antigen and Uninfected of a 54K Dalton Cellular SV40 Present in SV40-Transformed Cells. *Cell* **17**: 43–52.

Litovchick L, Florens LA, Swanson SK, Washburn MP, Decaprio JA. 2011. DYRK1A protein kinase promotes quiescence and senescence through DREAM complex assembly. *Genes Dev* **25**: 801–813.

Litovchick L, Sadasivam S, Florens L, Zhu X, Swanson SK, Velmurugan S, Chen R, Washburn MP, Liu XS, DeCaprio JA. 2007. Evolutionarily Conserved Multisubunit RBL2/p130 and E2F4 Protein Complex Represses Human Cell Cycle-Dependent Genes in Quiescence. *Mol Cell* **26**: 539–551.

Liu D, Hornsby PJ. 2007. Senescent human fibroblasts increase the early growth of xenograft tumors via matrix metalloproteinase secretion. *Cancer Res* **67**: 3117–3126.

Liu Y, Sanoff HK, Cho H, Burd CE, Torrice C, Ibrahim JG, Thomas NE, Sharpless NE. 2009. Expression of p16INK4a in peripheral blood T-cells is a biomarker of human aging. *Aging Cell* **8**: 439–448.

Liu Y, Zhu H, Yan X, Gu H, Gu Z, Liu F. 2017. Endoplasmic reticulum stress participates in the progress of senescence and apoptosis of osteoarthritis chondrocytes. *Biochem Biophys Res Commun* **491**: 368–373.

Lloyd AC. 2013. XThe regulation of cell size. *Cell* **154**: 1194–1205.

Ludlow JW, DeCaprio JA, Huang C-M, Lee W-H, Paucha E, Livingston DM. 1989. SV40 large T antigen binds preferentially to an underphosphorylated member of the retinoblasoma susceptibility gene product family. *Cell* **56**: 57–65.

Lukas C, Falck J, Bartkova J, Bartek J, Lukas J. 2003. Distinct spatiotemporal dynamics of mammalian checkpoint regulators induced by DNA damage. *Nat Cell Biol* **5**: 255–260.

Luo Z, Li X, Zhao Z, Yang X, Xiao S, Zhou Y. 2017. MicroRNA-146a affects the chemotherapeutic sensitivity and prognosis of advanced gastric cancer through the regulation of LIN52. *Oncol Lett* **13**: 1386–1392.

Ly DH, Lockhart DJ, Lerner RA, Schultz PG. 2000. Mitotic misregulation and human aging. *Science (80-)* **287**: 2486–2492.

Macleod KF, Sherry N, Hannon G, Beach D, Tokino T, Kinzler K, Vogelstein B, Jacks T. 1995. p53-Dependent and independent expression of p21 during cell growth, differentiation, and DNA damage. *Genes Dev* **9**: 935–944.

Maeda T, Hobbs RH, Morghoub T, Guernah I, Zelent A, Cordon-Cardo C, Teruya-Feldstein J, Pandolfi PP. 2005. Role of the proto-oncogene Pokemon in cellular transformation and ARF

repression. *Nature* **433**: 278–285.

Magenta A, Cenciarelli C, De Santa F, Fuschi P, Martelli F, Caruso M, Felsani A. 2003. MyoD stimulates RB promoter activity via the CREB/p300 nuclear transduction pathway. *Mol Cell Biol* **23**: 2893–906.

Mages CF, Wintsche A, Bernhart SH, Müller GA. 2017. The DREAM complex through its subunit Lin37 cooperates with Rb to initiate quiescence. *Elife* **6**.

Malumbres M. 2014. Cyclin-dependent kinases. *Genome Biol* **15**: 1–10.

Malumbres M, Barbacid M. 2005. Mammalian cyclin-dependent kinases. *Trends Biochem Sci* **30**: 630–641.

Manceau G, Letouzé E, Guichard C, Didelot A, Cazes A, Corté H, Fabre E, Pallier K, Imbeaud S, Le Pimpec-Barthes F, et al. 2013. Recurrent inactivating mutations of ARID2 in non-small cell lung carcinoma. *Int J Cancer* **132**: 2217–2221.

Mannava S, Moparthy KC, Wheeler LJ, Natarajan V, Zucker SN, Fink EE, Im M, Flanagan S, Burhans WC, Zeitouni NC, et al. 2013. Depletion of deoxyribonucleotide pools is an endogenous source of DNA damage in cells undergoing oncogene-induced senescence. *Am J Pathol* **182**: 142–151.

Marceau AH, Felthousen JG, Goetsch PD, Iness AN, Lee HW, Tripathi SM, Strome S, Litovchick L, Rubin SM. 2016. Structural basis for LIN54 recognition of CHR elements in cell cycle-regulated promoters. *Nat Commun* **7**.

Marcotte R, Lacelle C, Wang E. 2004. Senescent fibroblasts resist apoptosis by downregulating caspase-3. *Mech Ageing Dev* **125**: 777–783.

Maréchal A, Zou L. 2013. DNA damage sensing by the ATM and ATR kinases. *Cold Spring Harb Perspect Biol* **5**.

Martens UM, Chavez EA, Poon SSS, Schmoor C, Lansdorp PM. 2000. Accumulation of short telomeres in human fibroblasts prior to replicative senescence. *Exp Cell Res* **256**: 291–299.

Martín-Caballero J, Serrano M, Flores JM, García-Palencia P. 2001. Tumor susceptibility of p21waf1/cip1-deficient mice. *Cancer Res* **61**: 6234–6238.

Masselink H, Vastenhouw N, Bernards R. 2001. B-myb rescues ras-induced premature senescence, which requires its transactivation domain. *Cancer Lett* **171**: 87–101.

McConnell BB, Starborg M, Brookes S, Peters G. 1998. Inhibitors of cyclin-dependent kinases induce features of replicative senescence in early passage human diploid fibroblasts. *Curr Biol* **8**: 351–354.

McEachern MJ, Krauskopf A, Blackburn EH. 2000. Telomeres and Their Control. *Annu Rev Genet* **34**: 331–358.

Mittnacht S, Lees J a, Desai D, Harlow E, Morgan DO, Weinberg R a. 1994. Distinct sub-populations of the retinoblastoma protein show a distinct pattern of phosphorylation. *EMBO J* **13**: 118–127.

Miyashita A, Fukushima S, Nakahara S, Yamashita J, Tokuzumi A, Aoi J, Ichihara A, Kanemaru H, Jinnin M, Ihn H. 2015. Investigation of FOXM1 as a Potential New Target for Melanoma. *PLoS One* **10**: 144241.

Moiseeva O. 2006. DNA Damage Signaling and p53-dependent Senescence after Prolonged beta-Interferon Stimulation. *Mol Biol Cell* **17**: 1583–1592.

Moiseeva O, Bourdeau V, Roux A, Deschenes-Simard X, Ferbeyre G. 2009. Mitochondrial Dysfunction Contributes to Oncogene-Induced Senescence. *Mol Cell Biol* **29**: 4495–4507.

Morancho B, Martínez-Barriocanal Á, Villanueva J, Arribas J. 2015. Role of ADAM17 in the non-cell autonomous effects of oncogene-induced senescence. *Breast Cancer Res* **17**: 106.

Moreno-Herrero F, De Jager M, Dekker NH, Kanaar R, Wyman C, Dekker C. 2005. Mesoscale conformational changes in the DNA-repair complex Rad50/Mre11/Nbs1 upon binding DNA. *Nature* **437**: 440–443.

Morgan DO. 1997. Cyclin-dependent kinases: engines, clocks, and microprocessors. *Annu Rev Cell Dev Biol* **13**: 261–291.

Mowla SN, Lam EWF, Jat PS. 2014. Cellular senescence and aging: The role of B-MYB. *Aging Cell* **13**: 773–779.

Müller GA, Engeland K. 2010. The central role of CDE/CHR promoter elements in the regulation of cell cycle-dependent gene transcription. *FEBS J* **277**: 877–893.

Müller GA, Quaas M, Schümann M, Krause E, Padi M, Fischer M, Litovchick L, Decaprio JA, Engeland K. 2012. The CHR promoter element controls cell cycle-dependent gene transcription and binds the DREAM and MMB complexes. *Nucleic Acids Res* **40**: 1561–1578.

Müller GA, Stangner K, Schmitt T, Wintsche A, Engeland K. 2016. Timing of transcription during the cell cycle: Protein complexes binding to E2F, E2F/CLE, CDE/CHR, or CHR promoter elements define early and late cell cycle gene expression. *Oncotarget* **26**: 7–8.

Müller GA, Wintsche A, Stangner K, Prohaska SJ, Stadler PF, Engeland K. 2014. The CHR site: Definition and genome-wide identification of a cell cycle transcriptional element. *Nucleic Acids Res* **42**: 10331–10350A.

Muñoz-Espín D, Cañamero M, Maraver A, Gómez-López G, Contreras J, Murillo-Cuesta S, Rodríguez-Baeza A, Varela-Nieto I, Ruberte J, Collado M, et al. 2013. XProgrammed cell senescence during mammalian embryonic development. *Cell* **155**: 1104–18.

Muñoz-Espín D, Serrano M. 2014. Cellular senescence: From physiology to pathology. *Nat Rev Mol Cell Biol* **15**: 482–496.

Munro J, Barr NI, Ireland H, Morrison V, Parkinson EK. 2004. Histone deacetylase inhibitors induce a senescence-like state in human cells by a p16-dependent mechanism that is independent of a mitotic clock. *Exp Cell Res* **295**: 525–538.

Murata Y, Wakoh T, Uekawa N, Sugimoto M, Asai A, Miyazaki T, Maruyama M. 2006. Death-associated protein 3 regulates cellular senescence through oxidative stress response. *FEBS Lett* **580**: 6093–6099.

Musa J, Aynaud M-M, Mirabeau O, Delattre O, Grünewald TG. 2017. MYBL2 (B-Myb): a central regulator of cell proliferation, cell survival and differentiation involved in tumorigenesis. *Cell Death Dis* **8**: e2895.

Nakamura AJ, Chiang YJ, Hathcock KS, Horikawa I, Sedelnikova OA, Hodes RJ, Bonner WM. 2008. Both telomeric and non-telomeric DNA damage are determinants of mammalian cellular senescence. *Epigenetics Chromatin* **1**: 6.

Narita M, Nũnez S, Heard E, Narita M, Lin AW, Hearn SA, Spector DL, Hannon GJ, Lowe SW. 2003. Rb-mediated heterochromatin formation and silencing of E2F target genes during cellular senescence. *Cell* **113**: 703–716.

Neelsen KJ, Zanini IMY, Herrador R, Lopes M. 2013. Oncogenes induce genotoxic stress by mitotic processing of unusual replication intermediates. *J Cell Biol* **200**: 699–708.

Nelson G, Kucheryavenko O, Wordsworth J, von Zglinicki T. 2018. The senescent bystander effect is caused by ROS-activated NF-κB signalling. *Mech Ageing Dev* **170**: 30–36.

Nelson G, Wordsworth J, Wang C, Jurk D, Lawless C, Martin-Ruiz C, von Zglinicki T. 2012. A senescent cell bystander effect: Senescence-induced senescence. *Aging Cell* **11**: 345–349.

Nicolay BN, Dyson NJ. 2013. The multiple connections between pRB and cell metabolism. *Curr Opin Cell Biol* **25**: 735–740.

Nishio K, Inoue A, Qiao S, Kondo H, Mimura A. 2001. Senescence and cytoskeleton: Overproduction of vimentin induces senescent-like morphology in human fibroblasts. *Histochem Cell Biol* **116**: 321–327.

Noda A, Ning Y, Venable SF, Pereira-Smith OM, Smith JR. 1994. Cloning of senescent cell-derived inhibitors of dna synthesis using an expression screen. *Exp Cell Res* **211**: 90–98.

Norbury C, Nurse P. 1992. Animal Cell Cycles and Their Control. *Annu Rev Biochem* **61**: 441–

468.

Nurse P. 1975. Genetic control of cell size at cell division in yeast. *Nature*.

O'Hare MJ, Bond J, Clarke C, Takeuchi Y, Atherton AJ, Berry C, Moody J, Silver AR, Davies DC, Alsop AE, et al. 2001. Conditional immortalization of freshly isolated human mammary fibroblasts and endothelial cells. *Proc Natl Acad Sci U S A* **98**: 646–51.

Ohanna M, Giuliano S, Bonet C, Imbert V, Hofman V, Zangari J, Bille K, Robert C, Bressac-de Paillerets B, Hofman P, et al. 2011. Senescent cells develop a parp-1 and nuclear factor-κB-associated secretome (PNAS). *Genes Dev* **25**: 1245–1261.

Ohno-Iwashita Y, Shimada Y, Hayashi M, Inomata M. 2010. Plasma membrane microdomains in aging and disease. *Geriatr Gerontol Int* **10**: S41–S52.

Olovnikov AM. 1973. A theory of marginotomy. The incomplete copying of template margin in enzymic synthesis of polynucleotides and biological significance of the phenomenon. *J Theor Biol* **41**: 181–190.

Osorio FG, Soria-Valles C, Santiago-Fernández O, Freije JMP, López-Otín C. 2016. NF-κB signaling as a driver of ageing. In *International Review of Cell and Molecular Biology*, Vol. 326 of, pp. 133–174.

Paci P, Colombo T, Fiscon G, Gurtner A, Pavesi G, Farina L. 2017. SWIM: A computational tool to unveiling crucial nodes in complex biological networks. *Sci Rep* **7**.

Pang JH, Chen KY. 1994. Global change of gene expression at late G1/S boundary may occur in human IMR-90 diploid fibroblasts during senescence. *J Cell Physiol* **160**: 531–538.

Pardee AB. 1974. A Restriction Point for Control of Normal Animal Cell Proliferation. *Proc Natl Acad Sci* **71**: 1286–1290.

Park HJ, Wang Z, Costa RH, Tyner A, Lau LF, Raychaudhuri P. 2008. An N-terminal inhibitory domain modulates activity of FoxM1 during cell cycle. *Oncogene* **27**: 1696–1704.

Park WY, Park JS, Cho KA, Kim DI, Ko YG, Seo JS, Park SC. 2000. Up-regulation of caveolin attenuates epidermal growth factor signaling in senescent cells. *J Biol Chem* **275**: 20847–20852.

Parrinello S. 2005. Stromal-epithelial interactions in aging and cancer: senescent fibroblasts alter epithelial cell differentiation. *J Cell Sci* **118**: 485–496.

Passos JF, Nelson G, Wang C, Richter T, Simillion C, Proctor CJ, Miwa S, Olijslagers S, Hallinan J, Wipat A, et al. 2010. Feedback between p21 and reactive oxygen production is necessary for cell senescence. *Mol Syst Biol* **6**: 347.

Passos JF, Saretzki G, Ahmed S, Nelson G, Richter T, Peters H, Wappler I, Birket MJ, Harold G, Schaeuble K, et al. 2007. Mitochondrial dysfunction accounts for the stochastic heterogeneity in telomere-dependent senescence ed. T. De Lange. *PLoS Biol* **5**: 1138–1151.

Paulavich A, Hartwell L. 1995. A checkpoint regulates the rate of progession through S phase in S. cerevisiae in response to DNA damage. *Cell* **82**: 841–847.

Pavletich NP. 1999. Mechanisms of cyclin-dependent kinase regulation: Structures of Cdks, their cyclin activators, and Cip and INK4 inhibitors. *J Mol Biol* **287**: 821–828.

Pazolli E, Alspach E, Milczarek A, Prior J, Piwnica-Worms D, Stewart SA. 2012. Chromatin remodeling underlies the senescence- associated secretory phenotype of tumor stromal fibroblasts that supports cancer progression. *Cancer Res* **72**: 2251–2261.

Peng C. 1997. Mitotic and G2 Checkpoint Control: Regulation of 14-3-3 Protein Binding by Phosphorylation of Cdc25C on Serine-216. *Science (80-)* **277**: 1501–1505.

Penzo M, Massa PE, Olivotto E, Bianchi F, Borzi RM, Hanidu A, Xiang LI, Jun LI, Marcu KB. 2009. Sustained NF-kB activation produces a short-term cell proliferation block in conjunction with repressing effectors of cell cycle progression controlled by E2F or FoxM1. *J Cell Physiol* **218**: 215–227.

Petrova N V., Velichko AK, Razin S V., Kantidze OL. 2016. Small molecule compounds that

induce cellular senescence. *Aging Cell* **15**: 999–1017.

Pilkinton M, Sandoval R, Colamonici OR. 2007. Mammalian Mip/LIN-9 interacts with either the p107, p130/E2F4 repressor complex or B-Myb in a cell cycle-phase-dependent context distinct from the Drosophila dREAM complex. *Oncogene* **26**: 7535–7543.

Pines J. 1991. Cyclins: wheels within wheels. *Cell Growth Differ* **2**: 305–310.

Ping B, He X, Xia W, Lee D-F, Wei Y, Yu D, Mills G, Shi D, Hung M-C. 2006. Cytoplasmic expression of p21CIP1/WAF1 is correlated with IKKbeta overexpression in human breast cancers. *Int J Oncol* **29**: 1103–10.

Pluquet O, Pourtier A, Abbadie C. 2015. The unfolded protein response and cellular senescence. A Review in the Theme: Cellular Mechanisms of Endoplasmic Reticulum Stress Signaling in Health and Disease. *Am J Physiol - Cell Physiol* **308**: C415–C425.

Prieur A, Peeper DS. 2008. Cellular senescence in vivo: a barrier to tumorigenesis. *Curr Opin Cell Biol* **20**: 150–155.

Qu H, Qu D, Chen F, Zhang Z, Liu B, Liu H. 2010. ZBTB7 overexpression contributes to malignancy in breast cancer. *Cancer Invest* **28**: 672–678.

Quaas M, Müller GA, Engeland K. 2012. p53 can repress transcription of cell cycle genes through a p21WAF1/CIP1-dependent switch from MMB to DREAM protein complex binding at CHR promoter elements. *Cell Cycle* **11**: 4661–4672.

Rhodes DR, Yu J, Shanker K, Deshpande N, Varambally R, Ghosh D, Barrette T, Pandey A, Chinnaiyan AM. 2004. Large-scale meta-analysis of cancer microarray data identifies common transcriptional profiles of neoplastic transformation and progression. *Proc Natl Acad Sci* **101**: 9309–9314.

Robles SJ, Adami GR. 1998. Agents that cause DNA double strand breaks lead to p16(INK4a) enrichment and the premature senescence of normal fibroblasts. *Oncogene* **16**: 1113–1123.

Rodier F, Campisi J. 2011. Four faces of cellular senescence. *J Cell Biol* **192**: 547–556.

Rodier F, Coppé JP, Patil CK, Hoeijmakers WAM, Muñoz DP, Raza SR, Freund A, Campeau E, Davalos AR, Campisi J. 2009. Persistent DNA damage signalling triggers senescence-associated inflammatory cytokine secretion. *Nat Cell Biol* **11**: 973–979.

Rodier F, Munoz DP, Teachenor R, Chu V, Le O, Bhaumik D, Coppe J-P, Campeau E, Beausejour CM, Kim S-H, et al. 2011. DNA-SCARS: distinct nuclear structures that sustain damage-induced senescence growth arrest and inflammatory cytokine secretion. *J Cell Sci* **124**: 68–81.

Rovillain E. 2011. Dissecting the telomere-independent pathways underlying human cellular senescence. UCL (University College London).

Rovillain E, Mansfield L, Caetano C, Alvarez-Fernandez M, Caballero OL, Medema RH, Hummerich H, Jat PS. 2011. Activation of nuclear factor-kappa B signalling promotes cellular senescence. *Oncogene* **30**: 2356–2366.

Russell P, Nurse P. 1986. Schizosaccharomyces pombe and saccharomyces cerevisiae: A look at yeasts divided. *Cell* **45**: 781–782.

Ryan MD, King AMQ, Thomas GP. 1991. Cleavage of foot-and-mouth disease virus polyprotein is mediated by residues located within a 19 amino acid sequence. *J Gen Virol* **72**: 2727–2732.

Ryu SJ, Oh YS, Park SC. 2007. Failure of stress-induced downregulation of Bcl-2 contributes to apoptosis resistance in senescent human diploid fibroblasts. *Cell Death Differ* **14**: 1020–1028.

Sadaie M, Salama R, Carroll T, Tomimatsu K, Chandra T, Young ARJ, Narita M, Pérez-Mancera PA, Bennett DC, Chong H, et al. 2013. Redistribution of the Lamin B1 genomic binding profile affects rearrangement of heterochromatic domains and SAHF formation during senescence. *Genes Dev* **27**: 1800–1808.

Sadasivam S, DeCaprio JA. 2013. The DREAM complex: Master coordinator of cell cycle-dependent gene expression. *Nat Rev Cancer* **13**: 585–595.

Sadasivam S, Duan S, DeCaprio JA. 2012. The MuvB complex sequentially recruits B-Myb and FoxM1 to promote mitotic gene expression. *Genes Dev* **26**: 474–489.

Salama R, Sadaie M, Hoare M, Narita M. 2014. Cellular senescence and its effector programs. *Genes Dev* **28**: 99–114.

Salminen A, Huuskonen J, Ojala J, Kauppinen A, Kaarniranta K, Suuronen T. 2008. Activation of innate immunity system during aging: NF-kB signaling is the molecular culprit of inflamm-aging. *Ageing Res Rev* **7**: 83–105.

Salminen A, Kauppinen A, Kaarniranta K. 2012. Emerging role of NF-κB signaling in the induction of senescence-associated secretory phenotype (SASP). *Cell Signal* **24**: 835–845.

Sanders DA, Gormally M V., Marsico G, Beraldi D, Tannahill D, Balasubramanian S. 2015. FOXM1 binds directly to non-consensus sequences in the human genome. *Genome Biol* **16**.

Sanders YY, Liu H, Zhang X, Hecker L, Bernard K, Desai L, Liu G, Thannickal VJ. 2013. Histone modifications in senescence-associated resistance to apoptosis by oxidative stress. *Redox Biol* **1**: 8–16.

Sardet C, Vidal M, Cobrinik D, Geng Y, Onufryk C, Chen A, Weinberg RA. 1995. E2F-4 and E2F-5, two members of the E2F family, are expressed in the early phases of the cell cycle. *Proc Natl Acad Sci U S A* **92**: 2403–2407.

Schmit F, Cremer S, Gaubatz S. 2009. LIN54 is an essential core subunit of the DREAM/LINC complex that binds to the cdc2 promoter in a sequence-specific manner. *FEBS J* **276**: 5703–5716.

Schmit F, Korenjak M, Mannefeld M, Schmitt K, Franke C, Von Eyss B, Gagrica S, Hänel F, Brehm A, Gaubatz S. 2007. LINC, a human complex that is related to pRB-containing complexes in invertebrates regulates the expression of G2/M genes. *Cell Cycle* **6**: 1903–1913.

Sedivy JM, Capone JP, RajBhandary UL, Sharp PA. 1987. An inducible mammalian amber suppressor: Propagation of a poliovirus mutant. *Cell* **50**: 379–389.

Sedivy JM, van Deursen JM. 2013. Why do we grow old: is it because our cells just wear out, we run out of cells (or both), and what can we do about it? *Longev Heal* **2**: 7.

Seluanov A, Gorbunova V, Falcovitz A, Sigal A, Milyavsky M, Zurer I, Shohat G, Goldfinger N, Rotter V. 2001. Change of the Death Pathway in Senescent Human Fibroblasts in Response to DNA Damage Is Caused by an Inability To Stabilize p53. *Mol Cell Biol* **21**: 1552–1564.

Serrano M, Hannon GJ, Beach D. 1993. A new regulatory motif in cell-cycle control causing specific inhibition of cyclin D/CDK4. *Nature* **366**: 704–707.

Serrano M, Lin AW, McCurrach ME, Beach D, Lowe SW. 1997. Oncogenic ras provokes premature cell senescence associated with accumulation of p53 and p16(INK4a). *Cell* **88**: 593–602.

Shah MA, Schwartz GK. 2001. Cell cycle-mediated drug resistance: An emerging concept in cancer therapy. *Clin Cancer Res* **7**: 2168–2181.

Sharpless NE, Sherr CJ. 2015. Forging a signature of in vivo senescence. *Nat Rev Cancer* **15**: 397–408.

Shelton DN, Chang E, Whittier PS, Choi D, Funk WD. 1999. Microarray analysis of replicative senescence. *Curr Biol* **9**: 939–945.

Sherr CJ. 2000. The Pezcoller Lecture : Cancer Cell Cycles Revisited - Unit 4. *CANCER Res* **60**: 3689–3695.

Sherr CJ, Roberts JM. 1999. CDK inhibitors: positive and negative regulators of G1-phase progression. *Genes Dev* **13**: 1501–12.

Storer M, Mas A, Robert-Moreno A, Pecoraro M, Ortells MC, Di Giacomo V, Yosef R, Pilpel N, Krizhanovsky V, Sharpe J, et al. 2013. XSenescence is a developmental mechanism that contributes to embryonic growth and patterning. *Cell* **155**: 1119–30.

Stow JL, Murray RZ. 2013. Intracellular trafficking and secretion of inflammatory cytokines. *Cytokine Growth Factor Rev* **24**: 227–239.

Stracker TH, Theunissen JWF, Morales M, Petrini JHJ. 2004. The Mre11 complex and the metabolism of chromosome breaks: The importance of communicating and holding things together. *DNA Repair (Amst)* **3**: 845–854.

Studencka M, Schaber J. 2017. Senoptosis: non-lethal DNA cleavage as a route to deep senescence. *Oncotarget* **8**: 30656–30671.

Sulli G, Di Micco R, Di Fagagna FDA. 2012. Crosstalk between chromatin state and DNA damage response in cellular senescence and cancer. *Nat Rev Cancer* **12**: 709–720.

Szymczak AL, Workman CJ, Wang Y, Vignali KM, Dilioglou S, Vanin EF, Vignali DAA. 2004. Correction of multi-gene deficiency in vivo using a single “self-cleaving” 2A peptide-based retroviral vector. *Nat Biotechnol* **22**: 589–594.

Taganov KD, Boldin MP, Chang K-J, Baltimore D. 2006. NF- B-dependent induction of microRNA miR-146, an inhibitor targeted to signaling proteins of innate immune responses. *Proc Natl Acad Sci* **103**: 12481–12486.

Tai H, Wang Z, Gong H, Han X, Zhou J, Wang X, Wei X, Ding Y, Huang N, Qin J, et al. 2017. Autophagy impairment with lysosomal and mitochondrial dysfunction is an important characteristic of oxidative stress-induced senescence. *Autophagy* **13**: 99–113.

Takahashi K, Tanabe K, Ohnuki M, Narita M, Ichisaka T, Tomoda K, Yamanaka S. 2007. Induction of Pluripotent Stem Cells from Adult Human Fibroblasts by Defined Factors. *Cell* **131**: 861–872.

Takahashi K, Yamanaka S. 2006. Induction of Pluripotent Stem Cells from Mouse Embryonic and Adult Fibroblast Cultures by Defined Factors. *Cell* **126**: 663–676.

Takasugi M, Okada R, Takahashi A, Virya Chen D, Watanabe S, Hara E. 2017. Small extracellular vesicles secreted from senescent cells promote cancer cell proliferation through EphA2. *Nat Commun* **8**: 15729.

Takebayashi S ichiro, Tanaka H, Hino S, Nakatsu Y, Igata T, Sakamoto A, Narita M, Nakao M. 2015. Retinoblastoma protein promotes oxidative phosphorylation through upregulation of glycolytic genes in oncogene-induced senescent cells. *Aging Cell*, August.

Teixeira LK, Reed SI. 2013. Ubiquitin Ligases and Cell Cycle Control. *Annu Rev Biochem* **82**: 387–414.

Thorburn AM, Walton PA, Feramisco JR. 1993. MyoD induced cell cycle arrest is associated with increased nuclear affinity of the Rb protein. *Mol Biol Cell* **4**: 705–13.

Trimarchi JM, Lees JA. 2002. Sibling rivalry in the E2F family. *Nat Rev Mol Cell Biol* **3**: 11–20.

Tschöp K, Conery AR, Litovchick L, Decaprio JA, Settleman J, Harlow E, Dyson N. 2011. A kinase shRNA screen links LATS2 and the pRB tumor suppressor. *Genes Dev* **25**: 814–30.

Umbreit NT, Pellman D. 2017. Cancer biology: Genome jail-break triggers lockdown. *Nature* **550**: 340–341.

Van Den Heuvel S, Dyson NJ. 2008. Conserved functions of the pRB and E2F families. *Nat Rev Mol Cell Biol* **9**: 713–724.

Vaquerizas JM, Kummerfeld SK, Teichmann SA, Luscombe NM. 2009. A census of human transcription factors: Function, expression and evolution. *Nat Rev Genet* **10**: 252–263.

Vaziri H, Benchimol S. 1998. Reconstitution of telomerase activity in normal human cells leads to elongation of telomeres and extended replicative life span. *Curr Biol* **8**: 279–282.

Vermeulen K, Van Bockstaele DR, Berneman ZN. 2003. The cell cycle: A review of regulation, deregulation and therapeutic targets in cancer. *Cell Prolif* **36**: 131–149.

Virshup DM, Shenolikar S. 2009. From Promiscuity to Precision: Protein Phosphatases Get a Makeover. *Mol Cell* **33**: 537–545.

Volonte D, Zhang K, Lisanti MP, Galbiati F. 2002. Expression of Caveolin-1 Induces Premature Cellular Senescence in Primary Cultures of Murine Fibroblasts. Stress-Induced Premature Senescence Upregulates the Expression of Endogenous Caveolin-1. *Mol Biol Cell* **13**: 2502–2517.

Volonte D, Zou H, Bartholomew JN, Liu Z, Morel PA, Galbiati F. 2015. Oxidative stress-induced inhibition of Sirt1 by caveolin-1 promotes p53-dependent premature senescence and stimulates the secretion of interleukin 6 (IL-6). *J Biol Chem* **290**: 4202–4214.

Vredeveld LCW, Rowland BD, Douma S, Bernards R, Peeper DS. 2010. Functional identification of LRF as an oncogene that bypasses RASV12-induced senescence via upregulation of CYCLIN E. *Carcinogenesis* **31**: 201–207.

Waaijer MEC, Parish WE, Strongitharm BH, van Heemst D, Slagboom PE, de Craen AJM, Sedivy JM, Westendorp RGJ, Gunn DA, Maier AB. 2012. The number of p16INK4a positive cells in human skin reflects biological age. *Aging Cell* **11**: 722–725.

Wade Harper J, Adami GR, Wei N, Keyomarsi K, Elledge SJ. 1993. The p21 Cdk-interacting protein Cip1 is a potent inhibitor of G1 cyclin-dependent kinases. *Cell* **75**: 805–816.

Wajapeyee N, Serra RW, Zhu X, Mahalingam M, Green MR. 2008. Oncogenic BRAF Induces Senescence and Apoptosis through Pathways Mediated by the Secreted Protein IGFBP7. *Cell* **132**: 363–374.

Wanek K. 2011. Development of an shRNA screen to identify mediators of cellular senescence in human breast epithelial cells By. *Dr thesis, UCL (University Coll London)*.

Wang C, Jurk D, Maddick M, Nelson G, Martin-ruiz C, Von Zglinicki T. 2009a. DNA damage response and cellular senescence in tissues of aging mice. *Aging Cell* **8**: 311–323.

Wang G, Lunardi A, Zhang J, Chen Z, Ala U, Webster KA, Tay Y, Gonzalez-Billalabeitia E, Egia A, Shaffer DR, et al. 2013. Zbtb7a suppresses prostate cancer through repression of a Sox9-dependent pathway for cellular senescence bypass and tumor invasion. *Nat Genet* **45**: 739–746.

Wang J, Jacob NK, Ladner KJ, Beg A, Perko JD, Tanner SM, Liyanarachchi S, Fishel R, Guttridge DC. 2009b. RelA/p65 functions to maintain cellular senescence by regulating genomic stability and DNA repair. *EMBO Rep* **10**: 1272–1278.

Wang M, Kaufman RJ. 2014. The impact of the endoplasmic reticulum protein-folding environment on cancer development. *Nat Rev Cancer* **14**: 581–597.

Webley K, Bond JA, Jones CJ, Blaydes JP, Craig A, Hupp T, Wynford-Thomas D. 2000. Posttranslational modifications of p53 in replicative senescence overlapping but distinct from those induced by DNA damage. *Mol Cell Biol* **20**: 2803–8.

Weiss RS, Matsuoka S, Elledge SJ, Leder P. 2002. Hus1 acts upstream of Chk1 in a mammalian DNA damage response pathway. *Curr Biol* **12**: 73–77.

Westendorp B, Mokry M, Groot Koerkamp MJA, Holstege FCP, Cuppen E, De Bruin A. 2012. E2F7 represses a network of oscillating cell cycle genes to control S-phase progression. *Nucleic Acids Res* **40**: 3511–3523.

Whyte P, Buchkovich KJ, Horowitz JM, Friend SH, Raybuck M, Weinberg RA, Harlow E. 1988. Association between an oncogene and an anti-oncogene: the adenovirus E1A proteins bind to the retinoblastoma gene product. *Nature*.

Wiley CD, Campisi J. 2016. From Ancient Pathways to Aging Cells - Connecting Metabolism and Cellular Senescence. *Cell Metab* **23**: 1013–1021.

Wiley CD, Flynn JM, Morrissey C, Lebofsky R, Shuga J, Dong X, Unger MA, Vijg J, Melov S, Campisi J. 2017. Analysis of individual cells identifies cell-to-cell variability following induction of cellular senescence. *Aging Cell* **16**: 1043–1050.

Wiley CD, Velarde MC, Lecot P, Liu S, Sarnoski EA, Freund A, Shirakawa K, Lim HW, Davis SS, Ramanathan A, et al. 2016. Mitochondrial dysfunction induces senescence with a distinct

secretory phenotype. *Cell Metab* **23**: 303–314.

Williams GC. 1957. PLEIOTROPY, NATURAL SELECTION, AND THE EVOLUTION OF SENESCENCE. *Evolution (N Y)* **11**: 398–411.

Wu L, Timmers C, Malti B, Saavedra HI, Sang L, Chong GT, Nuckolls F, Giangrande P, Wright FA, Field SJ, et al. 2001. The E2F1-3 transcription factors are essential for cellular proliferation. *Nature* **414**: 457–462.

Wu M, Ye H, Shao C, Zheng X, Li Q, Wang L, Zhao M, Lu G, Chen B, Zhang J, et al. 2017. Metabolomics-Proteomics Combined Approach Identifies Differential Metabolism-Associated Molecular Events between Senescence and Apoptosis. *J Proteome Res* **16**: 2250–2261.

Yamakoshi K, Takahashi A, Hirota F, Nakayama R, Ishimaru N, Kubo Y, Mann DJ, Ohmura M, Hirao A, Saya H, et al. 2009. Real-time in vivo imaging of p16 ^{Ink4a} reveals cross talk with p53. *J Cell Biol* **186**: 393–407.

Yang G, Rosen DG, Zhang Z, Bast RC, Mills GB, Colacino JA, Mercado-Uribe I, Liu J. 2006. The chemokine growth-regulated oncogene 1 (Gro-1) links RAS signaling to the senescence of stromal fibroblasts and ovarian tumorigenesis. *Proc Natl Acad Sci* **103**: 16472–16477.

Yang H, Wang H, Ren J, Chen Q, Chen ZJ. 2017. cGAS is essential for cellular senescence. *Proc Natl Acad Sci* **114**: E4612–E4620.

Yosef R, Pilpel N, Papismadov N, Gal H, Ovadya Y, Vadai E, Miller S, Porat Z, Ben-Dor S, Krizhanovsky V. 2017. p21 maintains senescent cell viability under persistent DNA damage response by restraining JNK and caspase signaling. *EMBO J* **36**: 2280–2295.

Yosef R, Pilpel N, Tokarsky-Amiel R, Biran A, Ovadya Y, Cohen S, Vadai E, Dassa L, Shahar E, Condiotti R, et al. 2016. Directed elimination of senescent cells by inhibition of BCL-W and BCL-XL. *Nat Commun* **7**.

Yun MH. 2015. Changes in regenerative capacity through lifespan. *Int J Mol Sci* **16**: 25392–25432.

Yun MH, Davaapil H, Brockes JP. 2015. Recurrent turnover of senescent cells during regeneration of a complex structure. *Elife* **4**: 1–33.

Zhang HS, Gavin M, Dahiya A, Postigo AA, Ma D, Luo RX, Harbour JW, Dean DC. 2000. Exit from G1 and S phase of the cell cycle is regulated by repressor complexes containing HDAC-Rb-hSWI/SNF and RB-hSWI/SNF. *Cell* **101**: 79–89.

Zhang J, Pickering CR, Holst CR, Gauthier ML, Tlsty TD. 2006. p16INK4a modulates p53 in primary human mammary epithelial cells. *Cancer Res* **66**: 10325–10331.

Zhang X, Shi H, Wu J, Zhang X, Sun L, Chen C, Chen ZJ. 2013. Cyclic GMP-AMP containing mixed Phosphodiester linkages is an endogenous high-affinity ligand for STING. *Mol Cell* **51**: 226–235.

Zhao Z hong, Wang S fa, Yu L, Wang J, Chang H, Yan W li, Zhang J, Fu K. 2008. Overexpression of Pokemon in non-small cell lung cancer and foreshowing tumor biological behavior as well as clinical results. *Lung Cancer* **62**: 113–119.

Zhu W, Giangrande PH, Nevins JR. 2004. E2Fs link the control of G1/S and G2/M transcription. *EMBO J* **23**: 4615–4626.

Zhu Y, Tchkonia T, Pirtskhalava T, Gower AC, Ding H, Giorgadze N, Palmer AK, Ikeno Y, Hubbard GB, Lenburg M, et al. 2015. The Achilles' heel of senescent cells: from transcriptome to senolytic drugs. *Aging Cell* **14**: 644–658.

Zou L, Elledge SJ. 2003. Sensing DNA damage through ATRIP recognition of RPA-ssDNA complexes. *Science (80-)* **300**: 1542–1548.

Journal of Cell Signaling

Benedekova et al., J Cell Signal 2017, 2:3
DOI: 10.4172/2576-1471.1000155

Commentary OMICS International

Tumour Suppressors and Cellular Senescence

Marta Benedekova[1], **Ruchi Kumari**[1] **and Parmjit S Jat**[1*]

[1]*MRC Prion Unit at UCL, Institute of Prion Diseases Queen Square London WC1N 3BG, UK*

***Corresponding author:** Parmjit S Jat, MRC Prion Unit at UCL, Institute of Prion Diseases Queen Square London WC1N 3BG UK, E-mail: p.jat@prion.ucl.ac.uk

Received date: June 07, 2017; **Accepted date:** June 16, 2017; **Published date:** June 26, 2017

Commentary

Cellular senescence is a stable growth arrest that normal human diploid fibroblasts undergo after a finite number of divisions, as a result of progressive shortening of telomeres and other genotoxic as well as non-genotoxic stresses. It is an example of antagonistic pleiotropy, as it plays an important role in tumour suppression during early life whereas later in life, it leads to deleterious traits, such as disrupted tissue function, thereby promoting organismal ageing and age-related diseases. Elucidating and understanding the signalling pathways involved in regulating the senescent state, is therefore of great biological importance.

Cellular senescence is a stable growth arrest, that normal human diploid fibroblasts undergo after a finite number of divisions [1], as a result of progressive shortening of telomeres [2]. However, further stressors such as oncogenic activation, DNA damage, oxidative stress and other non-genotoxic stresses were later found to also trigger this arrested state [3]. Senescence is an example of antagonistic pleiotropy, playing an important role in tumour suppression during early life, as it is a natural barrier to carcinogenesis. Later in life, it leads to deleterious traits, such as disrupted tissue function, consequently promoting organismal ageing and age-related diseases. Hence, elucidating the signalling pathways involved in regulating the senescent state is of great biological importance.

Multiple stimuli are known to activate the p53/p21 and p16/pRB tumour suppressor pathways, which have clearly been established to mediate senescence; however, the critical downstream targets have yet

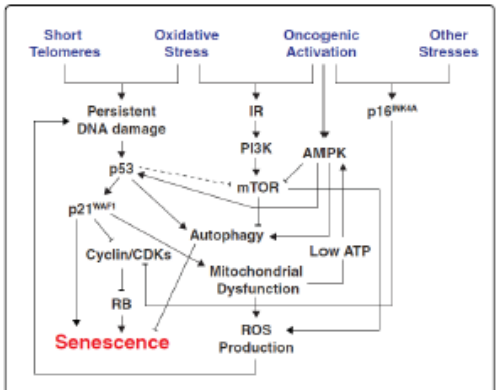

Figure 1: Schematic illustration of the signalling pathways involved in regulating cellular senescence.

The function of this complex has been characterised in quiescence [15], which suggests a potential role in senescence, but this remains to be verified. Although it is clear how p53 and pRB activation lead to quiescence, a greater understanding of downstream transcription factors and target genes involved in establishing senescence is essential,

BKB1R

▶ Bradykinin Receptors

BKB2R

▶ Bradykinin Receptors

BKR1

▶ Bradykinin Receptors

BKR2

▶ Bradykinin Receptors

BL34

▶ Regulator of G-Protein Signaling 1 (RGS1)

BL-AC/P26

▶ CD69

BMF (BCL-2-Modifying Factor)

▶ BCL-2 Family

BMK1

▶ MEK5/ERK5

BMYB

▶ B-Myb

B-Myb

Ruchi Kumari and Parmjit Jat
Department of Neurodegenerative Disease, Institute of Neurology, University College London, London, UK

Synonyms

BMYB; MYB proto-oncogene like 2; Myb-like protein 2; Myb-related protein B, MYBL2; v-myb